eMetN
METEOR JOURNAL

eJournal for meteor observers   **www.emetn.net**

This striking bright meteor was captured at 6h20m19.0 ± 0.1s UT on 2025 January 24. It had a peak absolute magnitude of −12.0 ± 1.0. It was listed in the SWEMN meteor database with the code SWEMN20250124_062019.   © José Madiedo.

Contents

Global Meteor Network report 2024

Paul Roggemans[1], **Peter Campbell-Burns**[2], **Milan Kalina**[3], **Mark McIntyre**[4],
James M. Scott[5], **Damir Šegon**[6], **and Denis Vida**[7]

[1] **Pijnboomstraat 25, 2800 Mechelen, Belgium**
paul.roggemans@gmail.com

[2] **UK Meteor Observation Network, Cavendish Gardens, Fleet, Hampshire, United Kingdom**
peter@campbell-burns.com

[3] **Czech Astronomical Society, Ondrejov, Czech Republic**
milank2010@gmail.com

[4] **UK Meteor Observation Network and Tackley Observatory, United Kingdom**
mark.jm.mcintyre@cesmail.net

[5] **University of Otago, Department of Geology, Dunedin, New Zealand**
james.scott@otago.ac.nz

[6] **Astronomical Society Istra Pula, Park Monte Zaro 2, 52100 Pula, Croatia**
damir@astro.hr

[7] **Department of Physics and Astronomy, University of Western Ontario, London, Ontario, N6A 3K7, Canada**
dvida@uwo.ca

A status report is presented for the Global Meteor Network. Since the start of the network, 1896600 meteor orbits have been collected until end of 2024, 387 different meteor showers have been identified among these orbits. During 2024 more than 237 new GMN cameras started contributing successfully paired meteors. 707554 orbits were collected in 2024. The development of the Global Meteor Network in different regions is described. The coverage of the camera fields of view is shown on maps.

1   Introduction

Over the past 20 years many video camera networks were created, both regional and national, with the aim of obtaining meteor trajectories through multi-station registrations. Most of these networks specialize in fireballs and meteorite droppers, others are dedicated to a fainter magnitude range comparable to what visual observers used to cover. The orbit data obtained by these networks brought a tremendous progress in our knowledge of meteoroid streams.

The Global Meteor Network is the most recent development in this domain. Its success builds on the many years of expertise of the Croatian Meteor Network, one of the pioneers in the field of video meteor observations and the origin of GMN (Gural and Šegon, 2009). Based on RMS, the significantly improved Raspberry Pi solution introduced by Zubović et al. (2015) and Vida et al. (2016), the Global Meteor Network began its operation at the end of 2018; its first six cameras located in New Mexico used IP cameras controlled by a Raspberry running its own dedicated software and reduction pipeline (Vida et al., 2021). GMN became the fastest growing meteor video network with 73 operational cameras at the end of 2019, 155 at the end of 2020, 341 at the end of 2021, 700 at the end of 2022, 1066 in 2023 and 1213 at the end of 2024. 179 older cameras were decommissioned and did not upload any data anymore in 2024.

2   Joining the Global Meteor Network

More information about this project can be found in Vida et al. (2020a; 2020b; 2021; 2022) and on the GMN website[1]. An informative video presentation about the Global Meteor Network project can be watched online[2]. Many sites and participants are still waiting to find partners to improve the coverage on their cameras. New participants are welcome to expand the network.

To obtain a camera for participation you can either buy it plug&play from Istream[3], or you buy the components and build your own camera for about 250 US$ or ~200 €. The RMS cameras are easy to build and operate. If you are interested in building your own camera you can find detailed instructions online[4].

The daily status of most (not all) meteor stations can be followed on the GMN weblog[5] or on the GMN status pages

---

[1] https://globalmeteornetwork.org/
[2] https://www.youtube.com/watch?v=MAGq-XqD5Po
[3] https://globalmeteornetwork.org/?page_id=136
[4] https://globalmeteornetwork.org/wiki/index.php?title=Build_A_Camera
[5] https://globalmeteornetwork.org/weblog/

per country[6]. The GMN results and data are publicly available and daily updated online[7]. The UK meteor network maintains a comprehensive archive[8] and daily update[9] which may inspire others. Their Wiki-page[10] may be helpful to people outside the UK as well as their github repos[11,12].

The meteor map[13] is an online tool for visualizing meteor cameras and ground tracks of observed meteors. Each participant can check the results obtained with each camera, check the location of the meteor trajectories and combinations with other camera stations. The tool has been described in an article (Dijkema, 2022). Milan Kalina developed another tool, "Meteorview[14]" to map meteor trajectories with several extra functionalities described in an article (Kalina, 2024).

As the static maps of camera FoVs presented in this report sometimes become overcrowded, the aggregated kml files valid for end of 2024 can be downloaded[15]. The individual up-to-date kml-files for all GMN cameras can be downloaded from the GMN website[16]. Camera operators are encouraged to point new cameras in function of optimal coverage with other cameras. Opening the kml files in Google Earth allows to toggle cameras on and off to get a better view on the actual coverage. Make sure to compare kml files at the same elevation (e.g. 100 km) and prevent 3D perspective by changing the properties in the Google Earth graphical interface to "clamped to ground" instead of the default setting "absolute".

If you have a dark site with a free view and if you are looking to make a scientifically useful contribution, with just five RMS cameras with 3.6 mm lenses (FoV 88° × 47°) pointed at azimuths 0° (North), 70°, 140°, 220° and 290°, between 35° and 40° elevation, you cover all the sky except your zenith. Avoid pointing a camera at the meridian (180° azimuth) as the transit of the Full Moon will take full effect in this position. Also do not point lower than 35° elevation: there are no meteors in the local scenery, trees or buildings. If you use 6 mm lenses, recommended where light pollution is an issue, you need six RMS to cover the sky with a royal overlap between the camera edges. Six cameras with 6 mm lenses (FoV 54° × 30°) pointed at azimuths 30°, 90°, 150°, 210°, 270° and 330°, between 35° and 40° elevation, would make you a key video meteor hub in the network. Building the cameras at the cost of the purchased components, or bought plug & play, both remain a low-cost project, affordable to many amateurs, observatories and societies.

The unavailability of Raspberry Pi because of production limitations due to Covid in former years has been meanwhile solved, but inspired people to explore alternative systems for unavailable RPi's. A cheap Linux PC can handle multiple cameras and a system has been developed to operate multiple GMN cameras using a single PC. Read the article written by Harman et al. (2023) and check the Wiki pages for the latest updates.

3   Annual GMN meeting 2024 (online)

The annual meeting of the Global Meteor Network got more than 100 people participating online from around the globe. The meeting took place in two sessions on February 24–25, 2024 in order to allow people from all time zones to participate. 19 presentations were given with enough time for questions and discussions, each session ended with a Q&A workshop session. Both sessions can be viewed online:

- Session 1 – February 24, 16^h00^m – 21^h00^m UTC[17]
- Session 2 – February 25, 00^h00^m – 03^h00^m UTC[18]

4   GMN camera coverage

The aim of the GMN is to cover all latitudes and longitudes to assure a global coverage of meteor activity in order to let no unexpected meteor event pass unnoticed. This is an ambitious goal especially for a project that depends for most efforts entirely on volunteers' work. In this report we describe the progress that was made by GMN during 2024 in different regions of the world. The status of the camera coverage is illustrated with maps showing the fields of view intersected at an elevation of 100 km in the atmosphere, projected and clamped to the ground. This way the actual overlap between the camera fields is shown without any effects of 3D perspectives. Where possible the camera ID has been mentioned on the plots. The status at the end of 2024 can be compared to the 2023 annual report (Roggemans et al., 2024).

Many RMS cameras with 4 mm optics have the horizon at the bottom of their field of view what results in a huge camera field at 100 km elevation. Rather few meteors will be bright enough to get registered near the horizon. The large distance between the camera station and the meteor also reduces the chances to obtain a useable triangulation. The number of paired meteors at the outskirts of these large camera fields is very small. However, cameras pointing so low towards the horizon turn out to be very useful regarding obtaining coverage at lower heights where meteorite dropping fireballs end their visible path. When looking for camera overlap, it is strongly recommended to look for an optimized overlap between cameras. An interesting study on this topic for the New Mexico Meteor Array has been

---

[6] https://globalmeteornetwork.org/status/
[7] https://globalmeteornetwork.org/data/
[8] https://www.ukmeteornetwork.org
[9] https://www.ukmeteors.co.uk/live/index.html
[10] https://github.com/markmac99/ukmon-pitools/wiki
[11] https://github.com/markmac99/ukmon-pitools
[12] https://github.com/markmac99/UKmon-shared
[13] https://tammojan.github.io/meteormap/

[14] https://www.meteorview.net/
[15] https://www.emeteornews.net/wp-content/uploads/2025/02/All_2024.zip
[16] https://globalmeteornetwork.org/data/kml_fov/
[17] https://www.youtube.com/watch?v=juOvRTtoqhs
[18] https://www.youtube.com/watch?v=MXhVIxrz2ks

published by Mroz (2021). Camera operators are encouraged to optimize their camera overlap.

The number of multi-station events mentioned per country corresponds to the number of orbits, unless an orbit was based on camera data from different countries, then it was counted once for each country. This can also be visualized on the MeteorMap[19] (Dijkema, 2022) or with MeteorView[20] (Kalina, 2024). The current camera coverage is presented per country or per region for reason of readability. To consider the real overlap for most European countries it is necessary to look at the camera coverage of neighboring countries. In several regions the camera coverage is too dense to visualize it in a single map. We strongly recommend to view the camera FoVs in Google Earth. The required kml-files have been grouped per country and can be downloaded for: Asia, Europe, North America, Africa and Southern hemisphere.

5.1 Austria

Austria got its first RMS (AT0002) generating orbits since August 2024, the second camera (AT0004) had its first orbits in October 2024. All together the two Austrian GMN cameras contributed 1702 orbits, most of which as a combination with GMN cameras in neighboring countries, see *Figure 1*.
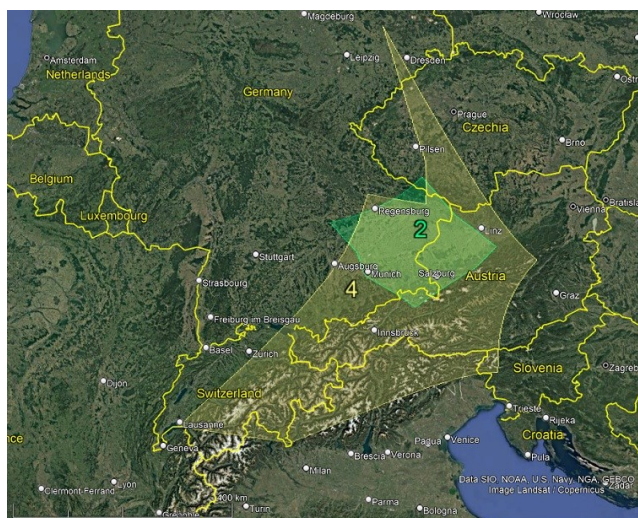

Figure 1 – GMN camera fields in 2024 intersected at 100 km elevation, for cameras active in Austria.

5.2 Australia

The first 31 meteor orbits by Australian RMS cameras were registered in September 2021 when the first five cameras got ready to harvest meteors. By the end of 2021, 12 cameras managed to obtain 1871 orbits in the final 4 months of 2021. A first breakthrough was achieved in 2022 as the number of RMS cameras in Australia increased to 29, good for 12460 orbits in 2022. The expansion of the network accelerated even more in 2023 with 66 operational cameras contributing 40712 orbits making Australia one of the major contributors to GMN. Nine cameras active in 2023 were decommissioned, but 31 new cameras were added in 2024. This resulted in a major breakthrough in 2024 with 88 cameras contributing as many as 100044 orbits (see

Table 5). Most cameras were installed in Western Australia (*Figure 3*) but significant progress was made in the eastern states of Australia with more cameras in Victoria, Queensland and New South Wales (*Figure 4*). Australia being a very large country, describing its camera networks as a single network is a bit unfair as it is like considering all European countries as a single EU network.
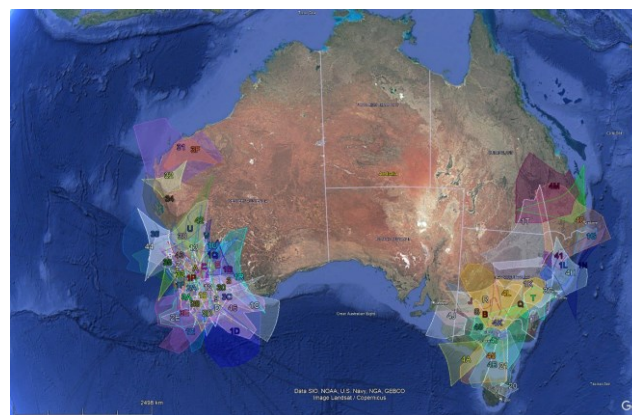

Figure 2 – GMN camera fields in 2024 intersected at 100 km elevation, for cameras active in Australia, global view.
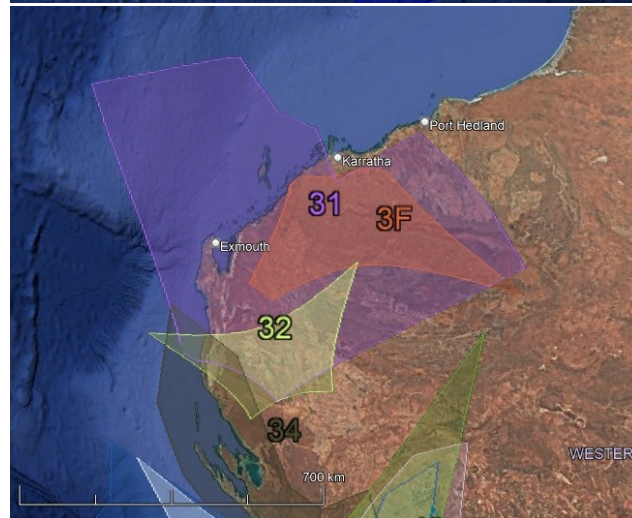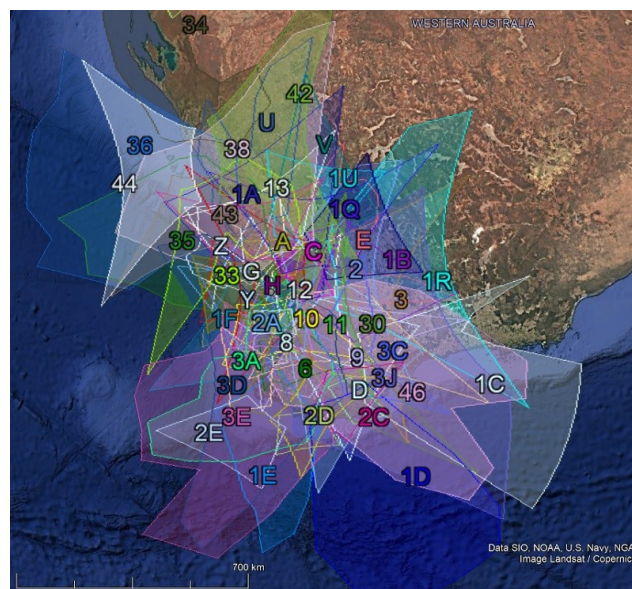

Figure 3 – GMN cameras in Western Australia in 2024 intersected at 100 km elevation. Note the expansion further north.

---

[19] https://tammojan.github.io/meteormap/
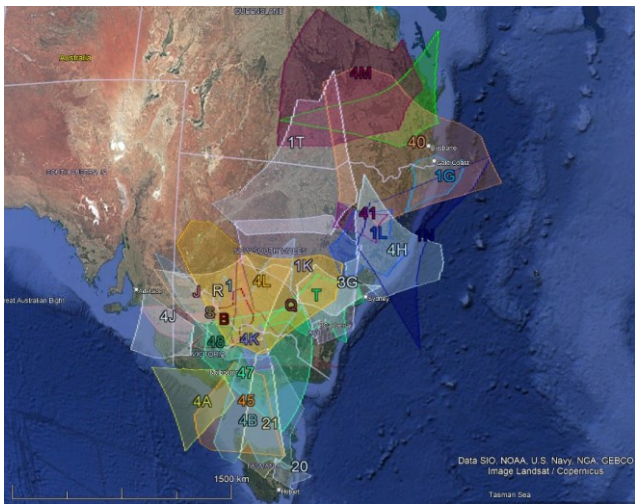
[20] https://www.meteorview.net/

Figure 4 – GMN camera fields in 2024 intersected at 100 km elevation, for cameras active in Australia (eastern states).

5.3 Belgium

Belgium had its first RMS cameras operational in early 2019. *Figure 5* shows the GMN coverage at the end of 2024 for Belgium. The map can be compared with the situation end of 2023 in the previous GMN annual report (Roggemans et al., 2024).
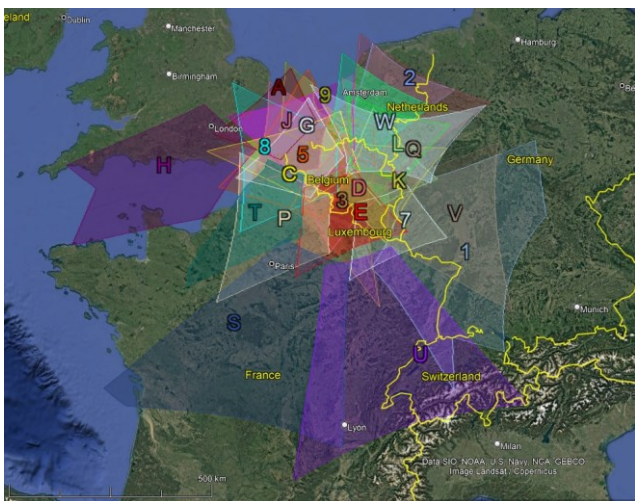

Figure 5 – GMN camera fields intersected at 100 km elevation, for 28 cameras installed in Belgium, status 2024.

Most of the Belgian RMS cameras are being installed for the reinforcement of the CAMS-BeNeLux network. For this purpose, the 6 mm lenses are preferred which have less distortion than the 3.6 mm and detect more fainter meteors. It started with 4 RMS cameras in 2019 expanding to 20 cameras in 2022 when exceptional favorable weather resulted in 23174 orbits. Although the weather was significantly less favorable in 2024, 34050 orbits were collected with 28 operational cameras. The only two decommissioned cameras so far will be hopefully reinstalled in 2025. Belgian cameras have many paired meteors with those in neighboring countries, France, Germany, Netherlands and the United Kingdom. Especially the overlap from cameras of the largest and most successful network in the UK result in many good combinations. Some cameras in Belgium have been installed to improve the coverage on Northern France.

5.4 Brazil

The BRAMON network had its first two RMS cameras getting paired meteors in October 2020 good for 40 orbits with two cameras in the last quarter of 2020. The network expanded to 13 operational cameras, good for 1645 orbits in 2021. In 2022 the number of cameras increased to 20 and 2760 orbits were obtained. In 2023 the number of cameras increased to 34 but the number of paired meteors dropped to 2331. With 37 cameras contributing to orbits in 2024, 4753 orbits were collected. Brazil is a huge country and most RMS cameras are installed in the southern part (*Figure 6*). Some cameras are installed waiting for coverage from other cameras. Further optimization of the network could increase the number of orbits a lot as these longitudes need more observing capacity to cover southern hemisphere meteor activity.
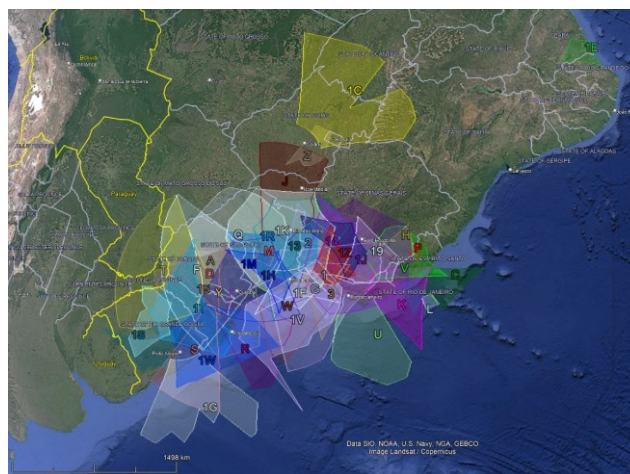
Figure 6 – GMN camera fields in 2024 intersected at 100 km elevation, for 37 cameras active in Brazil.

5.5 Bulgaria
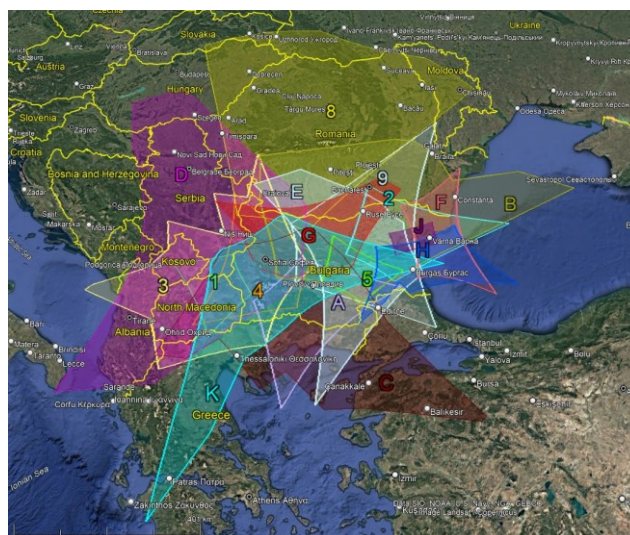
Figure 7 – GMN camera fields in 2024 intersected at 100 km elevation, for 17 cameras active in Bulgaria.

Bulgaria got its first RMS camera operational in June 2021 and got three cameras installed by the end of 2021 of which two had 419 multi-station events. In April 2022 a 4th RMS and in July 2022, two extra cameras were installed. With 6 cameras in 2022, 3877 orbits could be collected. Seven operational cameras had 3530 orbits in 2023. As many as

ten extra cameras were installed in 2024, good for 15058 meteor orbits. The Bulgarian RMS cameras also get paired meteors with cameras in Greece and in Romania (*Figure 7*).

5.6 Canada

Figure 8 – GMN camera fields intersected at 100 km elevation, for cameras active in Canada, Quebec and Ontario in 2024.

The Canadian GMN network got its first five operational RMS cameras providing orbits in June 2019 and expanded to 11 cameras by the end of 2019, good for 3599 orbits. The number of cameras increased to 17 by the end of 2020 with 10815 orbits registered. During 2021, 15 new camera IDs appeared in the list and 8809 orbits were recorded with 29 cameras in 2021, less than the year before despite the extra cameras. The number of cameras doubled from 29 to 58 in 2022 resulting in 16232 orbits. In 2023 the number of contributing cameras increased to 67 resulting in 15023 orbits. The number of operating cameras dropped to 51 in

2024, good for 18508 orbits. 29 Camera IDs that worked in previous years have disappeared from the list in 2024. Two smaller sub-networks existed, CAWE (Elginfield) which and CAWT (Tavistock) each of both networks had eight cameras, but ceased observing in 2024. A small network in the Calgary region of Alberta had its first orbits in 2022 (*Figure 9*) and continued in 2024. Most cameras are installed in Quebec and Southern Ontario, ideal for volunteers south of the Canadian border in the US. Some cameras in New Found Land still wait for a multi-station partner (*Figure 10*).

Figure 9 – GMN camera fields intersected at 100 km elevation, for cameras active in Canada, Alberta in 2024.

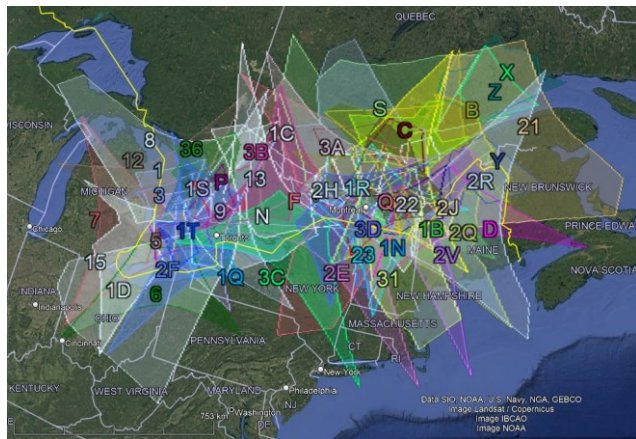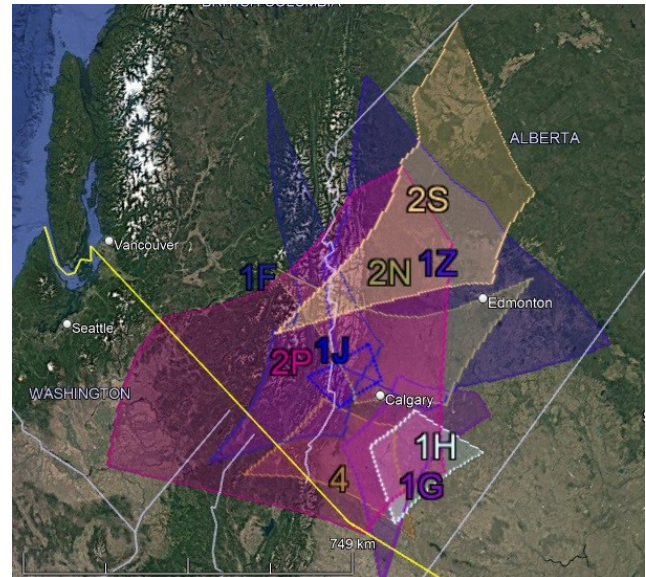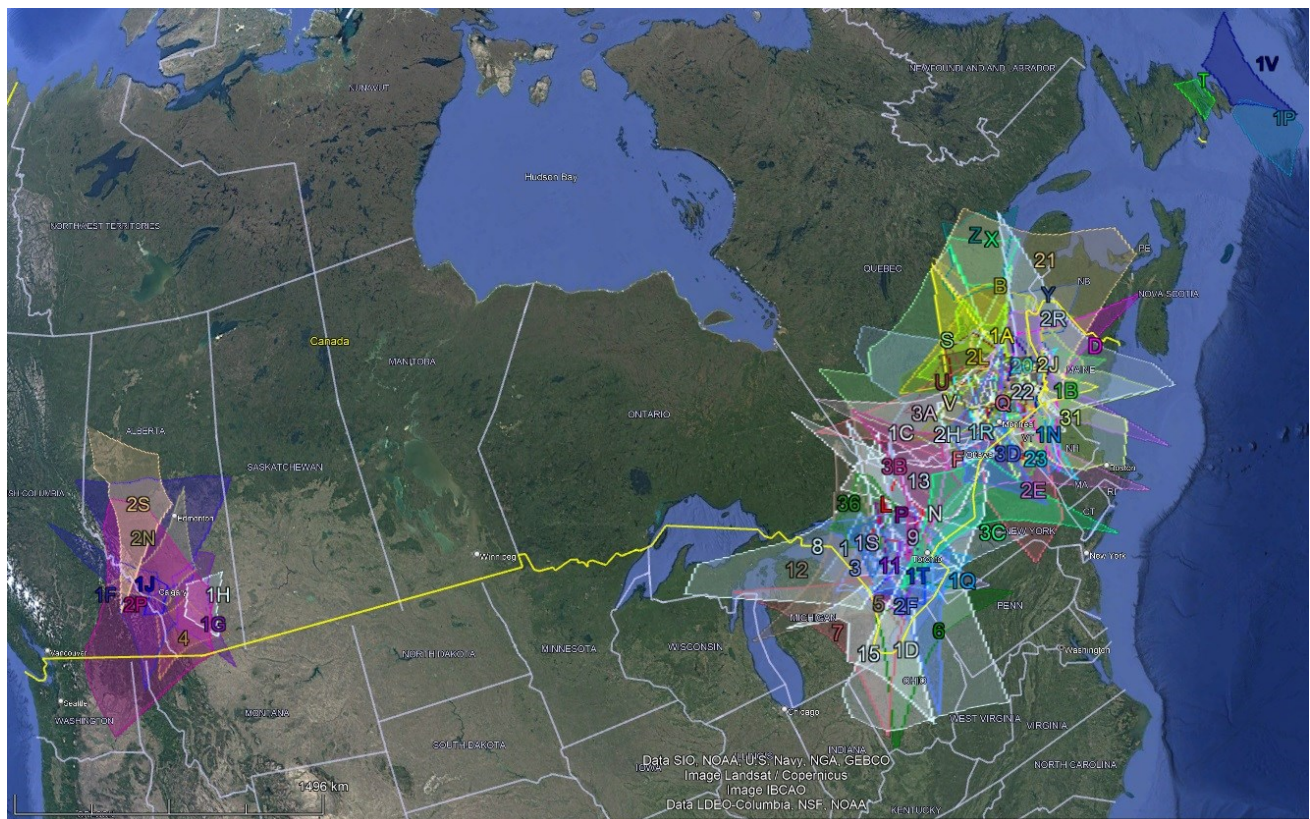*Figure 10* – GMN camera fields in 2024 intersected at 100 km elevation, for cameras active in Canada, overview.

5.7 Croatia

Croatia was the first European country in May 2019 to harvest orbits with three RMS cameras. By the end of 2019 Croatia had already 23 cameras successfully contributing in triangulations, good for 12221 multi-station events. The number of cameras increased to 32 in 2020 resulting in 35099 orbits that year. 38370 multi-station events were recorded in 2021 with 48 cameras. 2022 was slightly less successful with 31329 orbits and 45 operational cameras. In 2023 the number of cameras slightly decreased at 41 contributing to 27721 orbits. In 2024, 35727 orbits were collected with 43 operational cameras. Four new cameras were added in 2024 but 17 camera IDs from previous years didn't appear in the 2024 data anymore. Lots of cameras were running on RPi3, for years – and the time has come for them to be replaced. One camera operator passed away in 2023 and a number of cameras couldn't be reached anymore. In total Croatia contributed 180467 orbits to the GMN orbit database.

Figure 11 – GMN camera fields intersected at 100 km elevation, for cameras installed in Croatia, status 2024.

Croatia plays a major role in the coordination of GMN, maintaining the IstraStream service to produce and deliver new cameras for many countries and providing technical assistance to participants in the GMN project worldwide. The Croatian cameras provide a huge overlap on the neighboring countries (*Figure 11*). A number of Croatian cameras have a very small FoV to register fainter meteors with higher positional accuracy. To view these camera fields in detail we refer to the online KML files for consultation in Google Earth.

5.8 Cook Island

The Cook Islands is a nation in the South Pacific and its 15 islands are scattered over a vast area. The Global Meteor Network got a first camera installed at this geographically interesting location. So far, we wait for multi station coverage.

Figure 12 – GMN camera fields in 2024, intersected at 100 km elevation, for the camera active on the Cook Islands.

5.9 Czech Republic

The first three RMS in Czechia scored 163 orbits in 2020, with four cameras in 2021, 464 orbits were recorded and 2490 orbits with six cameras in 2022. A major breakthrough happened in 2023 as the number of cameras increased to 20, good for 11269 orbits. In 2024, 5 more cameras were installed and a total of 18248 orbits were collected (*Figure 13*). Only two cameras were not operational in the last months of 2024, but so far Czechia has no decommissioned cameras.

Since the end of 2022, the Czech and Slovak GMN camera operators are grouped in the CSMON (Czech & Slovak Meteor Observation Network), which helps the new and current meteor enthusiasts to get on board. In addition to individual amateur astronomers, there is an increasing number of public observatories getting equipped by RMS cameras, thanks to public funding. Latest advances in the SBC (Pi5) technology allows to multiply numbers of cameras on the same PC, i.e. make it even more accessible for low budgets.

Figure 13 – GMN camera fields in 2024, intersected at 100 km elevation, for cameras active in the Czech Republic.

5.10 Denmark

In October 2022 a first GMN camera got operational in Denmark, good for 55 orbits in 2022. In 2023 four cameras were active in Denmark which obtained 1386 orbits. A fifth camera was added in 2024 and 3360 orbits were collected (*Figure 14*). These northern cameras create possibilities for further camera coverage in southern Norway and Sweden as well as in Northern Germany.
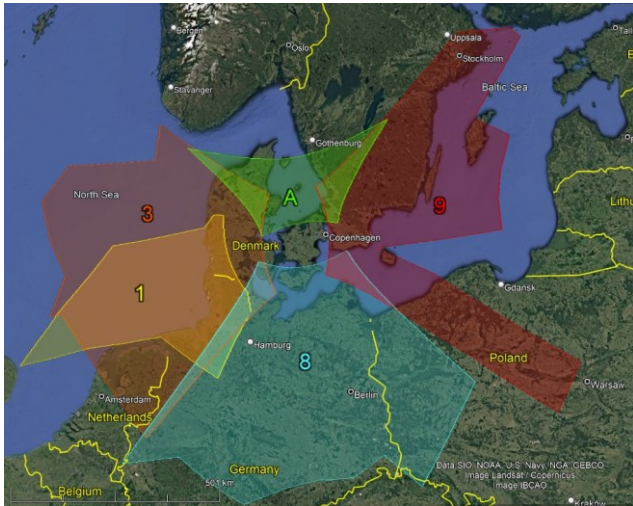

Figure 14 – GMN camera field in 2024 intersected at 100 km elevation, for cameras active in Denmark.

5.11 Finland

In October 2022 the first GMN cameras became operational at two sites in Finland, with 41 orbits as a first result. In 2023 there were five cameras active which resulted in 90 orbits and in 2024 three more cameras were installed and 204 orbits obtained by seven of the eight available cameras (*Figure 15*).
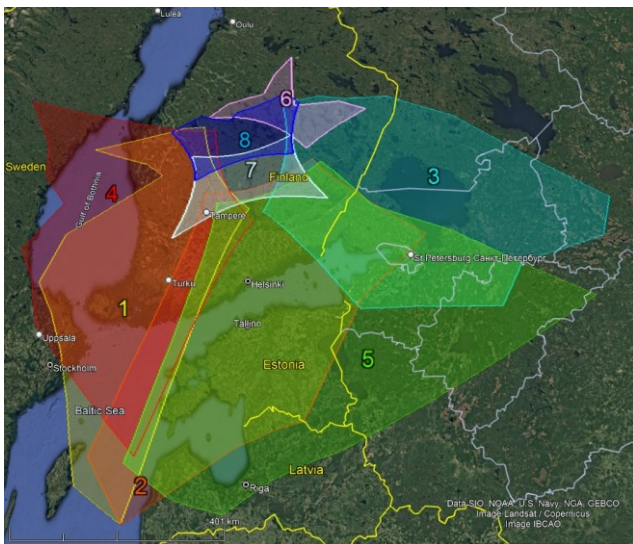
Figure 15 – GMN camera fields in 2024 intersected at 100 km elevation, for cameras active in Finland.

5.12 France

The number of RMS cameras in France increased gradually from 10 in 2020 to 14 devices in 2021 and 16 in 2022. More new cameras were installed in 2023 and 16682 orbits were obtained with 18 cameras, a much better result than in 2022 when 11990 orbits were obtained. In 2024 there were 19 operational cameras in France contributing 20591 orbits to the GMN dataset. In total 27 RMS cameras were installed since March 2020, but eight of them did not function anymore in 2023. A large part of France, the entire south-western, is still without GMN coverage (*Figure 16*).
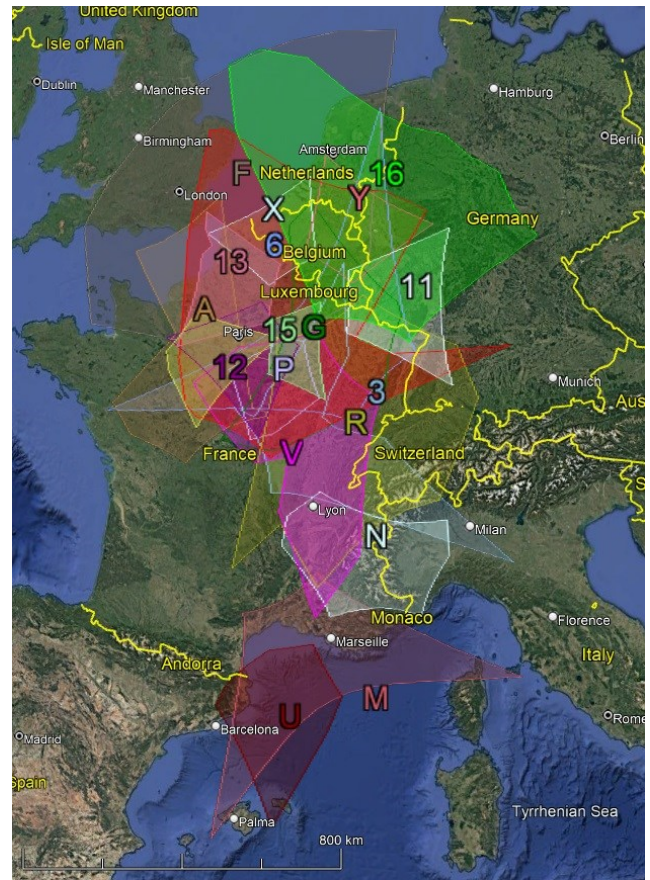

Figure 16 – GMN camera fields in 2024 intersected at 100 km elevation, for cameras active in France.
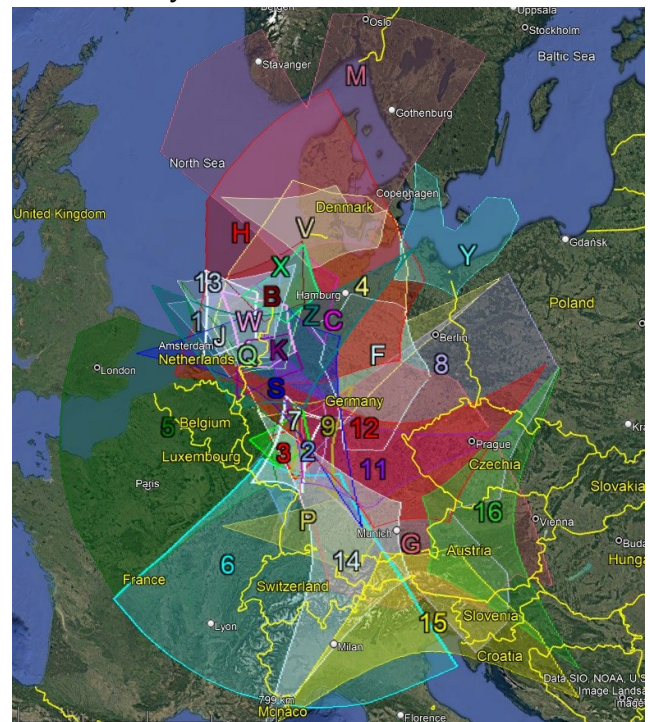
5.13 Germany

Figure 17 – GMN camera fields in 2024 intersected at 100 km elevation, for cameras active in Germany.

The first GMN camera in Germany had its first orbits in August 2019 with Belgian GMN cameras. By the end of 2019 there were four GMN cameras in Germany, good for 200 orbits. The number of cameras increased to 10 and the numbers of orbits to 3963 in 2020. With 12 cameras in 2021, 7009 orbits were collected, in 2022, with 18 cameras 9128 orbits were collected. In 2023 as many as 12194 orbits were recorded with 19 cameras. In 2024 the number of cameras in Germany increased with 11 to 30, good for 23240 orbits. Two cameras that were active in 2022 and 2023 did not function anymore in 2024. Some GMN cameras in the North-Western part of Germany also participate in the CAMS-BeNeLux network, supporting both GMN and CAMS (*Figure 17*).

5.14 Greece

In September 2022 the first GMN camera got operational in Greece, ideally pointed to overlap with some Bulgarian GMN cameras, good for 977 paired meteors in the four last months of 2022. Three extra cameras were installed and with four cameras 3375 orbits were obtained in 2023. Four more cameras were installed in 2024 and with eight operational cameras 8998 orbits were obtained (*Figure 18*).
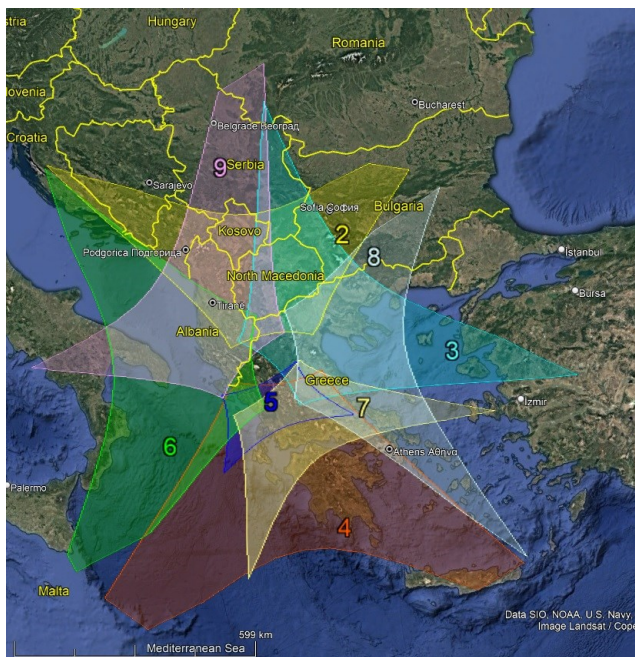
Figure 18 – GMN camera fields in 2024 intersected at 100 km elevation, for cameras active in Greece.

5.15 Greenland

The most northern GMN camera, GL0001, has been installed in the North West of Greenland at 77°28' northern latitude. During the late autumn and winter months, this site has almost permanent night time. The possibilities are considered to install a second camera at a favorable distance.
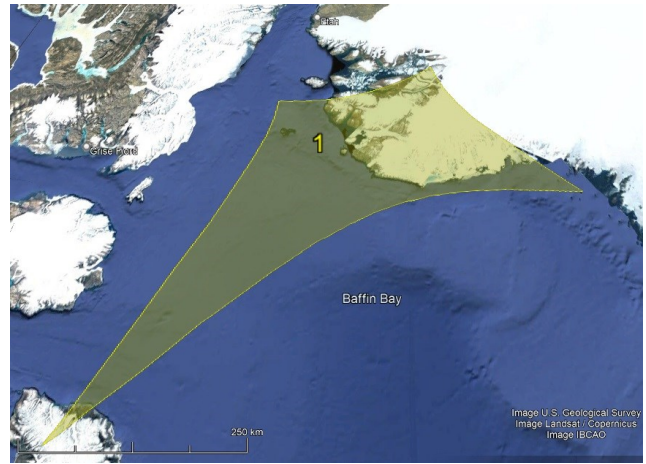

Figure 19 – GMN camera field in 2024 intersected at 100 km elevation in Greenland.

5.16 Hungary

A first GMN camera got operational in March 2022 in Hungary and by end of 2022, two Hungarian cameras had obtained 2114 orbits. One new camera was added in 2023 and last year, Hungarian cameras contributed to 7872 orbits. The number of cameras remained status quo in 2024 and produced 9627orbits, mainly paired meteors with Croatian and Czech cameras. Hungary has a long tradition in meteor astronomy and hopefully more GMN camera sites will get installed (*Figure 20*).
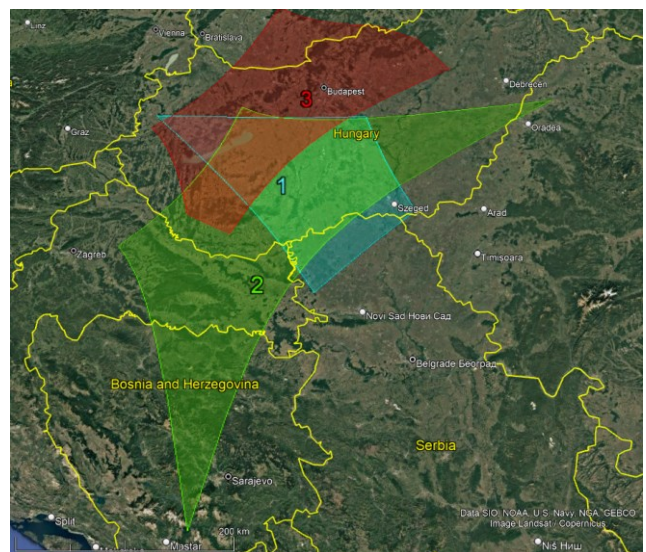

Figure 20 – GMN camera fields in 2024 intersected at 100 km elevation, for cameras active in Hungary.

5.17 Ireland

Ireland got a first GMN operational in October 2020 and a second one a month later, good for 120 orbits in 2020. With three cameras in 2021 the number of orbits increased to 424. 3490 orbits were recorded in 2022 with five GMN cameras. In 2023 the number of cameras remained unchanged but the number of orbits dropped to 1954. In 2024 two new cameras were added and one previously active RMS stopped uploading data. With six available cameras, 3706 orbits were obtained, the best year so far for Ireland. Most of the paired meteors were obtained thanks to the overlap provided by GMN cameras in the UK.
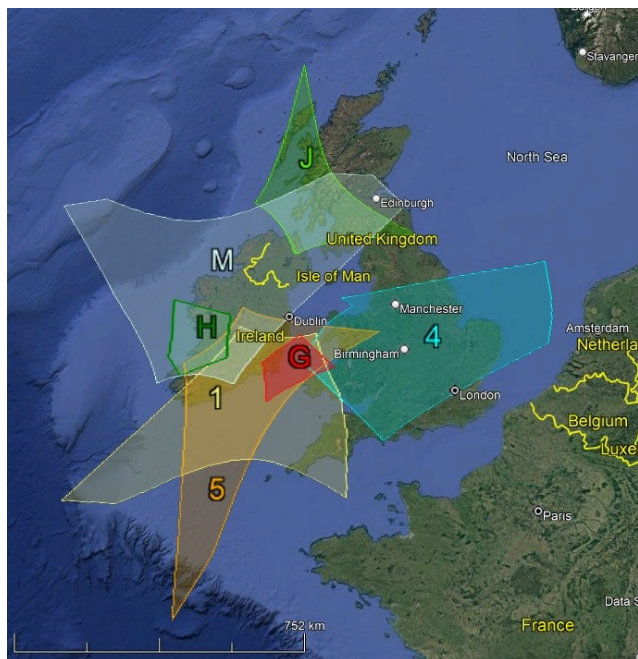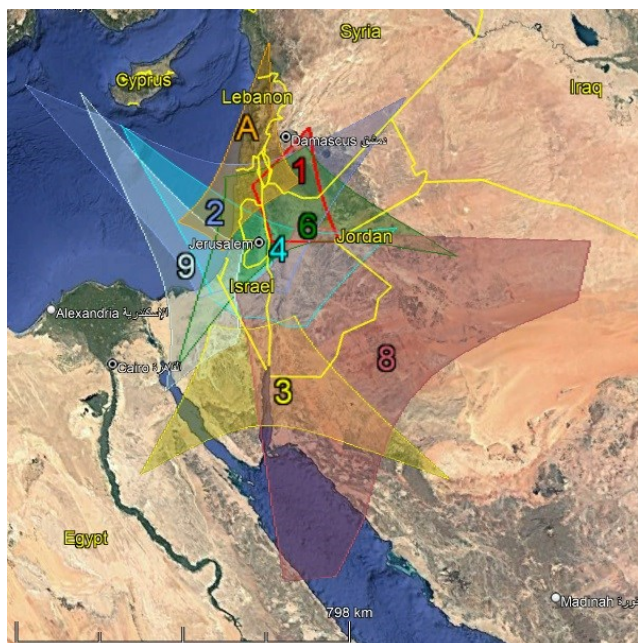
Figure 21 – GMN camera fields in 2024 intersected at 100 km elevation, for cameras active in Ireland.

5.18 Israel

Israel got its first three GMN cameras installed in November 2020, good for 553 orbits that year. In 2021 with three extra cameras 2009 orbits were obtained. In 2022 the cameras did not provide orbits during some time and one camera was discontinued, resulting in 975 orbits. In 2023, 1096 orbits were collected using six cameras. In 2024 an extra camera was installed and with seven cameras, 991 orbits were collected (*Figure 22*). So far two cameras were decommissioned.

Figure 22 – GMN camera fields in 2024 intersected at 100 km elevation, for cameras active in Israel.

5.19 Italy

Italy got its first GMN camera installed and contributing orbits in October 2019, good for 862 orbits in 2019. Italy remained with one GMN camera in 2020, which had as many as 5384 paired meteors with Croatian and Slovenian

cameras. Italy increased its number of cameras from one to five and these cameras were involved in 5447 multi-station events in 2021. An extra camera was added in Bologna in 2022 when 4943 orbits were collected. With seven cameras in 2023, 5064 orbits were obtained. In 2024, 6603 orbits were obtained with seven cameras (*Figure 23*). Three new cameras were installed in 2024 but three former cameras were decommisioned.
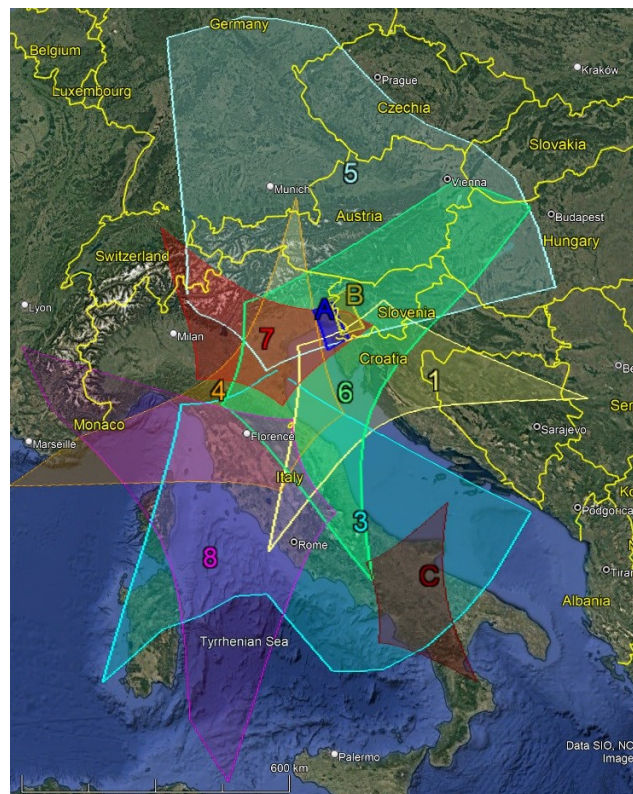

Figure 23 – GMN camera fields in 2024 intersected at 100 km elevation, for cameras active in Italy.
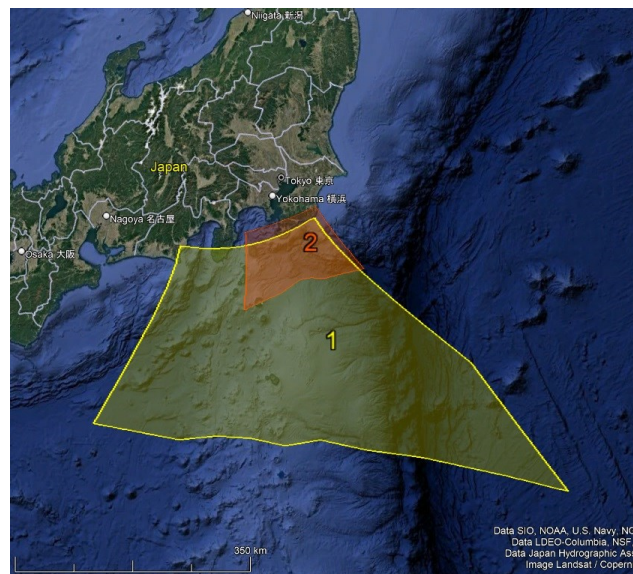
5.20 Japan

Figure 24 – GMN camera fields in 2024 intersected at 100 km elevation, for cameras active in Japan.

A first GMN camera got installed in Japan in 2022, waiting for some multi-station partners at suitable distance for triangulation. In 2023 a second camera was installed which

allowed to obtain 629 orbits. The network remained status quo in 2024 with two cameras and 606 orbits (*Figure 24*). Japan has the very active SonotaCo network which uses analog Watec cameras. RMS cameras deliver UFO capture output which may offer opportunities for the SonotaCo network to include GMN cameras in its network.

5.21 Korea (South)

A most impressive deployment of GMN cameras took place in 2022 in South Korea with a first few cameras obtaining orbits in September and as many as 47 GMN cameras installed in November and December 2022. The cameras were installed and pointed to obtain an optimal overlap resulting in 7711 orbits during the first year. In 2023 the number of cameras rapidly increased to 125 (!) collecting 34044 orbits. This fast deployment made the RMS network in South Korea a major contributor at a strategic geo location at the northern hemisphere for a 24 on 24-hour monitoring of meteor activity.
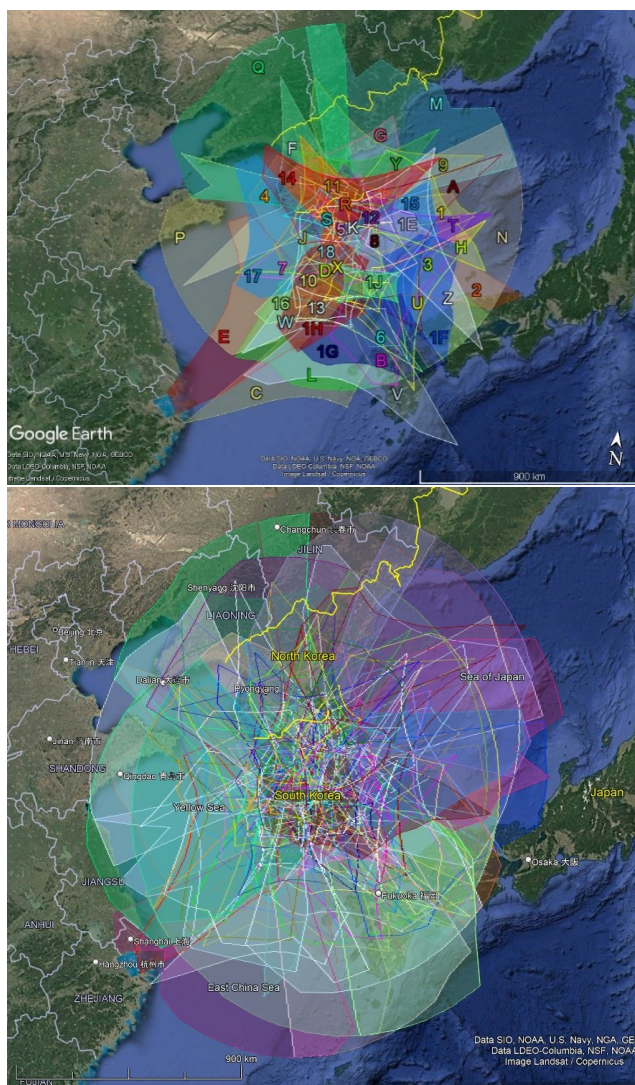

Figure 25 – GMN camera fields in 2022 (top) and in 2024 (bottom) intersected at 100 km elevation, for cameras active in South Korea.

In 2024 three cameras were decommissioned, with 122 operational cameras, 42477 orbits were collected. The dense coverage of overlapping camera fields in 2024 can be compared to the situation end of 2022 in *Figure 25*. If any

RMS cameras get installed in South-Western Japan, these would generate many paired meteors with the Korean cameras.

5.22 Luxembourg

In October 2022 a first GMN camera got installed in Luxembourg contributing to 622 orbits combining with Belgian, Dutch, French, German and even Czech GMN cameras (*Figure 26*). In 2023 this camera had 2018 paired meteors with orbits and in 2024, 2194 orbits were obtained. This camera also contributes GMN data to CAMS-BeNeLux.
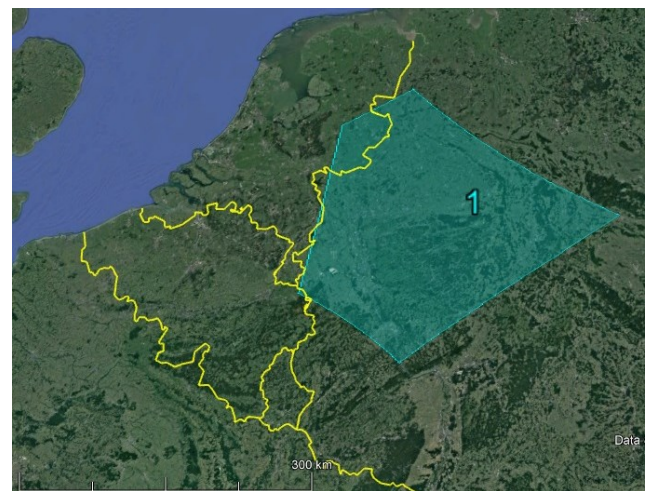

Figure 26 – GMN camera field in 2024 intersected at 100 km elevation, for cameras active in Luxembourg.
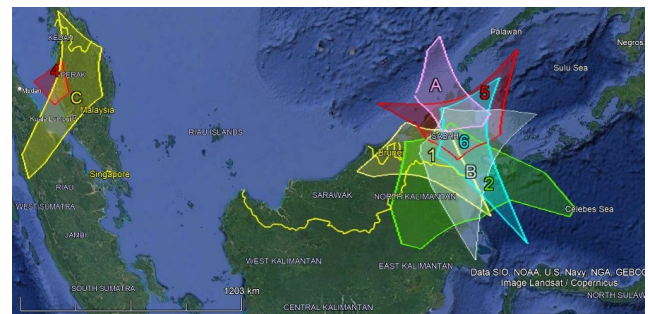
5.23 Malaysia

Figure 27 – GMN camera fields in 2024 intersected at 100 km elevation, for cameras active in Malaysia.

A first GMN camera had been installed in Malaysia in 2021 waiting for coverage from cameras installed at a suitable distance to get good triangulations. Some extra cameras got installed in 2022 and in June 2022 the first orbits were obtained. In total 50 orbits were collected in 2022 with three cameras. In 2023 a ten-fold of orbits, 551, were collected with five cameras. In 2024, 244 orbits were obtained with six cameras, two new cameras were added and two cameras were decommissioned (*Figure 27*). Further extensions of the Malaysian network are very welcome.

5.24 Mexico

An impressive deployment of GMN cameras took place in Mexico in 2022. The first few installed cameras obtained the first orbits in February 2022 and soon 12 cameras got installed with a good overlap. A total of 1769 meteor orbits

could be collected in 2022. The number of cameras increased to 15 in 2023 with 2953 orbits as a result. In 2024 13 cameras recorded 2871 orbits, two cameras were decommissioned. The efforts in Mexico are crucial in getting coverage for both the northern and especially the southern hemisphere at these longitudes (*Figure 28*).
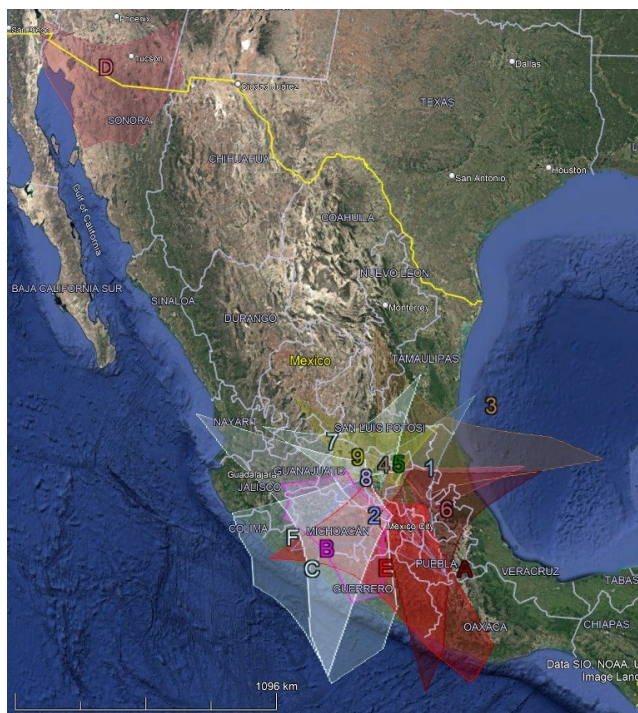

Figure 28 – GMN camera fields in 2024 intersected at 100 km elevation, for cameras active in Mexico.
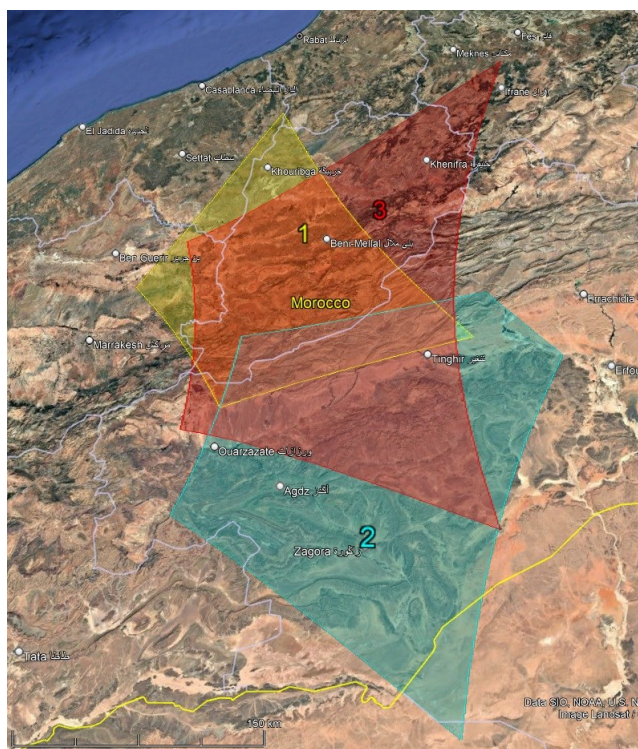
5.25 Morocco

Figure 29 – GMN camera fields in 2024 intersected at 100 km elevation, for cameras active in Morocco.

The first two GMN cameras obtained their first meteor orbits in May 2024, a third camera was added in July. The Moroccan GMN cameras collected 851 orbits in 2024, despite technical issues that hampered observations during many weeks (*Figure 29*).

5.26 Netherlands

The Netherlands started collecting orbits within GMN in August 2019 and had 278 orbits in this first year. The number of GMN cameras increased to 11 in 2020 with 4337 orbits as a result. The number of cameras remained unchanged in 2021 but the better overlap from neighboring countries resulted in 7605 orbits. Some cameras dropped off in 2022 and a few new ones were installed, resulting in 9139 orbits with 13 cameras. In 2023, 14 Dutch RMS cameras had 9421 orbits. In 2024 four new RMS cameras were installed, with a total of 18 cameras 17409 orbits were collected (*Figure 30*). The Netherlands have five decommissioned RMS cameras. Dutch cameras get mainly multi-station coverage from cameras in Belgium, Germany, the UK and Denmark.
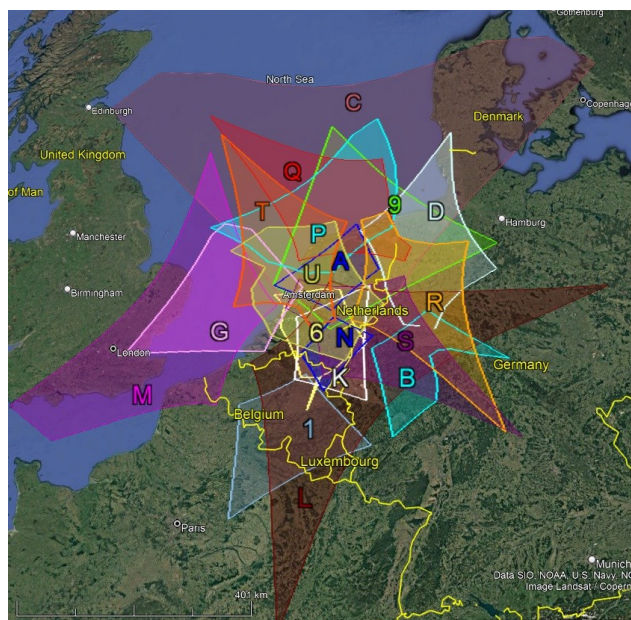

Figure 30 – GMN camera fields in 2024 intersected at 100 km elevation, for cameras active in the Netherlands.

5.27 New Zealand

The first two GMN cameras were installed in July 2021 in New Zealand and 1146 orbits were obtained that year. From March 2022 more cameras were installed month by month with an impressive deployment of strategically placed well pointed cameras covering the huge surface of the country. With 28 active cameras at the end of 2022, 6280 orbits were recorded. The New Zealand GMN network, known as Fireballs Aotearoa, was further expanded in 2023 and with a total of 111 cameras 47436 orbits were obtained, making New Zealand one of the most important providers of orbit data for the Southern Hemisphere. The density of the camera coverage can be seen in *Figure 31* and compared to the situation two years earlier. In 2024, 44 extra cameras became operational, three older cameras were decommissioned. With a total of 152 cameras, 147831 meteor orbits were collected. This makes New Zealand the greatest orbit contributor within the Global Meteor Network, doing better than GMN network in the USA that
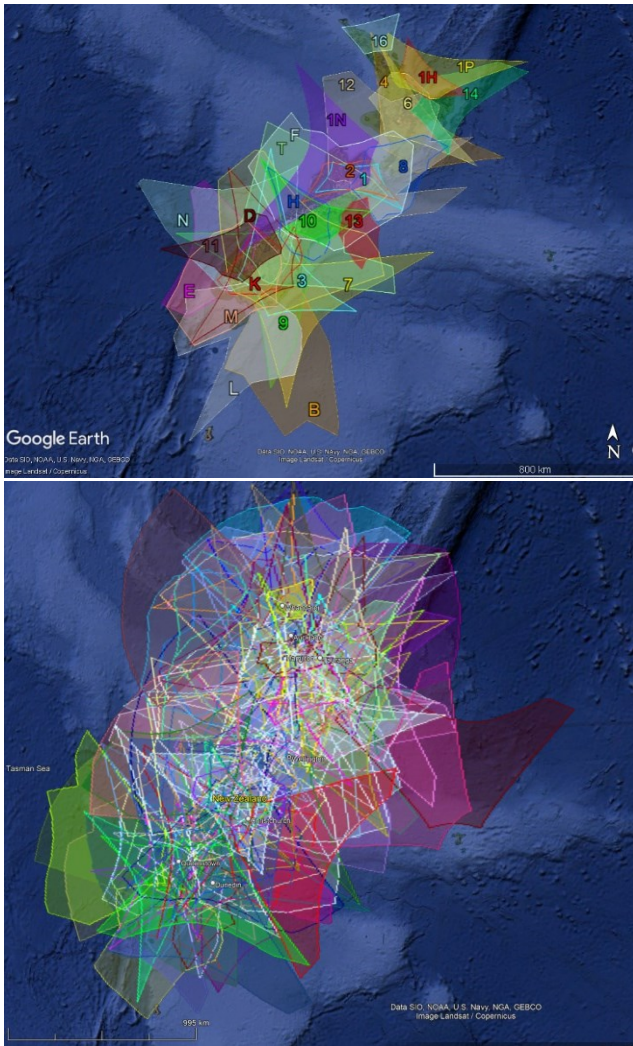
covers a much larger volume of atmosphere to intercept meteoroids.

The network imaged a bright fireball in March, with the trajectory indicating a high chance of a meteorite having been dropped. Together with other GMN members, a search was organized and a 810 gm L5 chondrite recovered. It is currently undergoing scientific analysis (Scott et al., 2024).

5.28 Norway

The two first GMN cameras were installed in Norway in December 2024, but so far without paired meteors as calibration failed. The cameras are pointed south and should combine well with cameras in Denmark, Germany and the United Kingdom (*Figure 33*).

Figure 33 – GMN camera fields in 2024 intersected at 100 km elevation, for cameras active in Norway.

Figure 31 – GMN camera fields in 2022 (top) and in 2024 (bottom) intersected at 100 km elevation, for cameras active in New Zealand.
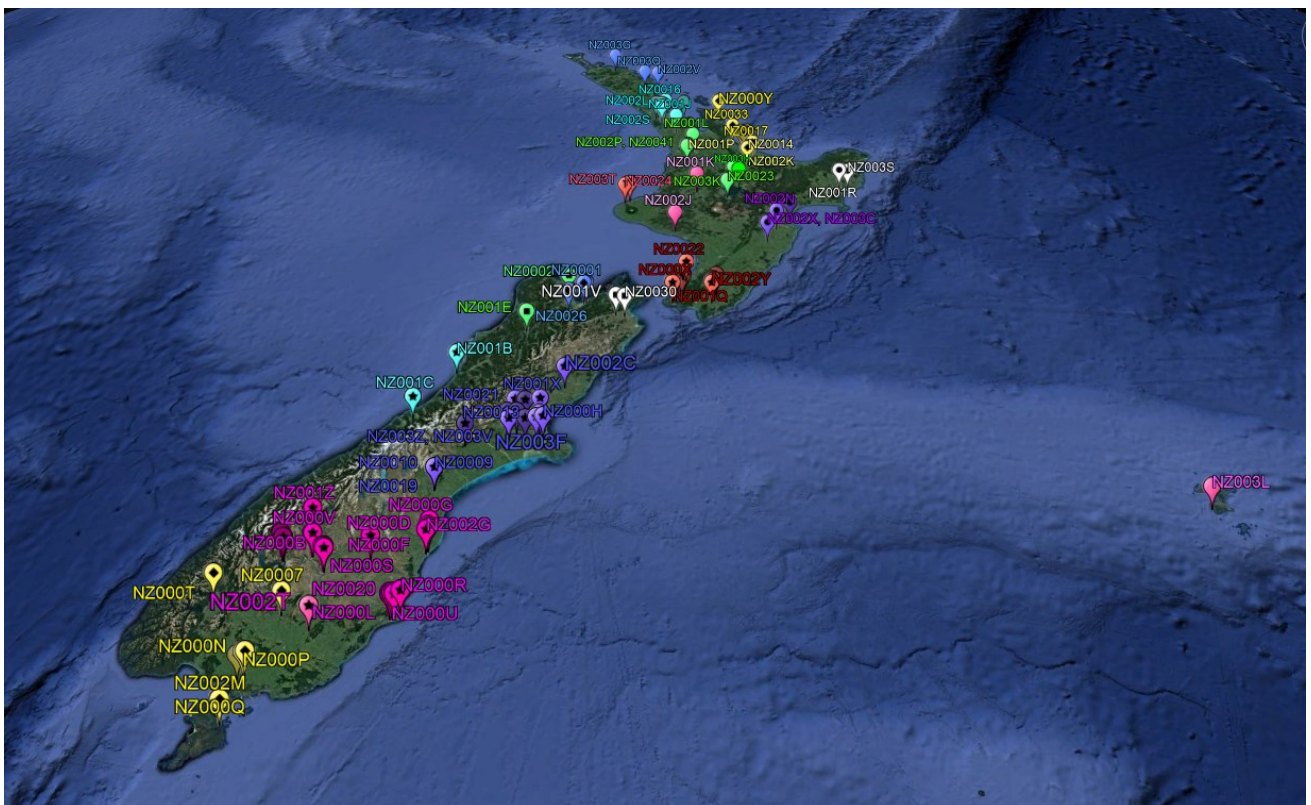

Figure 32 – GMN camera positions in New-Zealand, situation as at the end of 2023.

5.29 Poland

The first GMN camera got installed in September 2020 and remained long the only Polish GMN camera. In March 2022 two extra Polish GMN cameras got their first orbits. The cameras didn't function all the time but the number of orbits obtained increased from 67 in 2021 to 398 in 2022. In 2023 only two calmeras were active and 456 orbits were collected. In 2024 two new cameras were installed and 1759 orbits obtained (*Figure 34*). Polish GMN cameras get mainly paired meteors with cameras installed in Czechia.
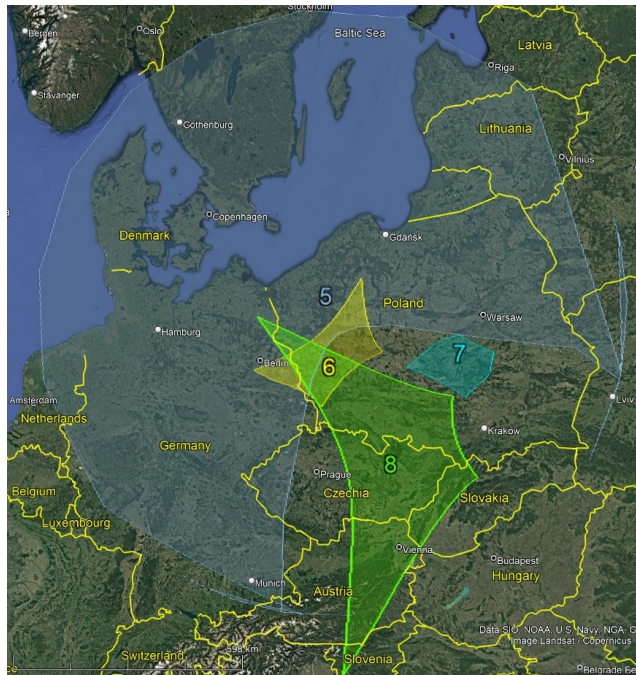

Figure 34 – GMN camera fields in 2024 intersected at 100 km elevation, for cameras active in Poland.

5.30 Portugal

Figure 35 – GMN camera field in 2024 intersected at 100 km elevation, for cameras active in Portugal.

A first GMN camera got meteor orbits in September 2022 in Portugal. A vast coverage from GMN cameras in Spain guarantees many paired meteors (*Figure 35*). In 2022, 398 orbits were recorded, in 2023 the total increased to 3322

orbits. A second camera was installed in January 2024 and with two cameras, 4413 orbits were obtained.

5.31 Romania

Romania got its first three RMS cameras installed in 2023. Operational since October 2023 and despite unfavorable weather, 417 orbits were collected. The network in Romania remained status quo in 2024, but RO0003 failed functioning since February. With only two functioning cameras, 4361 meteor orbits were collected. These cameras had many paired meteors with Bulgarian, Croatian, Czech and Hungarian cameras. Hopefully, more cameras will get installed in 2025.
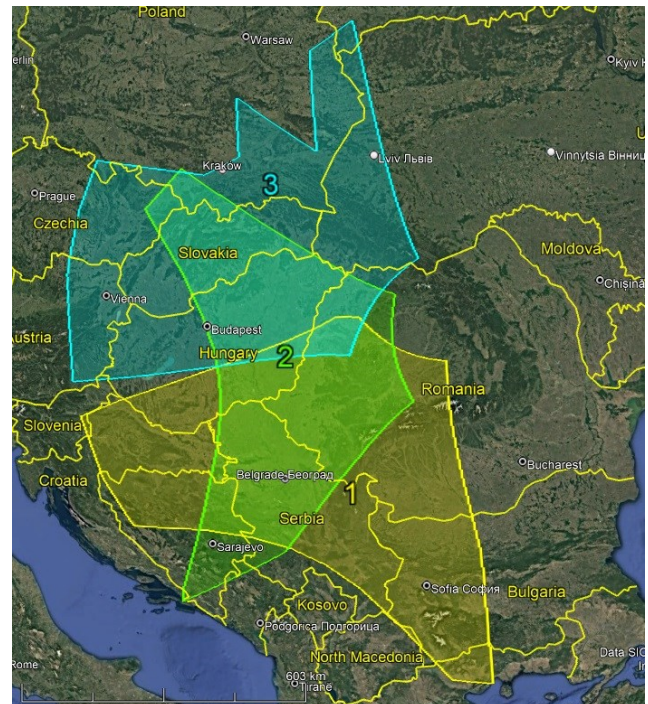

Figure 36 – GMN camera field in 2024 intersected at 100 km elevation, for cameras active in Romania.

5.32 Russia

The first two GMN cameras in Russia had orbits in July 2019. The first year had already 5715 orbits with 10 cameras. In 2020 the number of cameras increased to 21, good for as many as 13438 orbits. The number of RMS cameras having paired meteors remained stable at 21, but the number of orbits decreased to 6208 in 2021. Problems with the maintenance of some meteor stations reduced the number of paired observations. In 2022, 19 cameras in Russia had 5437 orbits. The number of Russian GMN cameras decreased further to 15 in 2023 and the number of paired meteors dropped to 1992. In 2024 seven new cameras were installed and with 22 cameras, 10939 meteor orbits were obtained. In total 12 of the formerly active cameras stopped contributing data.

Some single RMS devices (*Figure 37*) got installed elsewhere in Russia, waiting for coverage from other RMS cameras at a suitable distance. Some cameras are installed in the far east of Russia at longitude ~132° east and 50° north.
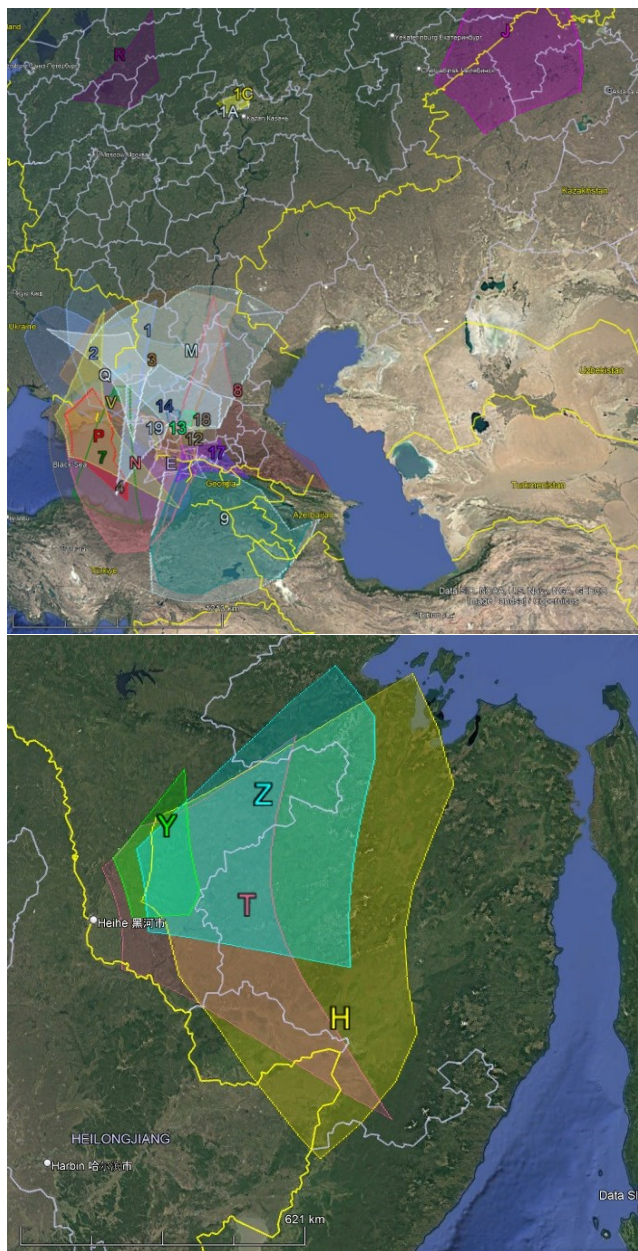
Figure 37 – GMN camera fields in 2024 intersected at 100 km elevation, for cameras active in Russia (West) (top) and in the far east (bottom).
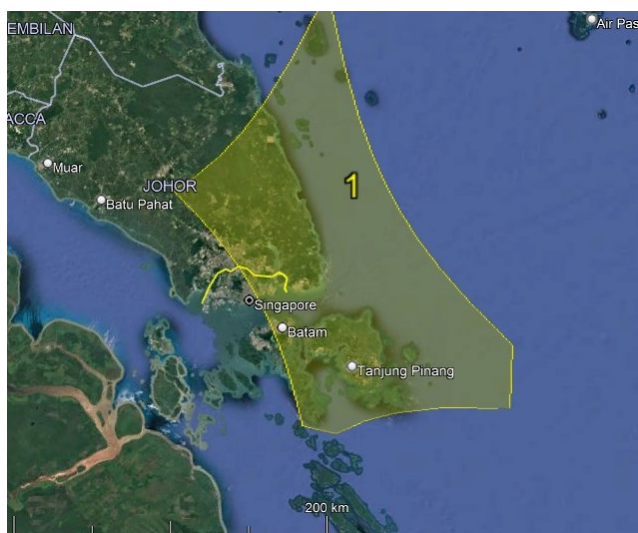
5.33 Singapore

Figure 38 – GMN camera fields in 2024 intersected at 100 km elevation, for cameras active in Singapore.

A first camera got installed in 2022 and is waiting for multi-station partners, no orbits could be obtained yet in 2024 (*Figure 38*).

5.34 Slovakia

Slovakia got its first camera in November 2021 with 37 paired meteors. In 2022, three GMN cameras got operational good for 2026 orbits. The number of cameras increased to four in 2023 and 5535 paired meteors with orbits were recorded by Slovakian cameras. In March 2024 a fifth camera was installed and last year 7532 orbits were obtained (*Figure 39*). Since the end of 2022, the Czech and Slovak GMN camera operators are grouped in the CSMON (Czech & Slovak Meteor Observation Network), which helps the new and current meteor enthusiasts to get on board.
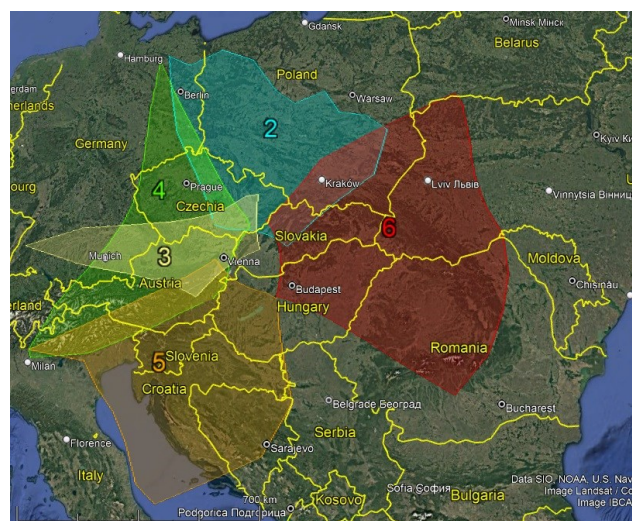
Figure 39 – GMN camera fields in 2024 intersected at 100 km elevation, for cameras active in Slovakia.

5.35 Slovenia

Figure 40 – GMN camera fields in 2024 intersected at 100 km elevation, for cameras active in Slovenia.

Slovenia got its first RMS contributing in August 2019 and a second RMS in August 2021. The coverage by cameras in neighboring Croatia resulted in 2753 orbits in 2019, 3999 in 2020 and 6001 in 2021. The two Slovenian cameras contributed to 5887 orbits in 2022. In 2023, four extra

cameras were installed and 6789 orbits were collected. The number of cameras remained status quo in 2024 with six, and 12208 orbits were obtained (*Figure 40*).

5.36 Spain

The GMN had its first orbits collected in Spain in April 2020. End of 2020, eight GMN cameras had collected 1207 orbits. A lot of progress was made in Spain in 2021 when the number of cameras increased from eight to 23. The 23 Spanish cameras were involved in 15113 multi-station events in 2021. The number of GMN cameras increased further to 30 in 2022 and resulted in 19301 orbits. In 2023, 22610 orbits were obtained with 35 cameras. In 2024 three new cameras were installed but six older cameras were decommissioned so that the number of operational cameras decreased to 32. 16771 meteor orbits were recorded during last year (*Figure 42*). Four cameras are installed at the Canary Islands (*Figure 41*).
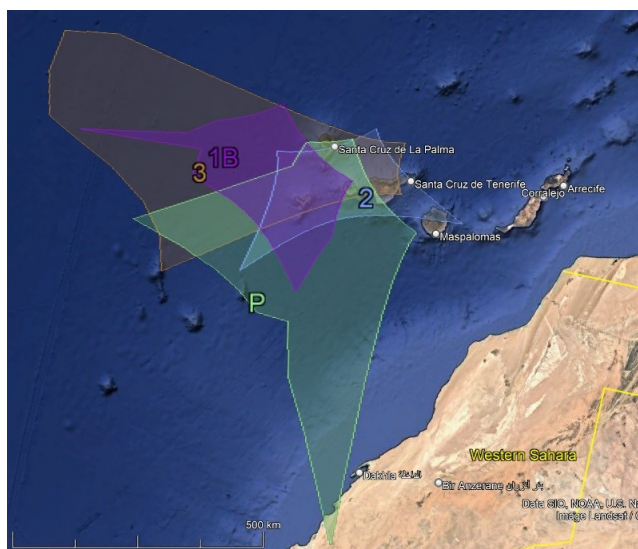

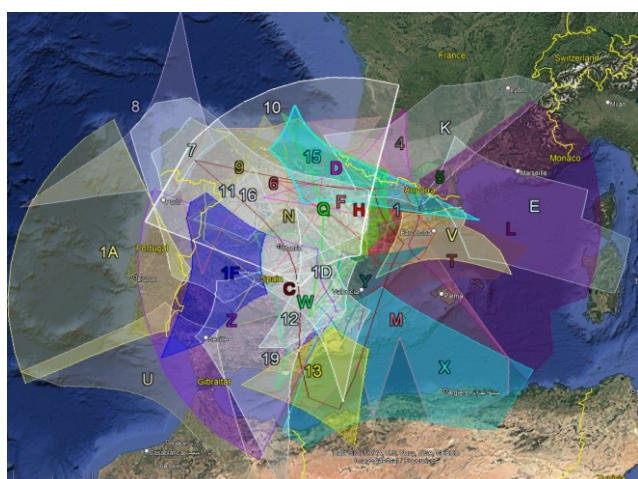*Figure 41* – GMN camera fields in 2024 intersected at 100 km elevation, for cameras active at the Canary Islands (Spain).

Figure 42 – GMN camera fields in 2024 intersected at 100 km elevation, for cameras active in Spain.

5.37 Switzerland

The first orbits were obtained in August 2021 but it took until May 2022 before extra cameras got installed and more orbits recorded. With five operational cameras 3439 orbits were obtained in 2022. The central location of Switzerland is ideal to obtain multi-station events with GMN cameras in the neighboring countries. The number of cameras remained unchanged in 2023 and the number of paired meteors increased to 4352. In 2024 one camera was decommissioned and with the remaining four cameras, 2383 meteor orbits were obtained (*Figure 43*).
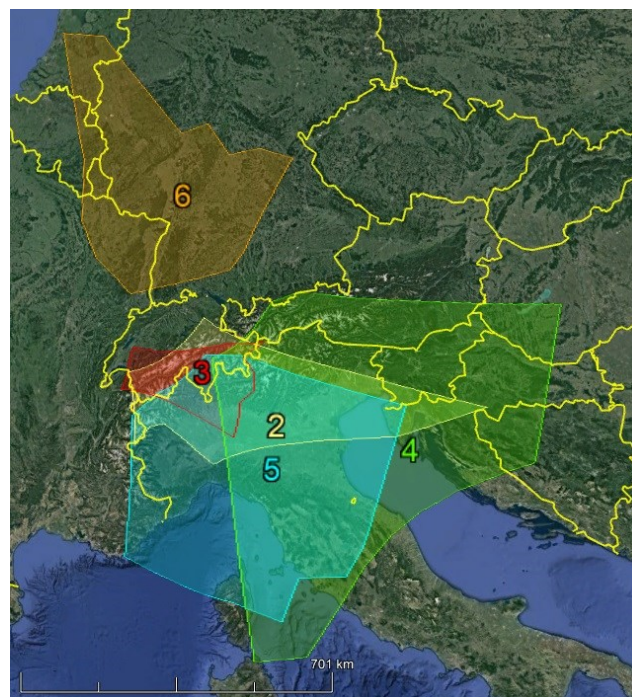
Figure 43 – GMN camera fields in 2024 intersected at 100 km elevation, for cameras active in Switzerland.

5.38 Tajikistan

The country has a long tradition in meteor astronomy and observations. In June 2024 two GMN cameras installed in Tajikistan had their first paired meteors. In total 411 meteor orbits were obtained despite technical issues that limited the time both cameras were operational (*Figure 44*).

Figure 44 – GMN camera fields in 2024 intersected at 100 km elevation, for cameras active in Tajikistan.

5.39 Ukraine

A first RMS camera contributes meteor data to Global Meteor Network in Ukraine, but so far, no paired meteors were recorded (*Figure 45*).

Figure 45 – GMN camera fields in 2024 intersected at 100 km elevation, for cameras active in Ukraine.

5.40 United Kingdom

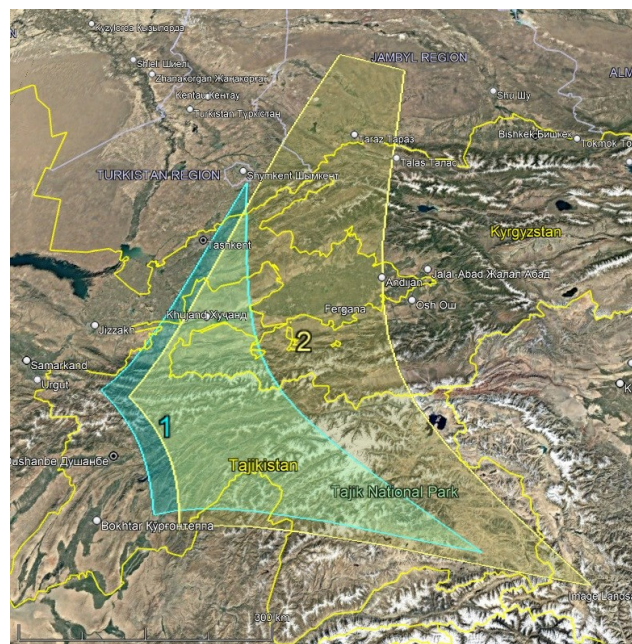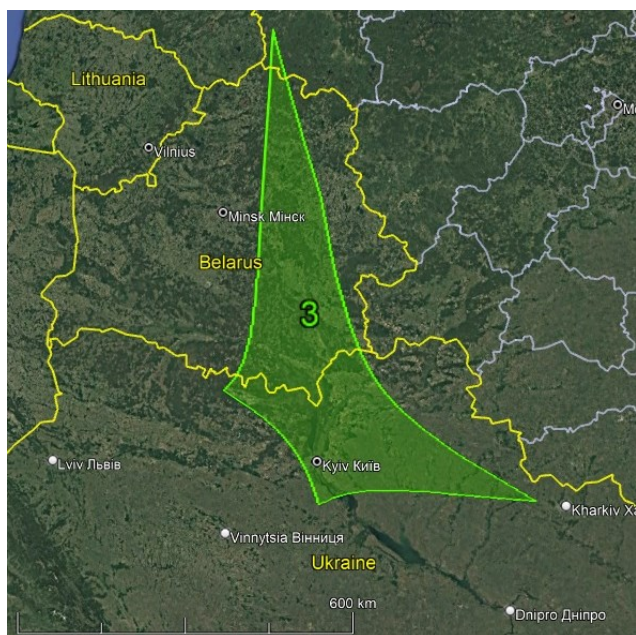*Figure 46* – GMN camera fields in 2024 intersected at 100 km elevation, for all cameras active in the United Kingdom.

The GMN got started with 13 cameras in 2020 in the UK contributing 1889 orbits. These numbers rapidly grew in 2021 to 97 cameras and 27430 orbits. The largest expansion came in 2022 when 191 cameras were contributing 78652 paired meteors. The network continued to grow throughout 2023 when 261 cameras contributed 84688. In 2024 the UK

had 95730 orbits. 31 older cameras were decommissioned. The vast majority of these cameras are part of the UK Meteor Network which now provides complete coverage of the UK and Eire (*Figure 46*), see also the kml file[21].

Cameras

UK active camera growth has now slowed somewhat, with about as many being decommissioned as newly commissioned. Although there are 312 cameras registered, only 292 were active during the year, of which 251 are members of UKMON.

Detections and matches

Around 1.3 million single-station observations were made by UK cameras in 2024, about 30% more than in the previous year. Roughly half of these were matched with other stations, generating 95730 confirmed meteor detections. 91% were detected by ten or fewer stations, with only 119 detected by 30 or more.

Many UK cameras overlap with those in Eire and continental Europe, leading to matches over quite a wide area. The furthest west was at longitude –12.38, roughly 100km off the western coast of Eire and the furthest east was at the longitude of Hannover in Germany while the northern and southern extremities were at the latitude of the Faroes and the Bay of Biscay, respectively. The map in *Figure 47* shows the extent of UKMON coverage.
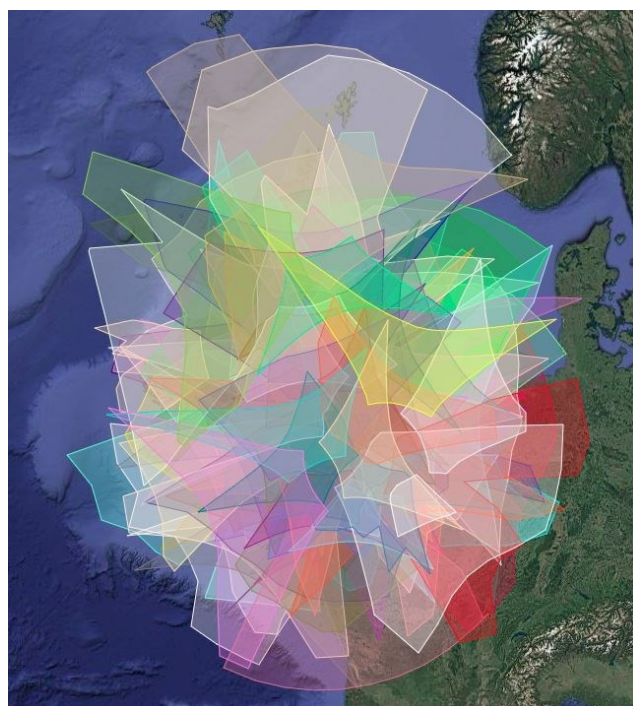
Figure 47 – UKMON camera fields in 2024 intersected at 100 km elevation, for cameras active in the United Kingdom.

The most interesting event of the year was the earthgrazing meteor of 7th July, which traversed Europe from Croatia to England taking 13 seconds to travel 840km. There is more about this event here[22] (McIntyre, 2024).

---

[21] https://www.emeteornews.net/wp-content/uploads/2025/02/UK_.kml

[22] https://www.emeteornews.net/2024/07/24/the-earth-grazing-meteor-of-july-2024/

In terms of fireballs, the UK Meteor Network has records of 43 that were detected during 2024. A few were potential meteorite droppers though unfortunately no rocks were found on the ground. The UK's terrain is not helpful in this respect, as bright fireballs seem to unerringly pick out the mountains of Scotland or Wales, or the peat bogs of the West Country!
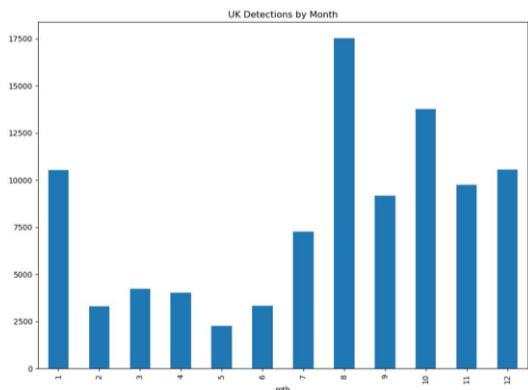
Figure 48 – The number of detections per month in the UK.

Showers

As one would expect the Perseid dominate though the Orionids were more prominent this year than the Geminids which were impacted by poor weather. The Quadrantids put on a better show than in 2023 due to better weather after Christmas. The top ten showers are shown in *Table 1* below. A total of 29844 shower meteors were detected in 347 different showers. At least ten meteors were detected in 199 showers and 79 showers had 50 or more detected members.

Table 1 – Top ten meteor showers in 2024 for the UK Meteor Network.

Shower	UK Matches
PER	8154
ORI	1872
GEM	1818
QUA	1424
SDA	779
STA	575
LEO	561
CAP	495
HYD	392
COM	435

Looking Forward

As RMS continues to improve, we should expect to see the number of meteor observations grow more slowly due to better filtration of non-meteors. On the other hand, we hope that a larger percentage of detections will be converted to matched events as improvements in the solver are implemented.

As of the end of January at least 170000 single-station detections had been made by UK cameras, leading to around 16000 confirmed matches.

5.41 United States

The American New Mexico Meteor Array was the pioneering network of the GMN as it started to harvest meteors in December 2018 with six cameras, producing the first 497 orbits for GMN. It remained the only data provider for GMN until May 2019 when the first 3 Croatian cameras started to deliver orbits. At the end of 2019, the number of US cameras had increased to 20 when the network collected 27643 orbits that year. In 2020, the 33 operational cameras in the US collected as many as 50607 orbits. With 72 RMS cameras registering paired meteors in the US, a total of 91901 orbits were obtained in 2021.

The number of GMN cameras involved in orbit determinations had increased to 100 in 2022, good for 114054 orbits. 2023 saw a further increase in cameras resulting in 120162 orbits. With 141 operational cameras in 2024, 135819 meteor orbits were collected. Until 2024 the USA had 16 decommissioned GMN cameras.
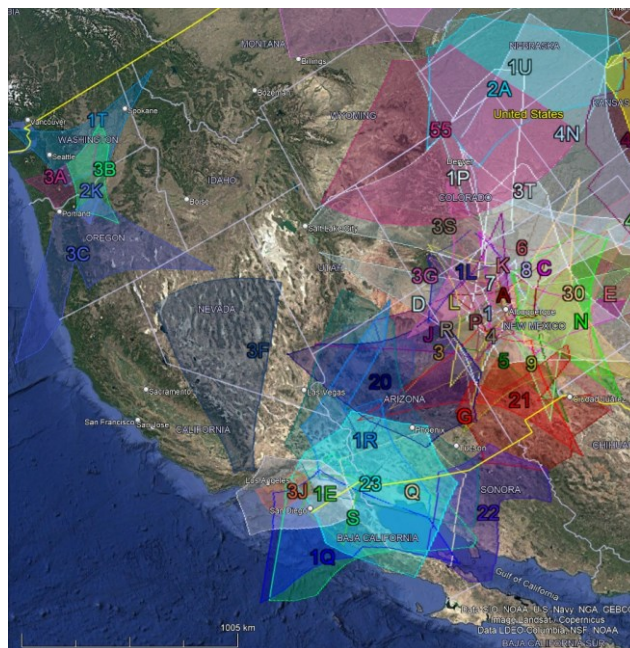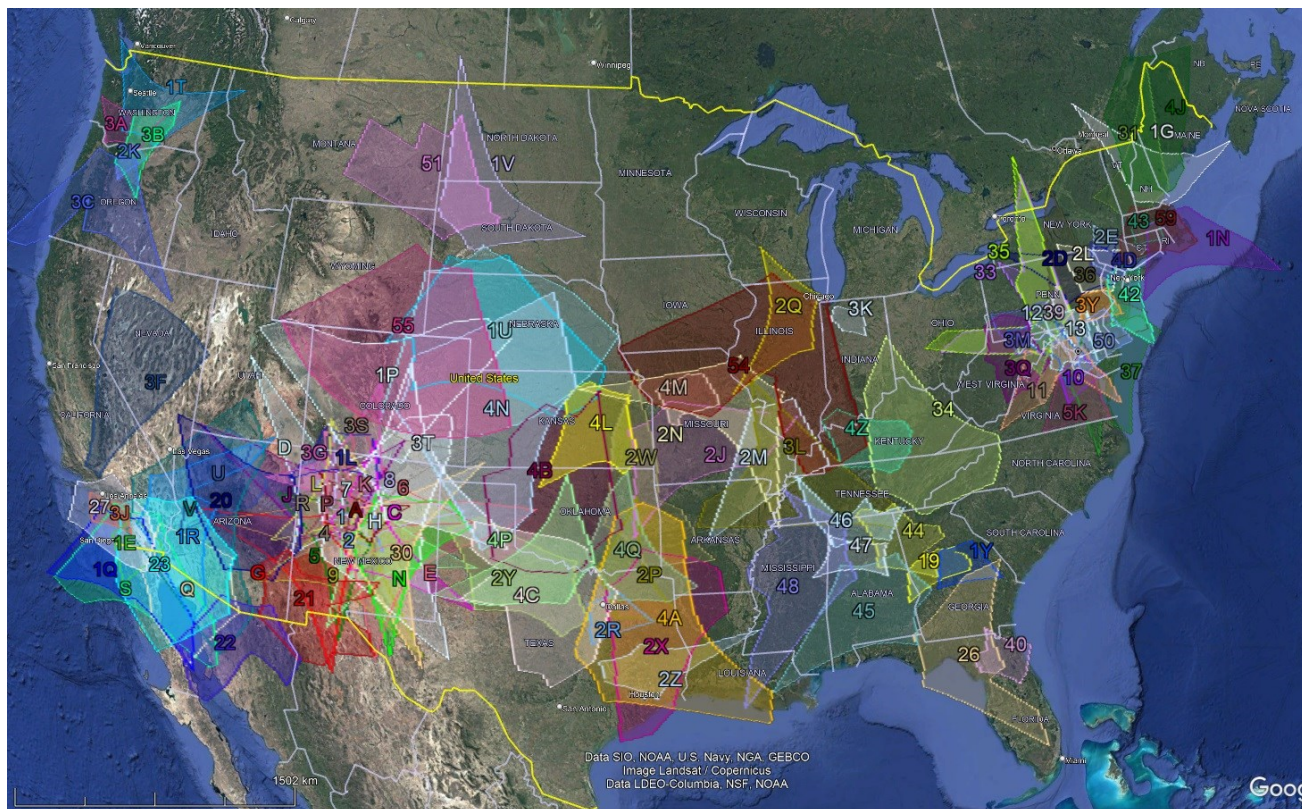

Figure 49 – GMN camera fields in 2024 intersected at 100 km elevation, for cameras in the western part of the USA.

Figure 50 – GMN camera fields in 2024 intersected at 100 km elevation, for cameras of the Lowell Observatory in Arizona.

Figure 51 – GMN camera fields intersected at 100 km elevation, global view for cameras installed in the USA, status 2024.

Figure 51 shows the GMN status like it was at the end of 2024 with 141 GMN cameras in the US, most of which belong to the New Mexico Camera Array and the Lowell Observatory in Arizona. Both networks are independent in neighboring states but have a large overlap. *Figure 50* shows the situation for the Lowell network in Arizona. The Lowell Observatory cameras also benefit coverage from other GMN cameras in the state as well as in California (*Figure 49*).

Figure 52 – GMN camera fields in 2024 intersected at 100 km elevation, for cameras in the north-eastern part of the USA.

GMN camera networks are emerging at several other sites in the US (*Figure 51*). The network reaches till Alaska at 65° northern latitude. Several cameras installed near the East Coast, south of the Canadian border connect to the

existing GMN network in Canada (*Figure 52*). The maps show where cameras in the US still wait for multi-station partners to set up cameras (*Figure 53*). Details are given in *Tables 5 and 6* for the Lowell network (USL), NASA network (USN) and USV network.
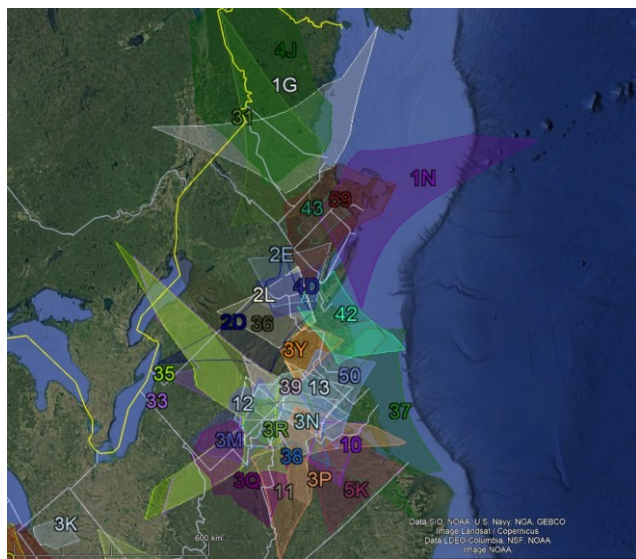

Figure 53 – GMN camera fields in 2024 intersected at 100 km elevation, for cameras in the south-eastern and central parts of the USA.

5.42 South Africa

The first two GMN cameras got installed end of 2022 but no paired meteors were obtained then. In 2023 the number of cameras increased to four and the first 200 orbits were obtained in South Africa. Major progress was made in 2024 when the number of operational cameras doubled and 2294 meteor orbits were recorded (*Figure 54*). The geographical position of South Africa makes this network of strategic interest for the coverage of southern hemisphere meteor activity.

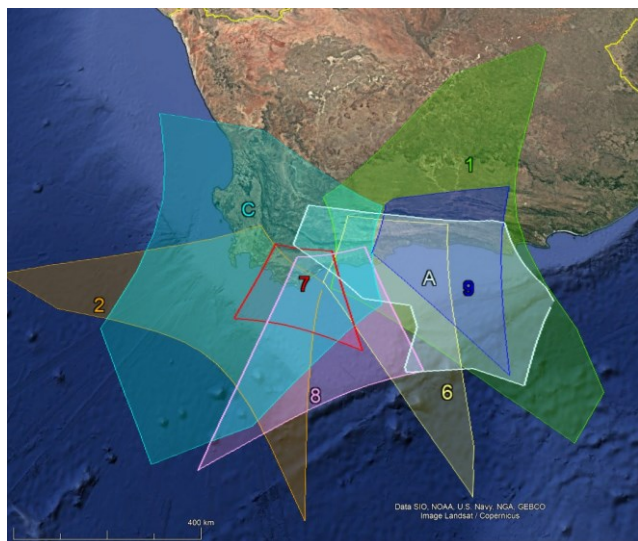*Figure 54* – GMN camera fields in 2024 intersected at 100 km elevation, for cameras active in South Africa.

5 GMN statistics 2024

When a first GMN status report got published, including all data until end October 2020, 140 operational cameras were involved and 144950 orbits had been collected (Roggemans, 2021). Meanwhile, we can compare six years of GMN work. *Figure 55* shows the accumulated number of orbits obtained and the number of contributing cameras during each calendar month. The rapid growth of the Global Meteor Network is obvious. The number of cameras involved in collecting orbits for GMN increased from 390 in 2021 to 700 in 2022, 1066 in 2023 and 1213 at the end of 2024.
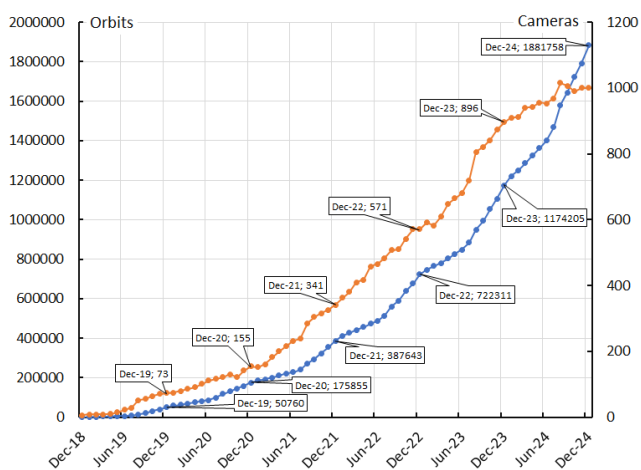

Figure 55 – The accumulated number of orbits (blue) and the actual number of operational cameras involved in triangulations (orange). The numbers at the end of each year are indicated.

Table 2 shows that only 29% of all orbits are collected during the first six months of each year, while 71% is obtained in the period July to December. The fast expansion of the Global Meteor Network also means that more

cameras were available towards the end of each year than at the beginning of each year, what also influenced the number of orbits obtained. The most important cause for the difference in number of orbits between the first and last six months is the meteor activity itself. Apart from the most active major meteor showers like the Perseids, Taurids, Orionids, Leonids and Geminids, the overall meteor activity is much higher during the second half of the year. This can be seen very well in *Figure 55* where the blue curve has a much steeper increase each second half of the year.

Although 1213 different cameras contributed paired meteors during 2024, only 1000 or 82% were successfully contributing during December (*Table 3*). The explanation is that this report is based on the camera IDs which occur in the orbit dataset and thus successfully recorded paired meteors. Apart from the 1000 successful cameras in December there were also a number of cameras functioning without having any paired meteors and thus not listed in the orbit dataset. Persistent unfavorable weather conditions sometimes prevent some cameras from getting paired meteors. A number of cameras struggled with technical issues. For instance, if a camera somehow is moved and has no calibration, no trajectories can be calculated.

Occasionally some hardware or network problem occur, if the connection with the camera board gets lost, the system may ping its camera unsuccessfully until the camera owner fixes the problem. Another hardware problem that is reported now and then is when the sd card crashes and needs replacement.

To prevent loss of valuable observing data, it is strongly recommended to look regularly at the camera status page[23] to check if all cameras report correctly to GMN. The GMN status page is another handy tool that shows all cameras per country color coding the status of all cameras in a single view[24].

In 2024, 237 new cameras contributed paired meteors, significantly less than previous year wen 430 new camera IDs were added. In total 1383 different camera IDs are listed in the orbit dataset, 179 of these camera IDs did not contribute to orbits in 2024, or 90 more than in 2023. *Table 5* lists the number of cameras active per country for each year since 2018. The number of camera IDs that contributed no paired meteors in 2024 has been also listed per country. In some cases, old devices were replaced by new, in other cases the camera owner somehow was unable to solve technical issues, had lack of time or lost interest. Some camera operators have died.

There is a remarkable status quo in the number of cameras that contribute paired meteors after August 2024. It is not clear if a software upgrade disabled a number of older cameras that failed to get restored.

---

[23] https://globalmeteornetwork.org/weblog/

[24] https://globalmeteornetwork.org/status/

Table 2 – Total number of orbits obtained by the Global Meteor Network cameras per calendar month for each year.

	2018	2019	2020	2021	2022	2023	2024	Tot
January	–	564	7539	9919	23727	23972	45613	111334
February	–	1284	5330	6529	14910	18602	31316	77971
March	–	537	5101	8767	15409	16310	33960	80084
April	–	876	7213	9655	15658	22713	38029	94144
May	–	1242	5654	10217	16951	22050	39834	95948
June	–	1523	5700	7954	13463	23125	38336	90101
July	–	1961	10973	11325	25226	35109	67402	151996
August	–	5387	19422	31292	47300	65155	112442	280998
September	–	6058	14012	21189	29984	44174	62041	177458
October	–	11978	13097	31501	48360	59134	81356	245426
November	–	7710	13228	30381	37895	54030	67862	211106
December	497	11143	17826	33059	45785	67520	89362	265192
Totals	497	50263	125095	211788	334668	451894	707553	1881758

Table 3 – Total number of operational cameras within the Global Meteor Network per calendar month.

	2018	2019	2020	2021	2022	2023	2024	Tot
January	–	9	75	152	363	591	910	1087
February	–	9	80	161	380	583	911	1089
March	–	9	86	182	410	609	940	1120
April	–	10	91	200	418	648	942	1153
May	–	15	101	216	458	665	956	1183
June	–	22	112	232	466	680	953	1183
July	–	29	117	239	483	720	969	1220
August	–	52	122	285	507	806	1016	1257
September	–	55	131	304	510	821	1007	1262
October	–	65	122	316	542	842	990	1257
November	–	71	142	326	571	873	1000	1261
December	6	73	155	341	571	896	1000	1284
Totals	6	76	173	390	700	1066	1213	1383

Table 4 – Total number of multi-station events contributing to an orbit result, recorded in each country for each year. The list is sorted on the country ID used in the camera ID. Subnetworks for some countries are counted in the grand total for the country.

	2018	2019	2020	2021	2022	2023	2024	Total
Austria (AT)	0	0	0	0	0	0	1702	1702
Australia (AU)	0	0	0	1871	12460	40712	100044	155087
Belgium (BE)	0	921	5500	8582	23174	25443	34050	97670
Bulgaria (BG)	0	0	0	419	3877	3530	15058	22884
Brazil (BR)	0	0	40	1645	2760	2331	4753	11529
Canada (CA)	0	3599	10815	8809	16232	15023	18508	72986
Canada (CAWE)	0	0	0	0	459	425	217	1101
Canada (CAWT)	0	0	0	0	0	193	211	404
Switzerland (CH)	0	0	0	3	3439	4352	2383	10177
Czech Republic (CZ)	0	0	163	464	2490	11269	18248	32634
Germany (DE)	0	200	3963	7009	9128	12194	23240	55734
Denmark (DK)	0	0	0	0	55	1386	3360	4801
Spain (ES)	0	0	1207	15113	19301	22610	16771	75002
Finland (FI)	0	0	0	0	41	90	204	335
France (FR)	0	0	3176	5601	11990	16682	20591	58040
Greece (GR)	0	0	0	0	977	3375	8998	13350
Croatia (HR)	0	12221	35099	38370	31329	27721	35727	180467
Hungary (HU)	0	0	0	0	2114	7872	9627	19613
Ireland (IE)	0	0	120	424	3490	1954	3706	9694
Israel (IL)	0	0	553	2009	975	1096	991	5624
Italy (IT)	0	862	5384	5447	4943	5064	6603	28303
Japan (JP)	0	0	0	0	0	629	606	1235
South Korea (KR)	0	0	0	0	7711	34044	42477	84232
Luxembourg (LU)	0	0	0	0	622	2018	2194	4834
Morocco (MA)							851	851
Mexico (MX)	0	0	0	0	1769	2953	2871	7593
Malasia (MY)	0	0	0	0	50	501	244	795
Netherlands (NL)	0	278	4337	7605	9139	9421	17409	48189
New Zealand (NZ)	0	0	0	1146	6280	47436	147831	202693
Poland (PL)	0	0	35	67	398	456	1759	2715
Portugal (PT)	0	0	0	0	327	3322	4413	8062
Romania (RO)	0	0	0	0	0	417	4361	4778
Russia (RU)	0	5715	13438	6208	5437	1992	10939	43729
Slovenia (SI)	0	2753	3999	6001	5887	6789	12208	37637
Slovakia (SK)	0	0	0	37	2026	5535	7532	15130
Tajikistan (TJ)							411	411
United Kingdom (UK)	0	0	1889	27430	78652	84688	95730	288389
USA (US)	497	27643	50607	91901	114054	120162	135819	540683
USA (USL)	0	0	2149	51425	79647	64903	64606	262730
USA (USN)	0	0	0	0	0	640	22	662
USA (USV)	0	0	0	0	3431	2099	1134	6664
Erroneous entry (XX)	0	0	0	8	28	0	123	159
South Africa (ZA)	0	0	0	0	0	200	2294	2494

Table 5 – Total number of operational cameras in each country for each year. Inactive devices and cameras without orbits are not counted. The list is sorted on the country ID used in the camera ID. Subnetworks for some countries are counted in the grand total for the country. The column 2024 (0) lists the number of cameras which had paired meteors before 2024 but did not appear in the 2024 data and are therefore considered as decommissioned.

	2018	2019	2020	2021	2022	2023	2024	Total	2024 (0)
Austria (A)	0	0	0	0	0	0	2	2	0
Australia (AU)	0	0	0	12	29	66	88	98	11
Belgium (BE)	0	4	4	10	20	23	28	30	2
Bulgaria (BG)	0	0	0	2	6	7	17	18	1
Brazil (BR)	0	0	2	13	20	34	37	44	8
Canada (CA)	0	11	17	29	51	51	46	72	28
Canada (CAWE)	0	0	0	0	7	8	4	8	4
Canada (CAWT)	0	0	0	0	0	8	1	8	7
Switzerland (CH)	0	0	0	1	5	5	4	5	1
Czech Republic (CZ)	0	0	3	4	6	20	25	25	0
Germany (DE)	0	4	10	12	18	19	30	32	2
Denmark (DK)	0	0	0	0	1	4	5	5	0
Spain (ES)	0	0	8	23	30	35	32	39	7
Finland (FI)	0	0	0	0	4	5	7	7	0
France (FR)	0	0	10	14	16	18	19	26	9
Greece (GR)	0	0	0	0	1	4	8	8	0
Croatia (HR)	0	23	32	48	45	41	43	59	17
Hungary (HU)	0	0	0	0	2	3	3	3	0
Ireland (IE)	0	0	2	3	5	5	6	8	2
Israel (IL)	0	0	3	6	5	6	7	9	2
Italy (IT)	0	1	1	5	5	7	7	10	3
Japan (JP)	0	0	0	0	0	2	2	2	0
South Korea (KR)	0	0	0	0	47	125	122	125	3
Luxembourg (LU)	0	0	0	0	1	1	1	1	0
Morocco (MA)	0	0	0	0	0	0	3	3	0
Mexico (MX)	0	0	0	0	12	15	13	15	2
Malasia (MY)	0	0	0	0	3	5	6	8	2
Netherlands (NL)	0	2	11	11	13	14	18	22	5
New Zealand (NZ)	0	0	0	2	28	111	152	155	3
Poland (PL)	0	0	1	1	3	2	4	5	1
Portugal (PT)	0	0	0	0	1	1	2	2	0
Romania (RO)	0	0	0	0	0	3	3	3	0
Russia (RU)	0	10	21	21	19	15	22	33	12
Slovenia (SI)	0	1	1	2	2	6	6	6	0
Slovakia (SK)	0	0	0	1	3	4	5	5	0
Tajikistan (TJ)	0	0	0	0	0	0	2	2	0
United Kingdom (UK)	0	0	13	97	191	261	283	311	31
USA (US)	6	20	33	72	100	128	141	155	16
USA (USL)	0	0	9	36	47	45	41	48	7
USA (USN)	0	0	0	0	0	3	1	4	3
USA (USV)	0	0	0	0	2	2	2	2	0
Erroneous entry (XX)	0	0	0	1	1	0	1	1	0
South Africa (ZA)	0	0	0	0	0	4	8	8	0

6 Meteor showers covered by GMN

Using the Working List of Meteor Showers[25] (Jenniskens et al., 2020; Jopek and Kaňuchová, 2017; Jopek and Jenniskens, 2011; Neslušan et al., 2020) as a reference, 387 of the showers listed could be associated with orbits collected by the Global Meteor Network. The number of orbits recorded for each of these showers is listed in *Table 6* for each year since 2018.

The GMN meteor shower association was originally based on the table of Sun-centered ecliptic shower radiant positions given in Jenniskens et al. (2018). However, in May 2023 it was concluded that the list had some imperfections and therefore it was decided to make GMN's own meteor shower list and redo the meteor shower associations from the past. The new reference list contains 387 meteor showers instead of the 425 in the previous list. For this reason, many entrees of the IAU MDC Working List of Meteor Showers have no matching orbits in the GMN database as most of these meteor showers are not included in the GMN list. Some of the showers are periodic and display only some activity once every few years, some showers have been detected only by radar in a fainter range of magnitudes than what GMN cameras cover and others are known as daylight meteor showers. While GMN is getting better coverage at the southern hemisphere, more of the low declination meteor showers will get covered. For many of the listed meteoroid streams their absence in the GMN orbit database can be explained because the evidence for the existence of the shower is still missing. One of the goals of the GMN project is to help to identify ghost meteor showers that should be removed from the Working List.

Table 6 – Total number of orbits according to the meteor shower association (IAU number + code) for each year.

IAU id	Meteor shower name	< 2020	2020	2021	2022	2023	2024	Total
Spo#-1	Sporadics	35918	88579	145663	231788	318794	519520	1340262
CAP#1	alpha-Capricornids	94	604	451	1147	1840	3845	8075
STA#2	Southern Taurids	765	838	1934	2178	3575	4564	14619
SIA#3	Southern iota-Aquariids	11	27	39	52	116	267	523
GEM#4	Geminids	2247	5959	9968	15800	19655	13814	69690
SDA#5	Southern delta-Aquariids	269	1271	1225	3190	4138	10056	20418
LYR#6	April Lyrids	30	531	743	1066	1451	1235	5086
PER#7	Perseids	1231	6192	11407	15126	22003	35890	93080
ORI#8	Orionids	2045	2501	4556	9576	10417	10664	41804
DRA#9	October Draconids	2	4	7	11	6	295	327
QUA#10	Quadrantids	13	561	1216	1070	1017	2798	6688
EVI#11	eta-Virginids	2	38	283	241	82	139	787
KCG#12	kappa-Cygnids	15	78	1773	85	107	180	2253
LEO#13	Leonids	272	683	953	1548	2362	2281	8371
URS#15	Ursids	88	244	169	325	402	745	2061
HYD#16	sigma-Hydrids	360	488	1613	1263	2737	4287	11108
NTA#17	Northern Taurids	344	579	965	1053	2397	2161	7843
AND#18	Andromedids	40	71	920	175	216	226	1688
MON#19	December Monocerotids	126	239	593	531	1291	1438	4344
COM#20	Comae Berenicids	272	574	680	1660	1686	2347	7491
AVB#21	alpha-Virginids	10	107	123	142	368	394	1154
LMI#22	Leonis Minorids	83	103	193	357	436	539	1794
EGE#23	Epsilon Geminids	100	116	347	510	624	753	2550
NOA#25	Northern October delta-Arietids	115	159	183	294	437	392	1695
NDA#26	Northern delta-Aquariids	99	393	476	774	1265	1792	4898
KSE#27	kappa-Serpentids	2	12	29	26	54	76	201
SOA#28	Southern October delta-Arietids	73	143	318	124	576	706	2013
ETA#31	eta-Aquariids	162	503	1321	2446	2575	7948	15117
NIA#33	Northern iota-Aquariids	64	132	215	230	382	623	1710
ZCY#40	zeta-Cygnids	10	120	203	303	347	357	1350
DLI#47	mu-Virginids	4	56	33	143	205	214	659

[25] https://www.ta3.sk/IAUC22DB/MDC2022/Roje/roje_lista.php?corobic_roje=0&sort_roje=0

IAU id	Meteor shower name	< 2020	2020	2021	2022	2023	2024	Total
TAH#61	tau-Herculids	0	0	1	1243	1	3	1248
GDE#65	gamma-Delphinids	1	6	27	26	36	45	142
SSG#69	Southern mu-Sagittariids	16	48	67	81	354	674	1256
SLY#81	September Lyncids	11	76	104	75	197	214	688
ODR#88	omicron-Draconids	3	18	17	46	31	53	171
PVI#89	January pi-Virginids	1	19	48	89	105	208	471
NCC#96	Northern delta-Cancrids	26	77	86	245	204	387	1051
SCC#97	Southern delta-Cancrids	49	121	104	278	272	498	1371
PIH#101	pi-Hydrids	79	127	290	469	649	1196	2889
ACE#102	alpha-Centaurids	0	0	0	29	40	319	388
BTU#108	beta-Tucanids	0	0	0	1	28	29	58
AAN#110	alpha-Antliids	3	20	10	61	48	76	221
DME#130	delta-Mensids	0	0	0	5	57	215	277
ELY#145	eta-Lyrids	7	39	148	209	181	289	880
NOP#149	Northern May Ophiuchids	4	22	12	18	61	110	231
SOP#150	Southern May Ophiuchids	3	9	25	15	70	144	269
EAU#151	epsilon-Aquilids	23	76	109	230	303	563	1327
NOC#152	Northern Daytime omega-Cetids	2	4	8	9	12	13	50
SSC#161	Southern omega-Scorpiids	10	7	38	21	50	102	238
NZC#164	Northern June Aquilids	63	331	304	709	1005	1966	4441
SZC#165	Southern June Aquilids	19	74	93	226	408	1287	2126
JBO#170	June Bootids	1	3	0	35	5	0	45
ARI#171	Daytime Arietids	6	14	32	34	46	90	228
JPE#175	July Pegasids	24	145	221	404	669	960	2447
PHE#176	July Phoenicids	1	0	11	49	221	650	933
OCY#182	omicron-Cygnids	1	20	20	31	34	41	148
PAU#183	Piscis Austrinids	5	33	40	52	104	352	591
GDR#184	July gamma-Draconids	8	124	66	175	127	322	830
EUM#186	epsilon-Ursae Majorids	0	13	6	14	22	33	88
PCA#187	psi-Cassiopeiids	4	19	33	56	80	71	267
BPE#190	beta-Perseids	8	27	33	96	75	151	398
ERI#191	eta-Eridanids	49	117	183	328	642	1614	2982
UCE#194	upsilon-Cetids	28	56	114	200	272	393	1091
AUD#197	August Draconids	92	237	320	460	714	858	2773
AUR#206	Aurigids	29	50	128	152	157	265	810
SPE#208	September epsilon-Perseids	85	220	411	310	833	865	2809
BAU#210	beta-Aurigids	41	118	159	250	340	374	1323
KLE#212	Daytime kappa-Leonids	2	4	6	7	24	12	57
NPI#215	Northern delta-Piscids	58	114	123	253	237	386	1229
SPI#216	Southern delta-Piscids	26	52	52	96	175	156	583
NDR#220	nu-Draconids	28	58	51	91	169	165	590
DSX#221	Daytime Sextantids	5	3	22	42	34	66	177
SOR#225	sigma-Orionids	43	76	118	218	310	394	1202
XDR#242	xi-Draconids	9	24	66	72	136	131	447
ZCN#243	zeta-Cancrids	1	9	22	15	26	25	99
NHD#245	November Hydrids	7	24	81	66	131	154	470
AMO#246	alpha-Monocerotids	25	22	40	73	80	138	403
NOO#250	November Orionids	232	273	821	1047	953	2127	5685

IAU id	Meteor shower name	< 2020	2020	2021	2022	2023	2024	Total
ALY#252	alpha-Lyncids	1	6	10	16	8	15	57
CMI#253	December Canis Minorids	34	60	100	158	189	298	873
PHO#254	Phoenicids	0	0	0	0	0	53	53
ORN#256	Northern chi-Orionids	115	127	233	376	423	611	2000
ORS#257	Southern chi-Orionids	185	247	525	688	971	1330	4131
OCT#281	October Camelopardalids	28	9	55	149	55	163	487
FTA#286	omega-Taurids	87	66	156	492	206	537	1631
DSA#288	Southern December delta-Arietids	39	76	111	220	259	355	1099
DNA#289	Northern December delta-Arietids	17	22	126	96	96	237	611
TPU#307	tau-Puppids	1	0	3	11	31	86	133
PIP#308	January pi-Puppids	19	16	36	66	108	321	585
MVE#318	mu-Velids	8	19	35	49	107	200	426
JLE#319	January Leonids	0	9	5	24	13	33	84
LBO#322	lambda-Bootids	1	15	29	70	56	86	258
XCB#323	xi-Coronae Borealids	0	17	31	41	65	92	246
EPR#324	epsilon-Perseids	0	12	3	12	17	17	61
EPG#326	epsilon-Pegasids	8	25	33	52	59	104	289
SSE#330	sigma-Serpentids	3	4	0	8	4	8	30
AHY#331	alpha-Hydrids	6	32	43	161	62	405	715
OCU#333	October Ursae Majorids	41	52	150	139	295	176	894
DAD#334	December alpha-Draconids	101	169	406	481	606	817	2681
XVI#335	December chi-Virginids	54	82	115	163	289	352	1109
DKD#336	December kappa-Draconids	106	35	293	149	423	668	1780
NUE#337	nu-Eridanids	234	423	850	1309	1849	2746	7645
OER#338	omicron-Eridanids	132	146	308	435	718	946	2817
PSU#339	psi-Ursae Majorids	30	25	124	62	150	291	712
TPY#340	theta-Pyxidids	23	39	63	154	194	400	896
XUM#341	January xi-Ursae Majorids	0	22	31	50	133	135	371
HVI#343	h-Virginids	10	148	6	2	7	116	299
FHE#345	f-Herculids	1	13	30	75	49	77	246
XHE#346	x-Herculids	3	33	53	96	84	123	395
BPG#347	beta-Pegasids	0	1	7	4	5	8	25
ARC#348	April rho-Cygnids	7	84	119	232	205	175	829
LLY#349	lambda-Lyrids	0	3	2	4	6	7	22
JMC#362	June mu-Cassiopeiids	3	23	56	66	44	69	264
PPS#372	phi-Piscids	66	286	354	841	952	1301	3866
ALN#376	August Lyncids	5	11	19	31	45	49	165
OLP#384	October Leporids	12	14	36	50	74	102	300
OBC#386	October beta-Camelopardalids	21	24	71	117	115	155	524
CTA#388	chi-Taurids	61	62	195	202	288	377	1246
THA#390	November theta-Aurigids	113	202	507	387	693	947	2962
NID#392	November i-Draconids	16	39	74	79	126	136	486
ACA#394	alpha-Canis Majorids	24	15	51	77	107	203	501
GCM#395	gamma-Canis Majorids	28	60	39	130	132	323	740
GUM#404	gamma-Ursae Minorids	0	30	19	54	162	103	368
DPI#410	delta-Piscids	2	12	17	54	98	69	254
CAN#411	c-Andromedids	18	130	205	411	439	652	1873
SIC#416	September iota-Cassiopeiids	5	32	43	42	82	108	317

IAU id	Meteor shower name	< 2020	2020	2021	2022	2023	2024	Total
SOL#424	September-October Lyncids	16	62	77	181	178	245	775
FED#427	February eta-Draconids	1	7	3	27	11	31	81
DSV#428	December sigma-Virginids	62	120	222	407	395	711	1979
ACB#429	alpha-Coronae Borealids	6	23	18	103	115	71	342
JIP#431	June iota-Pegasids	2	15	11	60	106	68	264
ZCS#444	zeta-Cassiopeiids	22	139	262	392	624	644	2105
KUM#445	kappa-Ursae Majorids	21	55	125	111	154	161	648
DPC#446	December phi-Cassiopeiids	12	11	71	89	40	357	592
AAL#448	April alpha-Librids	3	19	26	54	52	94	251
AED#450	April epsilon-Delphinids	3	15	27	48	49	93	238
CAM#451	Camelopardalids	3	1	2	6	6	2	23
MPS#456	May psi-Scorpiids	28	89	139	211	390	493	1378
JEC#458	June epsilon-Cygnids	5	41	61	43	128	107	390
JEO#459	June epsilon-Ophiuchids	39	28	10	47	110	90	363
AXC#465	August xi-Cassiopeiids	6	20	57	74	96	106	365
AOC#466	August omicron-Cetids	0	11	16	25	52	109	213
LAQ#473	lambda-Aquariids	9	22	23	44	104	56	267
ICE#476	iota-Cetids	11	42	32	36	60	68	260
TCA#480	tau-Cancrids	68	87	233	371	439	502	1768
NZP#486	November zeta-Perseids	8	20	17	50	43	55	201
NSU#488	November sigma-UrsaeMajorids	11	16	25	53	45	77	238
DEL#494	December Lyncids	20	36	127	93	169	214	679
DAB#497	December alpha-Bootids	5	13	20	47	52	31	173
FPL#501	February pi-Leonids	2	21	30	31	52	100	238
DRV#502	December rho-Virginids	37	47	129	140	173	263	826
AIC#505	August iota-Cetids	52	118	159	312	439	635	1767
FEV#506	February epsilon-Virginids	5	83	115	302	360	473	1343
UAN#507	upsilon-Andromedids	17	64	87	265	211	299	960
JRC#510	June rho-Cygnids	1	15	44	55	98	116	330
RPU#512	rho-Puppids	12	36	47	56	185	192	540
OMC#514	omega-Capricornids	0	13	16	34	120	223	406
OLE#515	omicron-Leonids	28	46	87	193	189	350	921
FMV#516	February mu-Virginids	1	22	32	105	116	149	426
ALO#517	April lambda-Ophiuchids	1	5	25	45	30	54	161
AHE#518	April102-Herculids	1	11	4	19	27	18	81
BAQ#519	beta-Aquariids	4	8	28	53	31	109	237
MBC#520	May beta-Capricornids	5	16	25	32	90	108	281
AGC#523	August gamma-Cepheids	15	54	72	169	103	260	688
LUM#524	lambda-Ursae Majorids	13	12	66	108	35	148	395
SLD#526	Southern lambda-Draconids	15	18	67	68	92	101	376
EHY#529	eta-Hydrids	58	97	241	287	473	632	1846
ECV#530	eta-Corvids	5	31	47	130	211	362	791
GAQ#531	gamma-Aquilids	6	18	60	73	94	114	371
JXA#533	July xi-Arietids	9	41	60	134	212	418	883
THC#535	theta-Cetids	1	4	11	20	29	91	157
TTB#543	22-Bootids	4	8	9	22	16	27	90
JNH#544	January nu-Hydrids	3	14	10	33	20	58	141
XCA#545	xi-Cassiopeiids	1	6	10	29	13	24	84

IAU id	Meteor shower name	< 2020	2020	2021	2022	2023	2024	Total
FTC#546	43-Cassiopeiids	12	57	63	83	149	167	543
KAP#547	kappa-Perseids	33	171	266	462	689	900	2554
FAN#549	49-Andromedids	3	56	77	112	156	132	539
PSO#552	pi6-Orionids	27	85	221	270	361	428	1419
OCP#555	October gamma-Camelopardalids	14	18	51	83	85	136	401
PTA#556	phi-Taurids	14	8	50	78	81	147	392
SFD#557	64-Draconids	29	53	101	111	191	202	716
MCB#559	beta-Canis Majorids	11	12	10	42	42	65	193
SSX#561	6-Sextantids	9	20	31	61	64	77	271
DOU#563	December omega-UrsaeMajorids	23	33	26	96	88	177	466
SUM#564	61-Ursae Majorids	16	14	13	40	23	81	203
OHY#569	omicron-Hydrids	9	22	34	128	225	511	938
FBH#570	February beta-Herculids	3	9	11	48	48	58	180
TSB#571	26-Bootids	2	9	11	29	28	48	129
SAU#575	63-Aurigids	6	18	19	41	60	56	206
CHA#580	chi-Andromedids	7	34	16	73	67	97	301
NHE#581	90-Herculids	5	66	88	130	190	160	644
JBC#582	January beta-Craterids	0	15	36	60	80	182	373
GCE#584	Cepheids-Cassiopeiids	11	28	50	84	102	169	455
THY#585	33-Hydrids	6	13	20	41	73	56	215
FNC#587	59-Cygnids	3	15	24	45	25	47	162
FCA#589	50-Cancrids	6	21	49	81	62	131	356
VCT#590	10-Canum Venaticids	1	5	2	14	5	30	58
ZBO#591	zeta-Bootids	3	20	28	52	49	92	247
PON#592	91-Piscids	3	10	18	30	39	61	164
TOL#593	28-Lyncids	16	19	62	77	126	117	433
RSE#594	Serpentids-Coronae Borealids	0	3	4	4	27	11	49
POS#599	72-Ophiuchids	4	44	89	156	173	256	726
ICT#601	iota-Craterids	4	8	10	27	28	86	167
KCR#602	kappa-Craterids	0	1	21	36	37	104	199
FAR#608	14-Aurigids	2	13	38	52	64	86	257
TLY#613	31-Lyncids	1	12	61	56	104	97	332
THD#618	12-Hydrids	2	6	16	30	12	64	132
XCS#623	xi2-Capricornids	20	78	99	248	814	499	1778
XAR#624	xi-Arietids	83	156	138	370	523	286	1639
LTA#625	lambda-Taurids	50	130	132	454	492	286	1594
LCT#626	lambda-Cetids	54	19	126	191	42	271	757
NPS#627	nu-Piscids	51	21	158	226	122	402	1031
STS#628	s-Taurids	123	62	208	3172	258	388	4334
ATS#629	A2-Taurids	84	124	176	326	706	228	1728
TAR#630	tau-Arietids	132	115	411	352	537	698	2377
DAT#631	delta-Arietids	167	58	374	553	227	877	2423
NET#632	November eta-Taurids	61	161	377	179	774	682	2295
PTS#633	p-Taurids	117	76	262	246	401	692	1911
TAT#634	tau-Taurids	99	157	210	487	606	670	2328
ATU#635	A1-Taurids	44	263	471	260	1090	969	3141
MTA#636	m-Taurids	60	33	172	121	182	432	1060
FTR#637	f-Taurids	120	156	404	1248	663	760	3471

IAU id	Meteor shower name	< 2020	2020	2021	2022	2023	2024	Total
DZT#638	December zeta-Taurids	15	18	39	47	97	66	297
AOA#640	August omicron-Aquariids	62	251	328	547	1117	2296	4663
JLL#644	January lambda-Leonids	41	83	107	134	231	249	886
BCO#647	beta-Comae Berenicids	8	40	69	99	82	117	423
TAL#648	22-Aquilids	6	82	113	216	317	431	1171
OAV#651	68-Virginids	18	32	67	128	385	273	921
OSP#652	omicron-Serpentids	4	10	21	30	36	96	201
RLY#653	R-Lyrids	4	34	33	88	71	94	328
APC#655	April phi-Capricornids	1	2	4	4	29	63	104
GSG#657	gamma-Sagittariids	0	2	12	13	27	60	114
EDR#658	epsilon-Draconids	2	14	22	30	19	44	133
EPS#660	epsilon-Scorpiids	3	15	30	25	61	143	280
OTH#661	110-Herculids	0	11	28	32	25	45	141
MUC#665	May upsilon-Cygnids	2	22	27	35	64	58	210
JMP#668	June mu-Pegasids	3	20	16	36	52	38	168
MCY#671	mu-Cygnids	0	3	9	20	9	32	73
MUA#679	mu-Aquariids	5	6	33	32	56	91	228
JEA#680	June epsilon-Arietids	6	9	12	19	22	33	107
OAQ#681	omicron-Aquariids	4	17	17	21	48	56	167
JTS#683	June theta-Serpentids	0	8	6	5	20	21	60
JPS#685	June beta-Pegasids	4	11	9	39	37	42	146
JRD#686	June rho-Draconids	0	1	7	17	26	15	66
KDP#687	kappa-Delphinids	0	9	5	7	8	19	48
TAC#689	tau-Capricornids	8	41	31	100	160	468	816
ZCE#691	zeta-Cetids	1	0	13	29	15	49	108
EQA#692	epsilon-Aquariids	15	119	239	373	159	1243	2163
ANP#693	August nu-Perseids	17	44	65	158	147	208	656
OMG#694	omicron-Geminids	32	73	111	180	217	283	928
APA#695	August psi-Aurigids	4	14	27	36	34	46	165
OAU#696	omicron-Aurigids	5	26	36	63	79	96	310
AET#698	August eta-Taurids	1	22	30	48	81	48	231
BCE#701	beta-Cepheids	2	8	7	24	37	93	173
ASP#702	August 78-Pegasids	1	12	9	17	13	23	76
OAN#704	omicron-Andromedids	18	83	107	135	197	250	808
ZPI#706	zeta-Piscids	24	51	80	132	174	210	695
BPX#707	beta-Pyxidids	0	2	4	19	15	102	142
RLM#708	R-Leonis Minorids	0	4	24	31	46	86	191
FDC#712	February delta-Cygnids	1	8	12	19	21	20	82
CCR#713	chi-Cancrids	5	10	9	19	25	13	86
RPI#714	rho-Piscids	34	62	89	143	181	250	793
ACL#715	alpha-Camelopardalids	60	162	286	401	557	607	2133
OCH#716	October chi-Andromedids	25	29	67	108	109	154	517
NGB#720	November gamma-Bootids	7	3	16	16	16	50	115
DAS#721	December alpha-Sextantids	13	6	38	19	23	73	185
FLE#722	15-Leonids	14	11	42	36	45	112	274
DEG#726	December epsilon-Geminids	18	37	12	85	76	119	365
ISR#727	iota-Serpentids	2	2	0	16	6	12	40
PGE#728	phi-Geminids	10	15	11	46	26	65	183

IAU id	Meteor shower name	< 2020	2020	2021	2022	2023	2024	Total
DCO#729	delta-Corvids	2	9	2	17	13	48	93
ATV#730	April theta-Virginids	1	6	1	4	7	22	42
FGV#732	February gamma-Virginids	3	12	14	33	41	27	133
MOC#734	March omicron-Cygnids	1	12	14	17	11	23	79
XIP#736	xi-Perseids	3	8	15	32	27	60	148
FNP#737	59-Perseids	1	4	2	15	4	25	52
RER#738	rho-Eridanids	3	13	31	47	78	238	413
LAR#739	lambda-Arietids	7	11	26	57	36	81	225
OSD#745	October 6-Draconids	7	18	40	66	83	84	305
EVE#746	e-Velids	11	13	123	195	942	1710	3005
JKL#747	January kappa-Leonids	8	23	44	101	52	153	389
JTL#748	January theta-Leonids	0	22	14	95	92	139	362
SMV#750	Southern March gamma-Virginids	6	50	94	186	229	397	968
KCE#751	kappa-Cepheids	17	42	39	78	87	109	389
MID#755	May iota-Draconids	0	4	3	11	6	5	29
CCY#757	chi-Cygnids	12	380	16	23	47	57	547
SCO#771	sigma-Columbids	1	2	9	9	27	25	74
KVE#784	kappa-Velids	0	2	28	103	99	404	636
TCD#785	theta-Carinids	0	0	9	41	75	343	468
SXP#786	6-Puppids	2	4	1	13	10	34	66
MBE#792	March beta-Equuleids	0	0	2	4	6	9	21
KCA#793	kappa-Cancrids	0	8	10	30	14	53	115
SED#796	September epsilon-Draconids	6	5	29	41	34	63	184
ADS#802	June Aquariids	0	8	9	18	46	68	149
LSA#803	lambda-Sagittariids	2	5	27	54	69	200	359
FLO#807	February Leonids	7	57	61	98	126	180	536
XCD#810	October Cetids	10	7	29	63	62	62	243
NAA#812	November alpha-Aurigids	5	20	27	32	64	59	212
CVD#814	January Canum Venaticids	0	6	6	34	48	24	118
UMS#815	August Ursae Majorids	0	10	9	15	16	16	66
CVT#816	February Canum Venaticids	1	5	13	15	23	20	78
OAG#818	October Aurigids	6	9	10	21	30	28	110
NUT#822	nu-Taurids	0	4	9	18	52	108	191
FCE#823	56-Cetids	10	20	26	54	85	129	334
DEX#824	December Sextantids	3	17	13	35	45	66	182
XIE#825	xi-Eridanids	14	12	22	25	69	111	267
ILI#826	iota1-Librids	4	36	42	69	126	282	563
NPE#827	nu-Pegasids	1	17	16	31	52	90	208
JSP#829	July 77-Pegasids	7	18	54	46	113	121	366
SCY#830	63-Cygnids	2	27	20	46	46	65	208
GPG#831	gamma-Pegasids	5	8	14	30	44	61	167
LEP#832	Leporids	3	1	5	12	27	85	136
KOR#833	kappa-Orionids	5	3	13	30	34	54	144
ACU#834	April theta-Centaurids	1	1	6	6	9	57	81
ABH#836	April beta-Herculids	0	2	8	17	22	30	79
CAE#837	Caelids	2	0	2	19	30	20	75
PSR#839	phi-Serpentids	1	9	17	22	29	53	132
TER#840	tau4-Eridanids	0	4	8	3	17	31	63

IAU id	Meteor shower name	< 2020	2020	2021	2022	2023	2024	Total
DHE#841	delta-Herculids	0	5	16	46	25	46	138
DMD#843	December mu-Draconids	1	5	5	9	13	25	59
DTP#844	December theta-Pyxidids	15	6	45	36	61	151	329
BEL#847	beta-Leonids	4	0	13	10	12	19	62
OPE#848	omicron-Perseids	2	4	4	9	8	2	31
SZE#849	September zeta-Eridanids	1	15	17	22	48	60	164
PCY#854	psi-Cygnids	1	17	25	67	69	71	251
ATD#855	August tau-Draconids	0	3	8	8	18	19	56
EMO#856	epsilon-Monocerotids	4	8	15	25	17	43	116
FPB#858	February phi-Bootids	3	20	15	75	81	62	259
MTB#859	March 12-Bootids	2	1	17	35	21	45	123
PAN#860	psi-Andromedids	0	3	12	28	22	15	80
JXS#861	June xi1-Sagittariids	1	9	4	15	33	26	89
SSR#862	16-Scorpiids	1	9	16	37	48	61	173
TLR#863	12-Lacertids	1	5	12	12	26	17	74
JSG#864	June 66-Pegasids	2	1	10	8	20	24	67
JES#865	June epsilon-Serpentids	4	4	3	15	25	25	80
ECB#866	epsilon-Coronae Borealids	2	5	9	8	6	17	49
FPE#867	52-Pegasids	3	10	2	38	17	44	117
PSQ#868	psi3-Aquariids	1	5	2	8	23	29	69
UCA#869	upsilon1-Cassiopeiids	0	10	5	25	29	65	134
JPG#870	July eta-Pegasids	0	11	8	11	10	27	67
DCD#871	delta-Cepheids	0	9	5	11	11	18	54
ETR#872	epsilon-Triangulids	2	9	16	32	39	84	184
OMI#873	omicron-Cetids	5	8	12	26	21	39	116
PXS#874	September xi-Perseids	13	44	45	75	113	82	385
TEI#875	tau9-Eridanids	4	2	13	19	24	42	108
ROR#876	rho-Orionids	9	11	20	49	43	79	220
OHD#877	omega-Hydrids	5	7	21	25	41	19	123
OEA#878	October epsilon-Aurigids	2	5	2	9	23	21	64
ATI#879	alpha-Taurids	7	11	28	35	58	56	202
YDR#880	Y-Draconids	12	13	28	40	50	42	197
TLE#881	theta-Leonids	1	1	21	19	9	19	71
PLE#882	phi-Leonids	3	7	10	20	20	25	88
NBP#884	November beta-Pyxidids	1	3	1	15	29	61	111
DEV#885	December epsilon-Virginids	4	11	7	32	16	69	143
ACV#886	alpha-Corvids	1	7	11	48	24	104	196
DZB#887	December zeta-Bootids	3	13	15	25	13	37	109
SCV#888	6-Corvids	0	2	10	10	21	43	86
YOP#889	Y-Ophiuchids	0	1	2	8	6	10	27
ESU#890	eta-Scutids	1	5	3	6	10	5	31
FSL#891	February sigma-Leonids	2	17	9	55	44	38	167
MCN#892	March Centaurids	0	0	3	9	5	22	39
EOP#893	eta-Ophiuchids	0	19	25	42	71	100	257
OTA#896	130-Taurids	11	21	11	42	61	41	198
OUR#897	October alpha-UrsaeMinorids	9	2	21	28	10	49	128
SGP#898	September gamma-Piscids	5	10	19	10	30	50	129
EMC#899	epsilon-Microscopiids	1	0	3	13	29	72	119

IAU id	Meteor shower name	< 2020	2020	2021	2022	2023	2024	Total
BBO#900	beta-Bootids	0	18	40	109	44	155	366
TLC#901	34-Lyncids	3	8	7	19	21	22	83
DCT#902	delta-Cetids	15	13	24	36	86	83	272
OAT#903	October alpha-Triangulids	8	12	7	25	35	51	146
OCO#904	omicron-Columbids	2	2	14	5	50	56	131
MXD#905	March xi-Draconids	0	7	6	7	11	7	38
ETD#906	eta-Draconids	0	13	18	34	27	17	109
MCE#907	mu-Cepheids	1	5	11	21	17	26	82
BTC#910	beta2-Cygnids	1	14	19	32	26	35	128
TVU#911	21-Vulpeculids	2	11	29	57	49	80	230
BCY#912	beta-Cygnids	1	17	23	39	46	74	201
DNO#915	delta-Normids	0	1	2	6	41	45	95
TAG#918	theta-Aurigids	4	10	17	41	18	37	131
ICN#919	iota-Centaurids	0	2	4	3	17	126	152
XSC#920	xi-Scorpiids	4	10	25	43	53	137	276
JLC#921	July lambda-Capricornids	3	15	6	22	27	48	124
SAN#924	62-Andromedids	1	3	20	5	26	16	72
EAN#925	eta-Andromedids	2	4	4	23	23	14	72
OCR#1033	omega-Carinids	0	0	0	0	6	19	25
ARD#1130	Arids	0	0	6	0	1	2	9
OZP#1131	October zeta-Perseids	0	0	6	1	0	0	7
		50760	125095	211788	334668	451894	707553	1896600

Table 6 serves as an inventory of what the GMN orbit database has available until end 2024. Of course, the number of shower members detected depends on the criteria used to associate a meteor with a known meteor shower radiant. The GMN shower association criterion assumes that meteors within 1° in solar longitude, within 3° in radiant, and within 10% in geocentric velocity of a shower reference location are members of that shower. Further details about the shower association are explained in Moorhead et al. (2020). This is a rather strict criterion since meteor showers often have a larger dispersion in radiant position and velocity. Therefore, using the orbit similarity criteria (Drummond, 1981; Southworth and Hawkins, 1963; Jopek, 1993) will certainly detect more shower candidates but at the risk of including sporadic orbits that fulfil similarity criteria by pure chance.

In 2024 Global Meteor Network detected some new meteor showers and contributed data about poorly known new meteor showers. The iota-Centaurids (ICN#919) meteor shower, in other years a minor shower, displayed enhanced activity in 2024 of relatively long duration. The outburst was observed by both the southern hemisphere CAMS networks and the Global Meteor Network in January 2024 (Jenniskens, 2024a). In March 2024 significant activity of beta-Tucanids was detected by the CAMS and GMN video camera networks (Jenniskens, 2024b). On 2024, April 27, a very short duration meteor shower was detected by GMN in the constellation of Hercules (Vida and Šegon, 2024). The GMN radiant plot for 2024, July 3–4 showed a new radiant source in the constellation of Fornax (Šegon et al., 2024a). A new shower was recorded during the first weeks of August 2024 (Jenniskens, 2024c). Another New meteor shower was detected in Cassiopeia on 4 September 2024 (Šegon et al., 2025a). Few weeks later on 23–24 September, again a new meteor shower was discovered in Ursa Minor (Šegon et al., 2025b). Finally, a new meteor shower was detected in Lyra on 26–27 October (Šegon et al., 2025c).

More information and detailed documentation about meteor showers can be found in the new reference work "Atlas of Earth's Meteor Showers" that appeared in October 2023 (Jenniskens, 2023).

The main goal of the GMN, not to let any meteor shower activity pass unnoticed is being achieved. Whenever some unexpected meteor activity occurs, the Global Meteor Network has good chances to cover it.

Acknowledgment

[26] https://creativecommons.org/licenses/by/4.0/

Martin, John Yules, John Burrin, Jon Bursey, Jonathan Alexis Valdez Aguilar, Jonathan Eames, Jonathan Mackey, Jonathan Whiting, Jonathan Wyatt, Jonathon Kambulow, Jorge Augusto Acosta Bermúdez, Jorge Oliveira, Jose Carballada, Jose Galindo Lopez, José María García, José-Luis Martín, Josef Scarantino, Josip Belas, Josip Krpan, Jost Jahn, Juan Luis Muñoz, Juergen Neubert, Julián Martínez, Jure Zakrajšek, Jürgen Dörr, Jürgen Ketterer, Justin Zani, Karen Smith, Karl Browne, Kath Johnston, Kees Habraken, Keith Maslin, Keith Biggin, Keith Christie, Kelvin Richards, Ken Jamrogowicz, Ken Lawson, Ken Gledhill, Ken Kirvan, Ken Whitnall, Kevin Gibbs-Wragge, Kevin Morgan, Kevin Faure, Klaas Jobse, Korado Korlević, Kyle Francis, Lachlan Gilbert, Larry Groom, Laurent Brunetto, Laurie Stanton, Lawrence Saville, Lee Hill, Lee Brady, Leith Robertson, Len North, Les Rowe, Leslie Kaye, Lev Pustil'Nik, Lexie Wallace, Lisa Holstein, Llewellyn Cupido, Logan Carpenter, Lorna McCalman, Louw Ferreira, Lovro Pavletić, Lubomir Moravek, Luc Turbide, Luc Busquin, Lucia Dowling, Luciano Miguel Diniz, Ludger Börgerding, Luis Fabiano Fetter, Luis Santo, Maciej Reszelsk, Magda Wisniewska, Manel Colldecarrera, Marc Corretgé Gilart, Marcel Berger, Marcelo Domingues, Marcelo Zurita, Marcio Malacarne, Marco Verstraaten, Marcus Rigo, Margareta Gumilar, Marián Harnádek, Mariusz Adamczyk, Mark Fairfax, Mark Gatehouse, Mark Haworth, Mark McIntyre, Mark Phillips, Mark Robbins, Mark Spink, Mark Suhovecky, Mark Williams, Mark Ward, Mark Bingham, Mark Fechter, Marko Šegon, Marko Stipanov, Marshall Palmer, Marthinus Roos, Martin Breukers, Martin Richmond-Hardy, Martin Robinson, Martin Walker, Martin Woodward, Martin Connors, Martin Kobliha, Martyn Andrews, Mary Waddingham, Mary Hope, Mason McCormack, Mat Allan, Matej Mihelčić, Matt Cheselka, Matt McMullan, Matthew Howarth, Matthew Finch, Max Schmid, Megan Gialluca, Mia Boothroyd, Michael Cook, Michael Mazur, Michael O'Connell, Michael Krocil, Michael Camilleri, Michael Kennedy, Michael Lowe, Michael Atkinson, Michał Warchoł, Michel Saint-Laurent, Mielke Sarkol, Miguel Diaz Angel, Miguel Preciado, Mike Breimann, Mike Hutchings, Mike Read, Mike Shaw, Mike Ball, Mike Youmans, Milan Kalina, Milen Nankov, Miles Eddowes, Minesh Patel, Miranda Clare, Mirjana Malarić, Muhammad Luqmanul Hakim Muharam, Murray Forbes, Murray Singleton, Murray Thompson, Myron Valenta, Nalayini Brito, Nawaz Mahomed, Ned Smith, Nedeljko Mandić, Neil Graham, Neil Papworth, Neil Waters, Neil Petersen, Neil Allison, Nelson Moreira, Neville Vann, Nial Bruce, Nicholas Hill, Nicholas Ruffier, Nick Howarth, Nick James, Nick Moskovitz, Nick Norman, Nick Primavesi, Nick Quinn, Nick Russel, Nick Powell, Nick Wiffen, Nicola Masseroni, Nigel Bubb, Nigel Evans, Nigel Owen, Nigel Harris, Nigen Harris, Nikola Gotovac, Nikolay Gusev, Nikos Sioulas, Noah Simmonds, Norman Izsett, Olaf Jakubzik Reinartz, Ole Alexander, Ollie Eisman, Pablo Canedo, Pablo Domingo Escat, Paraksh Vankawala, Pat Devine, Patrick Franks, Patrick Poitevin, Patrick Geoffroy, Patrick Onesty, Patrik Kukić, Paul Cox, Paul Dickinson, Paul Haworth, Paul Heelis, Paul Kavanagh, Paul Ludick, Paul Prouse, Paul Pugh, Paul Roche, Paul Roggemans, Paul Stewart, Paul Huges, Paul Breck, Paul Volman, Paul Jenkinson, Pedro Augusto de Jesus Castro, Penko Yordanov, Pete Graham, Pete Lynch, Peter G. Brown, Peter Campbell-Burns, Peter Davis, Peter Eschman, Peter Gural, Peter Hallett, Peter Jaquiery, Peter Kent, Peter Lee, Peter McKellar, Peter Meadows, Peter Stewart, Peter Triffitt, Peter Leigh, Peter Felhofer, Péter Molnár, Pető Zsolt, Phil James, Philip Gladstone, Philip Norton, Philippe Schaak, Phillip Wilhelm Maximilian Grammerstorf, Pierre Gamache, Pierre de Ponthière, Pierre-Michael Micaletti, Pierre-Yves Pechart, Pieter Dijkema, Predrag Vukovic, Przemek Nagański, Radim Stano, Rajko Sušanj, Raju Aryal, Ralph Brady, Raoul van Eijndhoven, Raul Truta, Raul Elias-Drago, Raymond Shaw, Rebecca Starkey, Reinhard Kühn, Reinier Ott, Rembert Melman, Remi Lacasse, Renato Cássio Poltronieri, René Tardif, Richard Abraham, Richard Bassom, Richard Croy, Richard Davis, Richard Fleet, Richard Hayler, Richard Johnston, Richard Kacerek, Richard Payne, Richard Stevenson, Richard Severn, Rick Fischer, Rick Hewett, Rick James, Rick Olupot, Ricky Bassom, Rob Agar, Rob de Corday Long, Rob Saunders, Rob Smeenk, Robert Longbottom, Robert McCoy, Robert Saint-Jean, Robert D. Steele, Robert Veronneau, Robert Peledie, Robert Haas, Robert Kiendl, Robert Vallone, Robert Bungener, Robin Boivin, Robin Earl, Robin Rowe, Robin Leadbeater, Roel Gloudemans, Roger Banks, Roger Morin, Roger Conway, Roland Idaczyk, Rolf Carstens, Roman Moryachkov, Romke Schievink, Romulo Jose, Ron James Jr, Ronal Kunkel, Roslina Hussain, Ross Skilton, Ross Dickie, Ross Welch, Ross Hortin, Russell Jackson, Russell Brunton, Ryan Frazer, Ryan Harper, Ryan Kinnett, Salvador Aguirre, Sam Green, Sam Hemmelgarn, Sam Leaske, Sarah Tonorio, Scott Kaufmann, Sebastiaan de Vet, Sebastian Klier, Seppe Canonaco, Seraphin Feller, Serge Bergeron, Sergio Mazzi, Sevo Nikolov, Simon Cooke-Willis, Simon Holbeche, Simon Maidment, Simon McMillan, Simon Minnican, Simon Parsons, Simon Saunders, Simon Fidler, Simon Oosterman, Simon Peterson, Simon lewis, Simon Lewis, Simon van Leverink, Simon Andersson, Slava Ilyin, Sofia Ulrich, Srivishal Sudharsan, Stacey Downton, Stan Nelson, Stanislav Korotkiy, Stanislav Tkachenko, Stef Vancampenhout, Stefan Frei, Stephane Zanoni, Stephen Grimes, Stephen Nattrass, Stephen M. Pereira, Steve Berry, Steve Bosley, Steve Carter, Steve Dearden, Steve Homer, Steve Kaufman, Steve Lamb, Steve Rau, Steve Tonkin, Steve Trone, Steve Welch, Steve Wyn-Harris, Steve Matheson, Steve Daniels, Steven Shanks, Steven Tilley, Stewart Doyle, Stewart Ball, Stuart Brett, Stuart Land, Stuart McAndrew, Sue Baker Wilson, Sylvain Cadieux, Tammo Jan Dijkema, Ted Cline, Terry Pundiak, Terry Richardson, Terry Simmich, Terry Young, Theodor Feldbaumer, Thiago Paes, Thilo Mies, Thomas Blog, Thomas Schmiereck, Thomas Stevenson, Thomas Duff, Tihomir Jakopčić, Tim Burgess, Tim Claydon, Tim Cooper, Tim Gloudemans, Tim Havens, Tim Polfliet, Tim Frye, Tioga Gulon, Tobias Westphal, Tobias Hinse, Tom Warner, Tom Bell, Tommy McEwan, Tommy B. Nielsen, Torcuill Torrance, Tosh White, Tracey Snelus, Travis Shao, Trevor Clifton, Ubiratan Borges, Urs

References

Dijkema T. J. (2022). "Visualizing meteor ground tracks on the meteor map". *eMetN Meteor Journal*, **7**, 73–75.

Drummond J. D. (1981). "A test of comet and meteor shower associations". *Icarus*, **45**, 545–553.

Gural P. and Šegon D. (2009). "A new meteor detection processing approach for observations collected by the Croatian Meteor Network (CMN)". *WGN, the Journal of the IMO*, **37**, 28–32.

Harman E., Eschman P., Massey B., and Olivera W. (2023). "Using GUI RMS on Linux to support multiple cameras". *eMetN Meteor Journal*, **8**, 185–196.

Jenniskens P., Baggaley J., Crumpton I., Aldous P., Pokorny P., Janches D., Gural P. S., Samuels D., Albers J., Howell A., Johannink C., Breukers M., Odeh M., Moskovitz N., Collison J., Ganju S. (2018). "A survey of southern hemisphere meteor showers". *Planetary and Space Science*, **154**, 21–29.

Jenniskens P., Jopek T.J., Janches D., Hajduková M., Kokhirova G.I., Rudawska R. (2020). "On removing showers from the IAU Working List of Meteor Showers". *Planetary and Space Science*, **182**, id. 104821.

Jenniskens P. (2023). Atlas of Earth's Meteor Showers. Elsevier, USA, ISBN: 978-0-443-23577-1, 824 pages.

Jenniskens P. (2024a). "Enhanced iota-Centaurids (ICN#919) activity in 2024". *eMetN Meteor Journal*, **9**, 53–55.

Jenniskens P. (2024b). "Enhanced activity of the beta-Tucanids (BTU, #108)". *eMetN Meteor Journal*, **9**, 159–160.

Jenniskens P. (2024c). "2024 Perseid-season meteor outburst with a radiant in Capricorn". *eMetN Meteor Journal*, **9**, 286–287.

Jopek T. J. (1993). "Remarks on the meteor orbital similarity D-criterion". *Icarus*, **106**, 603–607.

Jopek T. J. and Jenniskens P. M. (2011). "The Working Group on Meteor Showers Nomenclature: A History, Current Status and a Call for Contributions". In Meteoroids: The Smallest Solar System Bodies, *Proceedings of the Meteoroids Conference* held in Breckenridge, Colorado, USA, May 24-28, 2010. Edited by W.J. Cooke, D.E. Moser, B.F. Hardin, and D. Janches, NASA/CP-2011-216469., 7–13.

Jopek T. J. and Kaňuchová Z. (2017). "IAU Meteor Data Center - the shower database: A status report". *Planetary and Space Science*, **143**, 3–6.

Kalina M. (2024). "Meteorview – new meteor visualizing tool for the Global Meteor Network". *eMetN Meteor Journal*, **9**, 406–409.

McIntyre M. (2024). "The earth-grazing meteor of July 2024". *eMetN Meteor Journal*, **9**, 373–378.

Moorhead A. V., Clements T. D., Vida D. (2020). "Realistic gravitational focusing of meteoroid streams". *Monthly Notices of the Royal Astronomical Society*, **494**, 2982–2994.

Mroz E. J. (2021). "Optimizing Camera Orientation for the New Mexico Meteor Array". *eMetN Meteor Journal*, **6**, 562–567.

Neslušan L., Poručan V., Svoreň J., Jakubík M. (2020). "On the new design othe IAU MDC portal". *WGN, Journal of the International Meteor Organization*, **48**, 168–169.

Roggemans P., Cambell-Burns P., McIntyre M., Šegon D. and Vida D. (2023). "Global Meteor Network report 2022". *eMetN Meteor Journal*, **8**, 77–98.

Roggemans P., Campbell-Burns P., Kalina M., McIntyre M., Scott J. M., Šegon D., Stano R., Vida D. (2024). "Global Meteor Network report 2023". *eMetN Meteor Journal*, **9**, 56–89.

Roggemans P., Vida D., Scott J.M., Jenniskens P., Šegon D., and Rollinson D. (2024). "First observed meteors from comet 46P/Wirtanen (lambda-Sculptorids, LSC)". *eMetN Meteor Journal*, **9**, 6–14.

Scott J. M., Vida D., Behan D., Boothroyd M. R., Burgin D. L., Grieg D., McKellar P., Palmer M. C., Richardson T., Rowe J., Šegon D., Stayte J., Stevenson T., Wang T., Weterings J., Wyn-Harris S. (2024). "New Zealand's meteor camera network leads to recovery of the Tekapo/Takapō meteorite". *eMetN Meteor Journal*, **9**, 155–158.

Šegon D., Vida D., Roggemans P., Rollinson D., Scott J. M. (2024a). "New meteor shower in Fornax". *eMetN Meteor Journal*, **9**, 279–285.

Šegon D., Vida D., Roggemans P. (2025a). "New meteor shower in Cassiopeia, 4 September 2024". *eMetN Meteor Journal*, **10**, 5–11.

Šegon D., Vida D., Roggemans P. (2025b). "New meteor shower in Ursa Minor, 23–24 September 2024". *eMetN Meteor Journal*, **10**, 12–19.

Šegon D., Vida D., Roggemans P. (2025c). "New meteor shower in Lyra, 26–27 October 2024". *eMetN Meteor Journal*, **10**, 22–26.

Southworth R. R. and Hawkins G. S. (1963). "Statistics of meteor streams". *Smithson. Contrib. Astrophys.*, **7**, 261–286.

Vida D., Zubović D., Šegon D., Gural P. and Cupec R. (2016). "Open-source meteor detection software for low-cost single-board computers". In: Roggemans A. and Roggemans P., editors, *Proceedings of the International Meteor Conference*, Egmond, the Netherlands, 2-5 June 2016. International Meteor Organization, pages 307–318.

Vida D., Gural P., Brown P., Campbell-Brown M., Wiegert P. (2020a). "Estimating trajectories of meteors: an observational Monte Carlo approach - I. Theory". *Monthly Notices of the Royal Astronomical Society*, **491**, 2688–2705.

Vida D., Gural P., Brown P., Campbell-Brown M., Wiegert P. (2020b). "Estimating trajectories of meteors: an observational Monte Carlo approach - II. Results". *Monthly Notices of the Royal Astronomical Society*, **491**, 3996–4011.

Vida D., Šegon D., Gural P. S., Brown P. G., McIntyre M. J. M., Dijkema T. J., Pavletić L., Kukić P., Mazur M. J., Eschman P., Roggemans P., Merlak A., Zubrović D. (2021). "The Global Meteor Network – Methodology and first results". *Monthly Notices of the Royal Astronomical Society*, **506**, 5046–5074.

Vida D., Blaauw Erskine R. C., Brown P. G., Kambulow J., Campbell-Brown M., Mazur M. J. (2022). "Computing optical meteor flux using global meteor network data". *Monthly Notices of the Royal Astronomical Society*, **515**, 2322–2339.

Vida D., Šegon D. (2024). "New shower in Hercules". *eMetN Meteor Journal*, **9**, 161–164.

Zubović D., Vida D., Gural P. and Šegon D. (2015). "Advances in the development of a low-cost video meteor station". In: Rault J.-L. and Roggemans P., editors, *Proceedings of the International Meteor Conference*, Mistelbach, Austria, 27-30 August 2015. International Meteor Organization, pages 94–97.

A small Draconid outburst on October 8, 2024

Koen Miskotte

Dutch Meteor Society
`k.miskotte@upcmail.nl`

A Draconid outburst has been observed by visual meteor observers. Peak activity occurred around $\lambda_\odot$ = 191.12° with a maximum ZHR of 18 ± 6. These results nicely match the values found by the CMOR radar and the GMN video network.

1   Introduction

The Draconids are well-known from the large meteor storms of 1933 and 1946. The Draconid storm from 1933 was observed by the author's father-in-law (Dirk Teunissen) on his way home from school between Harderwijk and Ermelo. The meteor shower has since shown regular outbursts with ZHR values between 20 and 700. The last outbursts were in 2011 (Langbroek, 2011; Miskotte, 2012) and (Vandeputte, 2018; Miskotte, 2018; Miskotte, 2019). The one from 2011 showed multiple peaks that could be linked to a number of dust trails (Miskotte, 2012). In 2018 there was more of a "capped" peak or plateau with the ZHR fluctuating around 150 for a number of hours (Miskotte, 2019). All these outbursts were related to the perihelion of the parent body of the Draconids, the comet 21P/Giacobini-Zinner. Next year on March 25, this comet will be in perihelion again. The annual activity of the Draconids is not very significant, both visual observers and the video networks hardly see any Draconids then.

This year some extra activity was expected on October 8 caused by two dust trails of 21P/Giacobini-Zinner from 1852 and 1859. Both Peter Jenniskens and Jéremy Vaubaillon predicted times on October 8, 2024 roughly between 6^h and 7^h UT (Rendtel, 2024). Because these were old dust trails, both astronomers did not make a prediction for the expected ZHR values.

2   Draconid outburst?

As early as October 8 during the day, Pierre Martin from Canada reported his experiences to the author via messenger:

"*This past night October 7–8, I was out observing from late evening until early morning and not only saw a bright and stunning Aurora display, but also some decent Draconids activity! A minor outburst of low-level activity occurred with a few members visible every hour. It was easily the more active meteor source during the night. It is the most Draconids that I've seen in one night after the 2018 outburst. I did not observe a noticeable enhancement*

around the times that Jenniskens and Vaubaillon predicted the old dust trails but by then the radiant was very low. My observations were also quite "affected" by a brilliant aurora display, forcing me at times to meteor observe closer to the zenith or towards the western sky."

On October 12, the Draconid outburst observed by the Global Meteor Network was reported in CBET 5456 by D. Vida, A. Egal, P. Brown, and M. Campbell-Brown, University of Western Ontario; and W. Cooke and D. Moser, Meteoroid Environment Office, NASA (Vida et al., 2024). The outburst peaked with a ZHR of 15.7 ± 1.4 at solar longitude 195.08 ± 0.05 degrees (October 8, 2024 at 05^{h}15^m UT ± 1^h). The *ZHR* was calculated assuming a mass index of s = 2.0 and a population index r = 2.5. The total period of enhanced activity lasted about 10 hours. How to calculate the ZHR and flux from video data is published in (Vida et al., 2022). The well-known CMOR meteor radar also recorded this faint peak around solar longitude 195.133 ± 0.04 degrees. Preliminary modeling suggests that the outburst may have been caused by a dust trail ejected by comet 21P/Giacobini-Zinner in 1900.

The CAMS network has also clearly recorded more Draconids than normal.

3   Visual observations

As written, Pierre Martin reported all his experiences to the author. A few weeks later, all Draconid data uploaded to the IMO website was retrieved. In total, 7 observers observed the Draconids. These were *Pierre Martin* (Canada), *Jürgen Rendtel* (Germany), *Ina Rendtel* (Spain), *William Godley* (Oklahoma, US), *Ivan Sergey* (Belarus), *Wesley Stone* (Oregon, US) and the author (the Netherlands). Some observers made the following comments:

"*Saw a Draconid shoot from N to S while out letting our pup do his business, so sat out for 30 minutes in case something special might be happening. A couple more made a showing, but nothing dramatic so tiredness and work the next day called me back into the house. William Godley*".
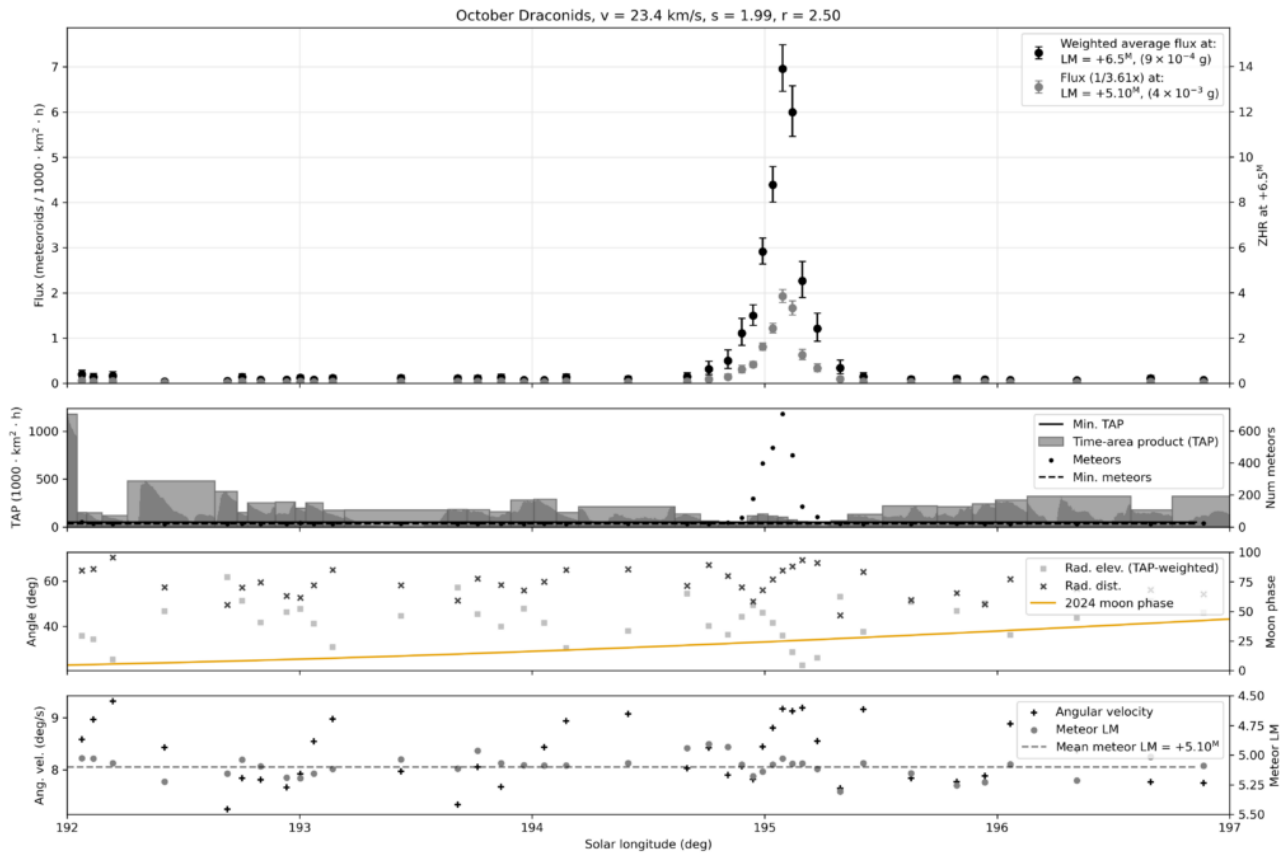
Figure 1 – ZHR and Draconid flux between $\lambda_{\odot}$ = 192–197 (Source: GMN[27]).

"*I got a bit of a late start as there was a decent auroral display early on. By the time I started counting, the aurora had settled down to a diffuse red glow in the northeast. Draconids were prominent and bright, especially early. Poor horizon elevation and aurora to the east, so I centered my view to the northwest and west, forsaking any shower associations of delta Aurigids or early Orionids*. Wesley Stone".
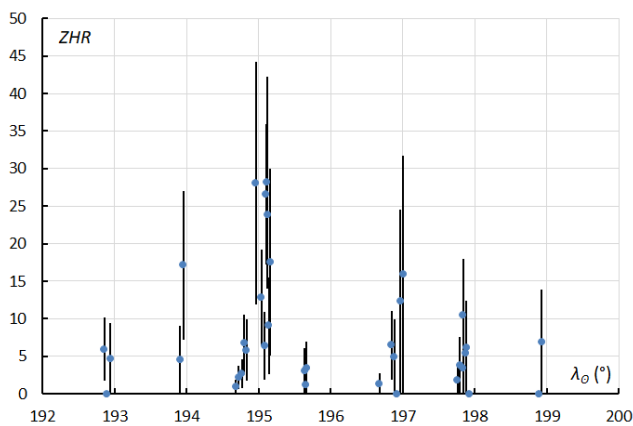
Figure 2 – All individual ZHRs of all observers. It is remarkable that also a few days before and after the maximum ZHR values between 2 and 10 are found. This concerns mostly observations at very low radiant position where for example one Draconid in an hour produces a ZHR of 5 or more. This graph therefore says little about the activity itself. Note: this ZHR values have not been corrected for zenith attraction.

In total, all these observers counted 65 Draconids. And taking into account that part of the data was obtained with low radiant angles below 25 degrees, this makes it a rather difficult analysis. To illustrate this, *Figure 2* shows all individual ZHR values of all Draconid observations. Only for the period of October 8, 2024 between 03^h45^m and 07^h45^m UT, the population index *r* was determined based on 52 Draconids: *r*[0:5] 2.36 ~ 0.32 (Steyaert, 1981). For the period outside this period, a population index *r* of 2.50 was used. The ZHR formula used is:

$$ZHR = \frac{n \cdot r^{6.5-lm}}{(\sin h)^{\gamma} \cdot C_p \cdot T_{eff}}$$

In large analyses where a lot of data is processed, certain requirements are imposed on the data. These requirements are:

- Reliable C_p determination;
- Minimum limiting magnitude rounded off 5.9;
- A minimum radiant height of rounded off 25 degrees.

The problem is that if we apply these rules to the few observations of the Draconids 2024, there is far too little data left to calculate with. That is why the standard requirements were adjusted so that more data remained to analyze.

- The minimum radiant heights between 7 October 19^h UT and 8 October 8^h UT are set at 10 degrees.

Minimum radiant heights before and after the aforementioned period are 20 degrees;

- If known, the C_p was included in the calculations, otherwise $C_p = 1.0$ was used;
- Limiting magnitude at least 5.5.

In the case of overlapping periods, the *ZHR* was determined using a weighted average. Because the Draconids have a very low geocentric velocity and the observations were often performed at low radiant positions, zenith attraction was taken into account in the *ZHR* calculations. Zenith attraction is an effect that mainly occurs with slow meteors. Due to the gravitational pull of the Earth, the direction and speed at which the meteor approaches the Earth changes. This also changes the position of the radiant, which then becomes somewhat higher. See also *Figure 3* (Rendtel, 2022–2024). Therefore, corrections were made for the zenith attraction for all radiant heights (Rendtel, 2022–2024). This results in a considerable difference in outcome, especially for the observations of Pierre Martin who observed with very low radiant positions. The results are in *Figures 4 and 5*, which show clear differences in outcome.
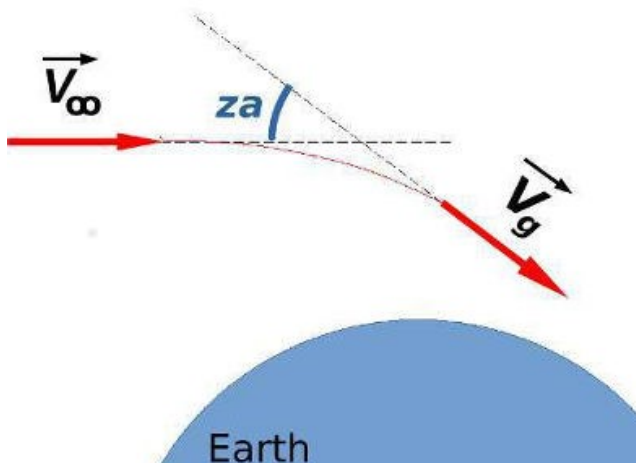
Figure 3 – Zenith attraction (angle *za*) of the radiant of a meteor approaching the Earth with velocity v_∞; the velocity vector changes in direction and magnitude in v_g. Figure is taken from Rendtel (2022–2024).
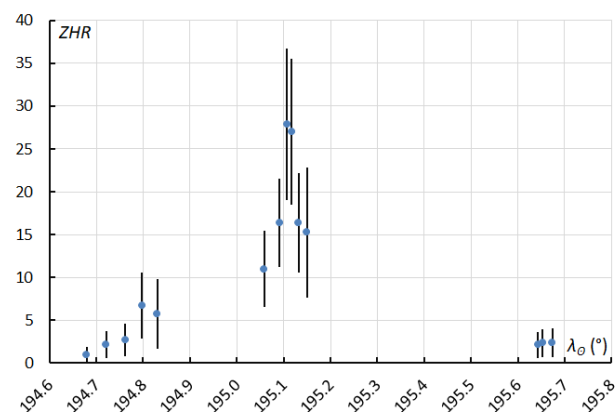
Figure 4 – The ZHR curve based on 5 observers, not corrected for zenith attraction. A maximum ZHR of 28 around solar longitude 195.1°. |
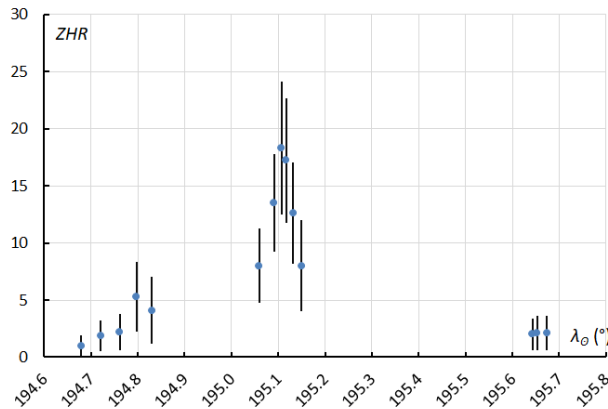
Figure 5 – The final ZHR curve where radiant positions are corrected for zenith attraction. This of course results in lower ZHR values due to the higher radiant heights.

The small Draconid outburst based on observations by *Pierre Martin* and *Wesley Stone* with a peak around $\lambda_\odot = 191.12°$ and a maximum *ZHR* of 18 ± 6 nicely matches the values found by the CMOR radar and the GMN video network. This also gives more confidence in the adjusted procedure followed. The individual *ZHR* values found between *Pierre Martin* and *Wesley Stone* also match well, especially after correcting for zenith attraction.

Also striking is the ascending curve between $\lambda_\odot = 194.6°$ and 194.9°. These are observations by *Ina Rendtel* who observed for 5 hours from northern Spain in the evening of October 7th under pitch-dark conditions (limiting magnitude 6.8). This seems to be a nice run-up to the somewhat higher activity observed by *Pierre Martin* and *Wesley Stone* around $\lambda_\odot = 195.1°$. The ZHR of 2 in the evening of October 8th is based on data from *Ivan Sergey* and the author. The fact that these two observers clearly saw low activity means that the increased activity may have lasted for 24 hours.

4   In summary

All in all, the result is not disappointing considering the small amount of data and the low radiant heights. The maximum time and maximum ZHR found correspond nicely with maximum times and *ZHR* values found by CMOR and GMN. This also gives confidence in the modified method used for this dataset.

Acknowledgments

References

Langbroek M. (2012). "Draconiden 2011 vanuit Dunkelsdorf en Kühlungsborn (noord Duitsland): visueel, met video en LiDAR". *Radiant*, **44**, 5–12.

Miskotte K. (2012). "Draconiden uitbarsting waargenomen, een eerste analyse". *Radiant*, **44**, 69–74.

Miskotte K. (2018). "Draconiden uitbarsting 8/9 oktober 2018!". *Radiant*, **50**, 125–126.

Miskotte K. (2019). "The outburst of the Draconid meteor shower in 2018: an analysis". *eMetN Meteor Journal*, **4**, 74–78.

Rendtel J. (2024). 2024 Meteor Shower Calendar, IMO.

Rendtel J. (2022–2024). Handbook for Meteor Observers, Chapter 7.3.3 The zenith correction factor, pages 140–143.

Steyeart C. (1981). "Populatie indexbepaling : methode en nauwkeurigheid". *Technische Nota nr. 5* VVS Werkgroep Meteoren, september 1981.

Vandeputte M. (2018). "Draconiden uitbarsting!". *Radiant*, **50**, 127.

Vida D., Blaauw Erskine R. C., Brown P. G., Kambulow J., Campbell-Brown M., Mazur M. J. (2022). "Computing optical meteor flux using global meteor network data". *Monthly Notices of the Royal Astronomical Society*, **515**, 2322–2339.

Vida D., Egal A., Brown P., Campbell-Brown M. (2024). 2024 Draconid Meteor Outburst, CBET 5456, Editor: Daniel W.E. Green.

The interesting Perseids of 2024:
An analysis of the visual observations

Koen Miskotte

Dutch Meteor Society
k.miskotte@upcmail.nl

It was possible to detect activity of the Jenniskens filament and/or the old dust trails of Vaubaillon, as well as to detect activity of the "new" peak around $\lambda_{\odot} = 141°$.

1 Introduction

The first quarter moon on August 12 meant that the Perseid maximum would be well observable in 2024. According to the IMO Meteor Shower Calendar (Rendtel, 2024), the Perseids would have their maximum on August 12 between 13h and 16h UT ($\lambda_{\odot} = 140.0°$ and 140.1°). This time is especially favorable for the western American coast and the Pacific. In addition, some extra activity was expected by a number of astronomers. Jérémie Vaubaillon calculated that on August 12 between 4^h and 11^h UT, the Earth would pass through five very old dust trails of comet 109P/Swift-Tuttle (Rendtel, 2024). Four of these were older than 1300 years. According to Peter Jenniskens, the Earth would pass through a weak filament on August 12 around 9^h UT, resulting in a population index r of 1.9 and an extra ZHR of 16 (Jenniskens, 2006).

Finally, the remark that in the years 2018–2022, increased Perseid activity was regularly observed up to 36 hours after the maximum (Jenniskens and Miskotte, 2021; Miskotte, 2019a; 2019b; 2020a; 2020b; 2021; Miskotte and Vandeputte, 2020a; 2020b; Miskotte et al., 2021a; 2021b; Roggemans, 2023). This year, too, this seems to have been the case according to radio observations (Ogawa and Sugimoto, 2024). In this analysis, it was examined whether anything was visually observed of the above-mentioned three phenomena.

2 Data

As in previous analyses, a number of quality requirements are imposed on the observations. These are:

- Reliable C_p determination;
- Minimum limiting magnitude rounded off to 5.9;
- A minimum radiant height of rounded off to 25 degrees;
- Suspiciously high or low ZHR values were removed.

A considerable amount of data was uploaded by the observers to the IMO website. For example, exactly 150 observers counted 20637 Perseids during 562 sessions. All data was checked to the quality requirements described above. A good C_p determination could be made for a few new observers. In the end, almost 72% of the data remained, which were 14852 meteors.

In this analysis, we will only discuss the meteor activity above Europe and America. This has one simple reason: there are hardly any visual observers active on the other continents. *Figure 1* gives a nice overview of the locations where observers were active.

In addition to data from the IMO website, data from one observer who does not report to IMO was also added.

Figure 1 – All locations where observers were active during the Perseids 2024 (source: IMO website).

3 Population index r

Before calculating the ZHR, the population index r must first be calculated. The population index r was calculated according to the method of Steyaert (1981). This resulted in *Table 1* and *Figure 2*.

In *Figure 3* we zoom in on the period from 10 August 2024 20^h UT to 14 August 02^h UT. Added to this are the filament passage expected by Peter Jenniskens at 9^h UT (black cross with predicted $r = 1.9$) and the period in which Jérémie Vaubaillon expected the old dust trails (green line). This clearly shows that the population index r was well below the normal value of 2.2 during the period of both predictions. An indication that the predictions were quite good. Also striking is the very high population index r near $\lambda_{\odot} = 140.67°$ (13 August 2024, 06^h18^m UT) and the sharp drop afterwards to low values. The start of the night of 13–14 August near $\lambda_{\odot} = 141.3°$ also shows very low r values. We will go into this in more detail in the next section.

Table 1 – Population index *r* Perseids 2024 based on the magnitude range –2 to +5.

M	D	T_m UT	$\lambda_\odot$	r	±	M	D	T_m UT	$\lambda_\odot$	r	±
7	29	22.21	126.92	1.91	0.35	8	12	8	139.77	1.77	0.23
7	30	22.46	127.89	2.22	0.37	8	12	9.48	139.83	2.27	0.24
8	3	23.13	131.75	2.34	0.33	8	12	10.55	139.87	1.99	0.23
8	5	23.43	133.67	2.27	0.15	8	12	19.7	140.24	2.11	0.56
8	6	22.93	134.61	2.06	0.18	8	12	20.83	140.28	1.97	0.12
8	8	1.50	135.67	1.77	0.36	8	12	21.53	140.31	2.16	0.08
8	8	23.57	136.56	2.17	0.29	8	12	22.5	140.35	2.12	0.07
8	9	23.40	137.51	2.15	0.18	8	12	23.48	140.39	2.18	0.06
8	10	20.66	138.36	2.16	0.26	8	13	0.44	140.43	2.13	0.07
8	10	21.78	138.40	2.33	0.18	8	13	1.53	140.47	2.02	0.08
8	10	22.59	138.43	2.30	0.18	8	13	2.43	140.51	2.2	0.12
8	10	23.71	138.48	2.29	0.10	8	13	4.3	140.58	2.52	0.29
8	11	0.48	138.51	2.24	0.10	8	13	6.3	140.66	3.03	0.18
8	11	1.18	138.54	2.25	0.10	8	13	8.33	140.74	2.6	0.2
8	11	1.23	138.54	2.34	0.14	8	13	10.33	140.82	1.85	0.22
8	11	5.82	138.72	2.70	0.32	8	13	21.58	141.27	1.66	0.19
8	11	20.91	139.33	2.30	0.16	8	13	22.1	141.29	1.93	0.19
8	11	21.55	139.35	2.15	0.11	8	13	22.59	141.31	2.02	0.14
8	11	22.47	139.39	2.21	0.07	8	13	23.23	141.34	2.02	0.14
8	11	23.54	139.43	2.29	0.06	8	14	0.38	141.39	2.34	0.2
8	12	0.53	139.47	2.09	0.06	8	14	1.48	141.43	2.22	0.24
8	12	1.52	139.51	2.06	0.07	8	14	9	141.73	2.54	0.26
8	12	2.30	139.54	2.06	0.11	8	14	23.3	142.30	2.19	0.12
8	12	3.86	139.60	2.07	0.38	8	15	9.9	142.73	1.97	0.56
8	12	5.97	139.69	1.83	0.36	8	17	1.75	144.32	2.01	0.39
8	12	7.56	139.75	1.82	0.32						
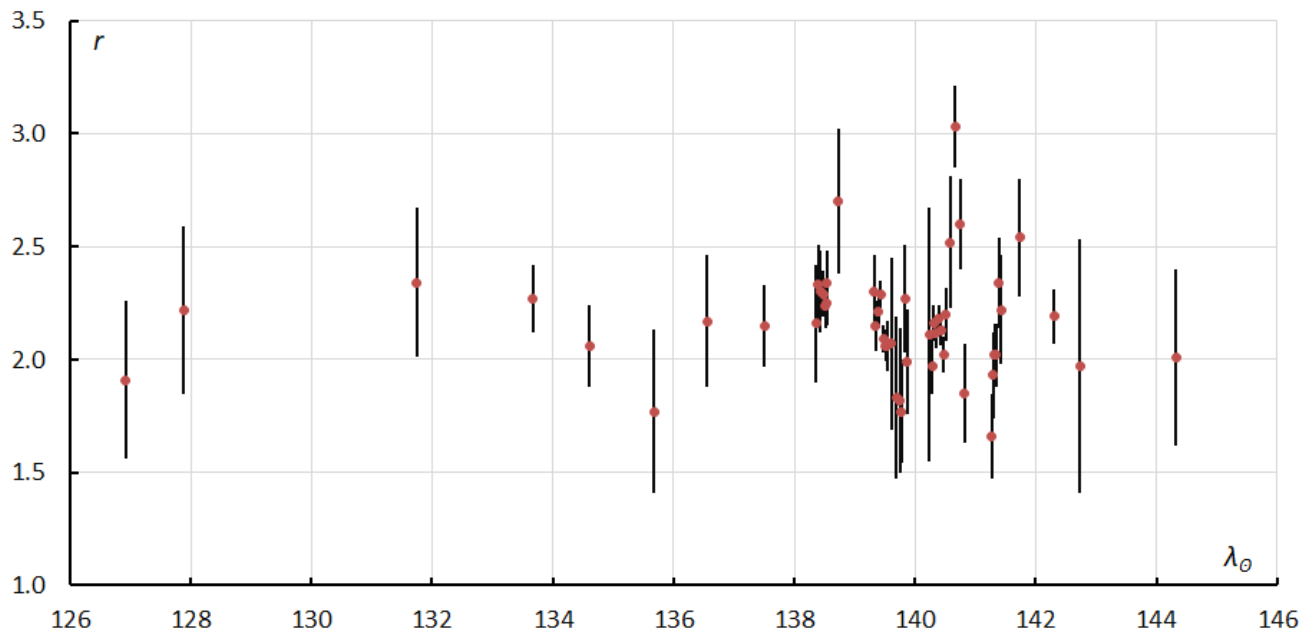
Figure 2 – The population index *r* of the Perseids between July 28 and August 30, 2024.
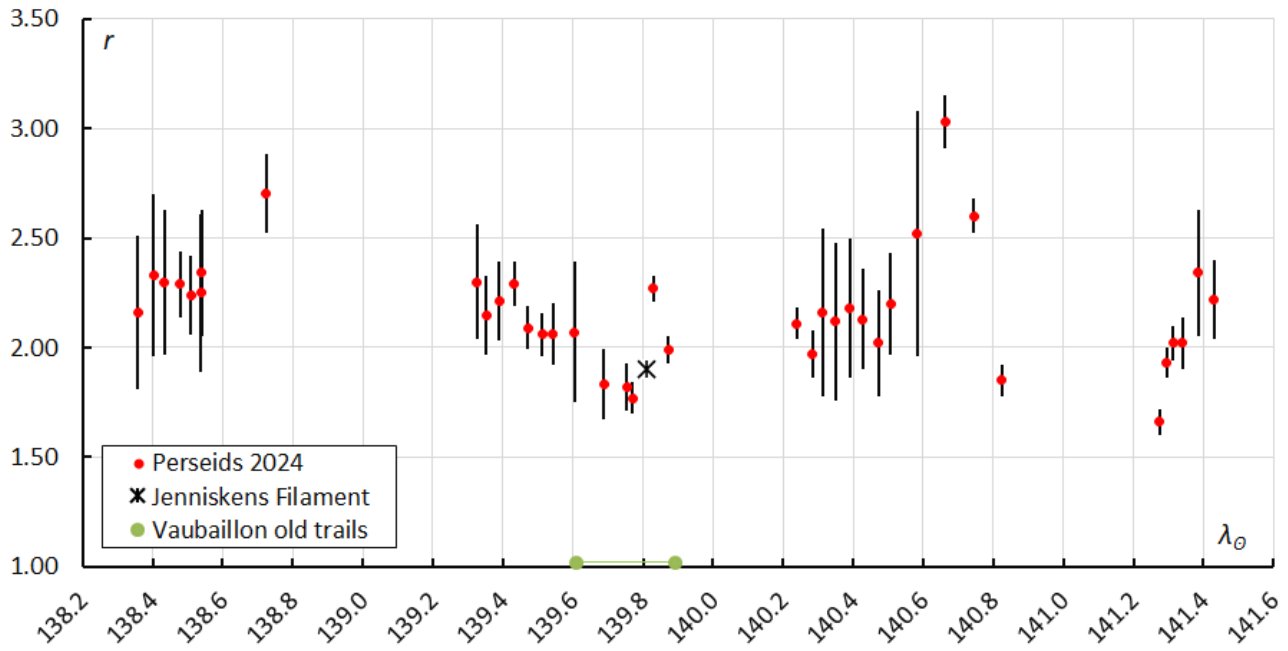
Figure 3 – Population index *r* Perseids 2024 and the expected position of the filament of Peter Jenniskens (2006) and the old dust trails of Jéremie Vaubaillion (Rendtel, 2024).

Table 2 – ZHR of the Perseids in 2024.

Month	Day	T_m	$\lambda_\odot$	periods	PER	ZHR	Dev	OBS
7	15	0.50	112.697	3	2	1.3	0.9	1
7	28	21.95	125.958	9	30	10.3	1.9	5
7	29	22.39	126.931	18	49	8.1	1.2	9
7	30	22.52	127.893	12	30	6.5	1.2	6
7	31	8.50	128.292	3	13	7.8	2.2	1
7	31	21.85	128.823	1	3	9.1	5.3	1
8	1	8.99	129.267	2	7	8.6	3.3	1
8	2	7.25	130.155	1	7	14.3	5.4	1
8	2	23.31	130.788	4	10	5.0	1.6	2
8	3	7.61	131.127	2	11	17.7	5.3	1
8	3	23.32	131.753	10	50	9.9	1.4	3
8	4	6.86	132.054	2	10	13.1	4.1	1
8	4	23.06	132.701	2	18	23.8	5.6	2
8	5	23.36	133.670	29	173	12.5	1.0	9
8	6	23.10	134.619	21	140	16.3	1.4	6
8	7	6.94	134.932	3	28	13.1	2.5	1
8	8	1.50	135.674	3	44	17.1	2.6	1
8	8	7.50	135.913	7	69	19.9	2.4	3
8	8	23.77	136.563	18	163	24.4	1.9	6
8	9	8.26	136.902	3	37	30.2	5.0	2
8	9	23.89	137.527	24	227	22.4	1.5	7
8	10	7.12	137.816	5	58	24.0	3.2	2
8	10	20.92	138.368	9	56	31.7	4.2	7
8	10	21.45	138.389	10	63	33.8	4.3	8
8	10	22.04	138.412	12	86	31.4	3.4	6
8	10	22.41	138.427	12	80	29.2	3.3	7
8	10	23.18	138.458	19	170	33.4	2.6	12
8	10	23.51	138.471	24	236	36.7	2.4	9

Month	Day	T_m	$\lambda_\odot$	periods	PER	ZHR	Dev	OBS
8	11	0.03	138.492	24	250	32.7	2.1	9
8	11	0.49	138.511	23	241	30.7	2.0	10
8	11	0.99	138.531	26	293	29.1	1.7	12
8	11	1.39	138.547	29	215	27.9	1.9	11
8	11	1.94	138.568	14	211	29.6	2.0	7
8	11	2.37	138.586	9	143	32.9	2.8	5
8	11	4.65	138.676	2	39	46.1	7.4	1
8	11	5.82	138.724	2	27	37.6	7.2	1
8	11	6.60	138.755	2	16	41.4	10.4	2
8	11	7.29	138.782	3	22	33.5	7.1	2
8	11	8.19	138.818	3	39	23.5	3.8	2
8	11	21.17	139.337	29	255	53.8	3.4	13
8	11	21.54	139.352	44	415	52.1	2.6	15
8	11	22.03	139.372	53	590	56.6	2.3	16
8	11	22.52	139.391	66	823	59.0	2.1	23
8	11	23.00	139.411	71	981	58.4	1.9	27
8	11	23.49	139.430	79	1170	55.7	1.6	28
8	11	23.91	139.447	69	1069	53.2	1.6	26
8	12	0.48	139.470	64	1108	54.2	1.6	22
8	12	0.93	139.488	57	1113	56.5	1.7	23
8	12	1.42	139.507	42	827	54.0	1.9	16
8	12	1.85	139.525	26	502	50.2	2.2	11
8	12	2.29	139.542	13	270	48.5	3.0	10
8	12	2.96	139.569	7	143	43.8	3.7	4
8	12	3.62	139.595	5	93	45.9	4.8	2
8	12	7.27	139.741	4	54	68.7	9.3	2
8	12	7.96	139.769	5	93	81.8	8.5	2
8	12	8.51	139.791	6	147	94.8	7.8	2
8	12	8.93	139.808	6	148	88.8	7.3	2
8	12	9.44	139.828	4	106	93.5	9.1	2
8	12	10.07	139.853	6	158	81.5	6.5	2
8	12	10.36	139.865	7	199	89.1	6.3	2
8	12	10.95	139.888	5	129	82.5	7.3	1
8	12	20.11	140.255	3	34	111.4	19.1	2
8	12	20.61	140.275	6	76	105.0	12.0	3
8	12	21.14	140.296	25	318	90.3	5.1	14
8	12	21.56	140.313	44	614	87.8	3.5	15
8	12	22.04	140.332	58	807	76.7	2.7	19
8	12	22.47	140.349	63	908	72.7	2.4	20
8	12	23.05	140.372	74	1221	72.0	2.1	21
8	12	23.48	140.390	80	1506	74.8	1.9	27
8	12	23.98	140.409	70	1373	71.0	1.9	22
8	13	0.48	140.429	61	1090	65.6	2.0	20
8	13	0.96	140.449	51	1094	63.0	1.9	19
8	13	1.47	140.469	43	1093	67.9	2.1	19
8	13	1.88	140.485	28	777	68.0	2.4	10
8	13	2.31	140.503	15	442	61.9	2.9	6
8	13	2.78	140.522	7	189	74.1	5.4	4

Month	Day	T_m	$\lambda_\odot$	periods	PER	ZHR	Dev	OBS
8	13	3.62	140.555	3	67	84.4	10.3	2
8	13	4.20	140.578	3	40	72.6	11.5	1
8	13	4.71	140.599	3	47	63.0	9.2	1
8	13	5.04	140.612	3	52	60.4	8.4	1
8	13	5.47	140.629	3	68	68.7	8.3	2
8	13	6.05	140.652	4	115	78.9	7.4	2
8	13	6.54	140.672	5	169	86.5	6.7	2
8	13	7.09	140.694	6	189	89.1	6.5	2
8	13	7.49	140.710	6	193	85.8	6.2	2
8	13	8.74	140.760	5	190	87.8	6.4	3
8	13	9.12	140.775	6	185	80.8	5.9	3
8	13	10.17	140.817	4	108	64.8	6.2	1
8	13	10.50	140.830	4	104	58.9	5.8	1
8	13	10.83	140.844	4	93	50.1	5.2	1
8	13	20.58	141.234	2	16	39.3	9.8	2
8	13	21.62	141.275	6	78	51.3	5.8	4
8	13	22.08	141.293	8	109	58.9	5.6	6
8	13	22.60	141.314	12	123	42.6	3.8	8
8	13	23.09	141.334	15	167	39.4	3.0	10
8	13	23.39	141.346	13	141	40.9	3.4	8
8	13	23.88	141.361	10	106	32.3	3.1	6
8	14	0.42	141.387	9	84	27.5	3.0	5
8	14	1.08	141.414	9	95	31.4	3.2	4
8	14	1.40	141.426	7	81	32.2	3.6	4
8	14	6.71	141.639	1	23	39.8	8.3	1
8	14	7.39	141.666	2	55	48.2	6.5	2
8	14	9.27	141.741	2	25	23.4	4.7	2
8	14	10.17	141.777	1	9	16.5	5.5	1
8	14	11.17	141.817	1	15	20.9	5.4	1
8	14	22.40	142.267	3	11	21.1	6.4	2
8	14	23.41	142.307	5	45	24.1	3.6	4
8	15	0.53	142.352	9	83	25.5	2.8	7
8	15	1.50	142.391	12	120	21.3	1.9	6
8	15	9.42	142.707	4	35	18.6	3.1	3
8	16	1.29	143.343	15	133	20.4	1.8	5
8	16	9.98	143.691	4	15	8.6	2.2	2
8	17	1.75	144.322	3	39	15.1	2.4	1
8	25	20.91	152.793	1	1	2.3	2.3	1
8	26	20.67	153.748	2	4	6.0	3.0	1
8	28	20.83	155.686	2	1	1.4	1.4	1
8	30	22.38	157.682	3	12	8.6	2.5	1
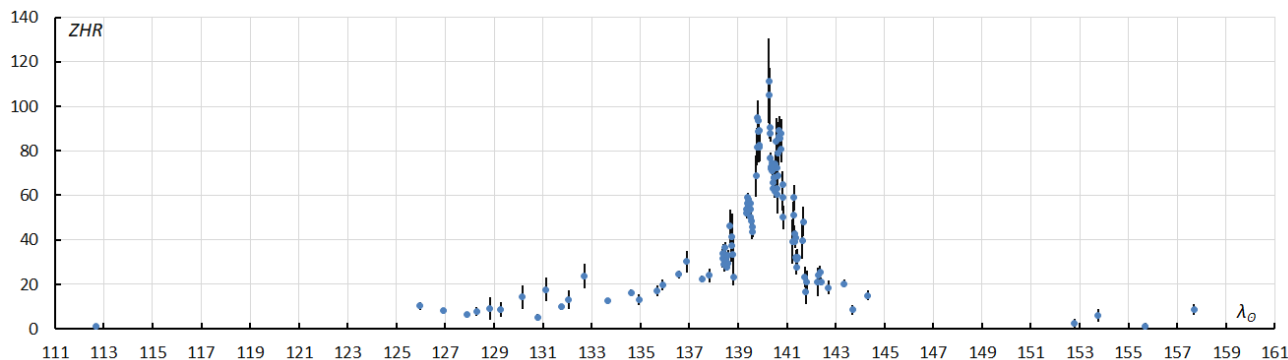
Figure 4 – ZHR Perseids in 2024.

4   Zenital Hourly Rate

To determine the Zenital Hourly Rate (*ZHR*) the meteor counts were used. The formula to calculate the *ZHR* is this:

$$ZHR \; = \; \frac{n \cdot r^{6.5-lm}}{(\sin h)^{\gamma} \cdot C_p \cdot T_{eff}}$$

For the period from 15 July to 10 August (0^h UT) hourly counts were used (0.67 to 2 hours), between 10 and 15 August shorter intervals were used (0.36 to 0.7 hours). This depends somewhat on how the data was supplied. Because some observers supply 30-minute counts, others 10-minute counts. For the latter, these are combined into 30-minute counts.

From all individual *ZHR* values that were calculated, the average *ZHR* was then calculated according to the principle of the weighted average. *Table 2* and *Figure 4* could be obtained from all *ZHR* calculations. The values calculated above were used as population index *r* values, all determined in the magnitude interval –2 to +5. For the single night in which this was not possible, the standard population index *r* for the Perseids (2.2) was used.

At first glance it seems like a normal Perseid year with a normal *ZHR* progression. However, this is more nuanced. We zoom in again to the period 10 to 15 August in Europe and America.

5   August 10–11: Europe and America

For this night we find the *ZHR* values that are normal around that period. Slowly increasing *ZHR*s between 30 and 40.

6   August 11–12: Europe and America

This night the observers in both Europe and America were also "treated" to a beautiful aurora show in addition to the Perseids. Especially the observers in the northern part of Europe saw the phenomenon, but the author also saw the aurora from the south of France.
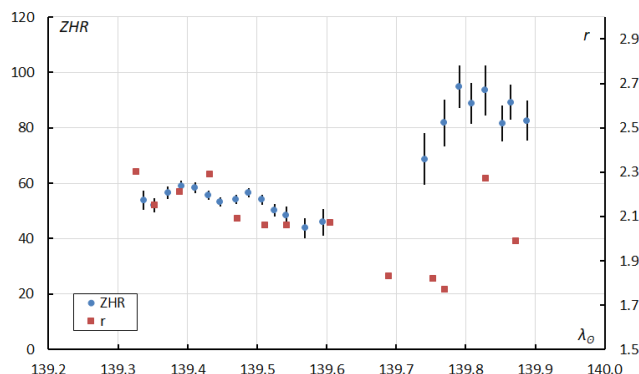
Figure 5 – ZHR and population index *r* of the Perseids on August 11–12, 2024.

Figure 5 shows the zoomed-in *ZHR* graph with the population index *r* added based on the magnitude interval [–2;5]. The Perseids *ZHR* over Europe was fairly stable with an average *ZHR* of 50 and values around the average population index *r*. At the end of the night, the *ZHR* and *r* value dropped slightly. In America it then got dark (from $\lambda_{\odot} = 139.7°$ onwards) and the *ZHR* appeared to be a lot higher. The *ZHR* increased from 70 to 90. Unfortunately, this concerned data from only two experienced observers, but both have been active for a very long time. A striking number of bright meteors resulted in a lower population index *r*, especially on August 12, 2024 between 7^h and 9^h UT respectively between $\lambda_{\odot} = 139.730°$ and $139.810°$. This coincided with the highest *ZHR* values that night (*ZHR* 95). After that, the *ZHR* decreased slightly, but not as fast as the rising edge increased. This may be related to the approaching annual Perseid maximum between solar longitude 140.0° and 140.1°, whereby the decrease was partly undone by the increase in Perseids belonging to the annual maximum. The increasing population index *r* could also be explained by this. Incidentally, the annual maximum was not observed because it ultimately fell after sunrise in America.

Peter Jenniskens gave a filament passage around 9^h UT with an extra *ZHR* of 16 (Rendtel, 2024). With the maximum *ZHR* of 95, this means that the *ZHR* without the filament was 80, a value that you would expect a few hours before the maximum. So, it seems like a consistent story. But in all fairness, we must also admit that the dust trail prediction of Jéremie Vaubaillon also fits in. In particular, the appearance

of bright Perseids (old dust trails) confirmed his prediction. It can be compared with the old dust trail story in 2023 on 12 Aug around 01^h UT, with the old dust trail from 68 BC. It leads to barely an increase in ZHR, but to a clearly lower population index r with a part of the bright Perseids belonging to the old dust trail.

Figure 6 shows the same graph as in *Figure 4*, but now supplemented with the radio ZHR_r curve. From the radio ZHR_r calculated by Hirofumi Sugimoto (Sugimoto,2017; Sugimoto and Ogawa, 2023) there is a peak around solar longitude 139.75° and a second peak around 140.03°. The latter may be the annual maximum, the first the filament of Peter Jenniskens and/or the old dust trails of Jéremie Vaubaillon. The first radio ZHR_r peak did not fall at exactly the same time as the visual peak. This may have to do with the brightness distribution of the meteors, where for example the radio peak consisted of many weak Perseids. But the latter remains speculation of course.

It must be said that the radio observation method is a completely different observation method. The numerical results cannot be compared with each other. The point here is to see whether the shape of the graph from the observed radio activity can be compared with what has been observed visually.
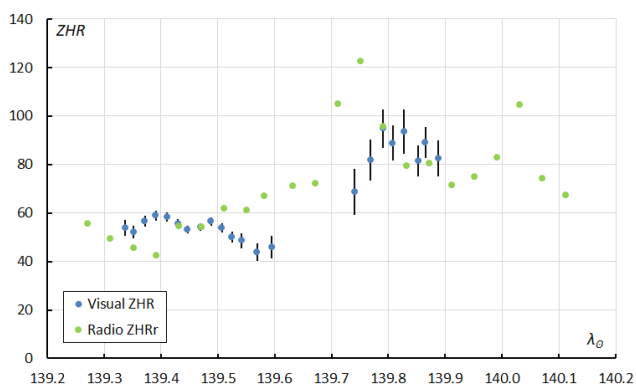
Figure 6 – Perseid visual ZHR and radio ZHR_r between 11 August 2024, 21^h UT and 12 August 2024, 11^h UT. The error bars of the US observers are larger because smaller numbers of meteors were used. The green points are the radio ZHR_r points. The annual maximum of the Perseids is usually between $\lambda_\odot = 140.0°$ and 140.1°.

7 August 12–13, 2024: Europe and America

Also, this night, aurora was visible from a large part of Europe. This night went as you would expect for Europe: decreasing ZHRs from 110 to 60, see *Figure 7*. However, as seen from America the ZHR started to rise again. A weak peak was detected on August 13, 2024 around 07^h–08^h UT (solar longitude ~140.7°) with a ZHR of 90. Maybe this was a recurrence of the peaks that previously occurred between

2018 and 2022? The population index r value behaved rather strangely, from a very high population index $r = 3.0$ a value of 1.8 was reached at the end of the night.
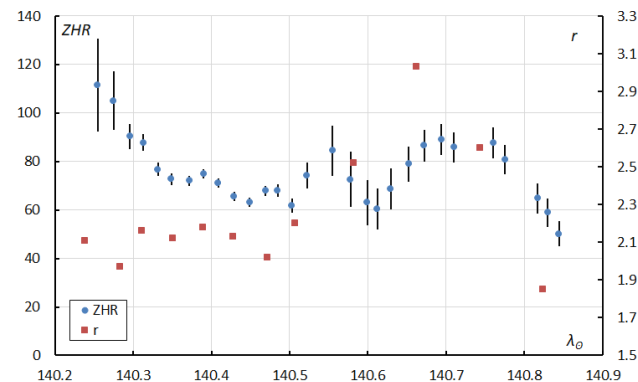
Figure 7 – Population index r and ZHR of the Perseids on August 12–13, 2024
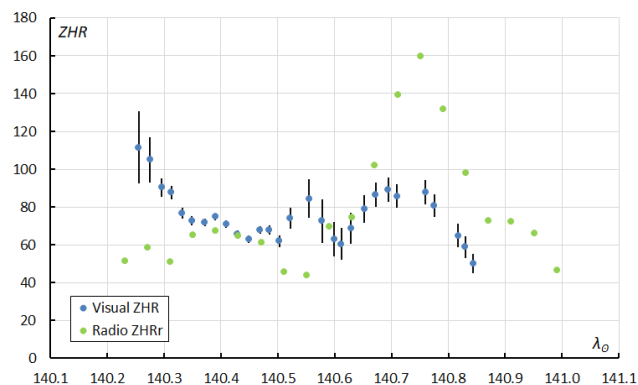
Figure 8 – Visual ZHR and Radio ZHR_r compared.

Radio observations confirmed the peak more clearly than the visual data, see *Figure 8*. This suggests that the peak consisted of fainter Perseids, just like in 2018. Bob Lunsford's observations at the end of the American night showed a low population index r: many bright Perseids. This may be a different structure than the visual and radio peak earlier that night. Of course, this is also speculation. These conclusions are based on observations from only three observers, but all have been active for many years. *Table 3* gives an overview of all years with the peak around $\lambda_\odot = 141°$.

8 August 13–14, 2014: Europe

When it got dark over Europe the population index r was still low, but we do not suggest that it was low the entire period in between. See also *Figure 9*. We simply do not know because there are no observations. It is also striking that the ZHR showed a peak of around 60 around the same time. After that the activity quickly decreased to a normal value of around 40 and a normal population index r. The author saw normal activity during the short clearing halfway through the night.

Table 3 – Comparison of the $\lambda_\odot$ = 141° outbursts of 2018, 2019,2020, 2021, 2022, 2023 and 2024.

	Visual				Radio		Remarks
Year	$\lambda_\odot$	*ZHR*	Pop. Index *r*	Year	$\lambda_\odot$	ZHR_r	
2018	140.935	86 ± 6	r[−2;5] 2.06 ± 0.05	2018	~	~	No outburst in radiodata
2019	~	~	~	2019	141.020	81 ± 4	No visual observations
2020	140.632	80 ± 15	r[−2;5] 2.31 ± 0.28	2020	140.612	84 ± 10	
	140.711	91 ± 16	r[−2;5] 2.49 ± 0.30		140.772	80 ± 6	
	140.765	91 ± 17	r[−2;5] 2.76 ± 0.28				
2021	141.489	195 ± 16	r[−1;5] 2.76 ± 0.22	2021	140.495	220 ± 20	
2022	~	~	~	2022	140.800	80 ± 15	Outburst?
2023	140.820	167 ± 39	r[−2:5] 2.13 ± 0.26	2023	140.820	126 ± 5	
2024	140.694	90 ± 7	r[−2;5] 2.80 ± 0.19	2024	140.750	160 ± 5	
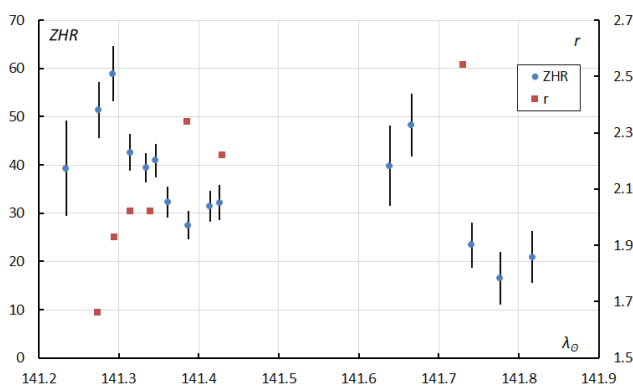
Figure 9 – Population index *r* and *ZHR* of the Perseids on August 13–14, 2024.

9   Summary

2024 brought an interesting Perseid appearance. Thanks to a careful selection of data based on fixed criteria it was possible to detect activity of the Jenniskens filament and/or the old dust trails of Vaubaillon, as well as to detect activity of the "new" peak around $\lambda_\odot$ = 141°.

10 Acknowledgments

References

Jenniskens P. (2006). Meteor showers and their Parent Comets, table 5d, p. 663, Cambridge University Press.

Jenniskens P., Miskotte K. (2021). "Perseid outburst 2021". *eMetN Meteor Journal*, **6**, 460–461.

Miskotte K. (2019a). "Perseïden 2018: een analyse van de visuele waarneemdata". *Radiant*, **41**, 27–35.

Miskotte K. (2019b). "The Perseids in 2018 analysis of the visual data". *eMetN Meteor Journal*, **4**, 135–142.

Miskotte K. (2020a). "Perseids 2020: again, enhanced Perseid activity around solar longitude 141?". *eMetN Meteor Journal*, **5**, 395–397.

Miskotte K. (2020b). "Perseids 2020 revisited". *Radiant*, **42**, 162–163.

Miskotte K. (2021). "Perseids 2020 revisited". *eMetN Meteor Journal*, **6**, 29–30.

Miskotte K., Vandeputte M. (2020a). "Perseïden 2019 Opnieuw een piek in activiteit rond zonslengte 141,0?". *Radiant*, **42**, 100–103.

Miskotte K., Vandeputte M. (2020b). "Perseids 2019: another peak in activity around solar longitude 141.0?". *eMetN Meteor Journal*, **5**, 25–29.

Miskotte K., Sugimoto H., Martin P. (2021a). "The big surprise: a late Perseid outburst!". *eMetN Meteor Journal*, **6**, 517–525.

Miskotte K., Sugimoto H., Martin P. (2021b). "De Perseïden uitbarsting van 14 augustus 2021". *Radiant*, **43**, 51–58.

Ogawa H., Sugimoto H. (2024). "2024 Perseids 2024 by worldwide radio meteor observations"., *eMetN Meteor Journal*, **9**, 350–352.

Rendtel J. (2024) Meteor Shower Calendar 2024, IMO.

Roggemans P. (2023). "Unusual Perseid activity in 2023". *eMetN Meteor Journal*, **8**, 288–289.

Steyeart C. (1981). Populatie indexbepaling: methode en nauwkeurigheid, Technische Nota nr. 5 VVS Werkgroep Meteoren, september 1981.

Sugimoto H. (2017). "The New Method of Estimating ZHR using Radio Meteor observations". *eMetN Meteor Journal*, **2**, 109–110.

Sugimoto H., Ogawa H. (2023). "Perseids 2023 by worldwide radio meteor observations". *eMetN Meteor Journal*, **8**, 285–287.

About spectrograms of meteor echoes at different stages of the radiant position of the Quadrantids 2025 – an AI/ML-investigation

Wilhelm Sicking

Augustin-Wibbelt-Straße 13, 48712 Gescher, Germany
`wil.sicking@gmail.com`

The Quadrantids 2025 were recorded with a new antenna and at a new, low-interference location. The recorded spectrograms were evaluated using Artificial intelligence (AI) / Machine Learning (ML). As in 2024, the data show a notch in the rate and a cluster of jagged meteor echoes around 9^h. The work confirms that the geometric relationships of the meteoroid and the radar cause the notch and jagged echoes.

It was found that a large number of the meteoroids decay according to the same pattern: in the 3D representation used, the head echoes have a bulbous shape shortly before their end and show pulsations. A few of these spectrograms are included in this work. In order to study this effect in more detail, a second meteor receiving system was recently installed. Interesting spectrograms of head echoes were recorded: they show pulsations of various kinds. First results are described in the next article.

1 Introduction

The major showers are particularly suitable for the study of meteor echoes: they provide plenty of echoes and it is known from which direction they come. Head echoes, only trail echoes and head echoes together with a trail echo were recorded. In the literature, the trail echoes are referred to as specular trails. The jagged echoes are created when a meteoroid moves almost parallel to the radar beam (Sicking, 2024b). With these echoes, no or only a weak head echo can be seen in my recordings. These echoes are referred to as non-specular trails. Head echoes are created by reflection from the plasma that directly surrounds the meteoroid and move at approximately the same speed as the meteoroid (Close et al., 2007). In this article, as in 2024, the spectrograms at different stages of the 2025 Quadrantids are examined.

2 Setup

Meteor echoes are recorded on the GRAVES frequency of 143.05 MHz. GRAVES is a high-performance radar for observing satellites and space debris. It is located in France near Dijon. With four planar phased array antennas, it transmits a powerful CW (continuous wave) carrier around the clock. The four antenna arrays transmit one after the other in a southerly direction. According to my own measurements, the switching time is 1.6 s. In the literature, so-called high power large aperture (HPLA) radars were used for investigations into head echoes. The GRAVES transmitter is also, in principle, an HPLA radar. Because the power is concentrated on a narrower beam than with normal HPLA radar systems, a high equivalent isotropically radiated power (EIRP) is obtained, so that this radar can deliver stronger echoes than if the same power were distributed over a large opening angle. One disadvantage, however, is that an echo is overlooked if the system is transmitting in a different direction. However, echoes that are illuminated by side lobes or the back lobe are also

visible. The sensitivity is then of course lower. In this case, dips can be seen in long trail echoes, see *Figure 1 top*.
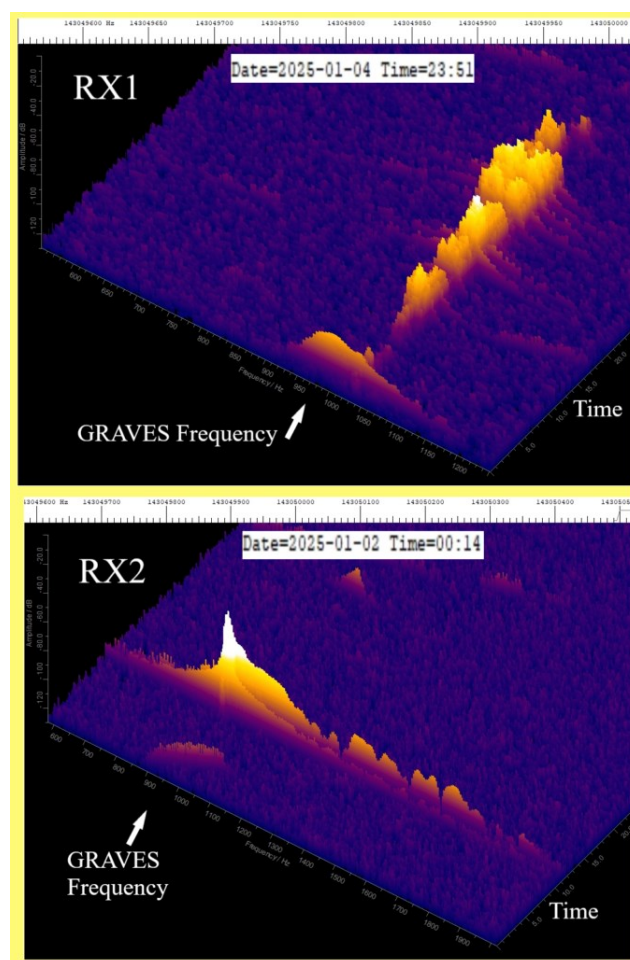
Figure 1 – The figure shows a Spectrum Lab (SL) output from each system. In the upper part, SL is set to record large echoes as completely as possible. The setting below is optimal for long head echoes. A bulge and pulsations are clearly visible. The original Spectrum Lab graphs have been cut off on the right side so that the graphs fit well into eMetN's two-column format.

The same image also shows the GRAVES glitches that are produced by switching the antennas. The head echo was not recorded.

To receive the meteor echoes, I now use a so-called eggbeater antenna. It consists of two loops rotated at 90° to each other and a reflector made of radials. The antenna has a vertical opening angle of 120° and is clockwise circularly polarized. Close to the horizon, this antenna is horizontally polarized. It has proven to be useful for meteor reception of GRAVES echoes, as only a small amount of signal intensity is received from the horizon. In particular, direct reception of the GRAVES carrier is prevented in this way. The antenna is located at the clubhouse of the local association N62 Wüllen of the German Amateur Radio Club at the southern end of the facility, see *Figure 2*.

Figure 2 – Photo of the clubhouse of OV-N62. It is a former NATO radio tower. (Photo: The author) The inset shows the loops of the eggbeater antenna and the moon. The red dot shows the location of the antenna. The building next to the red dot is a bunker from the Cold War era.

A low-noise preamplifier with a frequency range of 140–150 MHz and a noise figure of 0.25 dB is connected directly to the antenna. The preamplifier is connected to the receivers via a 60 m long coaxial cable. I am currently using two identical receiving systems. The receivers are Icom IC-R8600. The antenna signal is split by an antenna splitter. Optocouplers are inserted in the USB cables between the receivers and the PCs. This means that there are no crashes even after very long operating times. Spectrum-Lab (SL) by Wolfgang Buescher (DL4YHF) is used as the recording software. SL generates plots every 20 seconds with the corresponding date and time in the file name, which are later analyzed using machine learning-based software that I developed (Sicking, 2024a; 2024b). The only difference

between the two systems is the settings of Spectrum Lab. One system delivers the data as usual for later evaluation via AI / ML. The focus here is on capturing the trail echoes as completely as possible and also large echoes, see *Figure 1 top*. In the second system, Spectrum Lab is set to record as much of the head echo as possible, see *Figure 1 bottom*.

I trained the neural network used in the summer of 2024. The neural network can detect objects of 4 classes. So far, 880 plots have been labeled. The dataset is estimated to contain up to 3000 spectrograms of artificial stars, backgrounds, meteors, and jagged meteors. The test-train-split is 1:3. For training, I use a gaming PC with a Nvidia graphics card with CUDA cores. Training takes about 90 epochs of 60 s each. I select the best model manually in debug mode and through test runs. The spectrograms for training the jagged echoes mostly come from the Quadrantids 2024. For details see my paper Sicking (2024b).

3   Result and discussion

Figure 3 documents January 3, 2025 and gives an overview of the quality of the recording. The green and red dots represent meteor echoes. The sizes of the echoes are plotted logarithmically. A dip at 9^h a.m., the notch, is visible. The red dots, which appear more frequently around 9^h a.m., represent the jagged echoes. These are echoes that have no head echo because the radar beam and the flight path are almost parallel. Here the radiant of the Quadrantids had an azimuth of 0°.

The green dots represent the normal echoes with head echoes. These arise when the flight path is more or less perpendicular to the radar direction. The satellites and space debris are also logged. That are the light blue dots. Yellow dots are interference or moon echoes. The rough evaluation of the raw data from *Figure 3* is shown in the histograms in *Figure 4*.

The yellow histogram shows the rate and the red histogram shows the rate weighted by the sizes of the meteors. The notch in the red bars in *Figure 4* is more pronounced than in the yellow bars because the perspective, the radar beam here runs parallel to the flight path, makes the echoes near the notch appear smaller than if they were observed further out. At the minima of these two histograms, the light blue histogram of the jagged echoes has a maximum. A more detailed analysis follows in the subsection 3.2. A comparison of the notch with the notch from 2024 (Sicking, 2024b) shows that it is now less pronounced. The reason for this is the omnidirectional antenna used, which captures more echoes from all directions than a directional antenna facing GRAVES. I published a direct comparison between an omnidirectional antenna and a directional antenna in 2022 (Sicking, 2022).
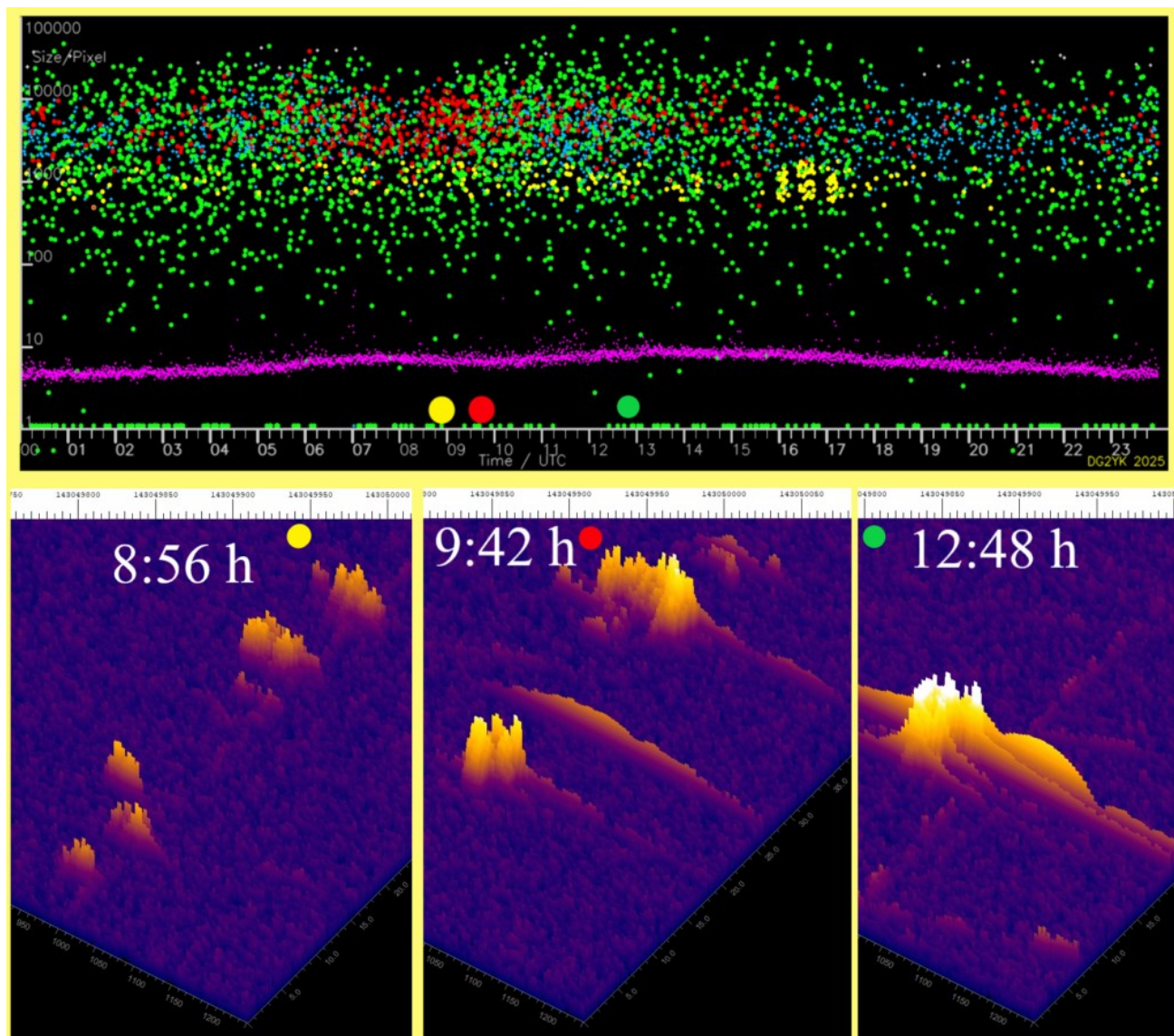
Figure 3 – Measured meteor sizes as a function of time, recorded on January 3, 2025. Each point represents an echo. 3141 echoes were recorded. The green dots represent the normal echoes. The red dots mark the jagged echoes. A decrease in the rate (green dots) and a strong increase in the red dots can be seen at 9^h a.m. The blue dots show the satellite echoes. The yellow dots show detected moon echoes and other interference. The noise floor is entered as a purple trace. In the lower part, typical spectrograms from the indicated times are shown. They are: jagged echoes without head echo, two jagged echoes with little head echo and a normal meteor echo consisting of trail echo, head echo and the GRAVES glitches. The pulsations can be seen on the head echo of the spectrogram from 12^h48^m. Small pulsations are also visible at 9^h42^m.

3.1 About the satellites and AI

The lower histogram in *Figure 4* shows the registered satellites. In the 4320 plots that are recorded daily, there is hardly a single recording without satellites or space debris. Therefore, automatic evaluation without AI / ML seems almost impossible to me. The AI software can distinguish satellites from meteors very well because of their comb-like shape. The distribution over the day has always looked very similar in recent weeks: They always have two maxima at 4^h–5^h a.m. and around 11^h a.m. *Figure 5* shows a typical recording from 11^h44^m a.m. The AI software also recognizes faint echoes, see the satellite echo at the top left. The large satellite echo (score 0.99) also clearly shows the antenna switching. The switching does not lead to a total loss of signal, but only to a weakening of the echo.

3.2 A closer look at the distribution of the jagged echoes and the rates weighted according to the size of the echoes

Figure 6 shows the echoes divided into four classes of different sizes and the percentage of jagged echoes. The small echoes have a secondary maximum at the minimum of the notch. The number of larger meteors decreases. This shows that large echoes now appear smaller in perspective and appear in the class of small echoes. The maximum of the yellow curve at the minimum of the notch is therefore a confirmation of the theory that at an azimuth of 0°, i.e. when a meteoroid moves almost parallel to the radar beam, a decrease in the reflecting surface makes the echoes appear smaller. The notch is now created because the echoes here partially fall below the observation threshold. At this time, the trail is only illuminated from the front. The system registers the jagged echoes, which then show a maximum,

see the red curve in *Figure 6*. Head echoes are not or only weakly visible in this situation, as can be seen in *Figure 3* or (Sicking, 2024b). What is surprising is that the intensity of the jagged echoes is relatively high. The reason for this is probably that when the track is illuminated from the front, the radar beams only see a small surface, while in the depth of the track they encounter many particles.
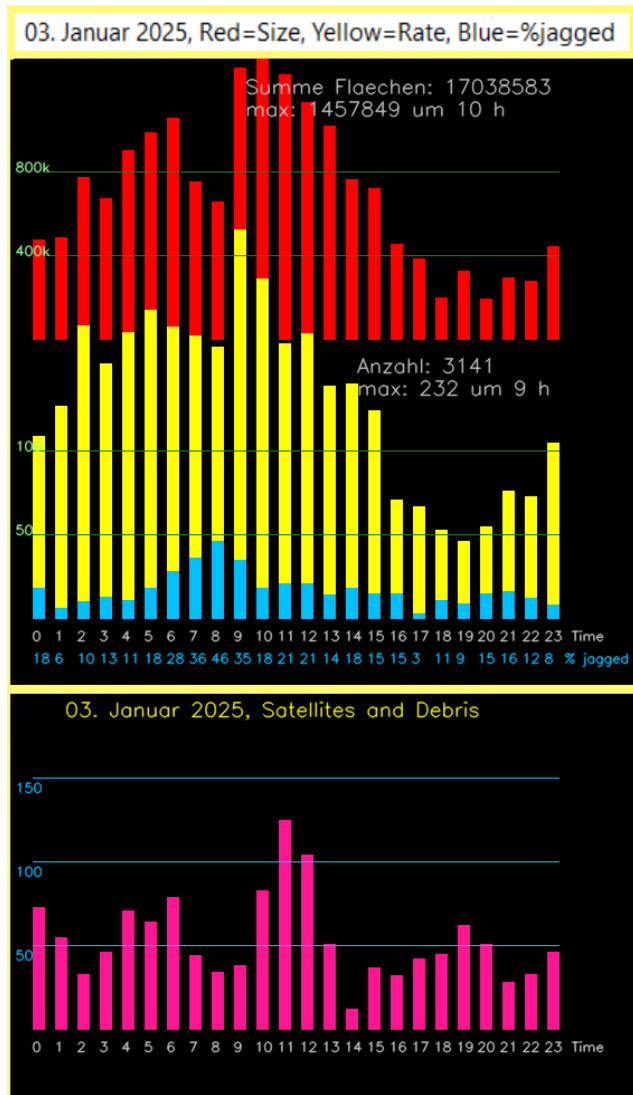
Figure 4 – The yellow histogram shows the rate and the red histogram shows the rate weighted by the size of the meteors. The notch at 9ʰ a.m. is clearly visible. The light blue histogram shows the percentage of jagged echoes. The lower histogram shows the registered satellites.
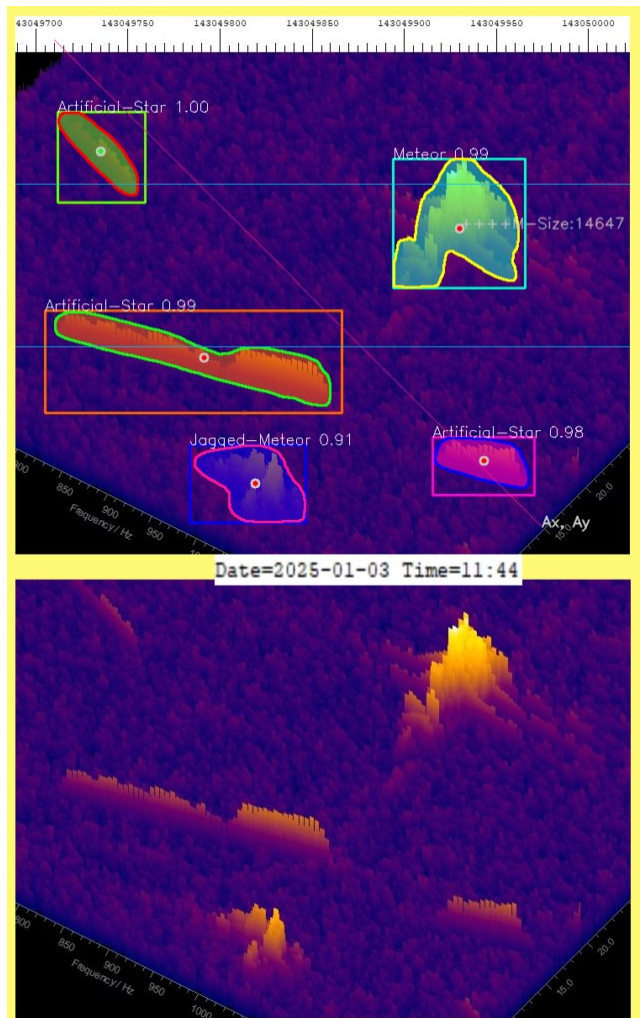
Figure 5 – Spectrum-Lab plot and AI analysis from $11^{h}44^{m}$ a.m. on January 3rd. The figure was created with the debug feature. Since the label are very small, only sections of the original plot were used. The area between the light blue lines is 20 s long. Only this area is evaluated.
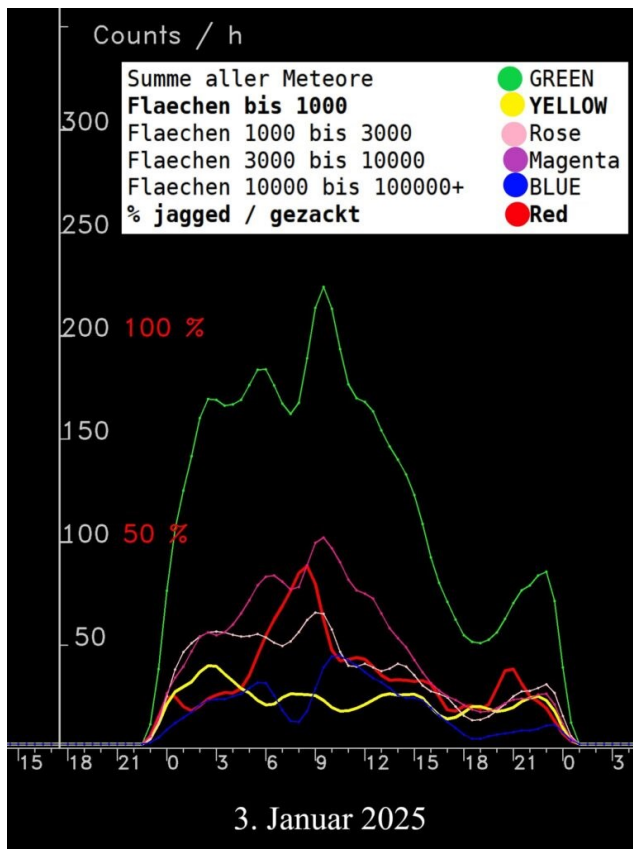
Figure 6 – Meteor rates for different echo sizes and the percentage distribution of jagged echoes from the Quadrantids on January 3, 2025. The blue line represents the rate of large echoes over 10000 pixels, the purple/magenta line shows the medium-sized echoes (3000 to 10,000 pixels), the pink line shows the echoes (1000 to 3000 pixels), and the yellow line shows the small echoes (under 1000 pixels). Finally, the green trace shows the rate of all echoes. The yellow trace (echoes under 1000 pixels) shows a local maximum where the notch and all other meteor sizes have a minimum. The red trace shows the percentage of jagged echoes. This curve shows a maximum approximately where the larger echoes show a local minimum. The curves were smoothed with a fixed Gaussian-like filter with coefficients 0.25, 0.71, 1.0, 0.71 and 0.25.

4   Conclusion

The work shows that the geometric relationships of the meteoroid and the radar cause the notch and the jagged echoes: If the meteoroid moves more or less parallel to the radar beam, jagged echoes and small echoes are created. This then appears to reduce the rate, which then causes the notch in the rate. The more pronounced notch in the rate weighted by the sizes is caused by the fact that large echoes appear smaller.

Acknowledgments

References

Close S., Brown P., Campbell-Brown M., Oppenheim M., Colestocka P. (2007). "Meteor head echo radar data: Mass–velocity selection effects". *Icarus*, **186**, 547–556.

Sicking W. (2022). "Radio observations on the Perseids and some other showers in August and September 2022". *eMetN Meteor Journal*, **7**, 407–410.

Sicking W. (2024a). "Meteor detection using Artificial Intelligence and Machine Learning". *eMetN Meteor Journal*, **9**, 29–36.

Sicking W. (2024b). "About spectrograms of meteor echoes at different stages of the radiant position – an AI/ML-investigation". *eMetN Meteor Journal*, **9**, 103–112.

2D and 3D spectrograms of meteor head echoes that possibly show meteoroid fragmentation

Wilhelm Sicking

Augustin-Wibbelt-Straße 13, 48712 Gescher, Germany
`wil.sicking@gmail.com`

Meteor head echoes were recorded using 2D and 3D spectrograms with the GRAVES radar. Various types of pulsations are visible. According to the literature, fragmentation of the meteoroids and the resulting interference could be the cause. Some rare spectrograms show the decay of the meteoroid below the GRAVES frequency, which is normally seen above or at this frequency. These echoes show pulsations that differ from those of the head echoes. A possible explanation is given. Further studies with improved resolution are planned.

1 Introduction

Head echoes are caused by reflections from the plasma that directly surrounds the meteoroid. The plasma moves at about the same speed as the meteoroid (Close et al., 2007). In the 3D representation used, the newly recorded head echoes have a bulbous shape shortly before their end and show pulsations. Pulsating meteor events were observed with the EISCAT UHF radar system (Kero et al., 2008). The authors postulate that reflections from fragments lead to interference that causes the pulsations. I received the reference to fragmentation of the head echoes from Prof. Asta Pellinen-Wannberg. I asked her whether she knew of any literature on "oscillations" on head echoes.

2 Setup

The setup was described in detail in the previous article (Sicking, 2025). In order to be able to examine the head echoes in detail, one system now records 2D spectrograms, the other system logs the data in the 3D format previously used. The 2D graphic has the advantage that the temporal progression of the head echo can be seen. This means that the 2D spectrogram can be used to determine whether the head echo continues below the GRAVES frequency of 143.05 MHz or whether it is a GRAVES glitch. The speed can also be seen to a certain extent. However, amplitude changes such as the pulsations and relative sizes of the echoes can only be seen in the 3D representation. Both systems have now been set up so that head echoes can be recorded optimally. *Figure 1* shows on the left side a spectrogram in the 3D setting previously used. This means that even large trail echoes can be recorded. The image on the right side is optimal for head echoes.

The GRAVES carrier frequency is marked with red dots. 950 Hz on the scale corresponds to the transmitter frequency of 143.05 MHz. This is the "zero Doppler frequency" (hereinafter referred to as "zero frequency"). Very small echoes, the GRAVES carrier itself or the trail echoes can often be seen at this frequency.

The original Spectrum Lab diagrams have been cropped at the sides to make the figures fit nicely into eMetN's two-column format. The original Spectrum Lab time and date markers have always been used.
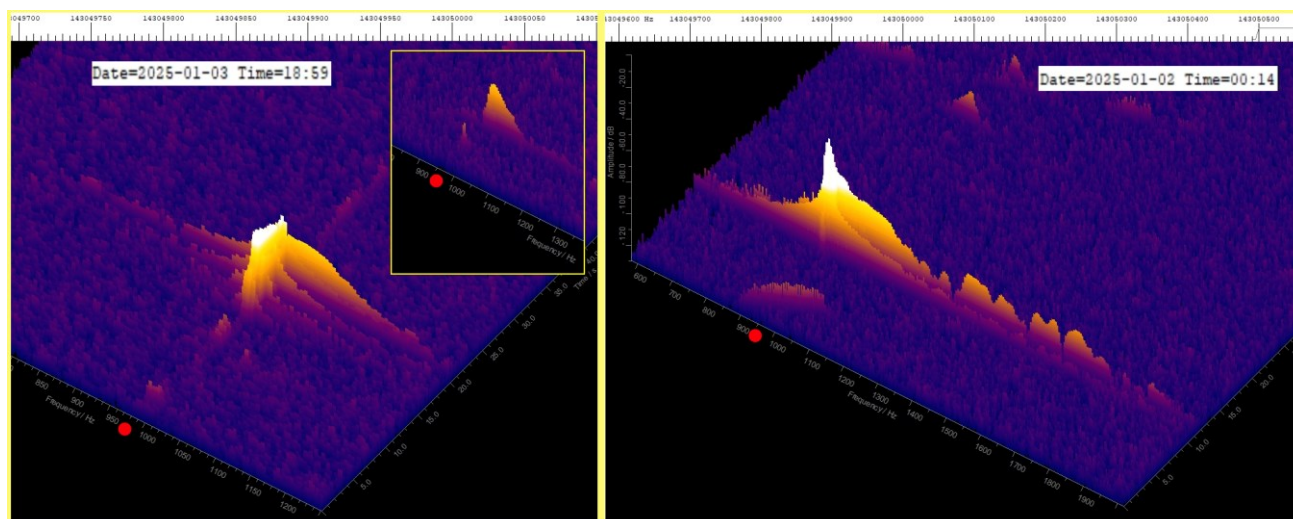
Figure 1 – Spectrograms from January 3, 6ʰ59ᵐ p.m. (left, earlier representation for large trail echoes) and from January 2, 2025, 12ʰ14ᵐ a.m. (right, current representation).
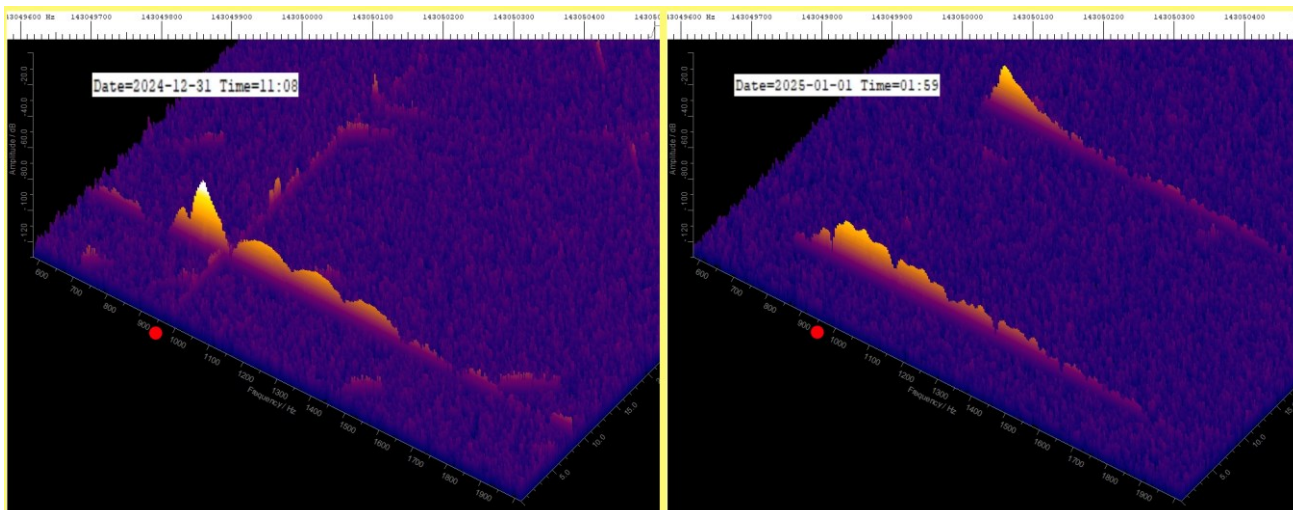
Figure 2 – A head echo from December 31. 2024, 11ʰ08ᵐ and two head echoes from January 1, 2025, 1ʰ59ᵐ.
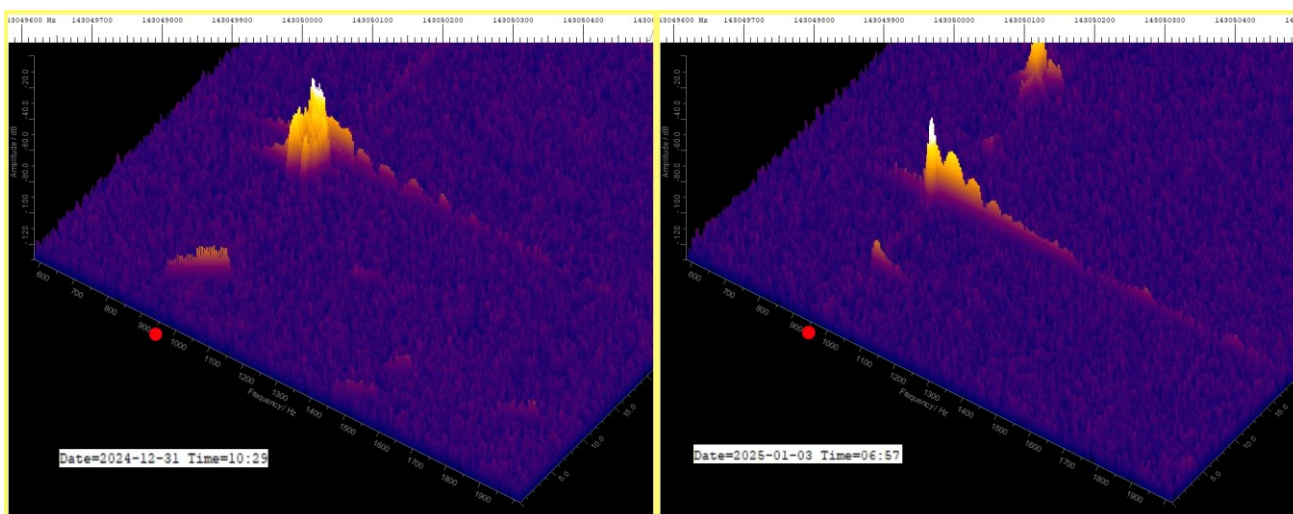
Figure 3 – Two head echoes from January 3, 2025, 6ʰ57ᵐ and from December 31, 10ʰ29ᵐ.

3   Result and Discussion

The spectrogram in *Figure 1* on the left side shows an echo from January 3ʳᵈ. Spectrum Lab is set up to capture large trail echoes as completely as possible. This means, however, that head echoes are lost. Typical echoes from a large and a small meteor are shown. Shortly before the end of the head echo, a bulge can be seen. The amplitude of the reflection from the plasma increases sharply here. This bulge clearly shows the explosion or decay of the meteoroid. For small meteoroids, this is the end of the disintegration, see the inset, for example. Further examples of small meteors can be found in the other figures. For larger explosions, the trail echo at the zero frequency usually follows. The spectrogram in the right image from January 2ⁿᵈ, 2025 at 0ʰ14ᵐ a.m. shows a bulge near the small trail echo as well as complex pulsations across the entire range. The zero frequency at 950 Hz is marked with the red dot. The spectrogram also extends below the zero frequency to the left edge. Without a 2D representation, which was not yet available here, details cannot be seen. A GRAVES glitch can be seen on the trail echo.

As written above, Kero et al. explain pulsations on the head echo by interference caused by reflections from the plasma. In detail: the radar waves reflected by parallel flying particles surrounded by plasma add up or attenuate depending on the phase shift. This process is called interference or fading. Causes of the phase shift can be the changing distance and the Faraday rotation. The fluctuations initially look like oscillations, but they are not, since the Doppler shift is plotted on the X-axis. I prefer the term fading.

Figure 2 shows on the right side two head echoes from January 1, 2025, 1ʰ59ᵐ a.m. The front echo shows complex pulsations. The rear head echo appears to come from just one particle. In *Figure 2* on the left from December 31, 2024, 11ʰ08ᵐ a.m., two particles appear to interfere very harmoniously. In the left image, the zero frequency is faintly visible in the spectrogram. The setup was optimized to minimize the carrier (Sicking, 2025).

Two head echoes with higher frequency pulsations from January 3, 2025, 6ʰ57ᵐ a.m. and December 31, 10ʰ29ᵐ a.m. are shown in *Figure 3*.

Evaluation with 2D and 3D spectrograms

Both systems are currently configured to record head echoes optimally. In the following three images, the 2D images were stretched in the Y direction, i.e. in the time axis, using the graphics program IrfanView and then displayed together with the 3D plot.
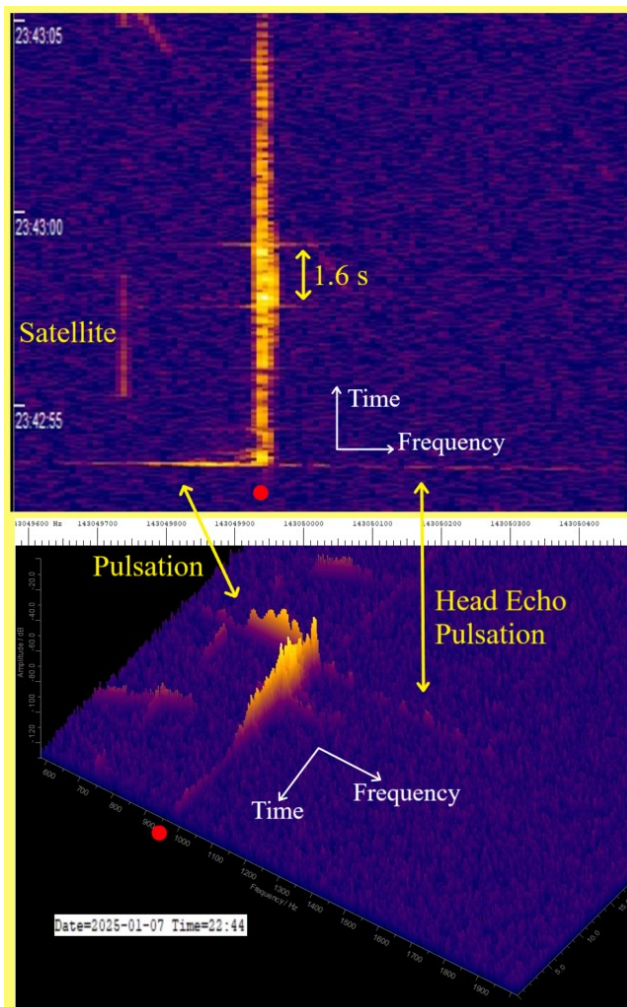
Figure 4 – Comparison of a 2D and a 3D spectrogram, see text.

Figure 4 shows a 2D and a 3D representation of one and the same meteor echo. Above the zero frequency, i.e. to the right of the red dot, a weak head echo with pulsations can be seen. Below the zero frequency, i.e. to the left of the red dot, the 3D spectrogram shows the bulbous spectrum with clear and very beautiful pulsations.

The recording was made on January 7, 2025 at 10^h44^m p.m. The 2D plot shows that the parts of the head echo above and below the zero frequency and the trail echo belong to one meteor echo. Using the GRAVES glitches as time markers, you can determine that the head echo was in the center of a 1.6 s window of the GRAVES transmitter. The local time is displayed in the upper part, on the left edge of the image. The two recording PCs have the same time setting. Spectrum Lab shows a one-minute difference between the times on the left edge and the time/date stamps. The cause is not yet known.

Usually the decay, i.e. the bulbous spectrum, appears above the zero frequency, i.e. to the right of the red dot, see e.g.

Figure 1, the right image. The echoes are then shifted to higher frequencies, as the meteoroid is moving towards the radar. In this case, the bulbous spectrum with the pulsations is below the zero frequency. This means that the meteoroid has moved away from the radar at this point. This is followed by the trail echo, which of course appears again at the zero frequency.

The spectrograms in *Figures 1 to 3* also show that a significant portion of the spectrograms are below the zero frequency, i.e. to the left of the red dot. The geometry of the flight path relative to the radar, i.e. a flyby, is probably important for the registration of pulsations. Further investigations will follow.
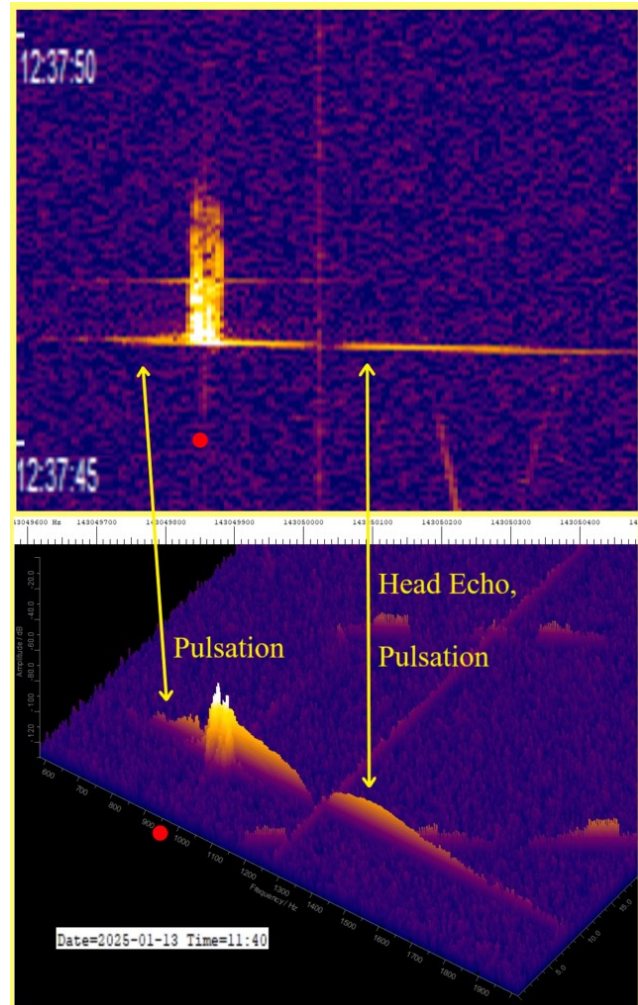
Figure 5 – Images from January 13, 2025 at 11^h40^m a.m. A slow pulsation above the zero frequency and a faster pulsation below can be seen. Some satellite echoes are in the image. The carrier in the center of the image is a disturbance that occurs occasionally at midday.

Figure 5 shows a similar image to *Figure 4*. However, the head echo is much more pronounced and shows a slow pulsation with a minimum in the center of the image. A weak pulsation below the zero frequency with a short period can be seen. The 2D plot confirms that this is not a satellite or a GRAVES glitch.

Figure 6 shows a head echo with a slow pulsation, like *Figure 5*, but weaker than in *Figure 5*. There is no head echo signal below the zero frequency (left of the red dot). The

bulbous spectrum above the zero frequency (right of the red dot) and the trail echo shows the standard decay.
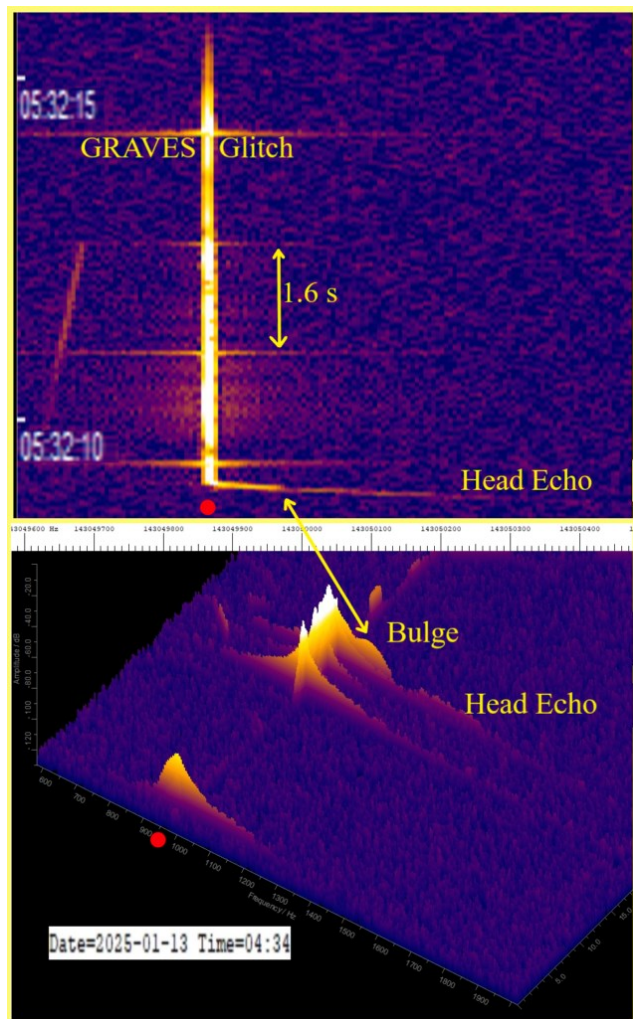
Figure 6 – Recordings from January 13, 2025 at 4ʰ34ᵐ a.m. In the 2D representation, it is clearly visible that there is no head echo below the zero frequency. Because of the glitches, the 3D representation is confusing in this area. Echoes like the echo at the zero frequency are always present in large numbers.

Figure 7 shows three interesting meteor echoes. They have only a weak or no head echo, no trail echo, but pulsations on the echo below the zero frequency, comparable to the pulsations in *Figure 4*. The spectra are essentially below the zero frequency, see also *Figure 8*. This means that the meteoroid with its plasma cloud is moving away from the radar. So, the radar is looking at the plasma cloud from behind. The interferences that cause the pulsations are probably caused by reflections at the interfaces of the ionized gases, whose reflection behavior changes due to turbulence.

This assumption is plausible because the pulsations are very similar in all spectrograms (compare *Figures 4 and 7*), and the pulsations are still very pronounced at low Doppler shift (at the left edge), although the intensity of the echo has already decreased significantly there. I have a few more images of this type, but such spectrograms are rare.
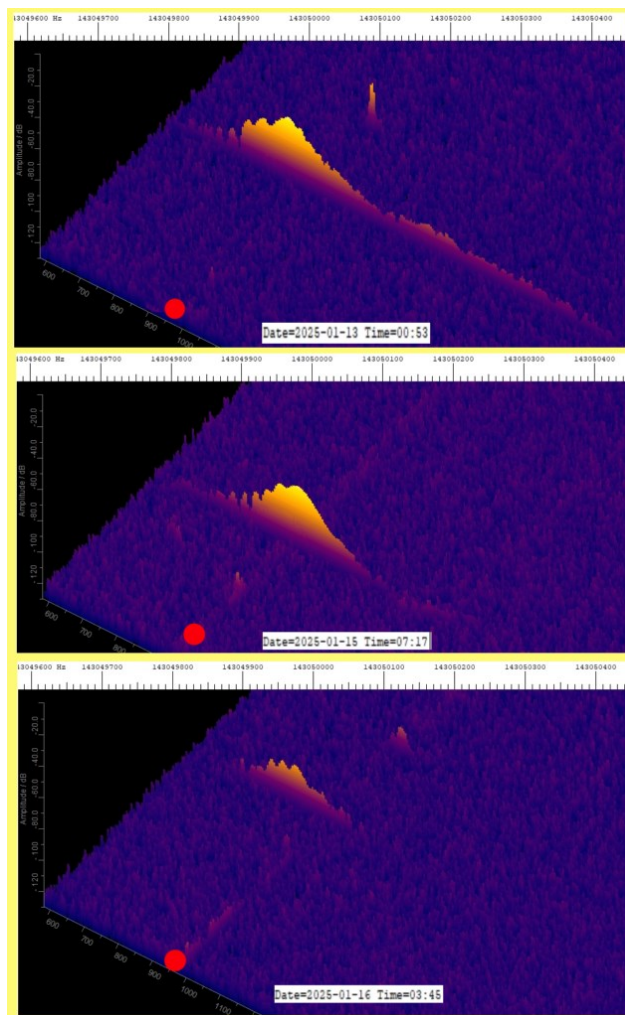
Figure 7 – Three spectrograms showing the bulge with pulsations below the zero frequency, indicated by the red dot.

Finally, *Figure 8* compares the 2D spectrograms from *Figure 6* from January 13, 2025 at 4ʰ34ᵐ a.m. and *Figure 7*, top spectrogram, from January 13, 2025 at 0ʰ53ᵐ a.m. The original 2D spectrograms were first copied exactly together and then stretched identically by a factor of 15. The graph shows that the lower head echo extends below zero frequency and that the maximum of the explosion is below the zero frequency. In the upper image, the explosion / bulge is above the zero frequency. It can also be seen (at least with the help of a graphics program) that the lower head echo is faster, probably due to the trajectory.

4 Conclusion

The 3D representation of the spectrograms obtained with the powerful GRAVES radar provides well-resolved 3D spectrograms of head echoes. My previous work had already shown that the 3D spectrogram can be used to detect when meteoroids and radar beams are parallel. In this work it was shown that the GRAVES radar can be used to study pulsations. For further investigations I will improve the resolution of the 2D spectrograms to below 10 ms if possible.
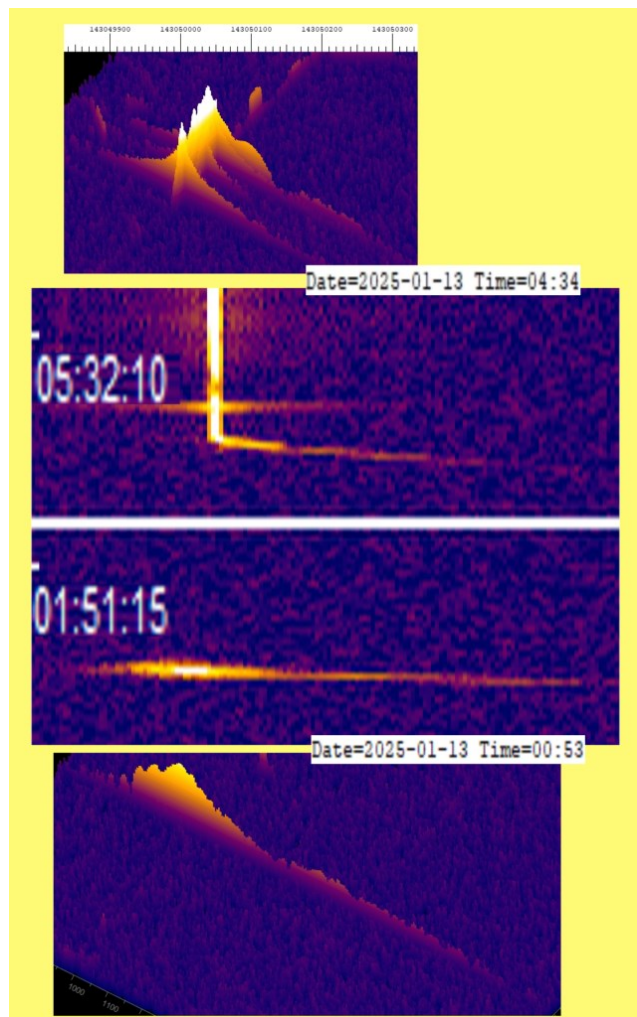
Figure 8 – Comparison of the 2D spectrograms from *Figure 6* from January 13, 2025 at 4ʰ34ᵐ a.m. and from *Figure 7*, top spectrogram, from January 13, 2025 at 0ʰ53ᵐ a.m. The time digits were stretched independently and may not be to scale. The two 3D images are not to scale. The times at the edge have an offset. The trail echo marks the zero frequency.

Acknowledgments

References

Close S., Brown P., Campbell-Brown M., Oppenheim M., Colestocka P. (2007). "Meteor head echo radar data: Mass–velocity selection effects". *Icarus*, **186**, 547–556.

Kero J., Szasz C., Pellinen-Wannberg A., Wannberg G., Westman A., and Meisel D. D. (2008). "Three-dimensional radar observation of a submillimeter meteoroid fragmentation". *Geophysical Research Letters*, **35**, L04101.

Sicking W. (2025). "About Spectrograms of Meteor Echoes at Different Stages of the Radiant Position of the Quadrantids 2025 – an AI/ML-Investigation". *eMetN Meteor Journal*, **10**, 115–119.

December 2024 CARMELO report

Mariasole Maglione[1], Lorenzo Barbieri[2]

[1] **Gruppo Astrofili Vicentini, Italy**
mariasole@astrofilivicentini.it

[2] **CARMELO network and AAB: Associazione Astrofili Bolognesi, Italy**
carmelometeor@gmail.com

The CARMELO network (Cheap Amateur Radio Meteor Echoes LOgger) is a collaboration of SDR radio receivers aimed at detecting meteor echoes. This report presents the data for December 2024.

1 Introduction

December is the month of the Geminids (GEM), a very unusual shower because it originates not from a comet but from an asteroid, 3200 Phaeton. The peak of the Geminids was recorded by the CARMELO network on the night of December 13–14. Minor showers were also present, with a slight increase in activity between December 22 and 24 and the peak of the Ursids.

2 Methods

The CARMELO network consists of SDR radio receivers. In them, a microprocessor (Raspberry) performs three functions simultaneously:

- By driving a dongle, it tunes the frequency on which the transmitter transmits and tunes like a radio, samples the radio signal and through the FFT (Fast Fourier Transform) measures frequency and received power.
- By analyzing the received data for each packet, it detects meteor echoes and discards false positives and interference.
- It compiles a file containing the event log and sends it to a server.

The data are all generated by the same standard, and are therefore homogeneous and comparable. A single receiver can be assembled with a few devices whose total current cost is about 210 euros.

To participate in the network read the instructions on this page[28].

3 December data

In the plots that follow, all available at this page[29], the abscissae represent time, which is expressed in UT (Universal Time) or in solar longitude (Solar Long), and the ordinates represent the hourly rate, calculated as the total number of events recorded by the network in an hour divided by the number of operating receivers.

In *Figure 1*, the trend of signals detected by the receivers for the month of December.

## 4 Geminids

December's star is the Geminid meteor shower (GEM), a fast-moving shower that is likely to disappear completely in less than a hundred years.
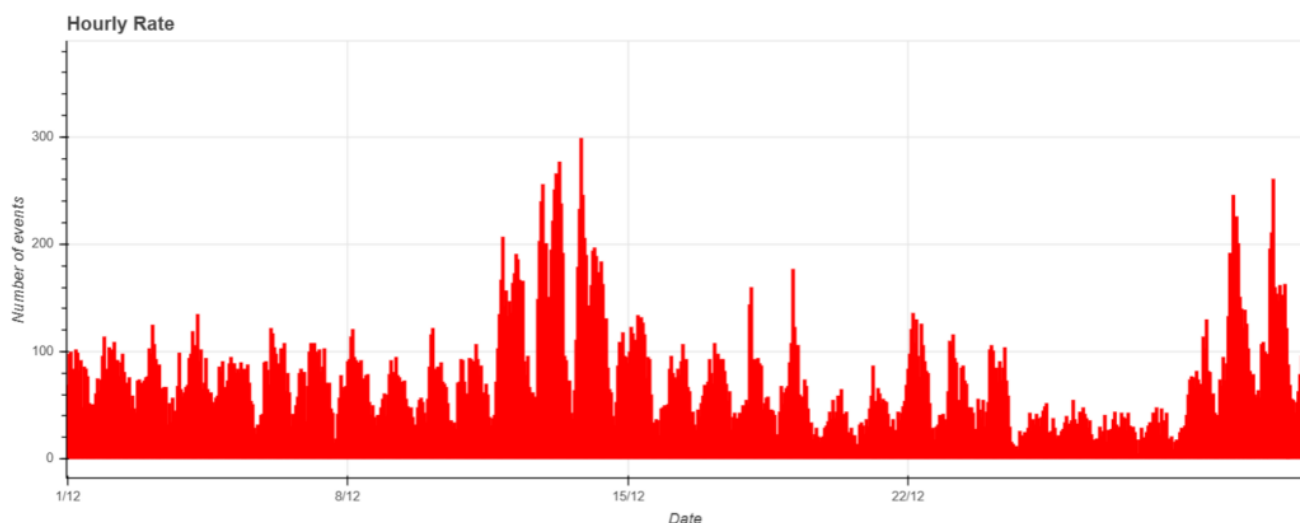
Figure 1 – December 2024 data trend.

---

[28] http://www.astrofiliabologna.it/about_carmelo

[29] http://www.astrofiliabologna.it/graficocarmelohr
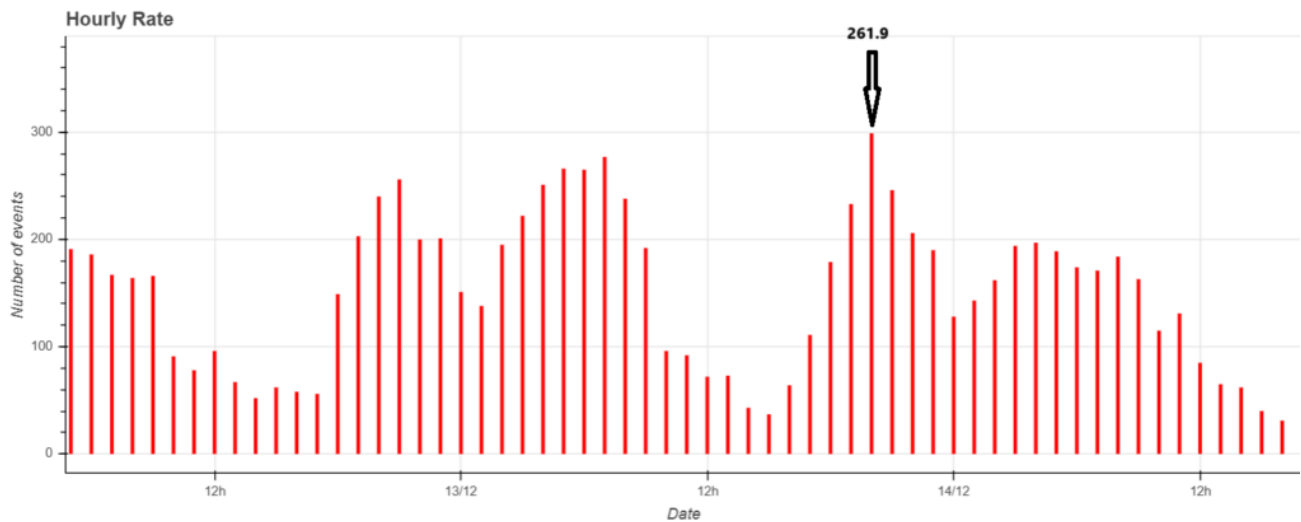
Figure 2 – Period of maximum activity of the Geminid shower between December 13 and 14, with maximum peak at solar longitude 261.9°.

Geminids represent a unique case among meteor showers: their origin is not linked to a comet, but to an asteroid, 3200 Phaethon (Jenniskens, 2006a). Discovered in 1983 with the Infrared Astronomical Satellite (IRAS), 3200 Phaethon is an Apollo-type asteroid with a highly elliptical orbit, which intersects those of Mars, Earth, Venus and Mercury and brings it very close to the Sun, closer than any other known asteroid. This close passage generates extremely high temperatures, capable of exceeding 750°C, enough to cause sublimation of some surface materials and the release of debris. This debris constitutes the very material that originates the Geminids.

Models suggest that debris is produced in significant quantities each time the asteroid passes close to the Sun, and is distributed along its orbit in a compact, well-defined trail.

Geminids are usually active from December 2 to December 19. In recent years, the *ZHR* (Zenithal Hourly Rate) has remained constant with 120–150 meteors recorded per hour with a peak of activity between December 13 and 14.

The radiant of the shower, or the point in the sky where the meteors appear to come from, is located in the Gemini constellation, near the bright star Castor. For skies in the Northern Hemisphere, it rises around 18^h and sets around 9^h local time.

This year, the presence of the nearly Full Moon (and bad weather, in Italy) hampered visual observation. As for radio observations, the CARMELO network receivers recorded a high rate on both the night of December 13 and the night between December 13 and 14, with a maximum peak and hourly rate of 299 events at 20^{h}00^m UT on the 13th, at solar longitude 261.9° (*Figure 2*).

5   Ursids

Ursids (URS) are another December meteor shower, active annually between the 17th and 26th of the month but much less abundant than the Geminids. Ursids are produced by debris left behind by comet 8P/Tuttle, a periodic comet that crosses the Solar System with an orbit of about 13.6 years.

The radiant is located in the Ursa Minor constellation, near the star beta Ursae Minoris (Kochab).

Ursids usually reach their peak activity between December 22 and 23, with an average frequency of 5–10 visible meteors per hour under normal conditions, but with occasional outbursts that can increase the number of meteors.

Also in 2024, activity increased slightly between December 22 and 24 (*Figure 3*), particularly between solar longitudes 270.4° and 270.6°.

Peter Jenniskens (2006b) analyzed the behavior of the Ursids, identifying a main trail of the shower that initially formed near the progenitor body, comet 8P/Tuttle. Jenniskens showed that the outburst, or peak of meteor activity, coincides with the time when the progenitor body is at aphelion (the farthest point from the Sun along its orbit). Through mathematical modeling, the author showed that Ursid meteoroids in fact tend to remain concentrated in a specific orbital resonance, with a ratio of 15/13. This resonance would be influenced by proximity to the 1/1 resonance with Jupiter.

Jenniskens in particular plotted the meteoroid distribution and shower passes year by year, covering the period from 1994 to 2004. In addition, he provided predictions for future events.

An interesting point to note is that our data turns out to be in excellent agreement with the predictions made by Jenniskens.

6   CARMELO update

As can be seen from the graph in *Figure 1* showing the trend for the month of December, the hourly rate of events increased in the last days of the month.
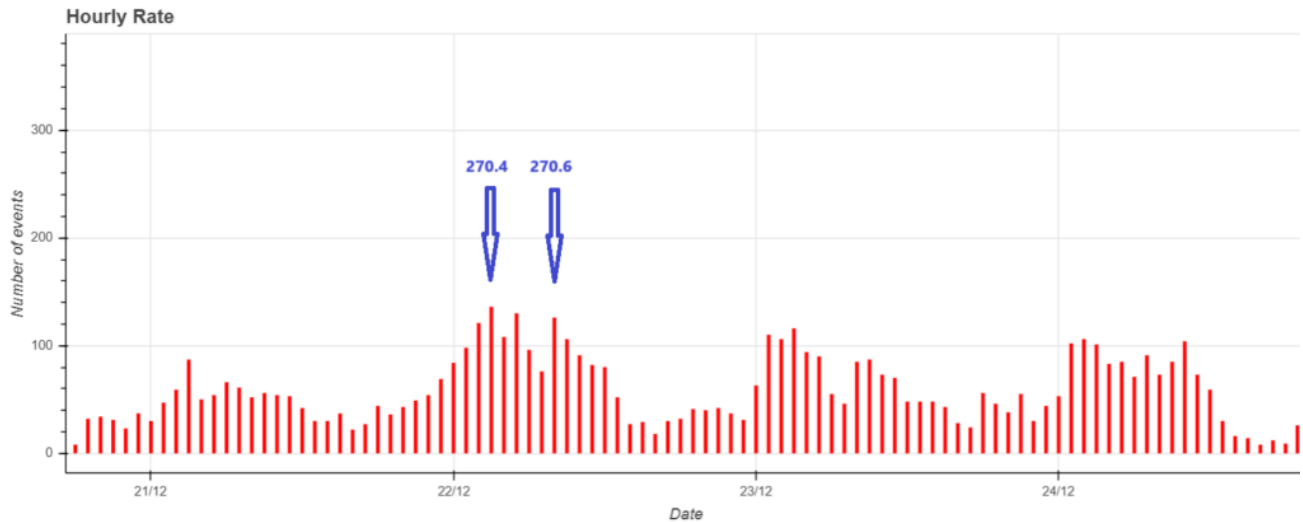
Figure 3 – Peak period of Ursid shower activity between December 22 and 24.

The reason for this increase is related to a recently performed update of CARMELO's software. With this new version, from now on CARMELO will record the radio power of each meteor echo and no longer the signal-to-noise ratio (SNR) value.

In addition, the bandwidth has been narrowed to 20 kHz, and the devices have been equipped with a new and more effective filter on false positives.

7 The CARMELO network

The network currently consists of 14 receivers, 13 of which are operational, located in Italy, the UK, Croatia and the USA. The European receivers are tuned to the Graves radar station frequency in France, which is 143.050 MHz. Participating in the network are:

- Lorenzo Barbieri, Budrio (BO) ITA;
- Associazione Astrofili Bolognesi, Bologna ITA;
- Associazione Astrofili Bolognesi, Medelana (BO) ITA;
- Paolo Fontana, Castenaso (BO) ITA;
- Paolo Fontana, Belluno (BL) ITA;
- Associazione Astrofili Pisani, Orciatico (PI) ITA;

- Gruppo Astrofili Persicetani, San Giovanni in Persiceto (BO) ITA;
- Roberto Nesci, Foligno (PG) ITA;
- MarSEC, Marana di Crespadoro (VI) ITA;
- Gruppo Astrofili Vicentini, Arcugnano (VI) ITA;
- Associazione Ravennate Astrofili Theyta, Ravenna (RA) ITA;
- Akademsko Astronomsko Društvo, Rijeka CRO;
- Mike German a Hayfield, Derbyshire UK;
- Mike Otte, Pearl City, Illinois USA.

The authors' hope is that the network can expand both quantitatively and geographically, thus allowing the production of better-quality data.

References

Jenniskens P. (2006a). Meteor showers and their parent comets. Cambridge University Press, pages 397–422.

Jenniskens P. (2006b): Meteor showers and their parent comets. Cambridge University Press, pages 263–265.

January 2025 CARMELO report

Mariasole Maglione[1], Lorenzo Barbieri[2]

[1] **Gruppo Astrofili Vicentini, Italy**
mariasole@astrofilivicentini.it

[2] **CARMELO network and AAB: Associazione Astrofili Bolognesi, Italy**
carmelometeor@gmail.com

The CARMELO network (Cheap Amateur Radio Meteor Echoes LOgger) is a collaboration of SDR radio receivers aimed at detecting meteor echoes. This report presents the data for January 2025.

1   Introduction

January opened with the peak of the Quadrantids, which is the main and dominant shower for the entire month, otherwise affected only by the passage of minor showers. The peak of the Quadrantids occurred on January 3.

2   Methods

The CARMELO network consists of SDR radio receivers. In them, a microprocessor (Raspberry) performs three functions simultaneously:

- By driving a dongle, it tunes the frequency on which the transmitter transmits and tunes like a radio, samples the radio signal and through the FFT (Fast Fourier Transform) measures frequency and received power.
- By analyzing the received data for each packet, it detects meteor echoes and discards false positives and interference.

- It compiles a file containing the event log and sends it to a server.

The data are all generated by the same standard, and are therefore homogeneous and comparable. A single receiver can be assembled with a few devices whose total current cost is about 210 euros.

To participate in the network read the instructions on this page[30].

3   January data

In the plots that follow, all available at this page[31], the abscissae represent time, which is expressed in UT (Universal Time) or in solar longitude (Solar Long), and the ordinates represent the hourly rate, calculated as the total number of events recorded by the network in an hour divided by the number of operating receivers.

In *Figure 1*, the trend of signals detected by the receivers for the month of January is shown.
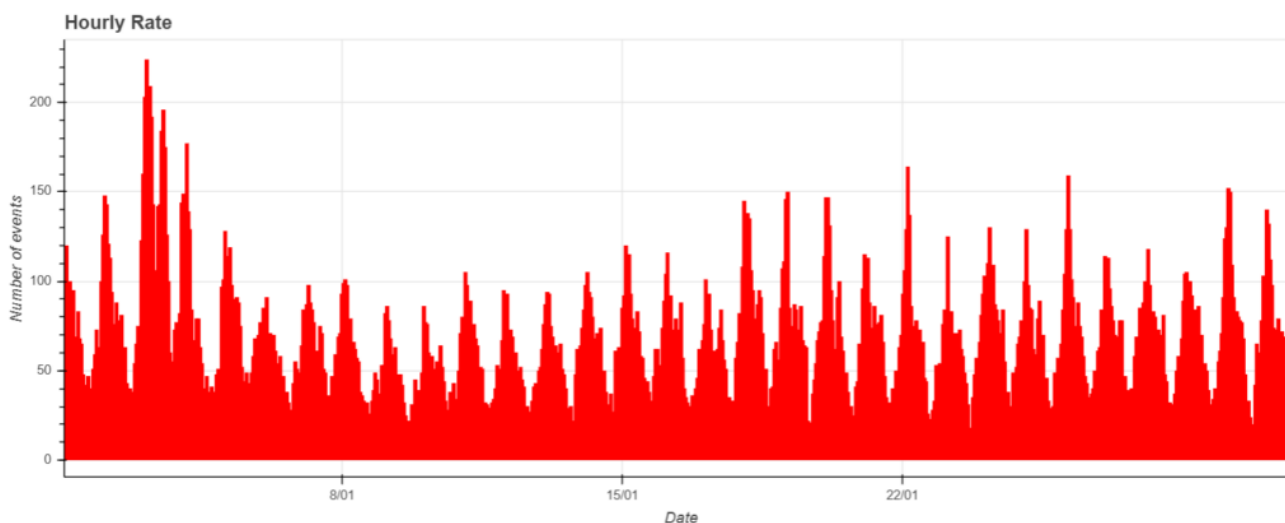
Figure 1 – January 2025 data trend.

---

[30] http://www.astrofiliabologna.it/about_carmelo

[31] http://www.astrofiliabologna.it/graficocarmelohr
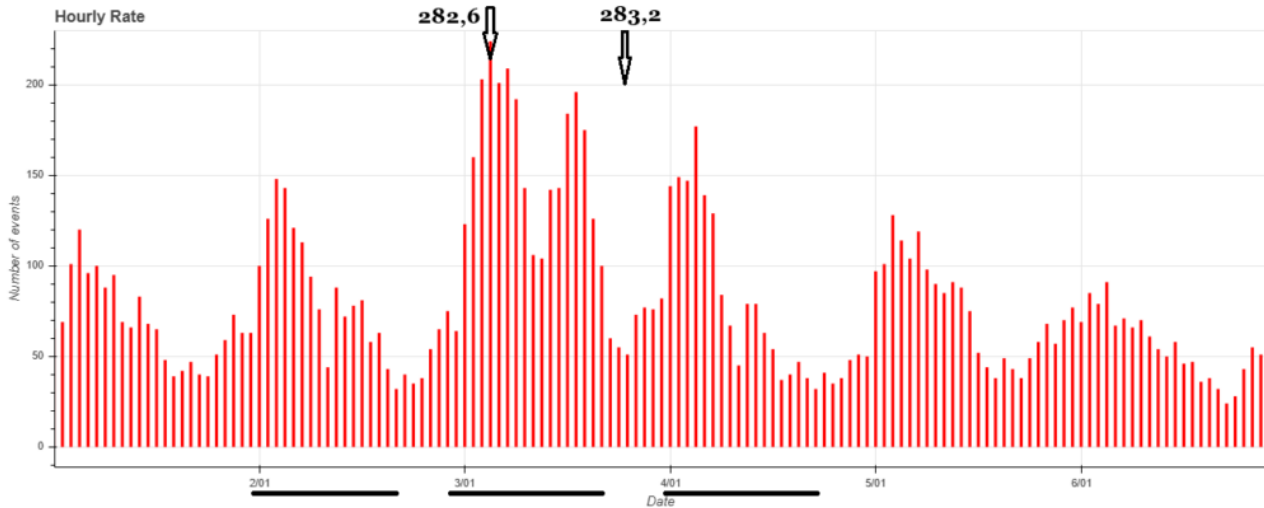
Figure 2 – Peak of maximum activity of the Quadrantids on January 3 detected at solar longitude 282.6°, and peak expected at 283.2° when the radiant was too low on the horizon.
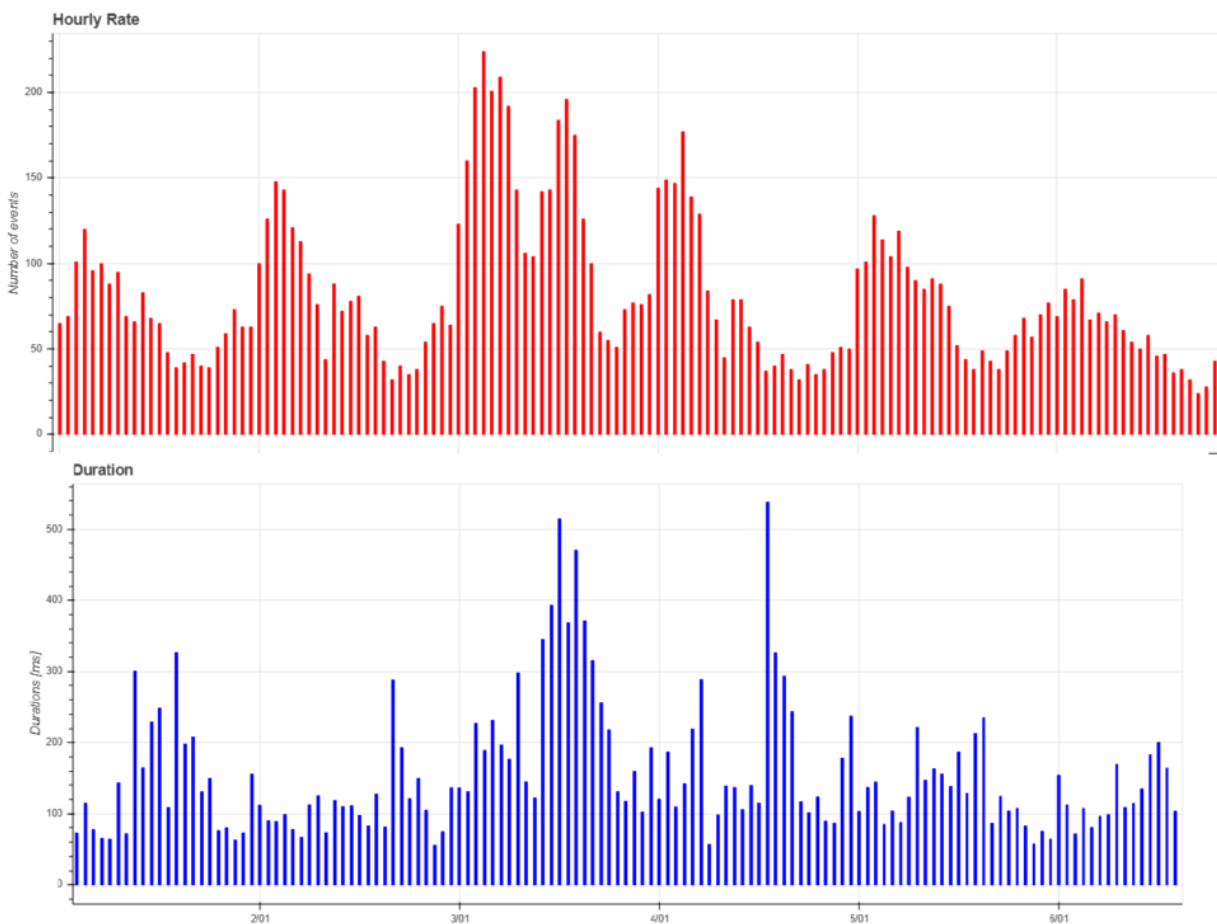
Figure 3 – Comparison of hourly rate and average duration of meteor echoes between January 1 and January 6.

4   Quadrantids

Among the annual meteor showers, the January Quadrantids usually stand out for their intensity, reaching peaks of activity between 60 and 200 meteors per hour. Despite this, they remain less well known than other more famous showers, such as the Perseids or Geminids. Their less notoriety is also due to the very short peak of activity, which lasts about 24 hours.

The radiant of the Quadrantids is located in the constellation Bootes, in a rather low position in the northern sky, between the head of the Dragon and the helm of the Big Dipper. The name is derived from Quadrans Muralis, an ancient constellation created in 1795 by the French astronomer Jérôme Lalande that included parts of Bootes and the Dragon, and which is not on the list of 88 constellations drawn up by the International Astronomical Union (IAU) in 1922 and published by Delporte (1930).

The origin of this swarm remains a debated topic. In 2003, following an observational campaign on minor bodies in the

Solar System, astronomer Peter Jenniskens found a possible progenitor body of the Quadrantids in the Near Earth (196256) asteroid 2003 EH1, a hypothesis that would make them one of the few meteor showers arising from an asteroid and not a comet, similar to the Geminids in December (Jenniskens, 2004). Since then, 2003 E1 has been considered the most likely progenitor body of the Quadrantids. It may itself be a fragment of comet C/1490 Y1, which was observed by Chinese, Japanese and Korean astronomers just over 500 years ago in 1490 (Lee et al., 2009).

This year, the maximum peak of the Quadrantids was expected on January 3 at solar longitude 283.2°, corresponding to 17^h UT. At that time, however, the radiant of the swarm was too low on the horizon for proper detection. The CARMELO network detected the maximum activity at 3^h UT on January 3 at solar longitude 286.6°, when the hourly rate was 224, and the Quadrantids' radiant was high in the sky to the northeast (*Figure 2*, with black strokes below highlighting the times of day when the radiant was high enough above the horizon for observation).

5 Quadrantids' composition

Figure 3 shows a comparison of the hourly rate and average duration of meteoric echoes on the days around the peak of Quadrantid activity.

Note how the three peaks on January 3 and 4 in the two graphs are very different: the central peak, around solar longitude 283° corresponding to 13^h UT on January 3, has much longer echoes; the average duration also reaches half a second.

This observation tells us a lot about the composition of this shower. In fact, the duration of a radio echo depends on the time it takes for the meteor to dissolve: the greater the number of ionized atoms (ions and free electrons), the longer the deionization process takes. The number of ionized atoms, or the density of the plasma, is proportional to the kinetic energy of the impacting bodies against the first molecules in the ionosphere: the more energetic the collision, the more atoms disintegrate, and thus the denser the meteor.

We know that kinetic energy is given by:

$$E_c = \tfrac{1}{2}\,mv^2$$

and we know that all meteors belonging to the same shower all travel at the same velocity *v*. It can therefore be deduced that the only parameter that varies is *m*, i.e., mass.

The graph thus shows that the Quadrantid shower can be described as a cylinder having a "shell" of smaller meteors on the outside, and a filament of larger meteors on the inside. This characteristic is typical of relatively young showers (in astronomical times, of course). With the passage of time, in fact, this composition tends to change,

either due to the effect of gravitational interactions with the major planets in the Solar System, or due to the pressure of solar radiation, which tends to move the more massive particles outward from the shower, thus generating a conformation that is no longer symmetrical.

Note how in the bottom graph in *Figure 3*, the spike in density increases toward solar longitude 284° (between January 4 and 5) is not a false positive, or a system error. It was also present at the passage of the Quadrantids in January 2023 and detected by CARMELO (Barbieri, 2023).

6 The CARMELO network

The network currently consists of 14 receivers, 13 of which are operational, located in Italy, the UK, Croatia and the USA. The European receivers are tuned to the Graves radar station frequency in France, which is 143.050 MHz. Participating in the network are:

- Lorenzo Barbieri, Budrio (BO) ITA;
- Associazione Astrofili Bolognesi, Bologna ITA;
- Associazione Astrofili Bolognesi, Medelana (BO) ITA;
- Paolo Fontana, Castenaso (BO) ITA;
- Paolo Fontana, Belluno (BL) ITA;
- Associazione Astrofili Pisani, Orciatico (PI) ITA;
- Gruppo Astrofili Persicetani, San Giovanni in Persiceto (BO) ITA;
- Roberto Nesci, Foligno (PG) ITA;
- MarSEC, Marana di Crespadoro (VI) ITA;
- Gruppo Astrofili Vicentini, Arcugnano (VI) ITA;
- Associazione Ravennate Astrofili Theyta, Ravenna (RA) ITA;
- Akademsko Astronomsko Društvo, Rijeka CRO;
- Mike German a Hayfield, Derbyshire UK;
- Mike Otte, Pearl City, Illinois USA.

The authors' hope is that the network can expand both quantitatively and geographically, thus allowing the production of better-quality data.

References

Delporte Eugène (1930). IAU: "Délimitation Scientifique des Constellations". At the University Press.

Jenniskens P. (2004). "2003 EH1 and the Quadrantid shower". *WGN, Journal of the International Meteor Organization*, **32**, 7–10.

Lee Ki-Won, Yang Hong-Jin, Park Myeong-Gu (2009). "Orbital Elements of Comet C/1490 Y1 and the Quadrantid shower". *Monthly Notices of the Royal Astronomical Society*, **400**, 1389–1393.

Barbieri Lorenzo (2023). "The 2023 Quadrantidis". *eMetN Meteor Journal*, **8**, 116–117.

Radio meteors December 2024

Felix Verbelen

Vereniging voor Sterrenkunde & Volkssterrenwacht MIRA, Grimbergen, Belgium
felix.verbelen@gmail.com

An overview of the radio observations during December 2024 is given.

1   Introduction

The graphs show both the daily totals (*Figure 1 and 2*) and the hourly numbers (*Figure 3 and 4*) of "all" reflections counted automatically, and of manually counted "overdense" reflections, overdense reflections longer than 10 seconds and longer than 1 minute, as observed here at Kampenhout (BE) on the frequency of our VVS-beacon (49.99 MHz) during the month of December 2024.

The hourly numbers, for echoes shorter than 1 minute, are weighted averages derived from:

$$N(h) = \frac{n(h-1)}{4} + \frac{n(h)}{2} + \frac{n(h+1)}{4}$$

Local interference and unidentified noise remained weak to moderate, and lightning activity was only detected on December 22nd.

The highlights of the month were, of course, the Geminids (*Figure 5*), while the Ursids were clearly present on December 22nd. An increase in reflections longer than 10 seconds was also noted on December 24th. In addition, there were some minor showers, especially at the beginning of the month.

This month, 9 reflections longer than 1 minute were observed here, spread throughout the month. A selection of these, along with some other interesting reflections is included (*Figures 6 to 17*). More of these are available on request.

In addition to the usual graphs, you will also find the raw counts in cvs-format[32] from which the graphs are derived. The table contains the following columns: day of the month, hour of the day, day + decimals, solar longitude (epoch J2000), counts of "all" reflections, overdense reflections, reflections longer than 10 seconds and reflections longer than 1 minute, the numbers being the observed reflections of the past hour.

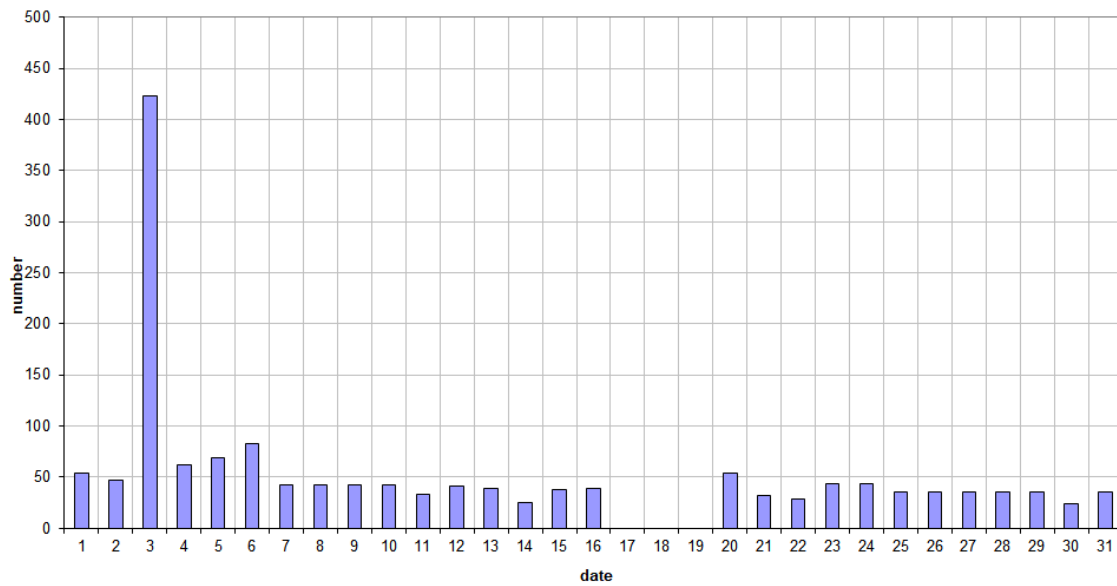[32] https://www.emeteornews.net/wp-content/uploads/2025/01/202412_49990_FV_rawcounts.csv
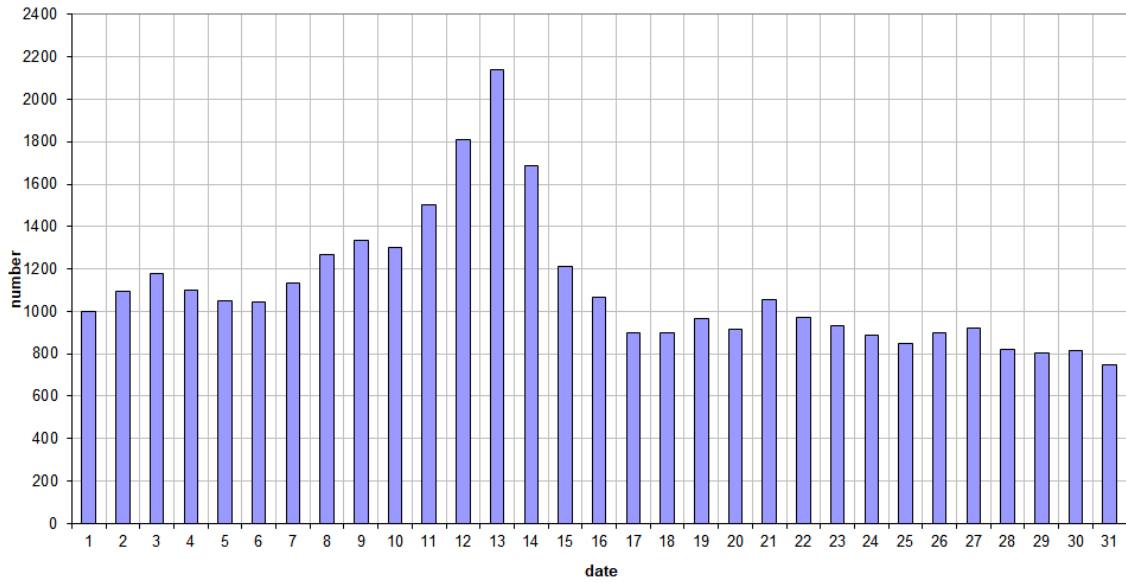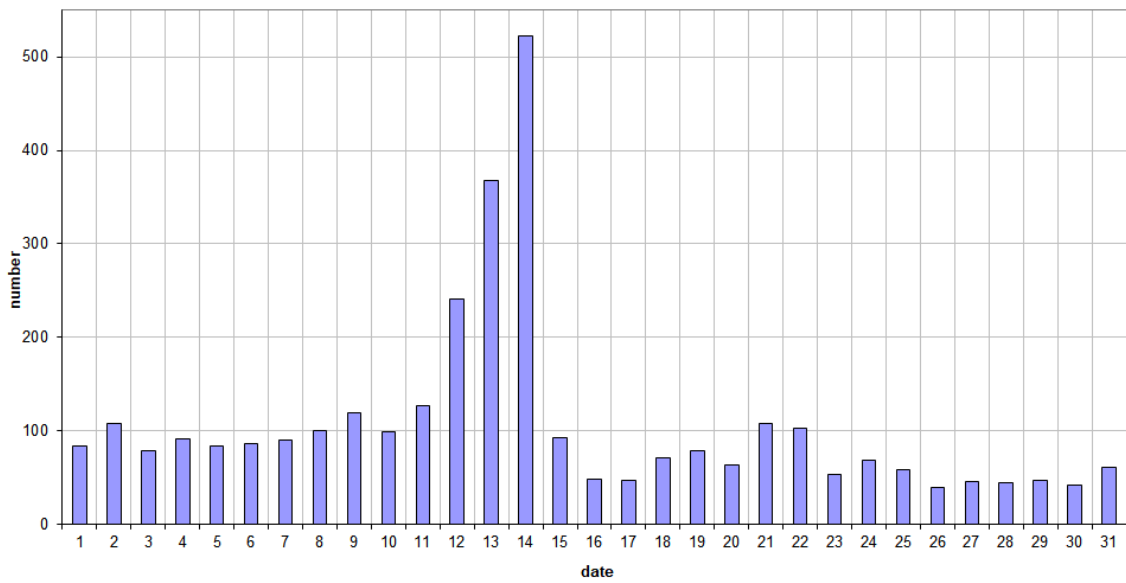
Figure 1 – The daily totals of "all" reflections counted automatically, and of manually counted "overdense" reflections, as observed here at Kampenhout (BE) on the frequency of our VVS-beacon (49.99 MHz) during December 2024.
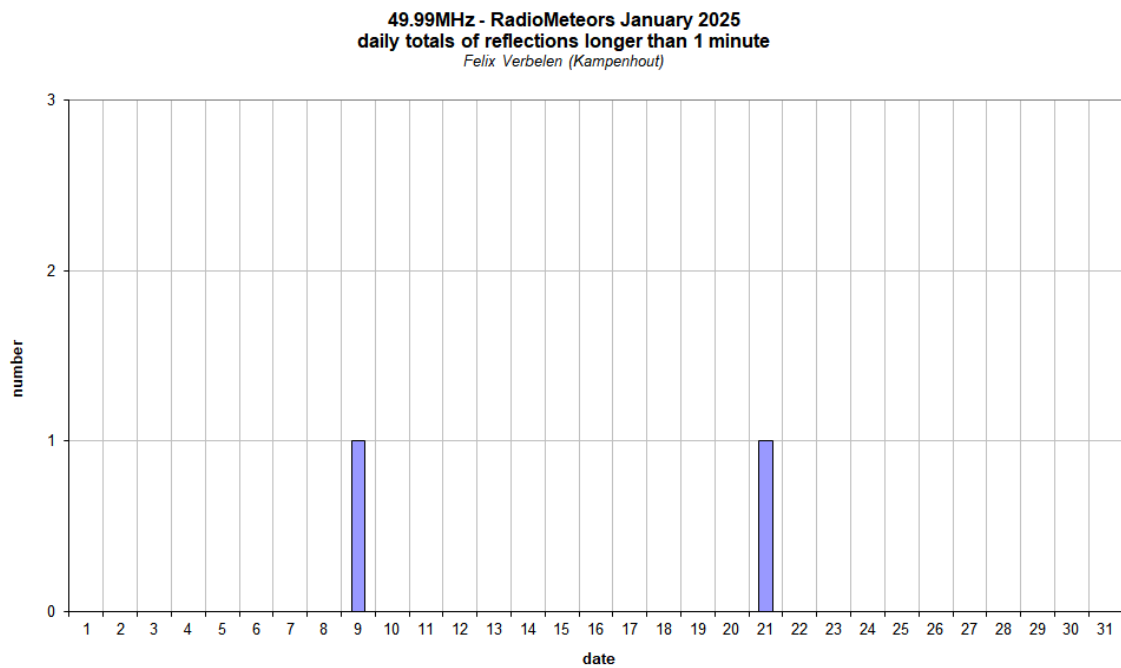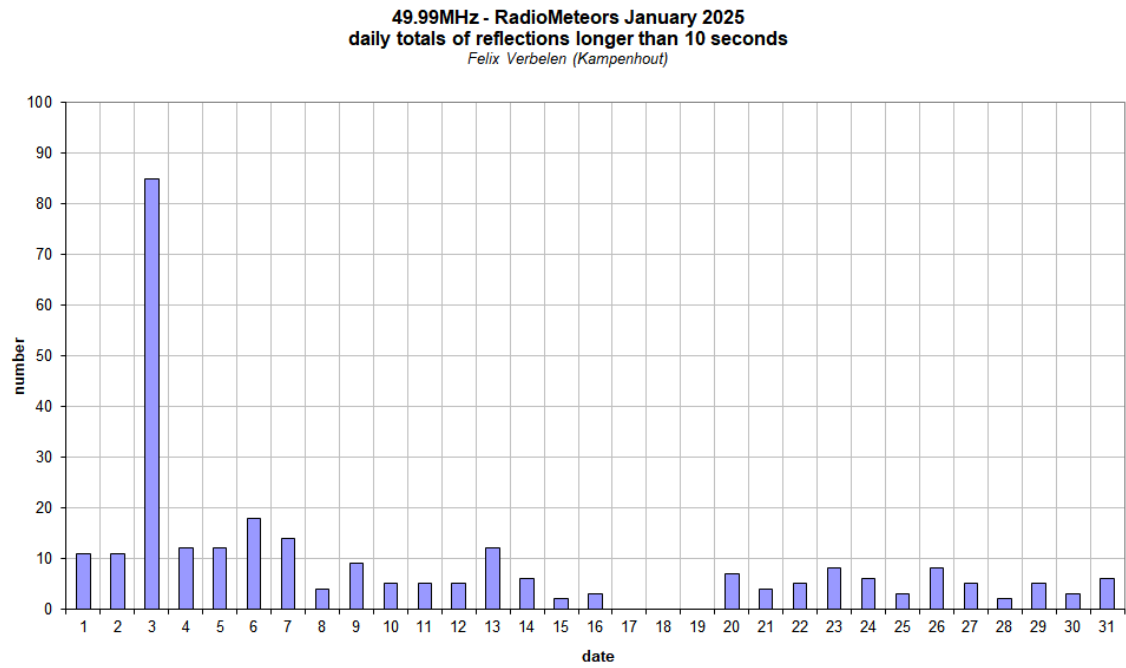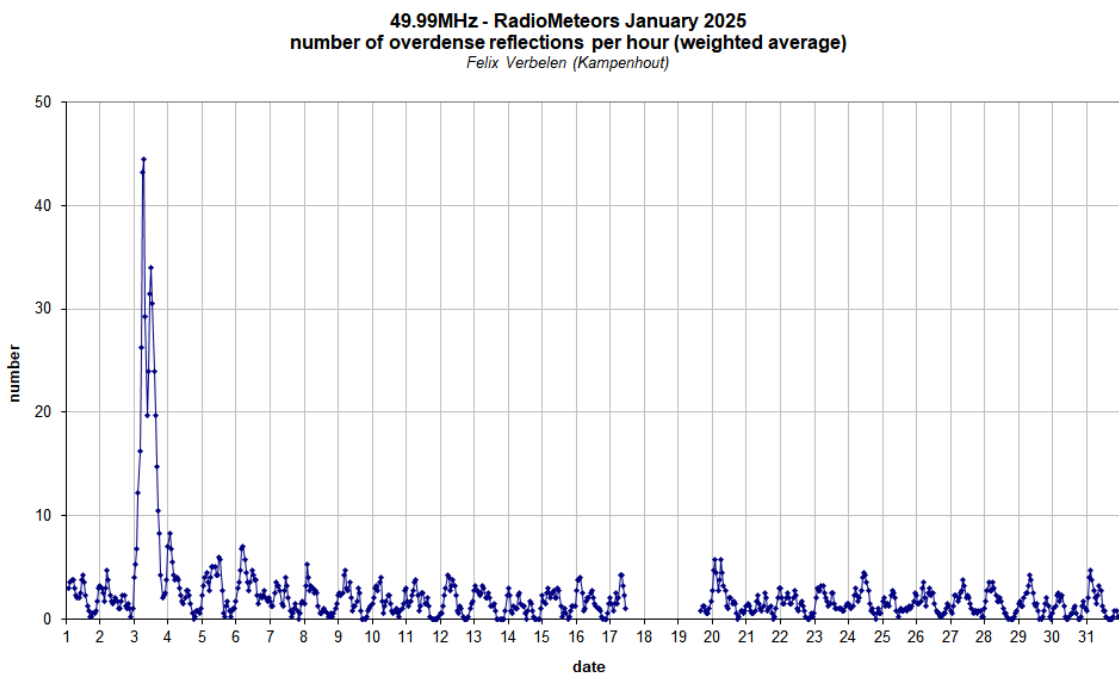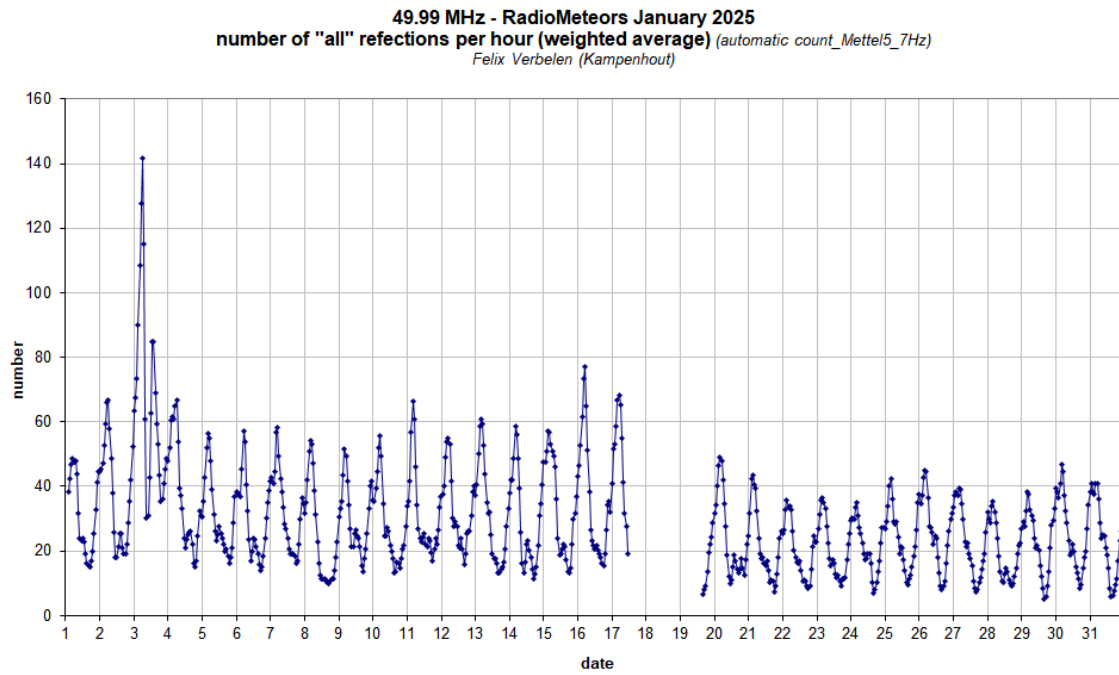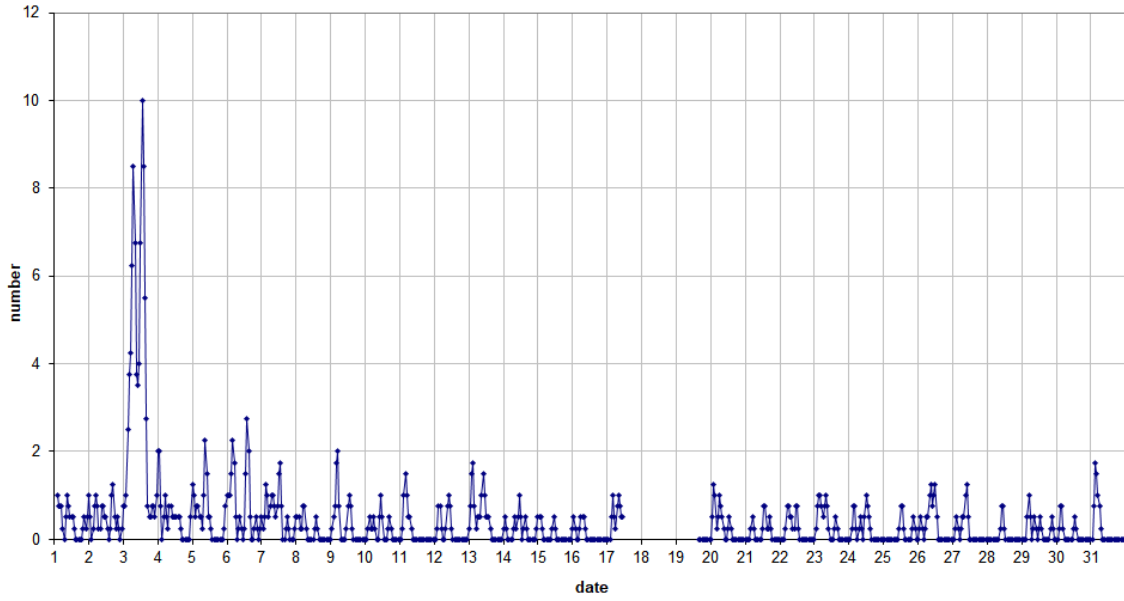
49.99MHz - RadioMeteors December 2024
daily totals of reflections longer than 10 seconds
Felix Verbelen (Kampenhout)
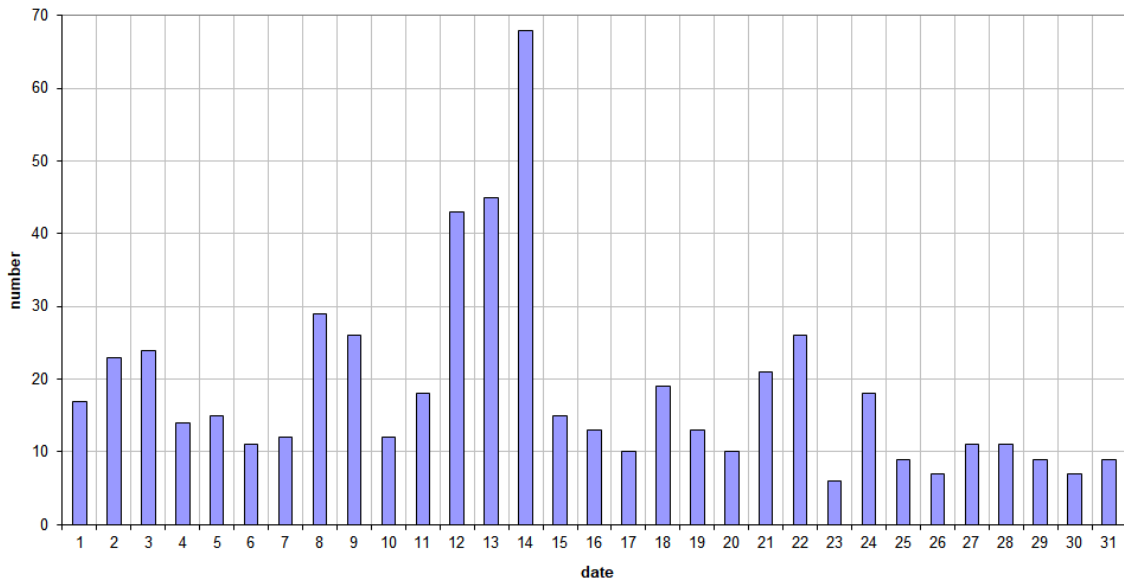
49.99MHz - RadioMeteors December 2024
daily totals of reflections longer than 1 minute
Felix Verbelen (Kampenhout)
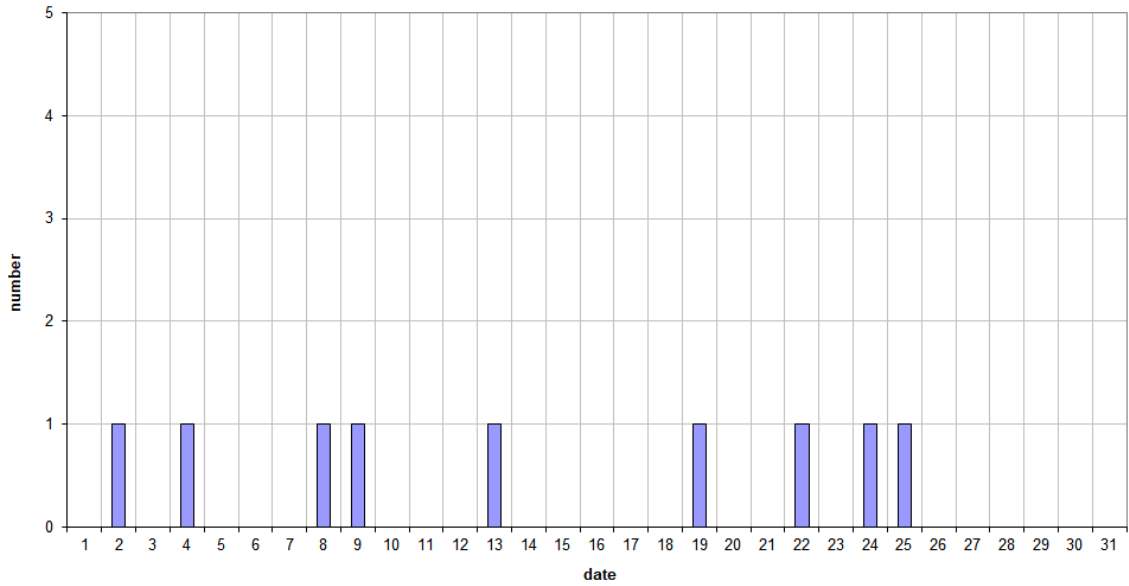
Figure 2 – The daily totals of overdense reflections longer than 10 seconds and longer than 1 minute, as observed here at Kampenhout (BE) on the frequency of our VVS-beacon (49.99 MHz) during December 2024.
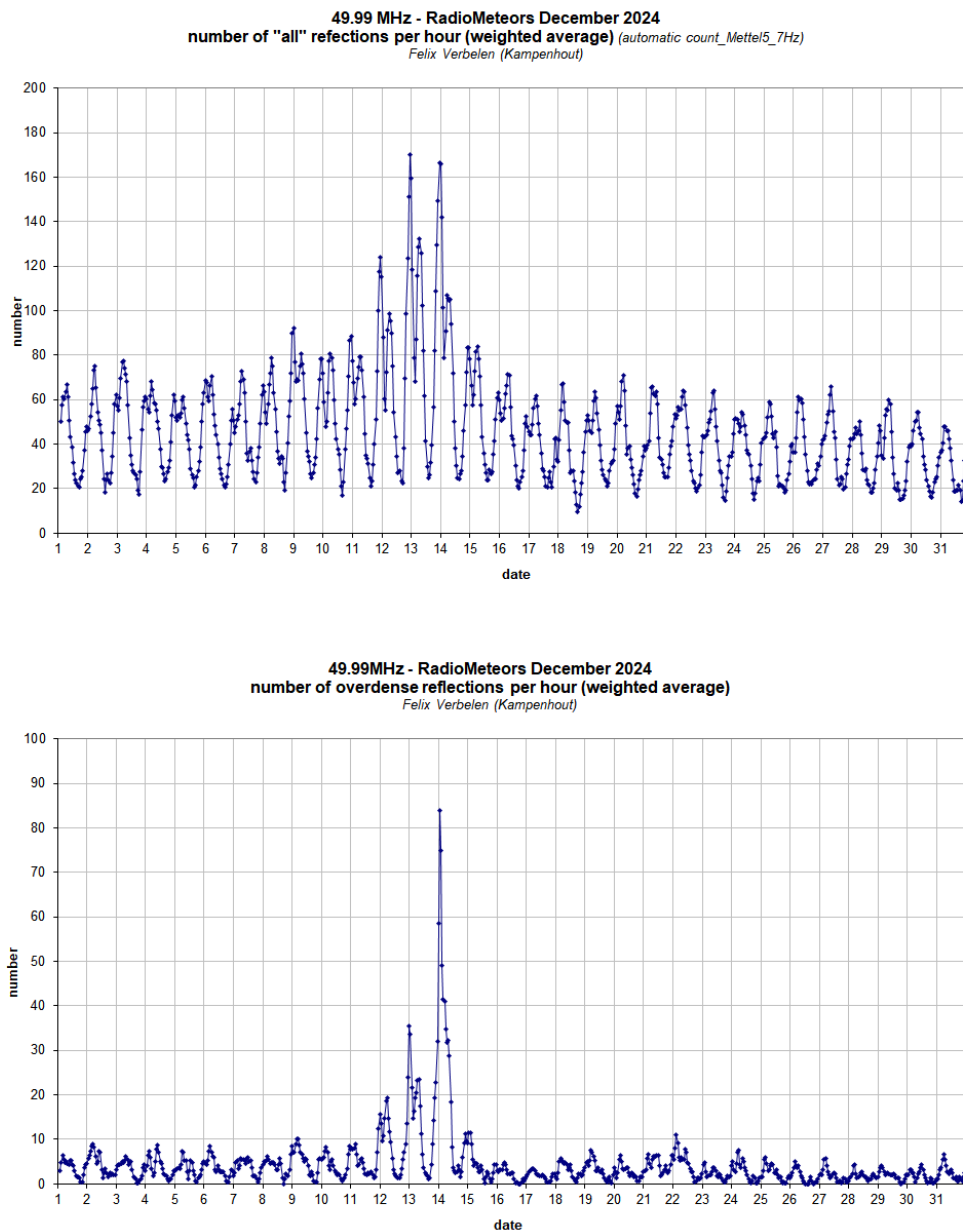
Figure 3 – The hourly numbers of "all" reflections counted automatically, and of manually counted "overdense" reflections, as observed here at Kampenhout (BE) on the frequency of our VVS-beacon (49.99 MHz) during December 2024.
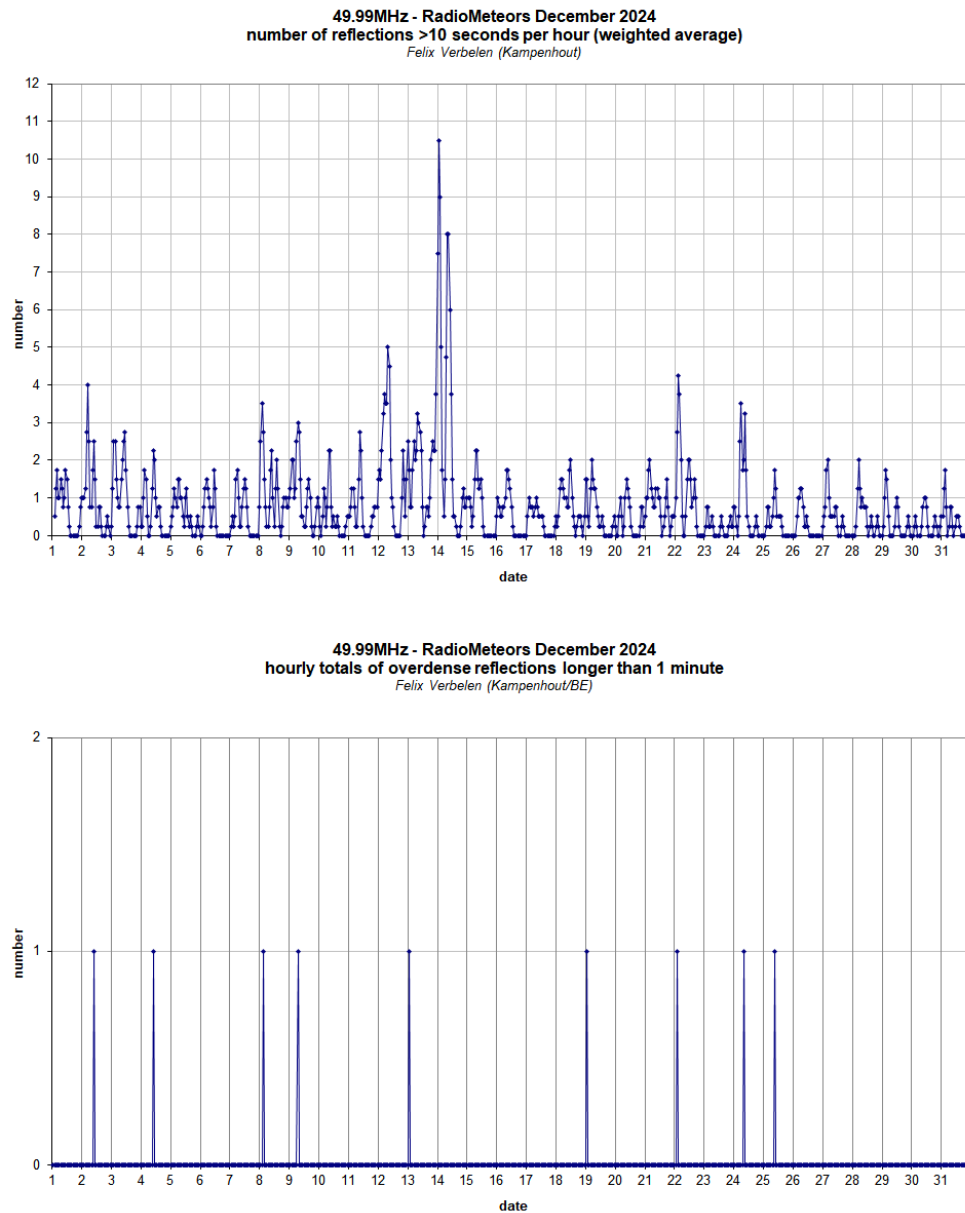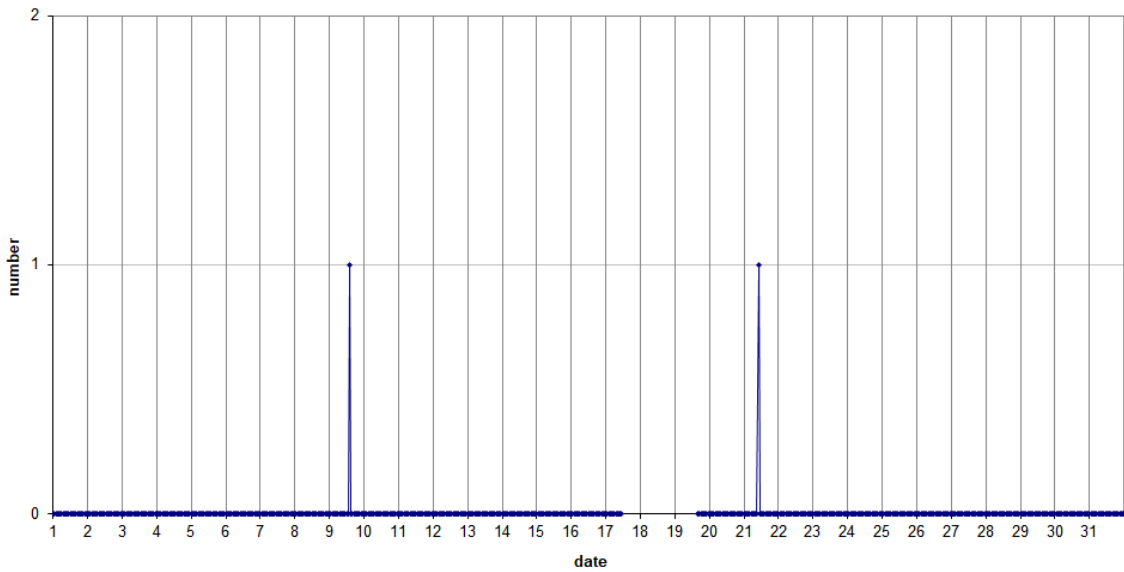
Figure 4 – The hourly numbers of overdense reflections longer than 10 seconds and longer than 1 minute, as observed here at Kampenhout (BE) on the frequency of our VVS-beacon (49.99 MHz) during December 2024.

Geminiden_20241214_49.99 MHz_selectie -- FV (Kampenhout/BE)
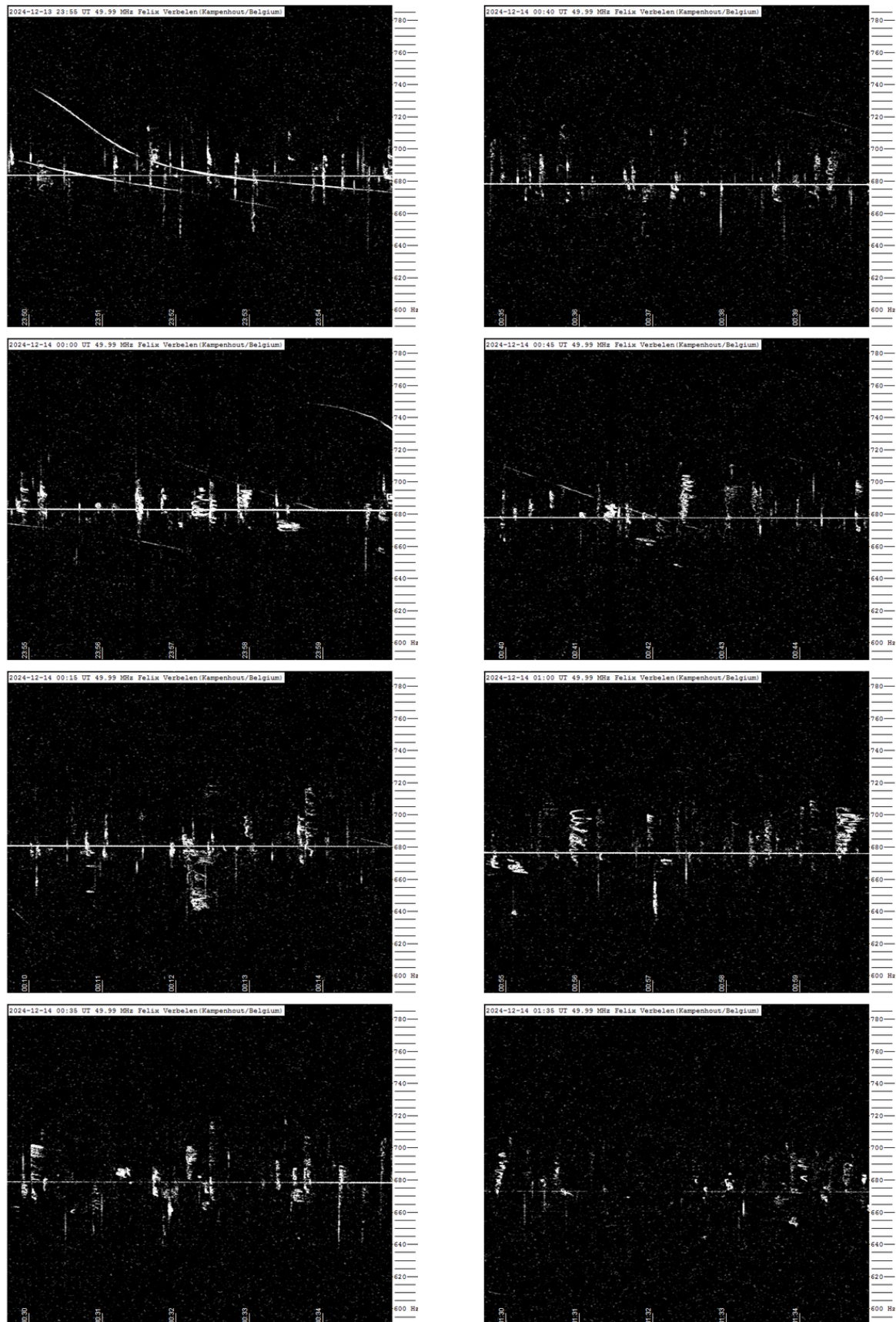
Figure 5 – Selection of meteor echoes during the Geminid maximum.
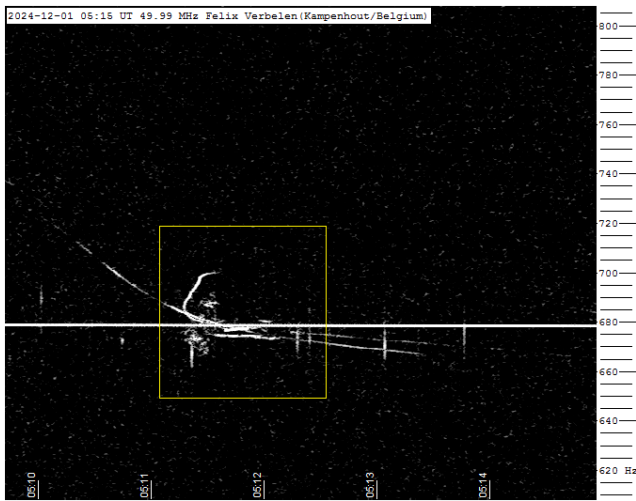
Figure 6 – Meteor echoes December 1, 5ʰ15ᵐ UT.
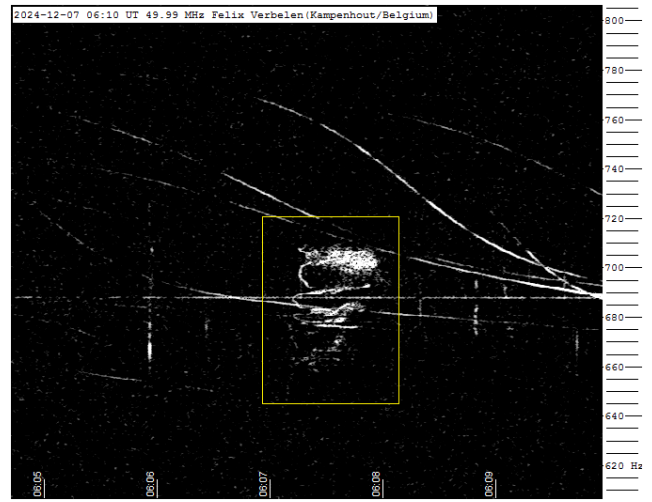
Figure 9 – Meteor echoes December 7, 6ʰ10ᵐ UT.
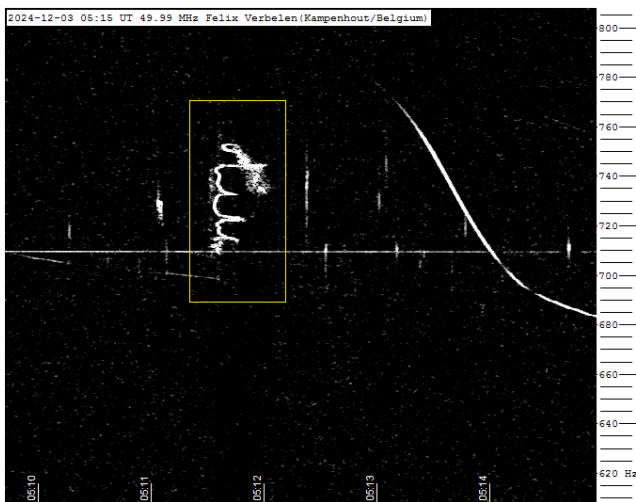
Figure 7 – Meteor echoes December 3, 5ʰ15ᵐ UT.
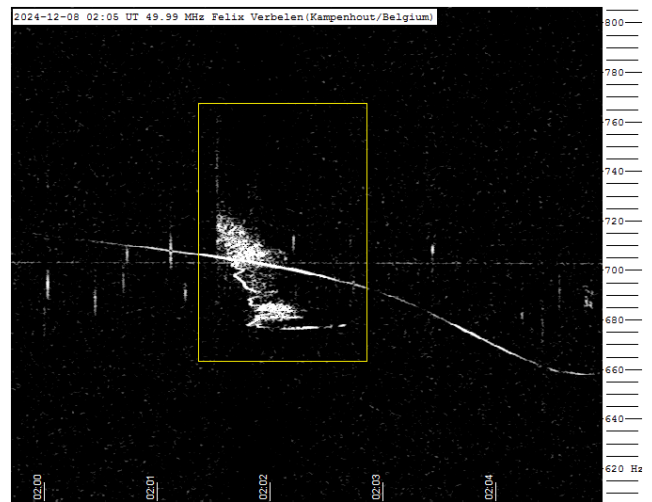
Figure 10 – Meteor echoes December 8, 2ʰ05ᵐ UT.
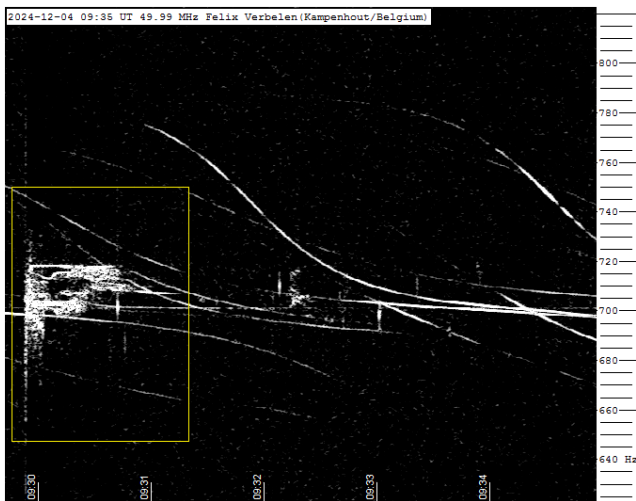
Figure 8 – Meteor echoes December 4, 9ʰ35ᵐ UT.
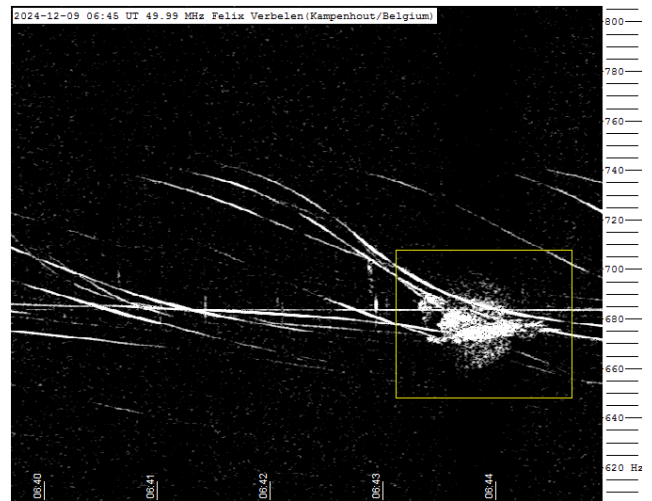
Figure 11 – Meteor echoes December 9, 6ʰ45ᵐ UT.
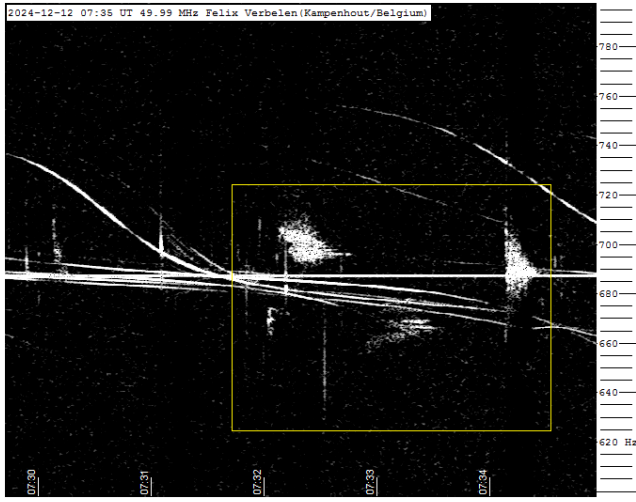
Figure 12 – Meteor echoes December 12, 7ʰ35ᵐ UT.
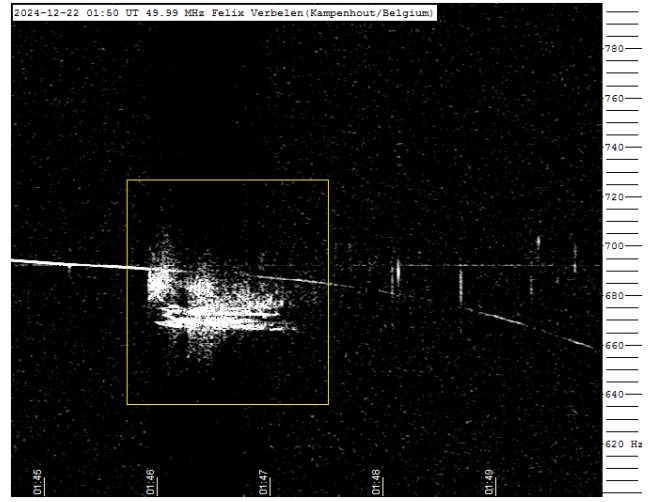
Figure 15 – Meteor echoes December 22, 1ʰ50ᵐ UT.
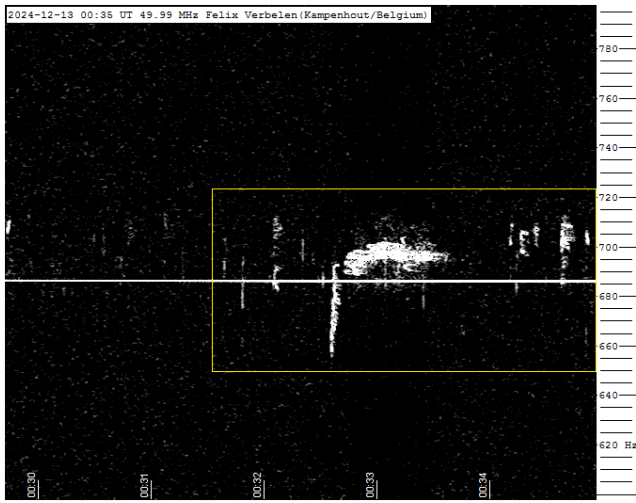
Figure 13 – Meteor echoes December 13, 0ʰ35ᵐ UT.
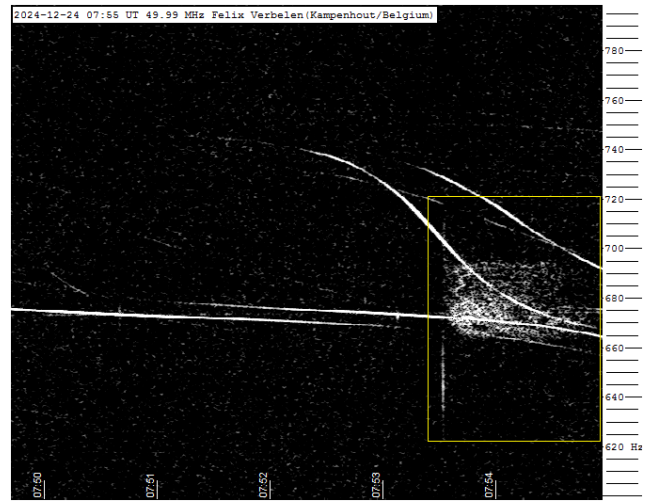
Figure 16 – Meteor echoes December 24, 7ʰ55ᵐ UT.
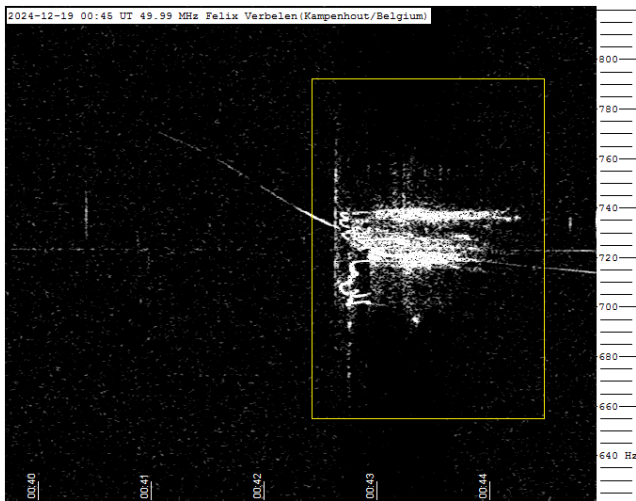
Figure 14 – Meteor echoes December 19, 0ʰ45ᵐ UT.
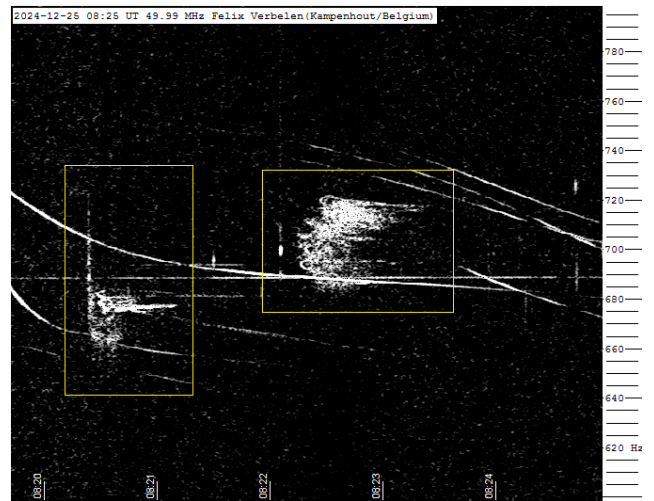
Figure 17 – Meteor echoes December 25, 8ʰ25ᵐ UT.

Radio meteors January 2025

Felix Verbelen

Vereniging voor Sterrenkunde & Volkssterrenwacht MIRA, Grimbergen, Belgium
`felix.verbelen@gmail.com`

An overview of the radio observations during January 2025 is given.

1   Introduction

The graphs show both the daily totals (*Figure 1 and 2*) and the hourly numbers (*Figure 3 and 4*) of "all" reflections counted automatically, and of manually counted "overdense" reflections, overdense reflections longer than 10 seconds and longer than 1 minute, as observed here at Kampenhout (BE) on the frequency of our VVS-beacon (49.99 MHz) during the month of January 2025.

The hourly numbers, for echoes shorter than 1 minute, are weighted averages derived from:

$$N(h) = \frac{n(h-1)}{4} + \frac{n(h)}{2} + \frac{n(h+1)}{4}$$

During this month, there were few local disturbances and no lightning activity was recorded, though solar flares (mostly type III) were observed almost daily.

However, during work near the beacon antenna, it was severely damaged, causing the beacon signal to fail between 13^{h}22^m UT on January 17th and 14^{h}40^m UT on January 19th.

Consequently, no observations were possible on 49.99 MHz during this period, and data are missing.

The highlight of the month was, as expected, the Quadrantid/Bootid meteor shower, which peaked on January 3rd. Some SpecLab images illustrating the intensity of the shower are attached (*Figure 5*).

The rest of the month was generally quiet, with a few minor showers. Only two reflections longer than 1 minute were observed this month, one of which (on January 21st) was particularly strong (*Figures 6 and 7*).

In addition to the usual graphs, you will also find the raw counts in cvs-format[33] from which the graphs are derived. The table contains the following columns: day of the month, hour of the day, day + decimals, solar longitude (epoch J2000), counts of "all" reflections, overdense reflections, reflections longer than 10 seconds and reflections longer than 1 minute, the numbers being the observed reflections of the past hour.

---

[33] https://www.emeteornews.net/wp-content/uploads/2025/02/202501_49990_FV_rawcounts.csv
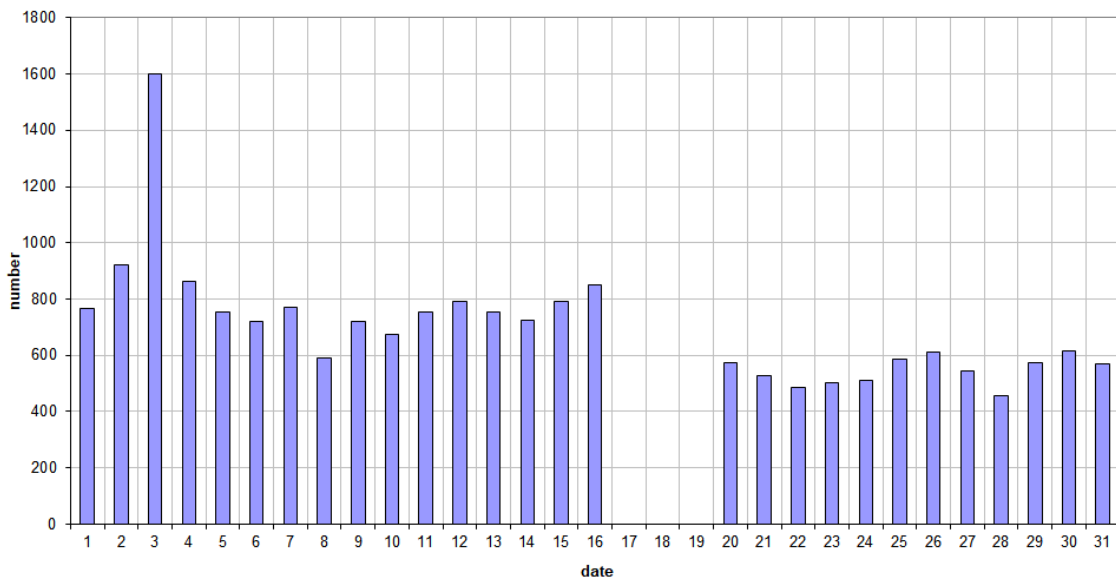
Figure 1 – The daily totals of "all" reflections counted automatically, and of manually counted "overdense" reflections, as observed here at Kampenhout (BE) on the frequency of our VVS-beacon (49.99 MHz) during January 2025.

Figure 2 – The daily totals of overdense reflections longer than 10 seconds and longer than 1 minute, as observed here at Kampenhout (BE) on the frequency of our VVS-beacon (49.99 MHz) during January 2025.

Figure 3 – The hourly numbers of "all" reflections counted automatically, and of manually counted "overdense" reflections, as observed here at Kampenhout (BE) on the frequency of our VVS-beacon (49.99 MHz) during January 2025.

49.99MHz - RadioMeteors January 2025
number of reflections >10 seconds per hour (weighted average)
Felix Verbelen (Kampenhout)

49.99MHz - RadioMeteors January 2025
hourly totals of overdense reflections longer than 1 minute
Felix Verbelen (Kampenhout/BE)

Figure 4 – The hourly numbers of overdense reflections longer than 10 seconds and longer than 1 minute, as observed here at Kampenhout (BE) on the frequency of our VVS-beacon (49.99 MHz) during January 2025.

Quadrantiden20250103_49.99 MHz-selectie (Felix Verbelen/BE)
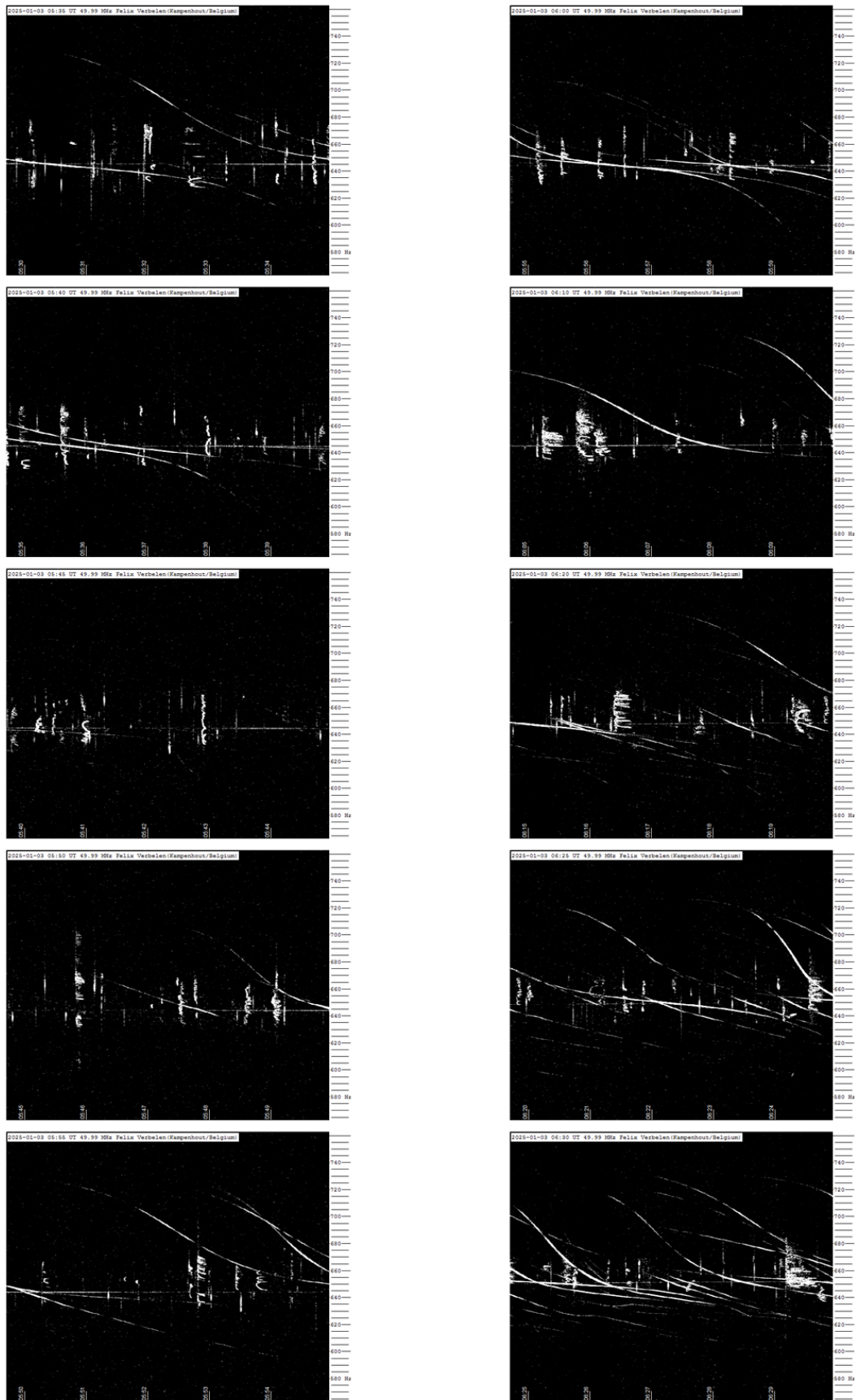
Figure 5 – Selection of meteor echoes during the Quadrantid 2025 activity.
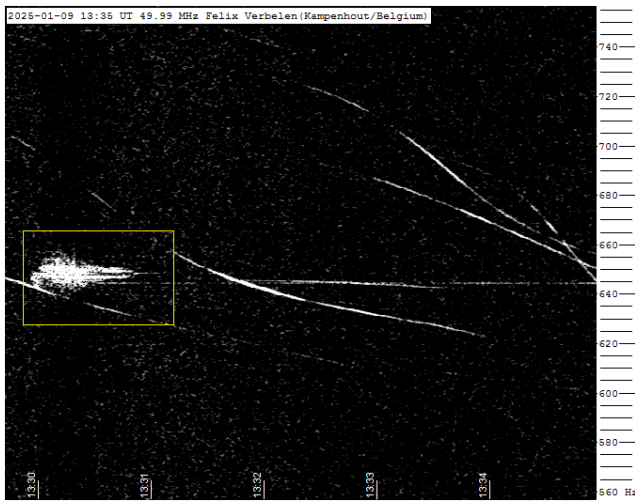
Figure 6 – Meteor echoes January 9, 13ʰ35ᵐ UT.
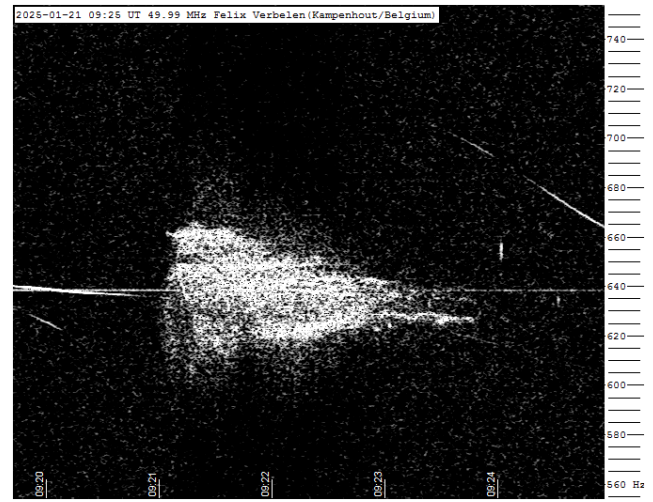
Figure 7 – Meteor echoes January 21, 9ʰ25ᵐ UT.

December 2024 report CAMS-BeNeLux

Carl Johannink

Am Ollenkamp 4, 48599 Gronau, Germany
c.johannink@t-online.de

A summary of the activity of the CAMS-BeNeLux network during the month of December 2023 is presented. This month we collected a total of 24353 meteors resulting in 3176 orbits.

1 Introduction

In December the Earth crosses dust of the Geminids, one of the highlights of meteor observing. Some nice minor showers are visible too. Combined with high sporadic activity this is a very attractive month for all meteor observers.

After the disappointing month of November, we hoped for better circumstances this month.

2 December 2024 statistics

December 2024 was, like last year, a somber month. Only a handful of complete clear nights occurred in large parts of the BeNeLux, France, Engeland, Germany and Denmark. And although the number of cameras and stations increased significantly compared with December months in the past, we have captured only 3176 orbits, resulting from 24353 recorded meteors.

In 8 nights, we could capture no orbit at all, and there were only a small number of nights in which we could collect more than 200 orbits. So, a meager result this year. See *Figure 1* and *Table 1*.

Table 1 – Number of orbits and active cameras in CAMS-BeNeLux during the month of December in the period 2012–2024.

Year	Nights	Orbits	Stations	Max. Cams	Min. Cams	Mean Cams
2012	12	117	6	7	–	2.4
2013	23	1053	10	25	–	15.7
2014	19	1540	14	37	–	25.8
2015	27	1589	15	49	8	33.8
2016	25	3492	21	58	25	48.3
2017	25	2804	22	86	49	68.9
2018	23	4908	21	78	52	69.8
2019	28	4124	21	82	64	72.8
2020	24	2693	24	86	56	72.4
2021	25	3072	25	84	67	76.0
2022	27	7680	31	97	73	84.8
2023	27	2751	41	119	101	109.0
2024	23	3176	49	125	111	117.5
Total	308	38999				

Figure 1 – Comparing December 2024 to previous months of December in the CAMS-BeNeLux history. The blue bars represent the number of orbits, the red bars the maximum number of cameras capturing in a single night, the green bars the average number of cameras capturing per night and the yellow bars the minimum number of cameras.

Around the Geminid maximum the central parts of the Netherlands got no sunshine at all for a period of 11 days in a row (December 9 – 19).

So, members from this stream could only be recorded by some stations in southern Belgium and Engeland, that had some clear nights in that time.

The highest number of orbits in one night was captured in December 26–27 and December 27–28, approximately 330 and 420 orbits each night. As said earlier, compared with December 2023, the number of stations, and consequently the number of active cameras, has increased significantly (see *Figure 1*).

This month, only 43% of all simultaneous meteors were captured by more than two stations. This confirms the bad weather this month.

On average, nearly 117 cameras at 49 stations were active during this month. Every night, at least 111 cameras captured meteors. The highest number of active cameras was 125 for a single night. These numbers are significantly higher than last year (*Figure 1*).

Unfortunately, the number of orbits was hampered by bad weather.

3   Conclusion

Results for December 2024 are, when compared to other years, only modest, although the number of cameras increased significantly.

Report on the sightings of a fireball over the skies of Matanzas and western Cuba

Yasmani Ceballos-Izquierdo[1] and Henry Delgado Manzor[2]

[1] **Calle 40, #2702 e/27 y 29, Madruga, Mayabeque, Cuba**
yasmaniceballos@gmail.com

[2] **Aeropuerto Internacional Juan Gualberto Gómez, Empresa Cubana de Navegación Aérea, Cuba**
delgadomanzor@gmail.com

On October 31, 2024, between 7^h11^m p.m. and 7^h13^m p.m., a luminous phenomenon was reported in the skies of western Cuba, primarily from Matanzas province. The event was marked by a rapidly distorting smoke trail, exhibiting characteristics consistent with a high-altitude bolide crossing. This report analyzes eyewitness accounts, rules out alternative explanations, and examines preliminary implications of the event.

1 Introduction

Fireballs captivate both the general public and the scientific community, while also enriching local culture through the documentation of notable historical events. In Cuba, there is a significant record of events related to fireballs and bolides. However, other luminous phenomena, such as airplane contrails, twilight effects from rocket launches, satellite passages, and the reentry of artificial objects, have sometimes been mistaken for these events (Ceballos-Izquierdo, 2024). Recently, misinterpretations of contrails as evidence of meteorite falls have become more common, as was the case with an event reported on January 22, 2023, in the province of Matanzas (Ceballos-Izquierdo, 2024). In this context, it is essential to thoroughly evaluate and document such phenomena to prevent misinterpretations and promote scientific understanding.

This report documents a singular event observed on October 31, 2024, in western Cuba, characterized by a smoke trail and coinciding visual reports from multiple provinces (*Figure 1*). Preliminary analysis suggests the passage of a bolide, which, based on its characteristics, could have produced meteorites. However, direct evidence of fragments on the ground has yet to be confirmed.

2 Discussion

Initial context of the event

The event was initially reported by social media users from Matanzas on October 31, 2024, between 7^h11^m p.m. and 7^h13^m p.m., who observed a notable smoke trail (*Figure 2*). At first glance, the trail did not resemble a typical aircraft contrail. Subsequently, witnesses from other provinces also reported the phenomenon, expanding the observation area.

Description of the trail and relevant observations

The observed trail initially appeared as a straight line but, within less than five minutes, acquired a twisted shape, a common feature of phenomena associated with fast-moving objects. This deformation may have been caused by upper atmospheric winds, which tend to curve and disperse trails left by rapidly moving objects. Twisted trails like this are characteristic of rotating meteoroids, and the observed density of the trail suggests that the object was of significant size. The absence of sound supports the hypothesis that the event occurred at such a high altitude that sound waves did not reach ground-level observers.

An observer from Playa, Havana, reported witnessing a bright blue light associated with the event, which left a visible trail in the sky. This detail is significant because the bluish coloration indicates a high-energy phenomenon, likely caused by intense friction as the object interacted with the upper layers of the atmosphere.

Preliminary interpretation

Cuba's atmospheric conditions, combined with the presence of domestic and international air traffic, often lead to confusion in the interpretation of celestial phenomena. As part of this investigation, various efforts were undertaken to gather accurate information and verify the situation in the area of observation.

The authors contacted the Control Tower of the Juan Gualberto Gómez International Airport in Varadero. Using their Multilateration (MLAT) system, it was confirmed that no aircraft were present in the area at the time of the sighting, ruling out the possibility of the phenomenon being related to aerial activity. Additionally, the authors consulted the National Center for Seismological Research (CENAIS) to review data from the Camarioca seismic station, located in northern Matanzas Province. This review yielded no positive results, as no explosions or unusual seismic activity were recorded in the region during the event.

Meteorological satellite imagery was also examined for evidence of lightning strikes, but no indicators associated with the observed phenomenon were found. Furthermore, an analysis of Florida's space activity records confirmed

that no rocket launches took place on the date and time of the event. This further reinforced the conclusion that neither aircraft nor space activities were involved.

The observed pattern and witness descriptions align with phenomena associated with bolides or fireballs. Such events occur when a meteoroid enters Earth's atmosphere and disintegrates, producing light and heat that create visible trails and, in some cases, meteorite fragments on the ground. However, it is noteworthy that specialized platforms for tracking such events, including NASA sensors, international bolide detection systems, and fireball reporting networks, did not detect this event. The authors reached out to these platforms but obtained no positive results. It is worth mentioning that bolides and even meteorite falls in Cuba have previously gone undetected by these systems, underscoring the importance of strengthening local capacities to identify and document these phenomena (Ceballos-Izquierdo et al., 2021, 2022).
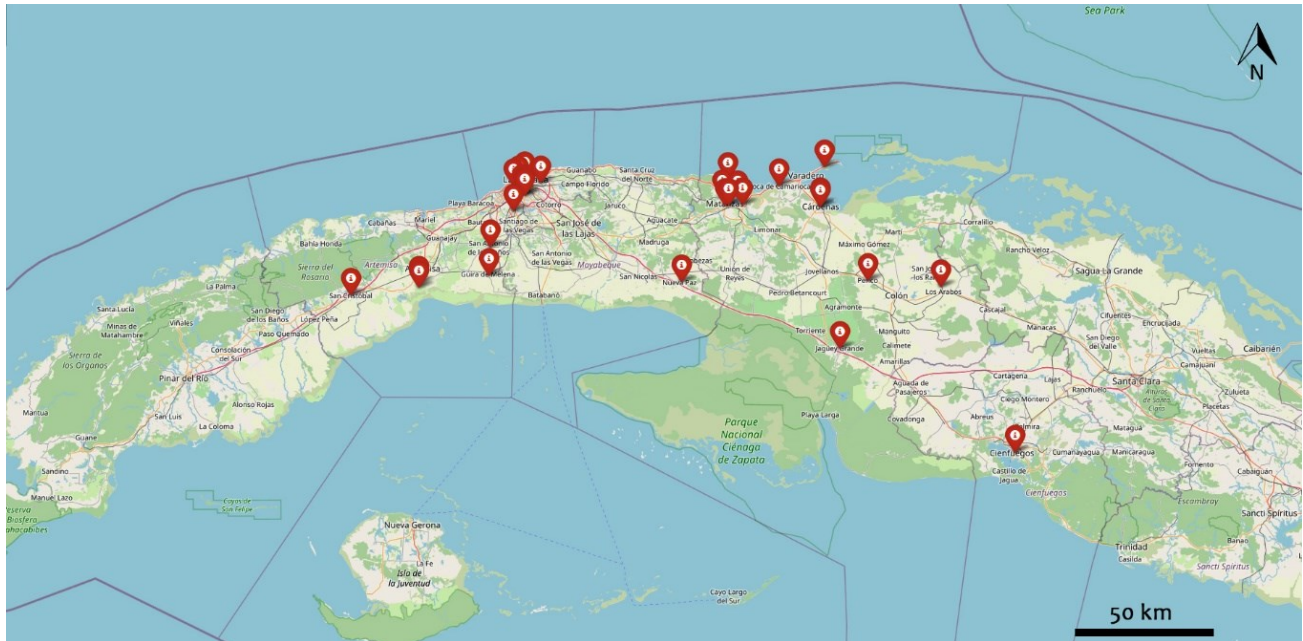
Figure 1 – General map of western Cuba showing the sightings of the trail and bolide from October 2024, marked in red.
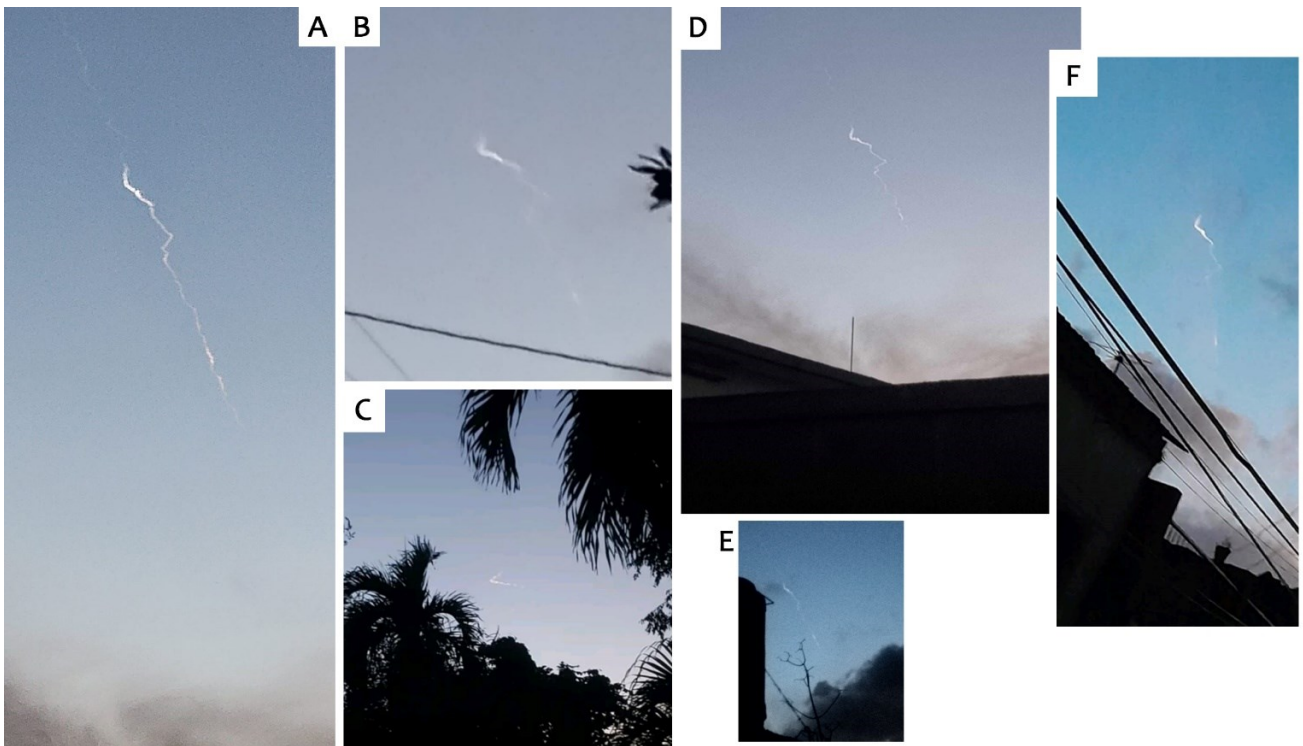
Figure 2 – Different aspects of the trail observed from various locations. Source: submitted to the authors by users on social media..

3 Conclusion

The phenomenon observed on October 31, 2024, over western Cuba exhibits characteristics typically associated with a bolide. The twisted trail, lack of sound, and reports of a bright blue light suggest a high-energy event occurring at a great altitude. However, the fall of associated meteorites has not yet been confirmed.

References

Ceballos-Izquierdo Y. (2024). "Twilight effect in Cuba after SpaceX's launch: What did observers really see?". *Revista Cubana de Física*, **41**, 1.

Ceballos-Izquierdo Y., Free D., Hughes A., Lucena F., Irizarry E., and Grullón M. E. (2022). "Bolas de fuego en el Caribe: Bases para futuras investigaciones". *Revista Cubana de Física*, **39**, 1.

Ceballos-Izquierdo Y., Orihuela J., Goncalves Silva G., Zurita M., Cardozo Mourão M., and Delgado Manzor H. (2021). "Meteorite and bright fireball records from Cuba". *Mineralia Slovaca*, **54**, 3–18.

A fireball with orbit beyond Saturn

Ventsislav Bodakov

Stellar Society, Sofia, Bulgaria
venzibo@gmail.com

At 23^{h}58^m UTC on 2024, November 19 a bright fireball was observed over Bulgaria by three Global Meteor Network cameras. The trajectory and orbit were computed. The orbit is inclined by 54 degrees and is extending beyond Saturn.

1 Introduction

Long time has passed since the last fireball was registered by the Bulgarian GMN cameras. That is why, when I was routinely checking the GMN camera status page and noticed the bright event I knew it might be interesting to analyze. One camera (BG000D) recorded the entire track of the fireball (*Figure 1*), another one (BG0004) up to the moment of the explosion (*Figure 2*), and a third one (BG0003) – part of it through the clouds (*Figure 3*).

Figure 1 – The fireball as seen from BG000D.

Figure 2 – The fireball as seen from BG0004.

Although the first two cameras captured the event, the brightness of the fireball saturating the camera sensor and the explosion itself made the meteor detector algorithm to not regard this as a regular meteor. The algorithm seeks the frames for a well-defined "centroid" of a meteor, which is hard or impossible to be determined in case of an overexposed, exploding fireball. Consequently, there was no detection entry in *radiants.txt, no presence in the detected stack and no FF file in Archive directory.

However, the brightness of the event triggered the fireball detector and it created an uncompressed "region-of-interest" video as FR file in the Archive directory. The third camera (BG0003) observed the meteor through cloud which greatly reduced the brightness and the meteor detection algorithm registered it. This effect helped for the accuracy of the trajectory estimation as we will see below.

Figure 3 – The fireball as seen from BG0003.

2 Fireball analysis

In such cases when a fireball is not detected by the algorithm at the meteor station and a detailed report and orbit estimation is needed, a manual reduction of the meteor data should be done. The data produced should then be correlated with a trajectory solver – in this case - Western Meteor Python Library. WMPL is a data analysis suite with the purpose of trajectory solving and orbit estimation, developed by the Western Meteor Physics Group at the University of Western Ontario.

The manual reduction of the fireball was done using SkyFit2, part of the RMS software of GMN meteor stations. The software was installed on Ubuntu 20.04.6 LTS virtual machine, along with the WMPL trajectory solver. The data reduction for BG000D and BG0004 was done using the FR files produced by the fireball detector in each station, which being uncompressed are better for the purpose compared to the compressed FF files. For a better accuracy first the field of view was recalibrated using the visible stars. Then the position of the fireball's centroid was marked in each frame. Once this process is done for each camera, SkyFit2 generates respective ECSV files as a result. This file contains data about the meteor position as coordinates in

time. As a second step in multi-station analysis these ECSV files were then analyzed and solved by WMPL with the additional option of 20 runs of the Monte Carlo method for a possible optimization of the error margins (Vida et al., 2019; 2020; 2021).

3 Results

The computed convergence angles between the planes of each camera and the fireball are all above the minimum of 3 degrees for a successful trajectory estimation. For BG0004 and BG000D it is 9.8 degrees, BG0003 and BG0004 – 15 degrees, and for BG0003 and BG000D – 25 degrees, which makes it the best intersection. A Google Earth 3D visualization of the trajectory and the plane intersections was generated with WMPL's Utils.TrajectoryKML tool (*Figure 4*).
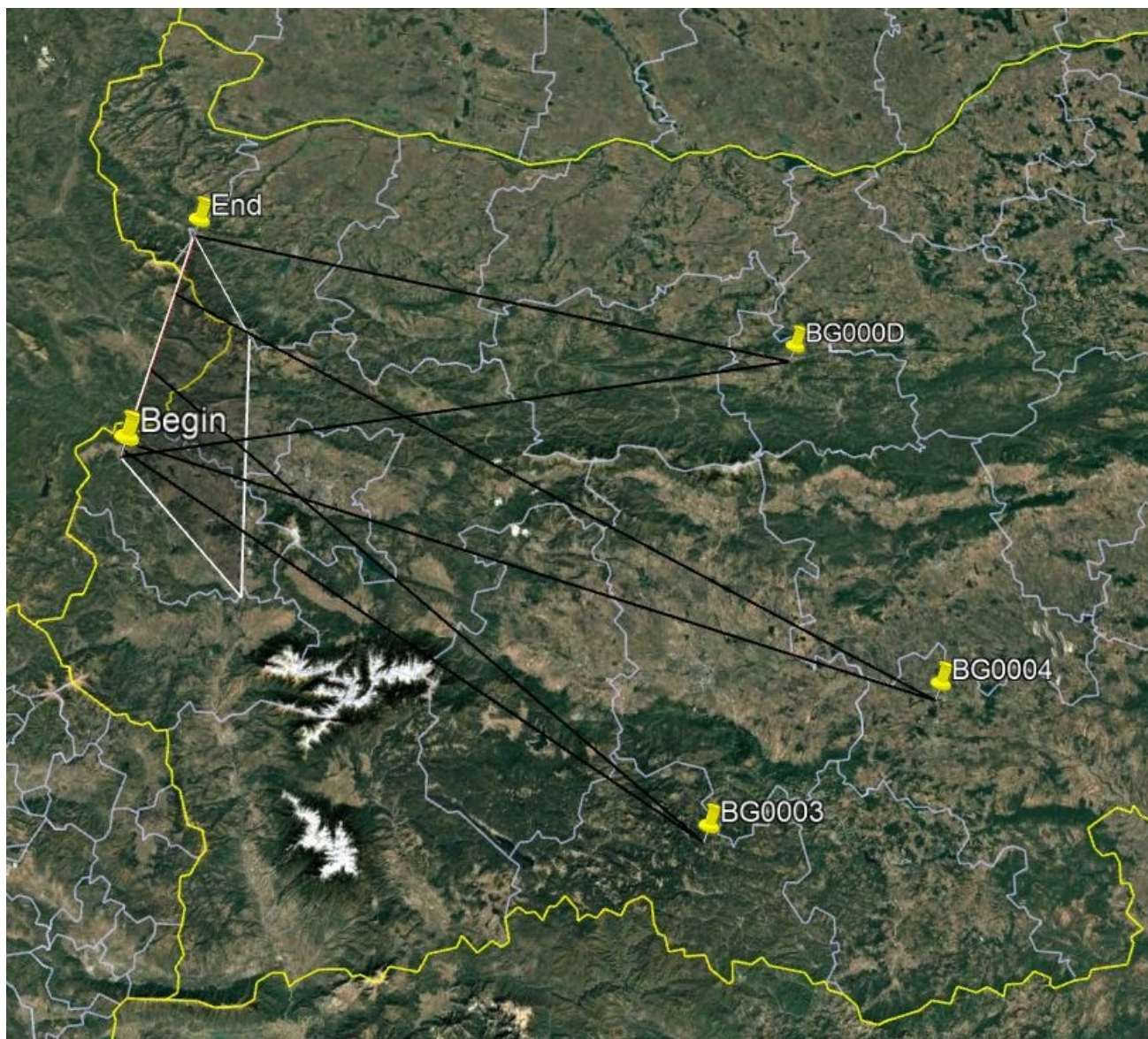
Figure 4 – Google Earth 3D visualization of the fireball trajectory.

The spatial residuals for BG000D, BG0004 and BG0003 are shown in *Figures 5, 6* and *7*, respectively. What attracts attention is that BG0003 has an excellent horizontal RMS deviation of 0.73m, possibly due to the well-defined fireball track dimmed by the clouds, allowing for a precise manual data reduction.

The meteoroid entered the atmosphere at an angle of 31.2 degrees, with an initial velocity of 40.3 km/s, burning up at an altitude between 114.9 km and 63.9 km. The detailed begin and end points of the trajectory with 95% confidence intervals are listed in *Table 1*.

Table 1 – End points of the fireball trajectory.

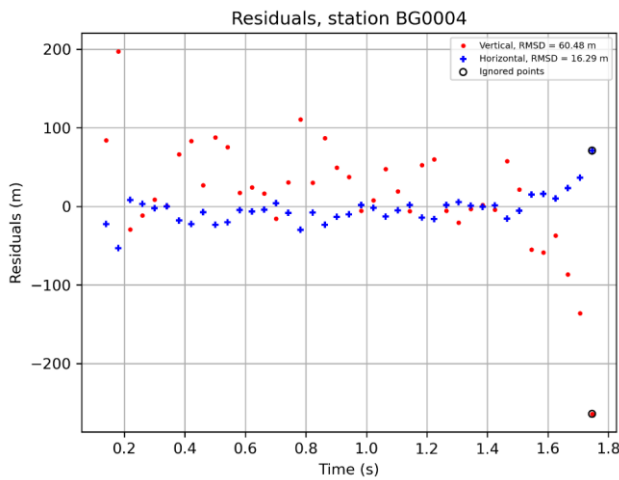| Parameters	Position
Latitude begin (°)	42.382274 ± 0.0001 (± 14.02 m)
Longitude begin (°)	23.102409 ± 0.0005 (± 38.95 m)
Height begin (m)	114918.85 ± 45.70
Latitude end (°)	43.148521 ± 0.0001 (± 16.44 m)
Longitude end (°)	23.070114 ± 0.0008 (± 66.76 m)
Height end (m)	63940.58 ± 44.83
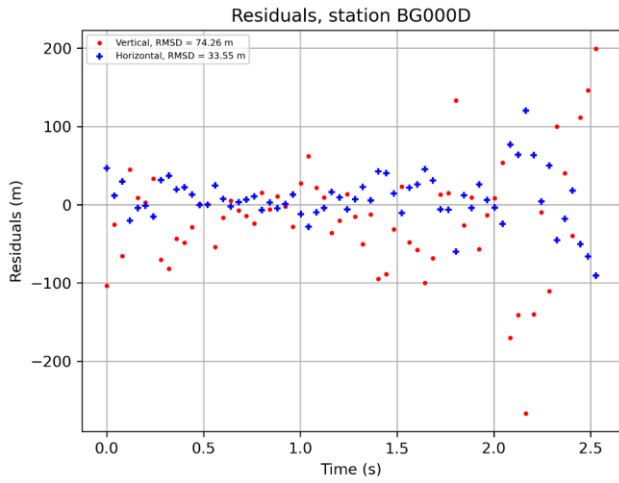
Figure 5 – BG000D spatial residuals.

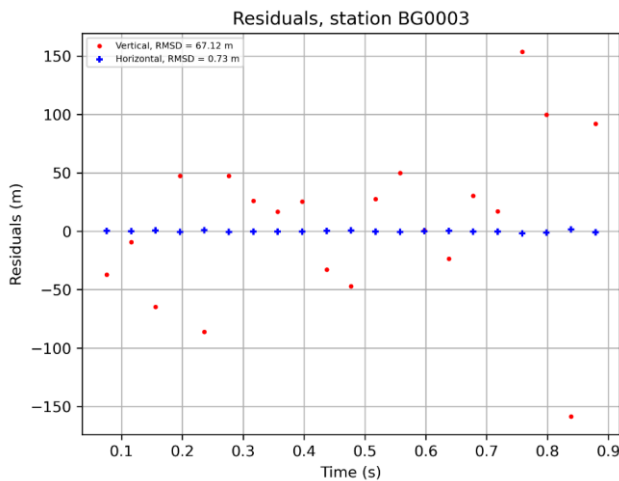*Figure 6 – BG0004 spatial residuals.*

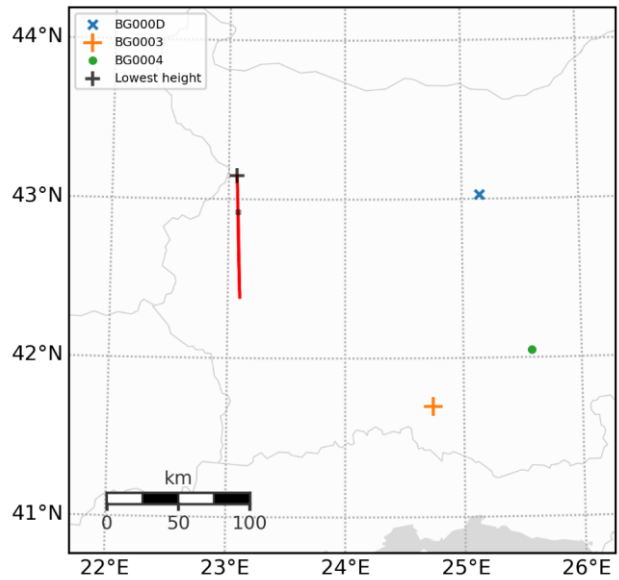*Figure 7 – BG0003 spatial residuals.*

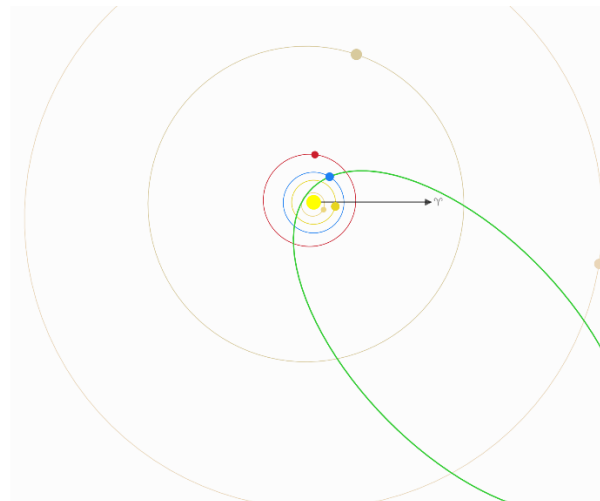*Figure 8 – Ground track of the fireball.*

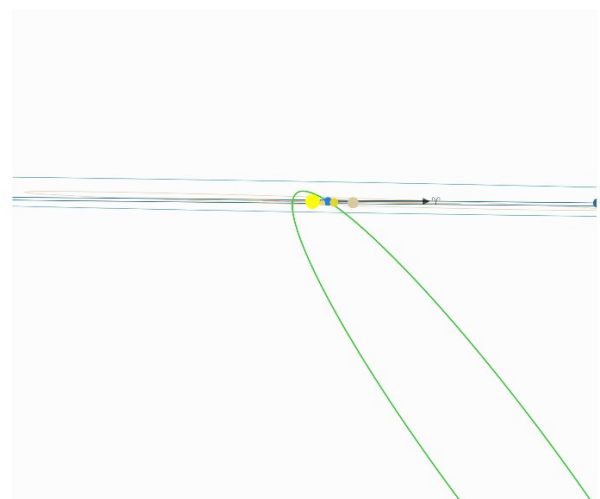*Figure 9 – The fireball orbit, top view.*

Figure 10 – The fireball orbit, side view.

Figure 8 shows a ground track representation of the fireball and the cameras that observed it. The black cross marks the lowest height at which the fireball was captured.

The orbit estimation shows that the fireball had an orbit extending beyond Saturn with an inclination of 54 degrees relative to the ecliptic – *Figures 9* and *10*.

No meteor shower could be associated therefore this fireball has been classified as a sporadic. The detailed orbital elements with 95% confidence intervals are specified in *Table 2*.

Table 2 – Orbital elements of the fireball.

Parameter	Value
Epoch JD	2460634.499
Solar longitude ($\lambda_{\odot}$)	237.809°
R.A. (α_g)	83.10 ± 0.05°
Dec. (δ_g)	−17.97 ± 0.04°
Geocentric velocity (v_g)	38.783 ± 0.015 km/s
λ_g	81.26 ± 0.06°
β_g	−41.20 ± 0.04
$\lambda_g - \lambda_{\odot}$	203.45 ± 0.06°
Semi-major axis (a)	13.7 ± 0.4 AU
Perihelion distance (q)	0.55917 ± 0.0005 AU
Eccentricity (e)	0.959 ± 0.001
Inclination (i)	54.058 ± 0.037°
Longitude of ascending node (Ω)	57.811 ± 0.000002°
Argument of perihelion (ω)	83.491 ± 0.049°
Longitude of perihelion (Π)	141.30 ± 0.05°
Mean anomaly (M)	359.245 ± 0.036°
Orbital period (T)	50.57 ± 2.28 years
Tisserand's parameter (T_j)	0.919 ± 0.011

4 Discussion

The calculated Tisserand's parameter with respect to Jupiter as perturbing body indicates a cometary Mellish-type object with $T_j = 0.919$.

The estimated orbit aphelion beyond Saturn may suggest that the object could be a "centaur" perturbed into this orbit by the giant planets. However, this cannot be proven with the current observation data.

Acknowledgments

References

Vida D., Gural P., Brown P., Campbell-Brown M., Wiegert P. (2019). "Estimating trajectories of meteors: an observational Monte Carlo approach - I. Theory". *Monthly Notices of the Royal Astronomical Society*, **491**, 2688–2705.

Vida D., Gural P., Brown P., Campbell-Brown M., Wiegert P. (2020). "Estimating trajectories of meteors: an observational Monte Carlo approach - II. Results". *Monthly Notices of the Royal Astronomical Society*, **491**, 3996–4011.

Vida D., Šegon D., Gural P. S., Brown P. G., McIntyre M. J. M., Dijkema T. J., Pavletić L., Kukić P., Mazur M. J., Eschman P., Roggemans P., Merlak A., Zubrović D. (2021). "The Global Meteor Network – Methodology and first results". *Monthly Notices of the Royal Astronomical Society*, **506**, 5046–5074.

The Southwestern Europe Meteor Network: some of the most bright bolides observed from October 2024 to January 2025

J.M. Madiedo[1], J.L. Ortiz[1], F. Aceituno[1], P. Santos-Sanz[1], J. Aceituno[2], E. de Guindos[2], D. Ávila[3], B. Tosar[4], A. Gómez-Hernández[5], J. Gómez-Martínez[5], A. García[6], M.A. Díaz[7], and A.I. Aimee[8]

[1] Departamento de Sistema Solar, Instituto de Astrofísica de Andalucía (IAA-CSIC), 18080 Granada, Spain
madiedo@cica.es, ortiz@iaa.es, fja@iaa.es, psantos@iaa.es

[2] Observatorio Astronómico de Calar Alto (CAHA), E-04004, Almería, Spain
aceitun@caha.es, guindos@caha.es

[3] Estación de Meteoros de Ayora, Ayora, Valencia, Spain
David_ayora007@hotmail.com

[4] Casa das Ciencias. Museos Científicos Coruñeses. A Coruña, Spain
borjatosar@gmail.com

[5] Estación de Registro La Lloma, Olocau, Valencia, Spain
curso88@gmail.com

[6] Estación de Meteoros de Cullera (Faro de Cullera), Valencia, Spain
antonio.garcia88@joseantoniogarcia.com

[7] Estación de Meteoros de Valencia del Ventoso, Badajoz, Spain
migandiaz@gmail.com

[8] Southwestern Europe Meteor Network, 41012 Sevilla, Spain
swemn.server@gmail.com

We present here the analysis of some of the most important bolides observed by the Southwestern Europe Meteor Network between October 2024 and January 2025. They were spotted over Spain. Their peak luminosity ranges from magnitude –6 to magnitude –13. Bolides included in this work were produced by different sources: the sporadic background, major meteoroid streams, and poorly-known streams.

1 Introduction

The Southwestern Europe Meteor Network (SWEMN) conducts the SMART project (Spectroscopy of Meteoroids by means of Robotic Technologies), which started operation in 2006 to analyze the physical and chemical properties of meteoroids ablating in the Earth's atmosphere. For this purpose, we employ an array of automated cameras and spectrographs deployed at meteor-observing stations in Spain (Madiedo, 2014; 2017). This allows to derive the luminous path of meteors and the orbit of their progenitor meteoroids, and also to study the evolution of meteor plasmas from the emission spectrum produced by these events (Madiedo, 2015a; 2015b). SMART also provides important information for our MIDAS project, which is being conducted by the Institute of Astrophysics of Andalusia (IAA-CSIC) to study lunar impact flashes produced when large meteoroids impact the Moon (Madiedo et al., 2015; 2018; 2019; Ortiz et al., 2015).

This report describes the preliminary analysis of 8 fireballs spotted by our meteor stations. This work has been fully written by AIMEE (acronym for Artificial Intelligence with Meteoroid Environment Expertise) by using as a source of information the recordings found in the fireball database of the SWEMN project (Madiedo et al., 2021; 2022).

2 Equipment and methods

The events presented here have been recorded by using Watec 902H2 and Watec 902 Ultimate cameras. Their field of view ranges from 62 × 50 degrees to 14 × 11 degrees. To record meteor spectra, we have attached holographic diffraction gratings (1000 lines/mm) to the lens of some of these cameras. We have also employed digital CMOS color cameras (models Sony A7S and A7SII) operating in HD video mode (1920 × 1080 pixels). These cover a field of view of around 70 × 40 degrees. A detailed description of this hardware and the way it operates was given in previous works (Madiedo, 2017). Besides digital CMOS cameras manufactured by ZWO (model ASI185MC) were used. The atmospheric paths of the events were triangulated by means of the SAMIA software, developed by J.M. Madiedo. This program employs the planes-intersection method (Ceplecha, 1987).

3 Description of the 2024 October 6 fireball

On 2024 October 6, at $3^h36^m36.0 \pm 0.1^s$ UT, our meteor stations captured this bright fireball (*Figure 1*). The event, which displayed a series of flares along its atmospheric trajectory, had a peak absolute magnitude of -7.0 ± 1.0. These flares occurred as a consequence of the sudden break-up of the meteoroid. The bolide was listed in our meteor database with the unique identifier SWEMN20241006_033636. The meteor can be viewed on YouTube[34].

Figure 1 – Stacked image of the SWEMN20241006_033636 "La Vereda" fireball.
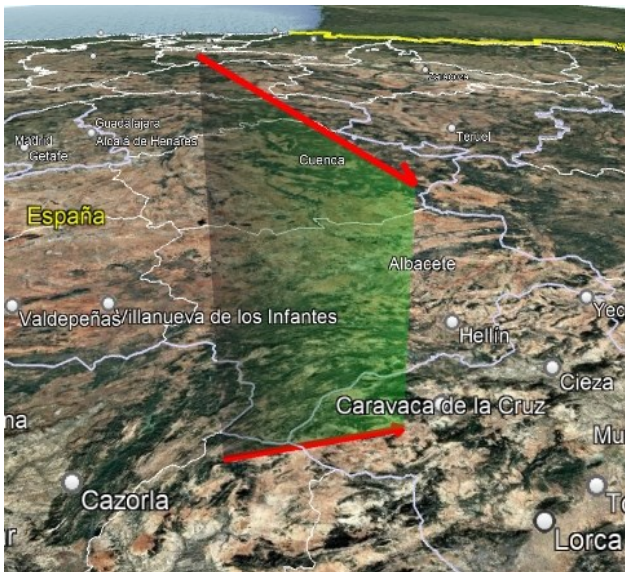
Figure 2 – Atmospheric path of the SWEMN20241006_033636 event, and its projection on the ground.

Atmospheric trajectory, radiant and orbit

According to the analysis of the trajectory in our atmosphere of the event it was obtained that this bolide overflew Granada and Murcia. The luminous event began at an altitude $H_b = 104.8 \pm 0.5$ km. The event penetrated the atmosphere till a final height $H_e = 70.7 \pm 0.5$ km. The apparent radiant was located at the equatorial coordinates $\alpha = 9.24°$, $\delta = +13.79°$. The meteoroid entered the

atmosphere with an initial velocity $v_\infty = 24.0 \pm 0.2$ km/s. *Figure 2* shows the calculated atmospheric path of the bolide. The heliocentric orbit of the meteoroid is drawn in *Figure 3*.

Table 1 – Orbital data (J2000) of the progenitor meteoroid before its encounter with our planet.

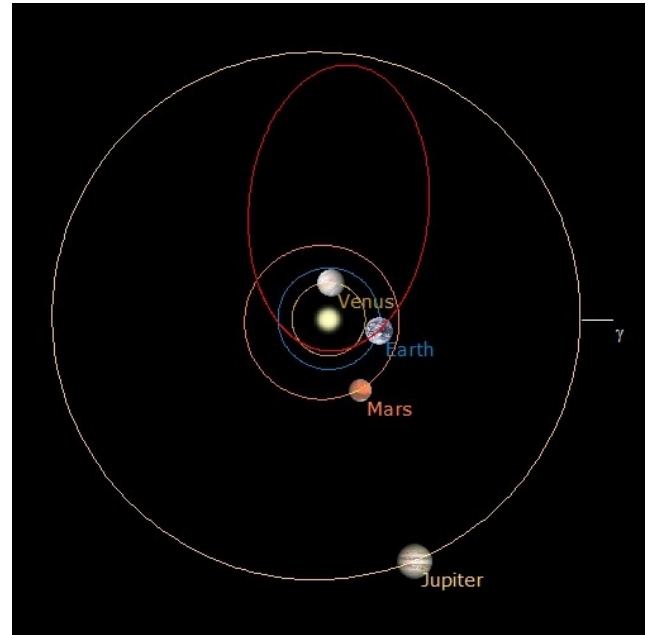| a (AU)	2.83 ± 0.08	ω (º)	261.9 ± 00.1
e	0.780 ± 0.007	Ω (º)	193.050335 ± 10^{-5}
q (AU)	0.622 ± 0.002	i (º)	5.64 ± 0.07

Figure 3 – Projection on the ecliptic plane of the orbit of the parent meteoroid of theº SWEMN20241006_033636 "La Vereda" event.

The name given to the bolide was "La Vereda", since the event was located over this locality during its final phase. The parameters of the heliocentric orbit of the parent meteoroid before its encounter with our planet can be found in *Table 1*, and the geocentric velocity yields $v_g = 21.6 \pm 0.2$ km/s. The Tisserand parameter referred to Jupiter ($T_J = 2.75$) shows that the meteoroid was moving on a cometary (JFC) orbit before entering the atmosphere. By taking into account this orbit and the radiant coordinates, the bright meteor was generated by the October epsilon Piscids (IAU code EPC#0234) (Molau and Rendtel, 2009).

4 Description of the 2024 October 7 fireball

On 2024 October 7, at $5^h24^m40.0 \pm 0.1^s$ UT, SWEMN meteor stations captured this very bright bolide (*Figure 4*). Its peak brightness was equivalent to an absolute magnitude of -12.0 ± 1.0. It presented a bright flare at the final part of its trajectory in the Earth's atmosphere as a consequence of the sudden disruption of the meteoroid. The bolide was included in our meteor database with the identifier SWEMN20241007_052440. A video containing images of

[34] https://youtu.be/iPgcrQvLVCw

the event and its trajectory in our atmosphere was uploaded to YouTube[35].

Figure 4 – Stacked image of the SWEMN20241007_052440 "San Román de la Cuba" bolide.
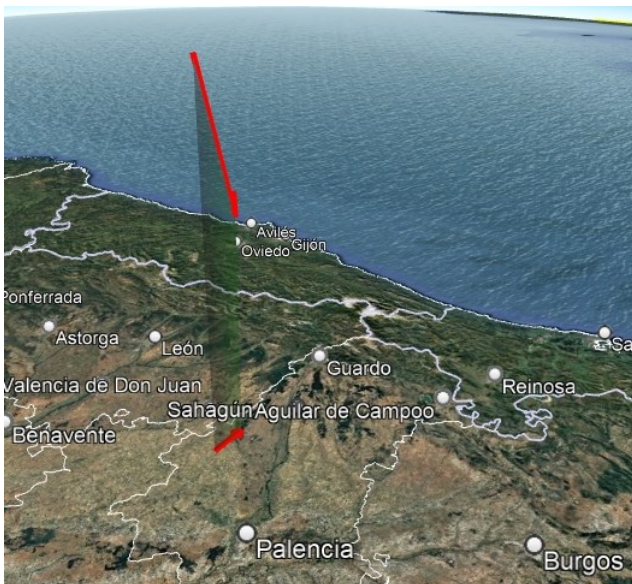

Figure 5 – Atmospheric path of the SWEMN20241007_052440 "San Román de la Cuba" meteor, and its projection on the ground.

Atmospheric path, radiant and orbit

This event overflew the province of Palencia (northern Spain). The luminous event began at an altitude $H_b = 123.7 \pm 0.5$ km. The bolide penetrated the atmosphere till a final height $H_e = 76.0 \pm 0.5$ km. The position inferred for the apparent radiant corresponds to the equatorial coordinates $\alpha = 90.50º$, $\delta = +27.46º$. The pre-atmospheric velocity concluded for the meteoroid yields $v_\infty = 69.9 \pm 0.2$ km/s. *Figure 5* shows the calculated atmospheric trajectory of the event. The heliocentric orbit of the meteoroid is drawn in *Figure 6*.
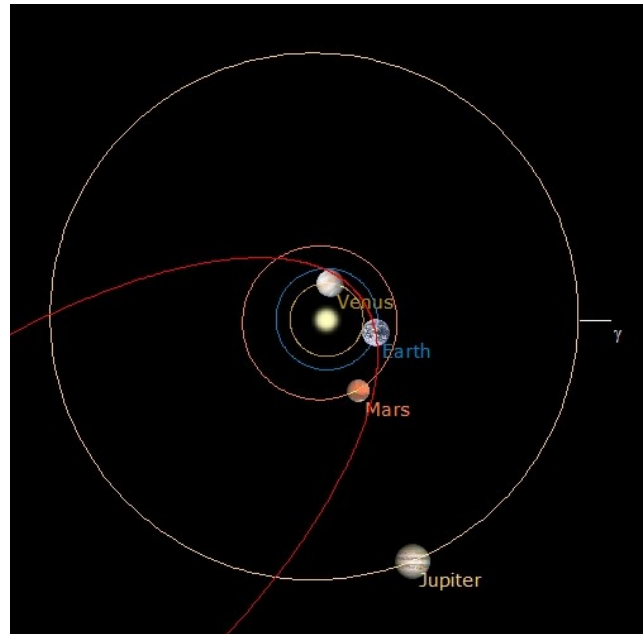
Figure 6 – Projection on the ecliptic plane of the orbit of the progenitor meteoroid of theº SWEMN20241007_052440 "San RomÃ¡n de la Cuba" event.

We named this event "San Román de la Cuba", because the bolide was located over this locality during its initial phase. *Table 2* shows the parameters of the orbit in the Solar System of the progenitor meteoroid before its encounter with our planet. The geocentric velocity of the meteoroid was $v_g = 69.0 \pm 0.2$ km/s. From the value obtained for the Tisserand parameter referred to Jupiter ($T_J = -0.59$), we found that the particle followed a cometary (HTC) orbit before entering the Earth's atmosphere. These values and the derived radiant position confirm that the bright meteor was associated with the sporadic background.

Table 2 – Orbital data (J2000) of the progenitor meteoroid before its encounter with our planet.

a (AU)	10.4 ± 2.0	ω (º)	232.7 ± 00.5
e	0.92 ± 0.01	Ω (º)	194.097158 ± 10^{-5}
q (AU)	0.810 ± 0.002	i (º)	172.70 ± 0.01

5   The 2024 November 7 bolide

On 2024 November 7, at $22^h33^m11.0 \pm 0.1^s$ UT, SWEMN cameras spotted this bright meteor. The maximum luminosity the event was equivalent to an absolute magnitude of -9.0 ± 1.0 (*Figure 7*). Its identifier in the SWEMN meteor database is SWEMN20241107_223311. A video showing the meteor was uploaded to YouTube[36]. The fireball could also be observed by a wide number of causal eyewitnesses.

---

[35] https://youtu.be/cde5fX8iRx4

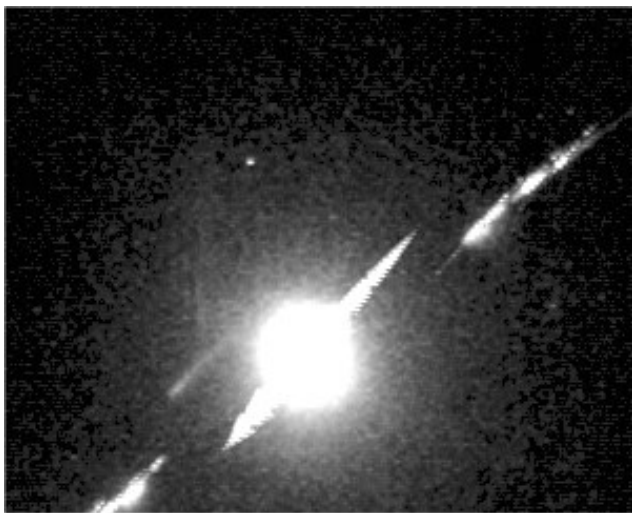[36] https://youtu.be/8w_353Maz5k

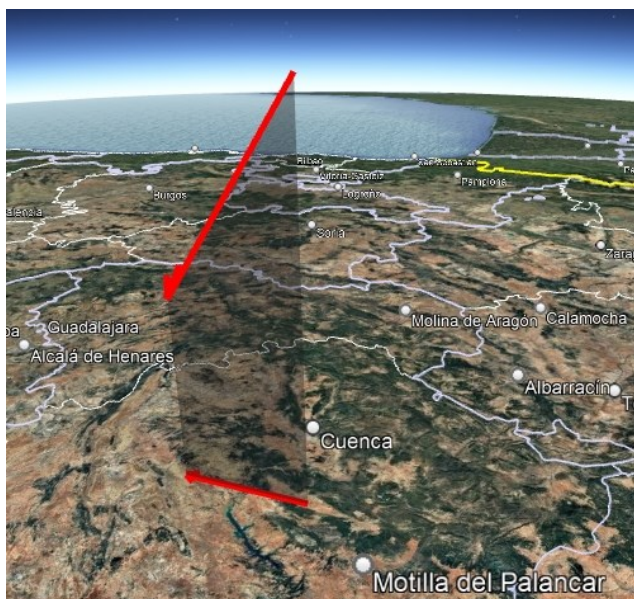*Figure 7* – Stacked image of the SWEMN20241107_223311 "Olmeda del Rey" meteor.

Figure 8 – Atmospheric path of the SWEMN20241107_223311 "Olmeda del Rey" event, and its projection on the ground.

Atmospheric path, radiant and orbit

By calculating the trajectory in the atmosphere of the bright meteor it was deduced that this fireball overflew the province of Cuenca. The luminous event began at an altitude $H_b = 103.9 \pm 0.5$ km. The meteor penetrated the atmosphere till a final height $H_e = 50.1 \pm 0.5$ km. The position obtained for the apparent radiant corresponds to the equatorial coordinates $\alpha = 59.03°$, $\delta = +24.79°$. Besides, we found that the meteoroid hit the atmosphere with a velocity $v_\infty = 33.7 \pm 0.2$ km/s. The calculated luminous path of the fireball is shown in *Figure 8*. The orbit in the Solar System of the progenitor meteoroid is shown in *Figure 9*.

The name given to the bright meteor was "Olmeda del Rey", since the event was located over this village during its initial phase. The parameters of the heliocentric orbit of the progenitor meteoroid before its encounter with our planet have been included in *Table 3*. The value calculated for the geocentric velocity was $v_g = 31.6 \pm 0.2$ km/s. The

Tisserand parameter referred to Jupiter ($T_J = 2.87$) indicates that the meteoroid followed a cometary (JFC) orbit before hitting the Earth's atmosphere. By taking into account these data and the calculated radiant location, the fireball was produced by the Northern Taurids (IAU shower code NTA#0017). So, the event was captured near the activity peak of this meteor shower. 2004 TG10 is the proposed progenitor body of this meteor shower (Jenniskens et al., 2016).

Table 3 – Orbital data (J2000) of the progenitor meteoroid before its encounter with our planet.

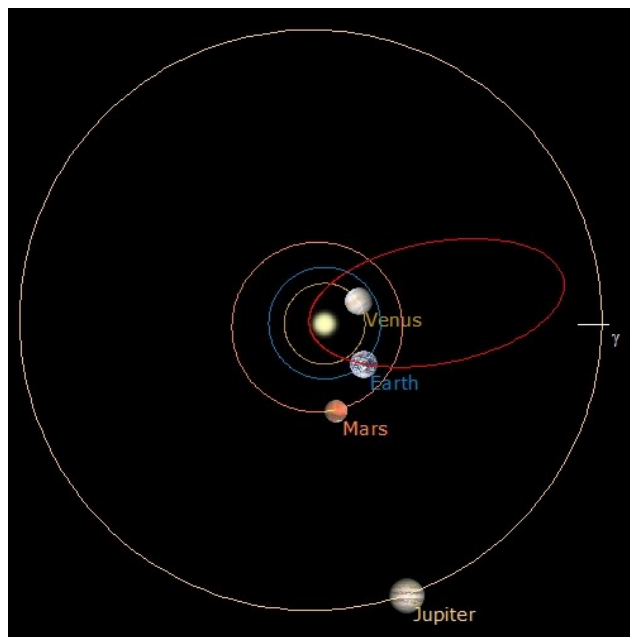| a (AU)	2.31 ± 0.06	ω (°)	303.2 ± 00.2
e	0.882 ± 0.003	Ω (°)	225.696503 ± 10^{-5}
q (AU)	0.271 ± 0.002	i (°)	5.79 ± 0.07

Figure 9 – Projection on the ecliptic plane of the orbit of the progenitor meteoroid of the SWEMN20241107_223311 "Olmeda del Rey" bolide.

6 Description of the 2024 December 14 fireball

We captured this event from the meteor-observing stations located at Huelva, La Hita (Toledo), Calar Alto, Sierra Nevada, La Sagra (Granada), and Sevilla (*Figure 10*). The fireball was spotted on 2024 December 14, at $20^h50^m58.0 \pm 0.1^s$ UT. It had a peak absolute magnitude of -6.0 ± 1.0. The identifier assigned to the fireball in the SWEMN meteor database is SWEMN20241214_205058. The bright meteor can be viewed on this video[37]. The meteor was witnessed by a wide number of casual observers.

Atmospheric path, radiant and orbit

The calculation of the trajectory in our atmosphere of the event allowed to conclude that this bolide overflew the province of Jaén (southern Spain). It began at an altitude

---

[37] https://youtu.be/NqJB5DTNOvU

$H_b = 99.5 \pm 0.5$ km, and ended at a height $H_e = 58.7 \pm 0.5$ km. The apparent radiant was located at the equatorial coordinates $\alpha = 113.61°$, $\delta = +33.32°$. The pre-atmospheric velocity inferred for the meteoroid yields $v_\infty = 36.1 \pm 0.2$ km/s. The obtained trajectory in the atmosphere of the fireball is shown in *Figure 11*. The heliocentric orbit of the meteoroid is drawn in *Figure 12*.
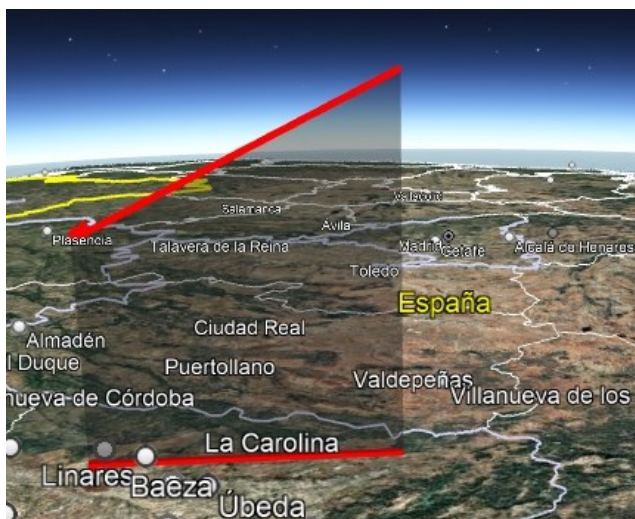

Figure 10 – Stacked image of the SWEMN20241214_205058 "Bailén" bolide.

Figure 11 – Atmospheric path of the SWEMN20241214_205058 "Bailén" event, and its projection on the ground.

This fireball was named "Bailén", because the bolide was located over this locality during its final phase. The parameters of the orbit in the Solar System of the progenitor meteoroid before its encounter with our planet have been listed in *Table 4*, and the geocentric velocity derived in this case was $v_g = 34.0 \pm 0.2$ km/s. The Tisserand parameter referred to Jupiter ($T_J = 4.31$) indicates that before colliding with the Earth's atmosphere the meteoroid was moving on an asteroidal orbit. By taking into account this orbit and the radiant coordinates, the event was generated by the Geminids (IAU shower code GEM#0004). Since the

Geminids peak on December 14, this fireball was recorded during this activity peak. 3200 Phaethon (=1983 TB) is the proposed parent body of this meteor shower (Jenniskens et al., 2016).

Table 4 – Orbital data (J2000) of the progenitor meteoroid before its encounter with our planet.

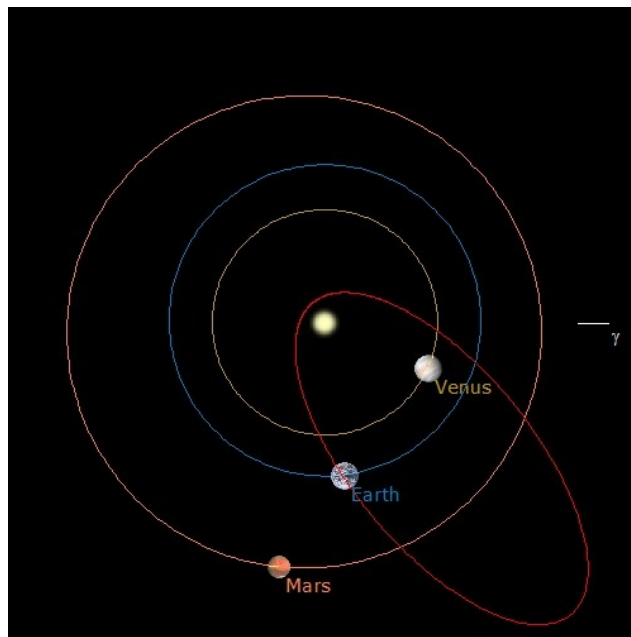| a (AU)	1.33 ± 0.01	ω (°)	323.25 ± 00.01
e	0.887 ± 0.002	Ω (°)	263.031820 ± 10^{-5}
q (AU)	0.150 ± 0.001	i (°)	24.5 ± 0.2

Figure 12 – Projection on the ecliptic plane of the orbit of the progenitor meteoroid of theº SWEMN20241214_205058 "Bailén" fireball.

7   The 2024 December 21 bolide

This bright meteor was spotted on 2024 December 21, at $0^h00^m47.0 \pm 0.1^s$ UT. Its maximum brightness was equivalent to an absolute magnitude of -8.0 ± 1.0 (*Figure 13*). It presented a bright flare at the terminal stage of its atmospheric path as a consequence of the sudden disruption of the meteoroid. It was included in the SWEMN meteor database with the code SWEMN20241221_000047. The event can be viewed on this YouTube[38] video.

Atmospheric path, radiant and orbit
As a result of the analysis of the trajectory in our atmosphere of the bolide it was found that this bright meteor overflew Spain, Portugal and the Atlantic Ocean. Its initial altitude was $H_b = 121.8 \pm 0.5$ km. The event penetrated the atmosphere till a final height $H_e = 86.8 \pm 0.5$ km. The apparent radiant was located at the equatorial coordinates $\alpha = 178.20°$, $\delta = +32.63°$. The meteoroid collided with the atmosphere with an initial velocity $v_\infty = 65.1 \pm 0.4$ km/s. The calculated trajectory in the atmosphere of the bright

---

[38] https://youtu.be/zCCuv_tl0fs

meteor is shown in *Figure 14*. The orbit in the Solar System of the meteoroid is shown in *Figure 15*.

Figure 13 – Stacked image of the SWEMN20241221_000047 "Araujo" bolide.

Figure 14 – Atmospheric path of the SWEMN20241221_000047 "Araujo" meteor, and its projection on the ground.
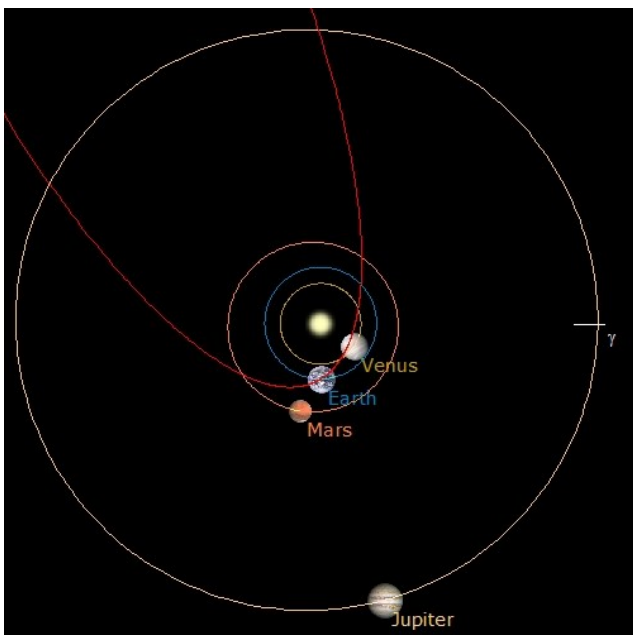

Figure 15 – Projection on the ecliptic plane of the orbit of the parent meteoroid of theº SWEMN20241221_000047 "Araujo" bolide.

We named this fireball "Araujo", because the event was located over this locality during its initial phase. The orbital parameters of the progenitor meteoroid before its encounter with our planet are listed in *Table 5*. The geocentric velocity of the meteoroid was $v_g = 63.8 \pm 0.4$ km/s. From the value derived for the Tisserand parameter with respect to Jupiter ($T_J = -0.24$), we found that before striking our atmosphere the particle was moving on a cometary (HTC) orbit. By taking into account these data and the derived radiant location, the bolide was generated by the 61 Ursae Majorids (IAU code SUM#0564) (Andreic et al., 2014).

Table 5 – Orbital data (J2000) of the progenitor meteoroid before its encounter with our planet.

a (AU)	11.5 ± 4.7	ω (º)	222.2 ± 00.8
e	0.92 ± 0.03	Ω (º)	269.263011 ± 10^{-5}
q (AU)	0.861 ± 0.002	i (º)	127.3 ± 0.2

8   The event on 2024 December 24

This bright bolide was recorded on 2024 December 24, at $20^h54^m12.0 \pm 0.1^s$ UT. It had a peak absolute magnitude of -8.0 ± 1.0 (*Figure 16*). Its code in the SWEMN meteor database is SWEMN20241224_205412. The bolide could also be observed by a wide number of causal eyewitnesses.

Figure 16 – Stacked image of the SWEMN20241224_205412 event.

Atmospheric path, radiant and orbit

This bright meteor overflew the provinces of Murcia, Almería and Granada (southeastern Spain). The luminous event began at an altitude $H_b = 99.2 \pm 0.5$ km. The bolide penetrated the atmosphere till a final height $H_e = 46.4 \pm 0.5$ km. The equatorial coordinates found for the apparent radiant are $\alpha = 102.43º$, $\delta = +11.71º$. The entry velocity in the atmosphere inferred for the progenitor meteoroid was $v_\infty = 25.2 \pm 0.2$ km/s. The orbit in the Solar System of the meteoroid is shown in *Figure 18*.

Table 6 contains the orbital parameters of the progenitor meteoroid before its encounter with our planet. The

geocentric velocity obtained for the particle yields $v_g = 22.3 \pm 0.2$ km/s. The value derived for the Tisserand parameter referred to Jupiter ($T_J = 4.51$) reveals that the meteoroid followed an asteroidal orbit before striking our atmosphere. These values and the derived radiant coordinates confirm that the bolide was produced by the sporadic component.

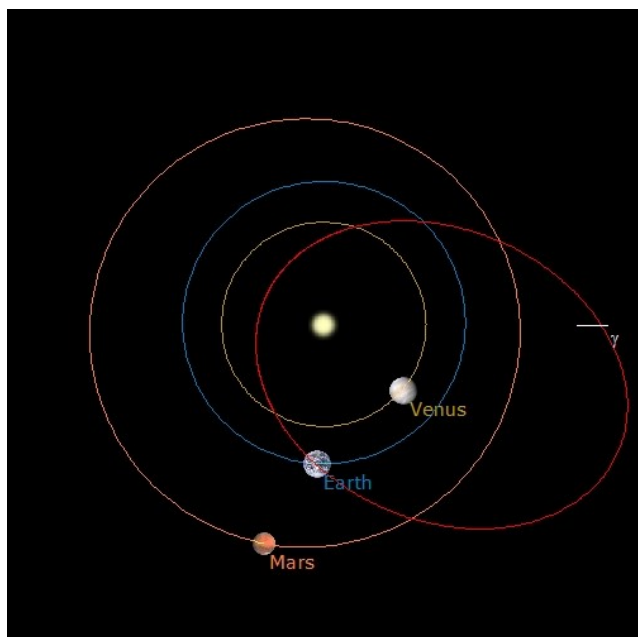*Figure 17* – Atmospheric path of the SWEMN20241224_205412 fireball, and its projection on the ground.

Figure 18 – Projection on the ecliptic plane of the orbit of the progenitor meteoroid of theº SWEMN20241224_205412 fireball.

Table 6 – Orbital data (J2000) of the progenitor meteoroid before its encounter with our planet.

a (AU)	1.38 ± 0.02	ω (º)	109.0 ± 00.6
e	0.666 ± 0.006	Ω (º)	93.190485 ± 10^{-5}
q (AU)	0.461 ± 0.004	i (º)	10.78 ± 0.09

---

[39] https://youtu.be/LLBWf2Pt-HE

9 Description of the fireball on 2025 January 9

This impressive event was captured on 2025 January 9, at $21^h08^m15.0 \pm 0.1^s$ UT (*Figure 19*). Its peak luminosity was equivalent to an absolute magnitude of -13.0 ± 1.0. It exhibited different flares along its trajectory in our atmosphere as a consequence of the sudden disruption of the meteoroid. The recordings clearly show that the meteoroid experienced fragmentation along the luminous trajectory of the event. The event was added to our meteor database with the identifier SWEMN20250109_210815. A video about this fireball can be viewed on YouTube[39]. Many casual eyewitnesses could also observe and report the bright meteor.

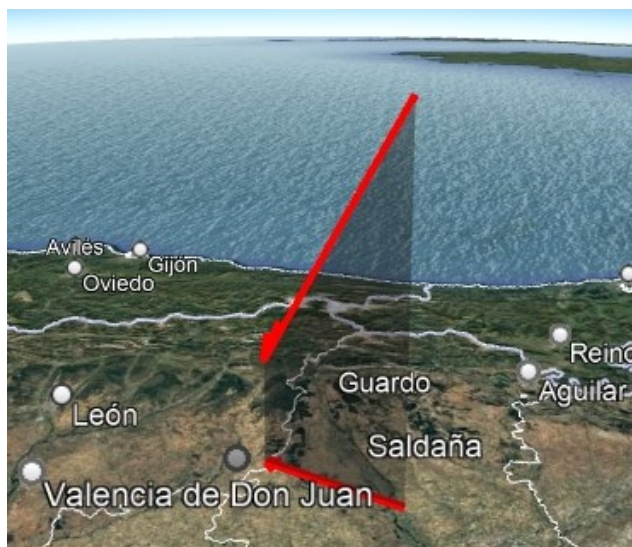*Figure 19* – Stacked image of the SWEMN20250109_210815 "Lomas" meteor.

Figure 20 – Atmospheric path of the SWEMN20250109_210815 "Lomas" bolide, and its projection on the ground.

Atmospheric path, radiant and orbit

It was inferred by calculating the path in the atmosphere of the fireball that this bolide overflew Palencia and León. Its initial altitude was $H_b = 85.8 \pm 0.5$ km. The event penetrated the atmosphere till a final height $H_e = 23.5 \pm 0.5$ km. From the analysis of the atmospheric path we also

obtained that the apparent radiant was located at the position $\alpha = 89.71°$, $\delta = +26.45°$. The entry velocity in the atmosphere concluded for the progenitor meteoroid was $v_\infty = 18.6 \pm 0.2$ km/s. *Figure 20* shows the obtained luminous path of the bright meteor. The orbit in the Solar System of the progenitor meteoroid is shown in *Figure 21*.

Table 7 – Orbital data (J2000) of the progenitor meteoroid before its encounter with our planet.

a (AU)	2.34 ± 0.08	ω (°)	235.4 ± 00.1
e	0.65 ± 0.01	Ω (°)	289.872435 ± 10^{-5}
q (AU)	0.813 ± 0.001	i (°)	0.50 ± 0.03
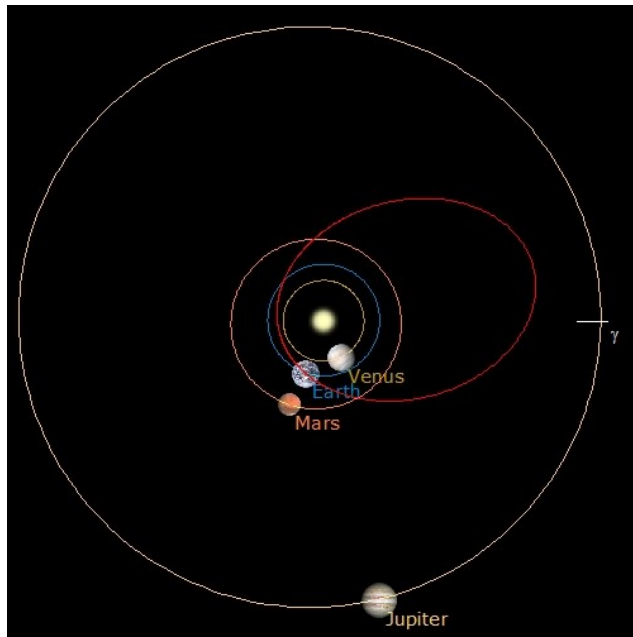
Figure 21 – Projection on the ecliptic plane of the orbit of the progenitor meteoroid of the SWEMN20250109_210815 "Lomas" event.

The bright meteor was named "Lomas", because the bolide was located over this locality during its initial phase. The orbital parameters of the parent meteoroid before its encounter with our planet have been included in *Table 7*, and the geocentric velocity derived in this case was $v_g = 14.7 \pm 0.3$ km/s. From the value estimated for the Tisserand parameter with respect to Jupiter ($T_J = 3.24$), we found that the meteoroid was moving on an asteroidal orbit before hitting our atmosphere. These parameters and the calculated radiant location confirm the sporadic nature of the fireball.

10 The 2025 January 24 event

This striking bright meteor was captured by our cameras at $6^h20^m19.0 \pm 0.1^s$ UT on 2025 January 24 (*Figure 22*). It had a peak absolute magnitude of -12.0 ± 1.0. It was listed in the SWEMN meteor database with the code SWEMN20250124_062019.

Atmospheric path, radiant and orbit
This bolide overflew the provinces of Albacete, Murcia, and Alicante, and also the Mediterranean Sea. Its initial altitude

was $H_b = 99.1 \pm 0.5$ km. The fireball penetrated the atmosphere till a final height $H_e = 40.4 \pm 0.5$ km. The apparent radiant was located at the equatorial coordinates $\alpha = 137.64°$, $\delta = -5.51°$. The meteoroid impacted the atmosphere with an initial velocity $v_\infty = 31.5 \pm 0.2$ km/s. The calculated atmospheric trajectory of the event is shown in *Figure 23*. The orbit in the Solar System of the progenitor meteoroid is shown in *Figure 24*.

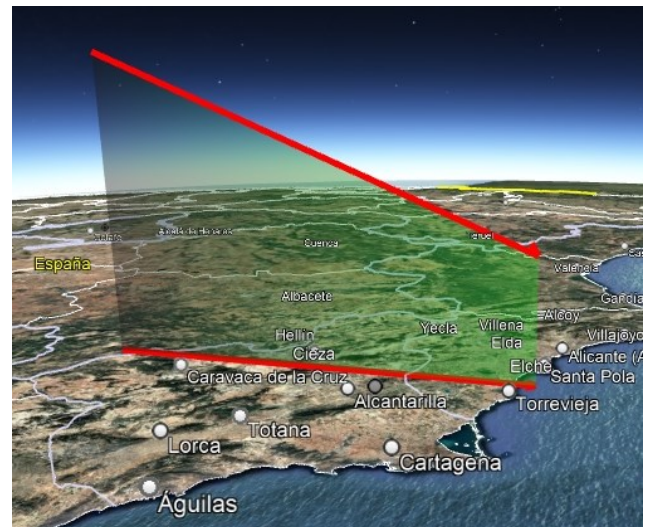*Figure 22* – Stacked image of the SWEMN20250124_062019 "Tobar" event.

Figure 23 – Atmospheric path of the SWEMN20250124_062019 "Tobar" bolide, and its projection on the ground.

Table 8 – Orbital data (J2000) of the progenitor meteoroid before its encounter with our planet.

a (AU)	2.0 ± 0.1	ω (°)	108.1 ± 01.7
e	0.797 ± 0.007	Ω (°)	124.162549 ± 10^{-5}
q (AU)	0.41 ± 0.01	i (°)	27.3 ± 0.2

We named this event "Tobar", since the bolide passed near the zenith of this locality during its initial phase. *Table 8* contains the parameters of the orbit in the Solar System of the parent meteoroid before its encounter with our planet, and the geocentric velocity derived in this case was $v_g = 29.9 \pm 0.2$ km/s. The Tisserand parameter referred to Jupiter ($T_J = 3.23$) indicates that the particle followed an asteroidal orbit before entering our atmosphere. By taking into account these values and the calculated radiant coordinates, it was concluded that the bolide was produced by the sporadic background.
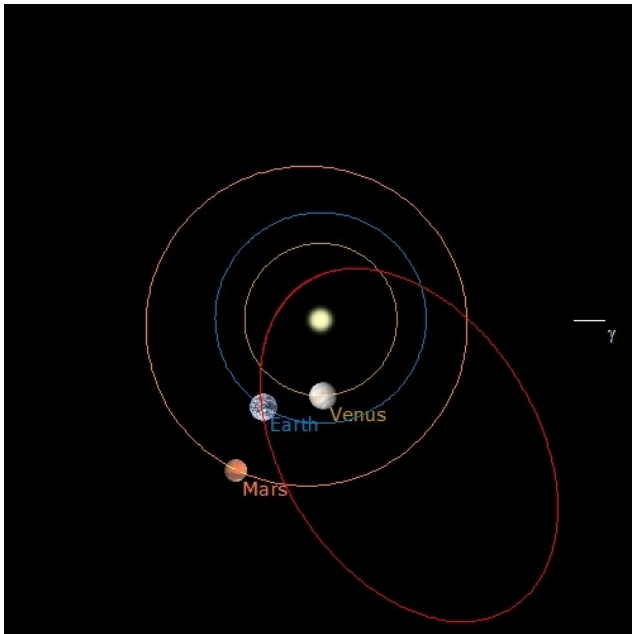
Figure 24 – Projection on the ecliptic plane of the orbit of the parent meteoroid of the SWEMN20231220_004521 meteor.

11 Conclusions

Some of the bright bolides recorded by SWEMN have been discussed in this work. Their peak luminosity ranges from magnitude –6 to magnitude –13.

The "La Vereda" fireball was recorded on October 6. Its peak magnitude was –7.0. The meteor event was produced by an October epsilon Piscid (EPC#0234) meteoroid and overflew the provinces of Granada and Murcia. The meteoroid followed a cometary (JFC) orbit before colliding with our atmosphere.

The second bolide described here was a fireball which was recorded on October 7 named "San Román de la Cuba". It reached a peak absolute magnitude of –12.0, and was associated with the sporadic component. This bolide overflew Palencia. The meteoroid followed a cometary (HTC) orbit before striking the Earth's atmosphere.

The next bolide described here was the "Olmeda del Rey" event. This was recorded on November 7. This Northern Taurid (NTA#0017) bolide had a peak absolute magnitude of –9.0 and overflew Cuenca. Before entering the Earth's atmosphere the meteoroid was moving on a cometary (JFC) orbit.

The next bolide described here was an event recorded on December 14 which was named "Bailén". This Geminid (GEM#0004) fireball had a peak absolute magnitude of –6.0 and overflew the province of Jaén.

The fifth bolide presented here was the "Araujo" event, which was recorded on December 21. Its peak magnitude was –8.0. The bolide was produced by a 61 Ursae Majorid (SUM#0564) meteoroid and overflew Spain, Portugal and the Atlantic Ocean. The meteoroid was moving on a

cometary (HTC) orbit before entering our planet's atmosphere.

Next, we have discussed an event recorded on December 24. It reached a peak absolute magnitude of –8.0, and belonged to the sporadic component. This meteor overflew the provinces of Murcia, Almería and Granada. Before entering our planet's atmosphere, the meteoroid was moving on an asteroidal orbit. The terminal height of this deep-penetrating meteor was of about 46 km.

The "Lomas" bolide was recorded on January 9. It reached a peak absolute magnitude of –13.0, and was also associated with the sporadic background. This meteor overflew the provinces of Palencia and León. Its parent meteoroid followed an asteroidal orbit before hitting our atmosphere. This deep-penetrating fireball reached an ending altitude of about 23 km.

And the last bolide described in this paper was the "Tobar" bolide, which was recorded on January 24. It reached a peak absolute magnitude of –12.0, and was associated with the sporadic component. This meteor overflew Albacete, Murcia, Alicante and the Mediterranean Sea. Before impacting the Earth's atmosphere the meteoroid was moving on an asteroidal orbit. The terminal altitude of this deep-penetrating meteor event was of about 40 km.

Acknowledgment

References

Andreic Z., Gural P., Segon D., Skokic I., Korlevic K., Vida D., Novoselnik F., and Gostinski D. (2014). "Results of CMN 2013 search for new showers across CMN and Sonotaco databases". *WGN, Journal of the International Meteor Organization*, **42**, 90–97.

Ceplecha Z. (1987). "Geometric, dynamic, orbital and photometric data on meteoroids from photographic fireball networks". *Bull. Astron. Inst. Cz.*, **38**, 222–234.

Jenniskens P., Nénon Q., Albers J., Gural P. S., Haberman B., Holman D., Morales R., Grigsby B. J., Samuels D. and Johannink C. (2016). "The established meteor showers as observed by CAMS". *Icarus*, **266**, 331–354.

Madiedo J. M. (2014). "Robotic systems for the determination of the composition of solar system materials by means of fireball spectroscopy". *Earth, Planets & Space*, **66**, 70.

Madiedo J. M. (2017). "Automated systems for the analysis of meteor spectra: The SMART Project". *Planetary and Space Science*, **143**, 238–244.

Madiedo J. M. (2015a). "Spectroscopy of a κ-Cygnid fireball afterglow". *Planetary and Space Science*, **118**, 90–94.

Madiedo J. M. (2015b). "The ρ-Geminid meteoroid stream: orbits, spectroscopic data and implications for its parent body". *Monthly Notices of the Royal Astronomical Society*, **448**, 2135–2140.

Madiedo J. M., Ortiz J. L., Organero F., Ana-Hernández L., Fonseca F., Morales N. and Cabrera-Caño J. (2015). "Analysis of Moon impact flashes detected during the 2012 and 2013 Perseids". *A&A*, **577**, A118.

Madiedo J. M., Ortiz J. L. and Morales N. (2018). "The first observations to determine the temperature of a lunar impact flash and its evolution". *Monthly Notices of the Royal Astronomical Society*, **480**, 5010–5016.

Madiedo J. M., Ortiz J. L., Morales N. and Santos-Sanz P. (2019a). "Multiwavelength observations of a bright impact flash during the 2019 January total lunar eclipse". *Monthly Notices of the Royal Astronomical Society*, **486**, 3380–3387.

Madiedo J. M., Ortiz J. L., Izquierdo J., Santos-Sanz P., Aceituno J., de Guindos E., Yanguas P., Palacian J., San Segundo A., and Avila D. (2021). "The Southwestern Europe Meteor Network: recent advances and analysis of bright fireballs recorded along April 2021". *eMetN Meteor Journal*, **6**, 397–406.

Madiedo J. M., Ortiz J. L., Izquierdo J., Santos-Sanz P., Aceituno J., de Guindos E., Yanguas P., Palacian J., San Segundo A., Avila D., Tosar B., Gómez-Hernández A., Gómez-Martínez J., and García A. (2022). "The Southwestern Europe Meteor Network: development of new artificial intelligence tools and remarkable fireballs observed from January to February 2022". *eMetN Meteor Journal*, **7**, 199–208.

Molau S., Rendtel J. (2009). "A Comprehensive List of Meteor Showers Obtained from 10 Years of Observations with the IMO Video Meteor Network". *WGN, Journal of the International Meteor Organization*, **37**, 98–121.

Ortiz J. L., Madiedo J. M., Morales N., Santos-Sanz P. and Aceituno F. J. (2015). "Lunar impact flashes from Geminids: analysis of luminous efficiencies and the flux of large meteoroids on Earth". *Monthly Notices of the Royal Astronomical Society*, **454**, 344–352.

Contributors:

- Aceituno F.
- Aceituno J.
- Aimee A.I.
- Ávila D.
- Barbieri L.
- Bodakov V.
- Campbell-Burns P.
- Ceballos-Izquierdo Y.
- de Guindos E.
- Delgado Manzor H.

- Díaz M.A.
- García A.
- Gómez-Hernández A.
- Gómez-Martínez J.
- Johannink C.
- Kalina M.
- Madiedo J.M.
- Maglione M.
- McIntyre M.
- Miskotte K.

- Ortiz J.L.
- Roggemans P.
- Santos-Sanz P.
- Scott J. M.
- Šegon D.
- Sicking W.
- Tosar B.
- Verbelen F.
- Vida D.